DRAFT

HVS Test Results on Fast-Setting Hydraulic Cement Concrete

Palmdale, California Test Sections, South Tangent

Report prepared for the California Department of Transportation

by:

Louw du Plessis
CSIR Transportek

David Bush
Dynatest, Inc.

Fritz Jooste,
CSIR Transportek

Dave Hung
University of California
Pavement Research Center

Clark Scheffy
University of California
Pavement Research Center

Jeffery Roesler
University of Illinois
Urbana-Champaign

Lorina Popescu
University of California
Pavement Research Center

John Harvey
University of California
Pavement Research Center

University of California
Institute of Transportation Studies
Pavement Research Center

July 2002

TABLE OF CONTENTS

LIST OF FIGURES

LIST OF PHOTOGRAPHS

LIST OF TABLES

1.0 INTRODUCTION

As part of the Caltrans Long Life Pavement Rehabilitation Strategies (LLPRS), a fast setting strength hydraulic cement concrete (FSHCC)/Type I/II Portland cement concrete (PCC) blend was evaluated under Heavy Vehicle Simulator (HVS) tests as detailed in the Test Plan for CAL / APT Goal LLPRS - Rigid Phase III (*1*).

Because it is expected to be used on projects where heavy trucks are expected to be allowed on the slabs within 4 to 8 hours after placement, this newly placed concrete is specified to obtain a flexural strength of 2.8 MPa within 4 to 8 hours of placement.

Two full-scale test sites, each approximately 210 m in length, were constructed using this concrete on either side of State Route 14 about 5 miles south of Palmdale, California. Various test sections were constructed at these two sites. The site in the southbound direction included sections with different thicknesses of concrete placed on compacted granular base. The site in the northbound direction included 200-mm concrete on cement treated base, with various design features: dowels, tied shoulders, widened lanes.(*2*)

This report documents the results of the tests on the southbound lanes, also referred to as the "South Tangent." Another report currently in being written presents the results of tests on the northbound lanes (North Tangent).

2.0 HVS TEST OBJECTIVES AND SCOPE OF WORK

The main objective of the series of tests on the South Tangent was to evaluate the fatigue behavior of the fast setting hydraulic cement concrete/Portland cement concrete blend under the influence of accelerated wheel loads. It was assumed that the behavior of this mix is similar to that of a pure FSHCC mix. Thirteen HVS tests were undertaken on the South Tangent during the period 07/15/1998 to 05/21/1999.

This report summarizes the results and observations of all HVS tests conducted on the South Tangent. Included in this report are all test sections on the plain jointed (no-dowels, no-tie bars, standard lane width) sections with concrete thicknesses of 100 mm, 150 mm, and 200 mm.

All of the data summarized in this report is included in the Pavement Research Center electronic database.

3.0 HVS TEST PROGRAM

The HVS tests on the South Tangent are listed in Table 3.1.

Table 3.1 HVS Tests on the South Tangent

HVS Test	Section Number	Slab Number*	Design Thickness (mm)	Slab Length (m)	Start Date	End Date	Temperature Control?
519FD	1A	4	100	5.80	07/15/98	07/19/98	Yes
520FD	1B	8	100	5.77	07/23/98	07/30/98	Yes
521FD	1C	12	100	5.76	08/10/98	08/28/98	Yes
522FD	1D	14	100	3.69	09/02/98	09/02/98	No
523FD	3A	17	150	5.47	09/14/98	09/29/98	Yes
524FD	3B	20	150	5.77	10/02/98	10/13/98	Yes
525FD	3C	23	150	3.91	10/15/98	10/18/98	No
526FD	3D	27	150	4.00	10/19/98	10/22/98	Yes
527FD	3C	22	150	3.58	10/26/98	01/21/99	No
528FD	5B	35	200	4.03	01/27/99	02/02/99	Yes
529FD	5A	31	200	3.94	02/07/99	03/04/99	No
530FD	5C	39	200	3.95	03/10/99	05/14/99	Yes
531FD	5D	42	200	3.70	05/19/99	05/21/99	Yes

* The HVS test was centered on this slab. Some areas of the adjacent slabs were also subjected to HVS testing.

The layout of all these sections with respect to the 210-m long full-scale test section on the South Tangent is detailed in an earlier report (*2*).

3.1 HVS Data Collection Schedule

Data were collected according to the intervals detailed in Table 3.2. Visual surveys of the test section were done on a daily basis and air, surface, and in-depth temperatures were recorded every 2 to 3 hours, 24 hours per day. Attempts were made to synchronize the data collection times in terms of number of repetitions for all the test sections, but this was not always possible. A summary of all the temperatures recorded can be found in Section 8 of this report; an example of the raw temperature data can be found in Appendix B. Complete temperature data can be accessed in the Pavement Research Center Database.

Table 3.2 Data Collection Schedules* for HVS Test Sections 519FD to 531FD

Repetitions	Test Section/Temperature Control?/Thickness (mm)												
	519FD	520FD	521FD	522FD	523FD	524FD	525FD	526FD	527FD	528FD	529FD	530FD	531FD
	Yes	Yes	Yes	No	Yes	Yes	No	Yes	No	Yes	No	Yes	Yes
	100 mm				150 mm					200 mm			
10	X	X	X	**	X	X	X	X	X	X	X	X	X
100					X	X	X	X	X				
500			X		X	X	X	X	X				
1,000		X	X		X	X	X	X	X				
2,100	X	X	X									X	X
3,500										X	X	X	X
5,000		X	X		X	X	End	X	X				
10,000			X		X			X	X				
15,000			X		X					X	X	X	X
20,000			X		X	X							
25,000	X	X						End	X	X			
30,000		X	X		X	X				X	X		X
35,000	X	X											
40,000		X	X		X	X			X				
50,000		X			X					X	X		X
55,000	X	X											
60,000	End	X			X	X			X				
70,000		End			X								
80,000										X		X	End
85,000										End		X	
90,000					X						X	X	
100,000			X			X			X		X	X	
125,000			X			End			X		X		
140,000			X		X						X		
150,000											X	X	
157,000			X		End				X				
168,000			End						X				
200,000									X		X	X	
215,000											X	X	

Repetitions	Test Section/Temperature Control?/Thickness (mm)												
	519FD	520FD	521FD	522FD	523FD	524FD	525FD	526FD	527FD	528FD	529FD	530FD	531FD
	Yes	Yes	Yes	No	Yes	Yes	No	Yes	No	Yes	No	Yes	Yes
	100 mm				150 mm					200 mm			
230,000									X		X		
245,000									X		X		
260,000									X		X	X	
310,000									X		X	X	
320,000											X	X	
335,000											X	X	
350,000									X		End	X	
400,000									X			X	
500,000									X			X	
600,000									X			X	
830,000									X			End	
900,000									X				
950,000									X				
1,000,000									X				
1,233,969									End				

* Note: The table shows the approximate data collection times.

** Test Section 522FD was a static test.

HVS loading was continued for each test section until the particular section was considered failed. The failure criterion was a crack in the slab. Although all data were recorded as indicated in Table 3.2, only the most significant results are presented in this summary report (complete data can be accessed in the Pavement Research Center Database). HVS Test Section 522FD was a static test and was not subjected to repetitive loading.

3.2 HVS Instrumentation Plan

In order to monitor the functional and structural behavior of the pavement under accelerated loading, various instruments were used. The description and function of these instruments and their recording mechanisms are described in previous reports *(1–3)*.

Vertical surface deflections were recorded using two Joint Deflection Measuring Devices (JDMDs) and one Edge Deflection Measuring Device (EDMD) on each test section. The JDMDs were positioned to record corner deflections; the EDMD was positioned to record the edge deflection in the middle of the slab. On a few sections, Multi Depth Deflectometers (MDDs) were installed to measure the vertical surface and in-depth deflections. An illustration of the placement of the JDMDs and EDMDs with respect to the concrete slabs and the HVS test pad is shown in Figure 3.1.

Surface deflections were also captured with the Road Surface Deflectometer (RSD) at certain sections. These results were merely used for calibration purposes between the RSD, JDMDs, and EDMDs and are not reported in this document. Further discussion of these instruments and their application can be found in Reference (*1, 2*)

Each test section was instrumented with thermocouples, which recorded the surface (0 mm), mid-depth, and bottom in-depth temperatures of the concrete structures. Other

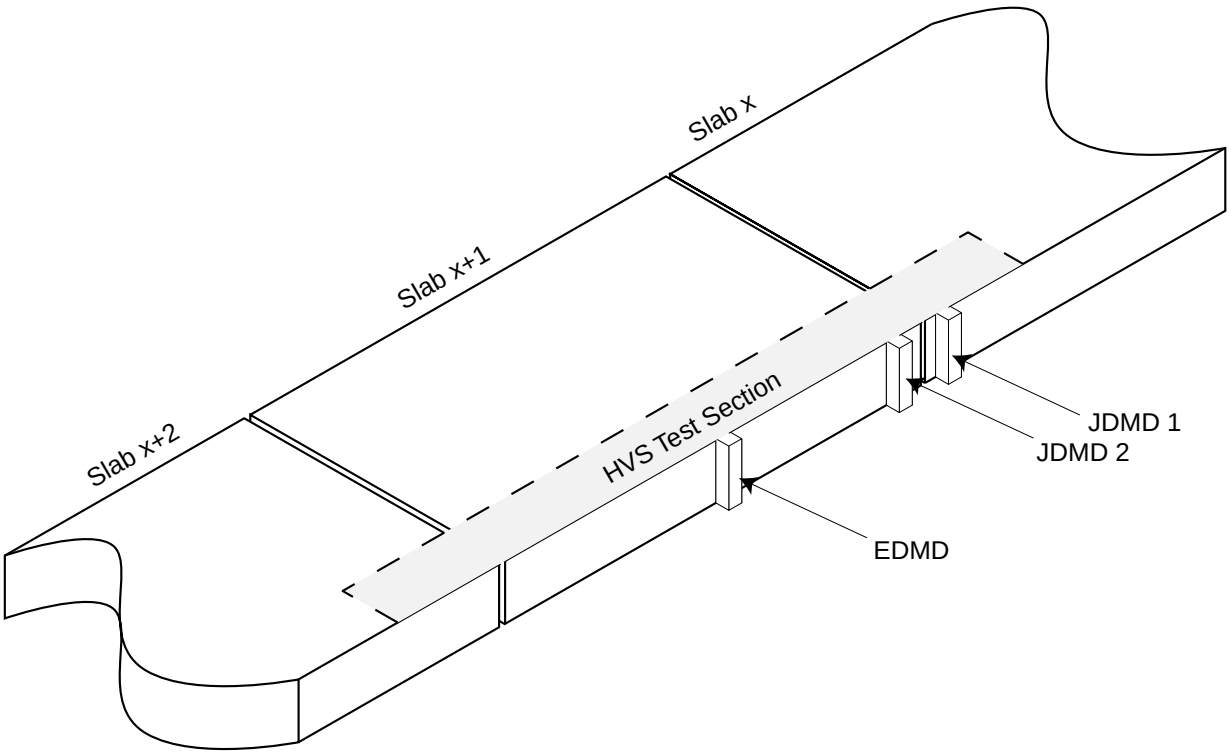

Figure 3.1. Illustration of the placement of JDMDs and EDMD.

environmental data, such as rainfall, and wind direction and speed were continuously recorded using a Davis automatic weather station.

Some sections were instrumented with strain gauges. At these sections, listed in Table 3.3, four strain gauges were placed inside the concrete slab along the edge of the slab. Two gauges were placed inside the slab 40 mm from the bottom of the slab, and two were placed 40 mm from the surface.

Two of the four were manufactured by Dynatest, which are uniaxial, and the other two were Tokyo Sokki PMR 60 6L gauges (designated by the abbreviation: PMR) each measuring in three directions. One Dynatest gauge was placed parallel to the direction of wheel travel in the middle of the center slab (midpoint), and the other one perpendicular to the direction of travel about 300 mm from the joint to the adjacent slab.

The two PMR gauges were placed 40 mm from the surface at the same locations. They were installed so that the two perpendicular arms (90 degrees apart) were placed in the longitudinal and transverse directions with respect to the slab. The third arm is between the other two at 45 degrees. Figure 3.2 illustrates the placement of the various strain gauges.

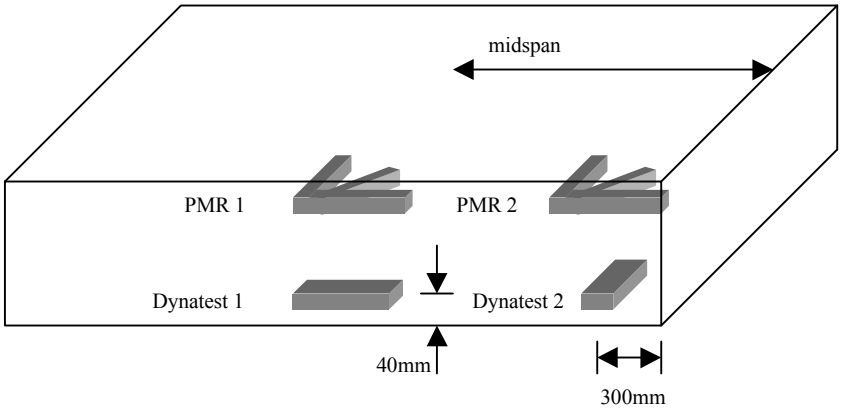

Figure 3.2. Illustration of the placement of the strain gauges with respect to the concrete slab

These strain gauges were used to monitor the changes in the strain state inside the concrete slab in two ways:

1. **Dynamic response:** changes in the elastic strain state due to the influence of the applied wheel load. This is illustrated in Figure 3.3. The figure shows the output of both Dynatest strain gauges with respect to the applied wheel load. Note that the gauges went through states of compression and tension as the wheel passed over them.
2. **Static response:** changes in the strain state of the pavement due to concrete hydration, setting, temperature, and shrinkage effects.

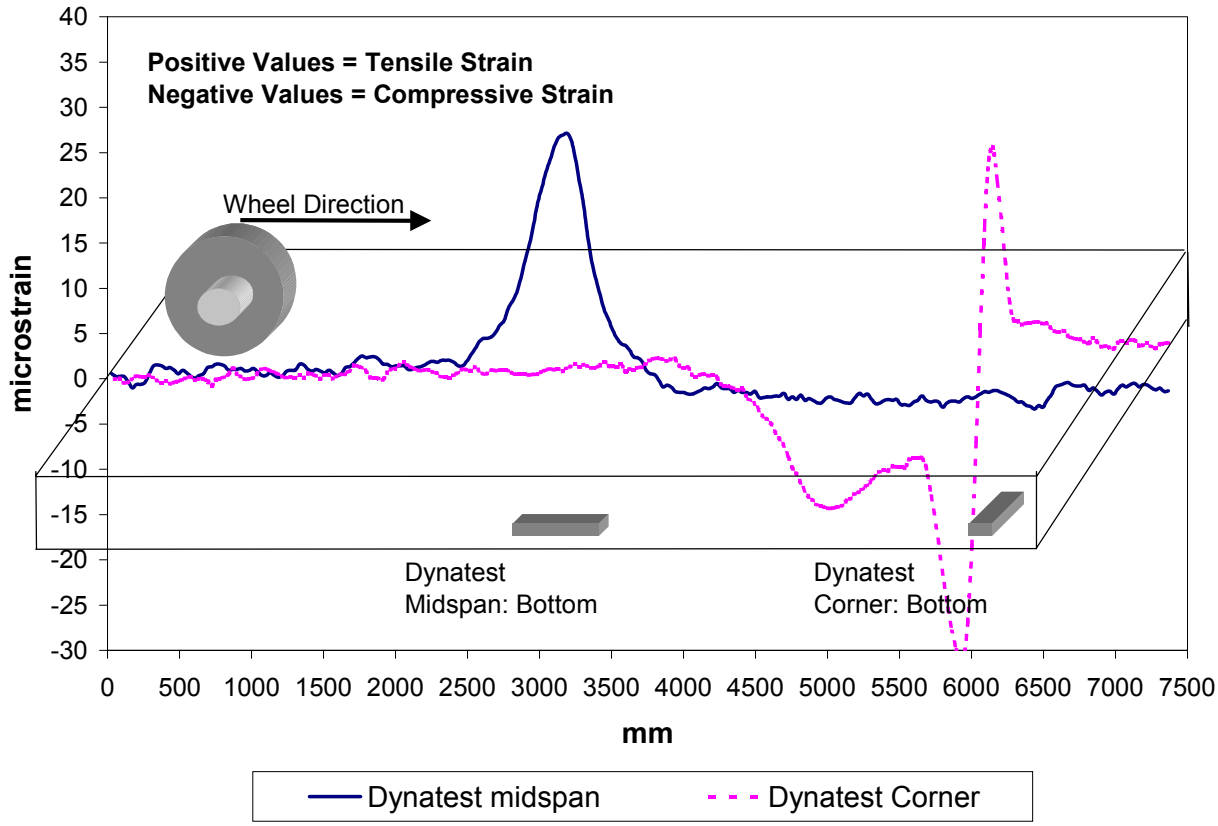

Figure 3.3. Illustration of the output of the strain gauges under the influence of an applied load.

The detailed instrumentation plan is given in Table 3.3.

3.3 HVS Loading Plan

The actual thickness of the slab varied over the length of the nominal 100-mm thick sections. In order to account for these variations, some changes in the loading were made from test to test. The actual loading applied can been seen in Table 3.4

All tests were done with the HVS trafficking in the bi-directional traffic mode, meaning that the wheel was loaded in both directions. All tests were performed with a channelized wander pattern, meaning that no lateral wander was introduced, and the wheel always traveled

Table 3.3 Instrumentation Plan For all HVS Sections on the South Tangent

Section Thickness	Pavement Section	Slab #	HVS Test Section	Thermo-couples	JDMD	Strain Gauges	MDD	RSD	CAM	FWD
100 mm	1A	3, 4, 5	519	x	x			x	x	
	1B	7, 8, 9	520	x	x	x		x		
	1C	11, 12, 13	521	x	x		x	x	x	
	1D	13, 14, 15	522		x					
150 mm	3A	16, 17, 18	523	x	x				x	
	3B	19, 20, 21	524	x	x	x				
	3C	22, 23, 24	525	x	x					
	3D	26, 27, 28	526	x	x					
	3C	21, 22, 23	527	x	x				x	
200 mm	5B	34, 35, 36	528	x	x	x			x	x
	5A	30, 31, 32	529	x	x					x
	5C	38, 39, 40	530	x	x		x			x
	5D	41, 42, 43	531	x	x		x			x

Table 3.4 Loading Plan for the HVS Tests

HVS Test	Number of Repetitions at Given Load											
	20 kN	**25 kN**	**35 kN**	**40 kN**	**45 kN**	**50 kN**	**60 kN**	**70 kN**	**80 kN**	**85 kN**	**90 kN**	**100 kN**
519FD		0 – 55,446				55,446 - 56,432						56,432 – 60,163
520FD			0 – 51,290									51,290 – 74,320
521FD	0 – 157,719								157,719 – 168,319			
522FD*	x	x	x	x	x	x	x	x	x	x	x	x
523FD					0 – 151,151							
524FD					0 – 119,784							
525FD					0 – 5,000							
526FD										0 – 23,625		
527FD			0 – 723,600	723,600- 1,233,969								
528FD				0 – 83,045								
529Fd				0 – 88,110			88,110 – 352,324					
530FD				0 – 64,227			64,227 – 816,674				816,674 – 846,844	
531FD				0 – 31,318				31,318 – 65,315				

* Test Section 522FD was a static test. Response data was recorded at various applied static loads.

along the edge of the slabs next to the asphalt shoulder. Wander was not introduced because it would have prolonged the time required to achieve fatigue cracking on each test section.

Channelized traffic represents the most critical case. The HVS repetitions to failure on the slab edge for this case can be extrapolated to a more typical traffic wander pattern through the use of modeling. In the modeling, the strains are calculated for the critical edge load as well as for the other load locations. Stresses calculated from the strains are related to repetitions to failure by fatigue laws. The HVS results are used to verify the fatigue law, which is then applied to the other load locations.

4.0 HVS RESULTS

The test results of the individual HVS tests are summarized in this section. The previous output report on the construction of the test sections at Palmdale gives complete details of the instrument layout (*1*). Data collection was undertaken at the intervals shown in Table 3.2. All dynamic data were measured when the HVS wheel was running at a creep speed of about 2 km/h, and in both directions. Further details of HVS data collection procedure for concrete can be found in a previous report (*3*). For fatigue analysis purposes, the appearance of a crack on the middle slab signified fatigue failure. In certain cases, the HVS tests were run longer to monitor the performance of the middle and adjacent slabs after the first appearance of fatigue cracks.

Because temperature differentials inside the concrete slab have a significant influence on the stress and strain state which in turn influences the surface deflection measurements, the temperature difference between the surface and the bottom of the concrete layer at the time of deflection measurements is also given along with the tabulated deflection data. Thermocouple data collection was not always in synchronization with regular data collection and in some cases, no data are available.

In the surface deflection graphs, temperature gradient data have been omitted to avoid unnecessary confusion as the graphs already have a significant amount of data displayed. Plots of all the temperature gradients can, however, be found in Section 8, which details the temperature results.

4.1 Test Section 519FD

Test Section 519FD was performed on slabs 3, 4, and 5 on the South Tangent. Slab 4 (total length of 5.8 m) was fully tested, together with part of the adjacent slabs (slabs 3 and 5) on

either side of joints 3 and 4. In order to minimize stresses and strains caused by temperature effects, the temperature control chamber was used during this test.

The test started with a 25-kN dual wheel load to 55,448 repetitions, after which the load was increased to 50 kN for another 1,000 repetitions. The final loading phase was performed at a 100-kN wheel load up to 60,163 repetitions, at which stage the pavement structure was cracked.

At the time of the test on Section 519FD, no thermocouples were installed.

4.1.1 Visual Observations, Section 519FD

The crack pattern, as it developed with time, can be seen in Figure 4.1. Prior to the start of any loading on Section 519FD, a crack starting at joint 4 and the edge of the slab had developed, most likely from construction traffic (Photograph 4.1).

After approximately 2,000 25-kN load repetitions, a longitudinal crack developed throughout the length of the middle slab (slab 4) between both joints, about 1.4 m from the edge (Photograph 4.2). This type of crack indicates a loss of support under the slab and/or excessive slab warping causing an unsupported edge (*4*). This crack was followed by two corner cracks on either side of slab 4 (one in slab 3 and one in slab 5), which developed at approximately 25,000 repetitions (Photographs 4.3 and 4.4). As the test progressed, more edge and corner cracks developed. The final crack pattern is displayed in Photograph 4.5 and Figure 4.1.

One interesting observation is the amount of permanent deformation along the edge of the slab. Prior to the HVS test, the concrete slab was flush with the asphalt concrete shoulder all along the edge of the concrete slab. As the test progressed, the concrete edge slowly started to move downward into the aggregate base. The total permanent deformation after 37,819

Photograph 4.1. Corner crack prior to start of test, Test Section 519FD.

Photograph 4.2. Longitudinal crack after 2,105 repetitions, Test Section 519FD.

Photograph 4.3. Corner crack on slab 5 after 25,000 repetitions, Test Section 519FD.

Photograph 4.4. Corner crack on slab 3 25,000 repetitions, Test Section 519FD.

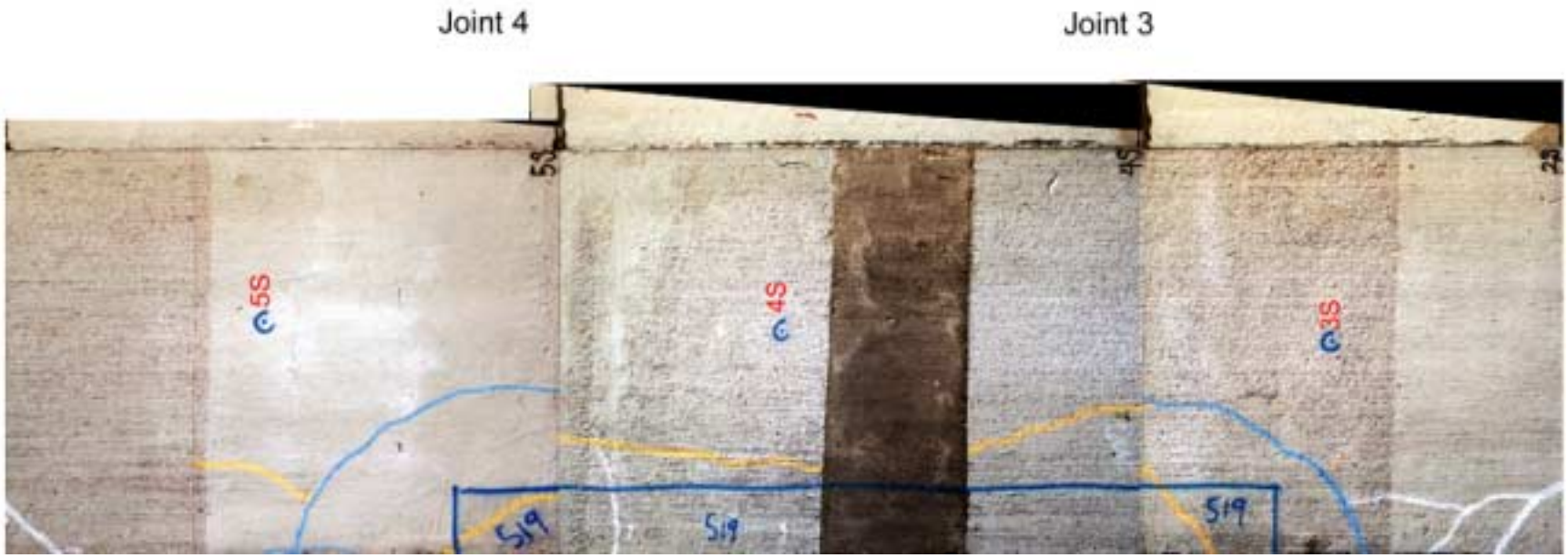

Photograph 4.5. Composite photograph of final crack pattern, Test Section 519FD.

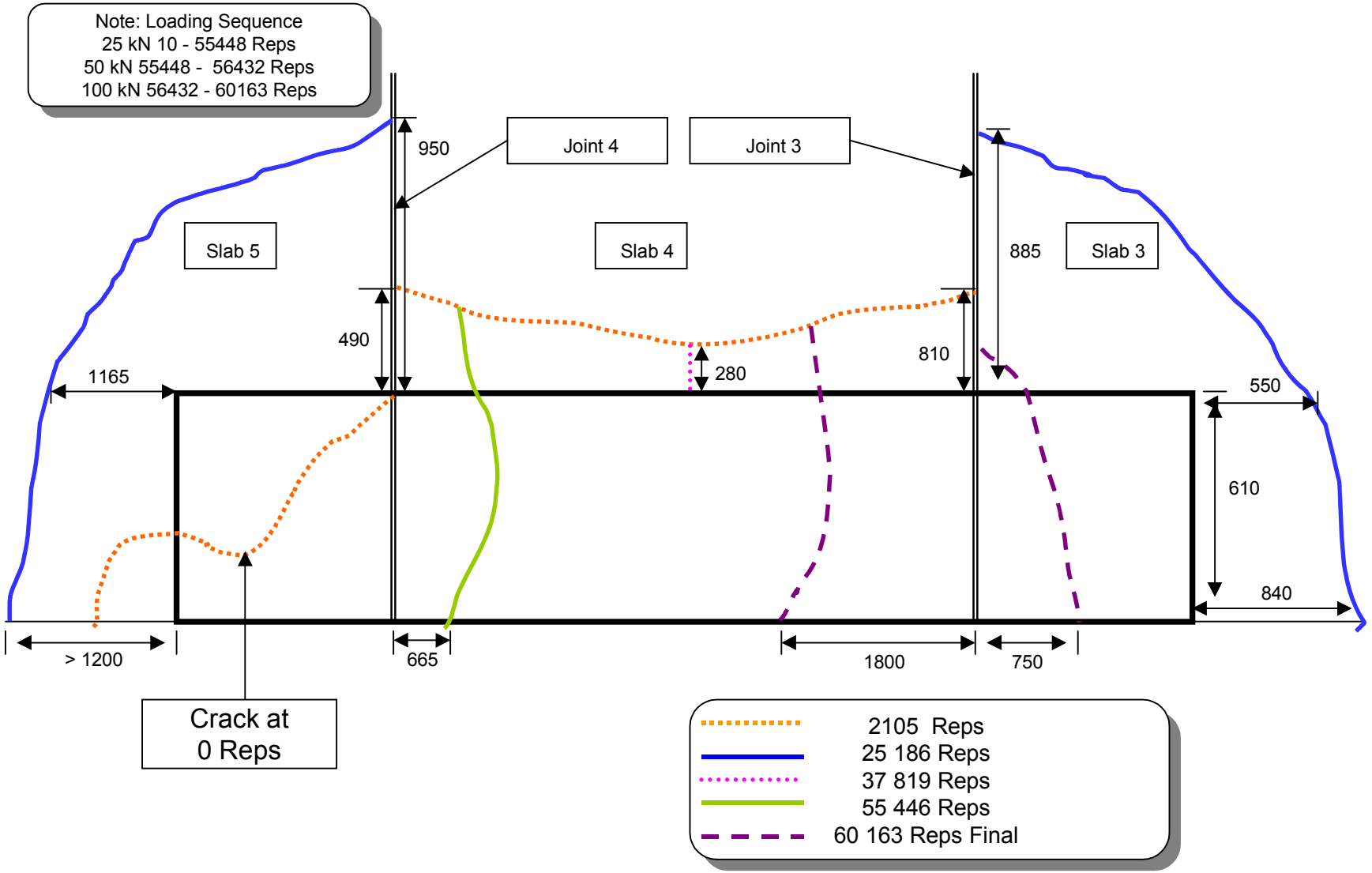

Figure 4.1. Schematic of crack development, Test Section 519FD (not to scale).

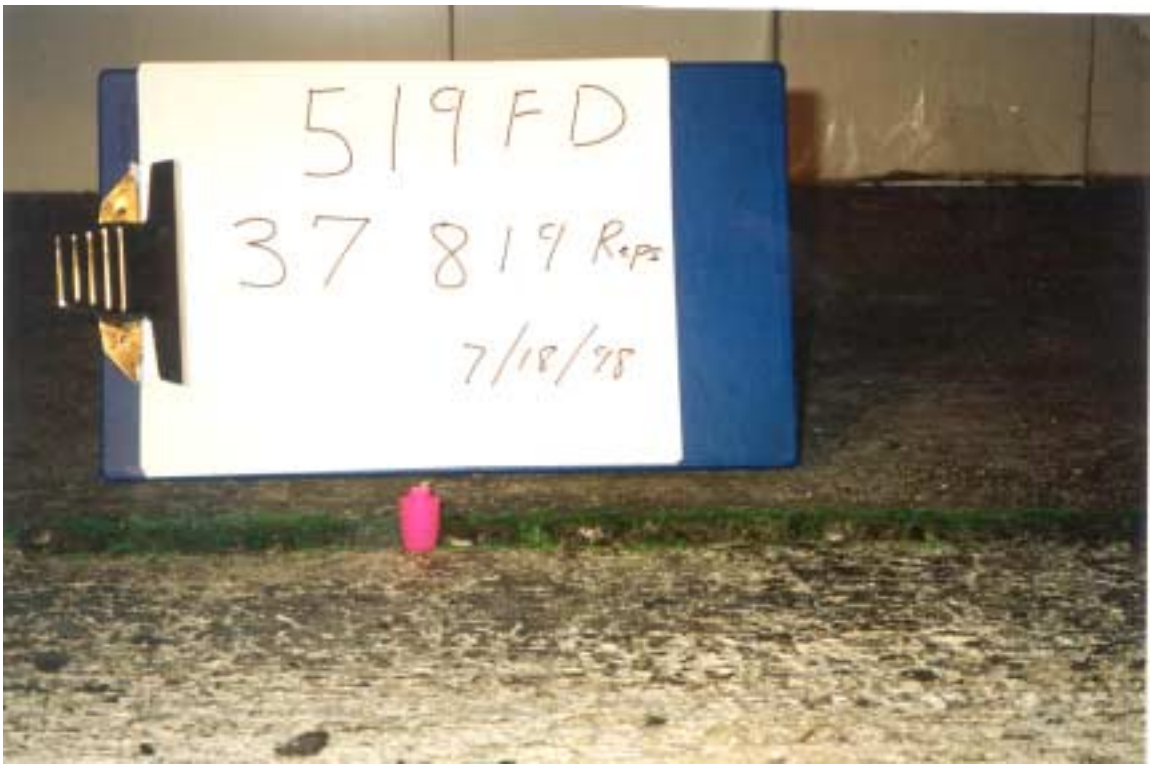

Photograph 4.6. Permanent deformation at shoulder after 37,000 repetitions, Test Section 519FD.

repetitions recorded along the edge at the interface between the concrete slab and the adjacent asphalt shoulder was around 20 mm (see Photograph 4.6).

4.1.2 JDMD and EDMD Data, Test Section 519FD

Two Joint Displacement Monitoring Devices (JDMDs) were placed on either side of joint 3 and one Edge Displacement Monitoring Device (EDMD) was placed on the edge of slab 4 at its midpoint (centrally between the two joints) to monitor the elastic movement of the slab. The maximum deflections at the midpoint edge of the middle slab and at the corner edge of joint 4 are summarized in Table 4.1.

Table 4.1 EDMD and JDMD Deflections, Test Load = 25 kN, Test Section 519FD

Repetitions	Deflections (m × 10^{-6})			Temperature Difference (Top-Bottom), °C
	Midpoint Edge, Slab 4	Corner, Joint 3		
		Slab 4 Side	Slab 3 Side	
10	1,762	4,553	4,669	NA
2,105	448	2,748	5,427	NA
10,658	335	2,248	5,038	NA
25,186	375	2,134	2,053	NA
37,819	380	2,239	1,842	NA
55,446	368	2,307	1,752	NA
60,163	426	5,842	3,597	NA

The data are shown graphically in Figure 4.2, which should be viewed together with the crack patterns (Photograph 4.5) in order to interpret the behavior correctly.

It is believed that a cavity under the edge of the slab caused the high initial deflections because of differential drying shrinkage in the FSHCC. This cavity, together with the applied edge loading, caused a bending moment all along the length of the slab which resulted in the longitudinal crack that developed after only 2,105 repetitions (Photograph 4.2). After this crack had developed, it was considered that the concrete slab re-seated onto the base course. This caused the cavity to close, which resulted in a significant decrease in edge deflections owing to the more effective support from the base and underlying layers. After the crack had been formed, the midpoint edge deflections decreased from 1,762 microns to 448 microns. This represents an 81 percent decrease in deflection at the midpoint. Similarly, the deflections on the slab 4 side of joint 3 experienced a 51 percent decrease in deflection.

On the slab 3 side of joint 3, the deflections stayed constant up to the point when the corner crack developed (25,186 repetitions) (see Photographs 4.3 and 4.4). At this point the deflections decreased by about 60 percent from the original N10 measurements, from 4,699 microns at the beginning of the test to 2,053 microns after 25,186 repetitions.

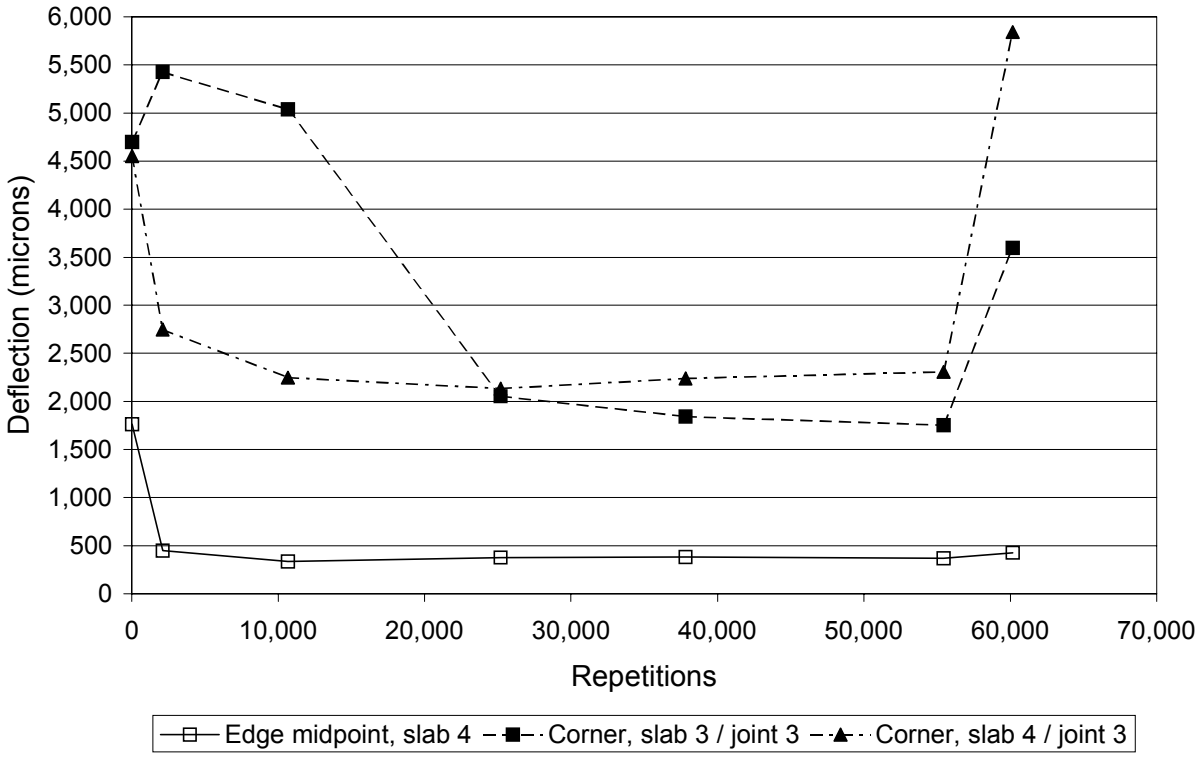

Figure 4.2. EDMD and JDMD deflections, test load = 25 kN, Test Section 519FD.

After 37,819 load repetitions, a maximum of approximately 20 mm of permanent deformation was recorded along the slab edge at the interface between the concrete slab and the adjacent asphalt shoulder (Photograph 4.6). This observation clearly illustrated the reason for the slab having had a longitudinal crack, i.e., the slab had to move downward to come in full contact with the base.

After the initial longitudinal crack (at 2,105 repetitions) and the corner cracks (at 25,186 repetitions), the deflections stabilized up to the point where the wheel load was increased (at 55,446 reps). A sharp increase in deflections was observed at this point as a result of the increased wheel load (Figure 4.2).

4.1.3 Load Transfer Efficiency, Test Section 519FD

The Load Transfer Efficiency (LTE) was calculated at joint 3 (the joint between slab 3 and slab 4) at 3 stages: at the beginning; after the first major longitudinal crack appeared (2,105 repetitions); and after two corner cracks appeared at 25,186 repetitions. These results are summarized in Table 4.2.

Table 4.2 Load Transfer Efficiency at Joint 3, Test Section 519FD

Repetitions	Load Transfer Efficiency (LTE), percent					
	From Slab 4 to Slab 3			From Slab 3 to Slab 4		
	$d_{unloaded}$, $m \times 10^{-6}$	d_{loaded}, $m \times 10^{-6}$	LTE	$d_{unloaded}$, $m \times 10^{-6}$	d_{loaded}, $m \times 10^{-6}$	LTE
10	3,571	4,671	*77*	2,809	4,616	*61*
2,105	2,768	4,051	*68*	1,126	5,405	*21*
25,186	562	2,142	*26*	89	2,057	*4*

LTE is defined as the ratio between the deflection on the unloaded slab with respect to the deflection on the loaded slab at the joint, and was calculated for the HVS wheel running over the joint in each direction.

The LTE was always higher when the HVS loaded wheel approached the joint from slab 4 than when it approached from slab 3. These results suggest that the crack that had formed at the bottom of the saw-cut joint is not perfectly vertical. Instead, as the crack formed, it traveled toward slab 4 such that slab 3 is providing more support (load transfer) when the load is approaching from slab 4 (from the left) than when it approaches from slab 3 (from the right).

The damaging effect of the repetitive load on the joint performance can be seen in Table 4.2 by the decrease in LTE with load repetitions. As the test progressed, the HVS wheel loading at the joint deteriorated the aggregate interlock between the two slabs causing a decrease in LTE. After 25 000 repetitions, the joint had deteriorated to such an extent that only 26 percent of the

deflection was transferred when the wheel was approaching from slab 4, and 4 percent when the HVS wheel was approaching from the slab 3 side.

4.1.4 CAM Data, Test Section 519FD

Crack activity measurements were taken at one location, on the longitudinal crack that had formed after 2,105 repetitions. The CAM was placed across this crack close to joint 4, which was the joint between slab 4 (the middle slab) and slab 5. The placement of the CAM can be seen in Photograph 4.3. An example of the horizontal and vertical movement from the CAM is given in Figure 4.3. The maximum and minimum CAM values are summarized in Table 4.3. CAM measurements were taken after the first 10,000 repetitions.

The sign convention of the output values of the CAM with respect to Figure 4.3 is as follows:

- vertical *positive* movements are when the left hand side of the crack (that is, the area between the crack and the AC shoulder) is moving *upward* relative to the right hand side (the area between the crack and the K-rail); vertical *negative* movements indicate that the left hand side of the crack is moving *downward* relative to the right hand side.
- horizontal *positive* movements indicate that the gap created by the crack is *closing*; horizontal *negative* movements indicate that the gap is *opening*.

Table 4.3 CAM Data, Test Load = 25 kN, Test Section 519FD

Repetitions	**Horizontal Movement, m × 10^{-6}**		**Vertical Movement, m × 10^{-6}**	
	Closing (+)	**Opening (-)**	**Positive**	**Negative**
10,658	1	24	1	58
25,186	5	24	2	57
37,819	16	31	1	79
55,446	49	38	51	73
60,163	127	15	479	70

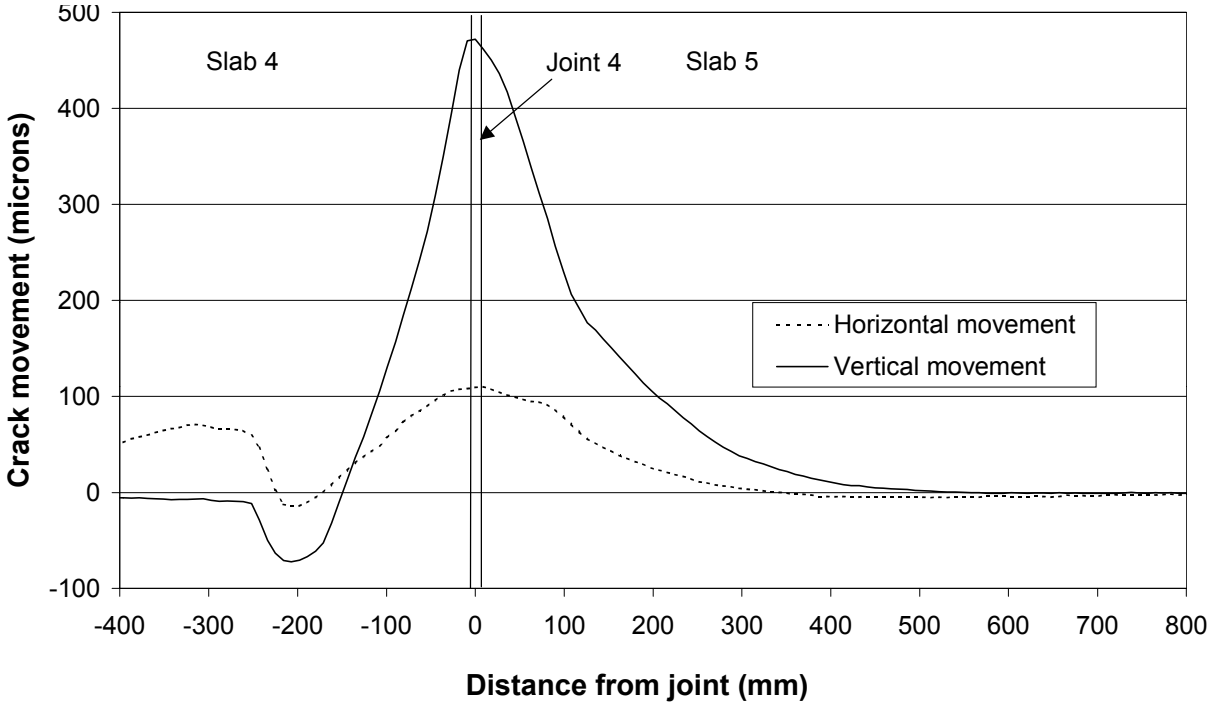

Figure 4.3. CAM response, Test Section 519FD.

These values are small, even after 60,000 load applications, but it is important to note that the CAM was placed over a crack, which was approximately 1 meter away from the applied load (see Photograph 4.3). The CAM results do not, therefore, reflect the crack activity under the influence of a load applied directly over the crack (as would be observed with normal traffic).

One interesting observation is that the crack activity increased as the test progressed, especially after the traffic wheel load was increased (from 25 kN to 50 kN and eventually to 100 kN). It seems as if the greater wheel loads caused a noticeable loss in horizontal contact between the aggregate on either side of the crack, hence the increased horizontal relative movement. This is likely due to rotation of the thin slab downward and away from the joint, which appears in both the horizontal and vertical deflection measurements.

The same can be said about the aggregate interlock, which was restricting the relative vertical movement across the crack. As the test progressed the interlock deteriorated and greater

relative vertical movements were recorded. Comparing the crack activity measured at 60,163 repetitions with the readings taken at 55,446 repetitions shows an increase in vertical positive movement from 50.7 to 478.7 microns. This suggests that the trafficked area between the crack and the AC shoulder got increasingly detached from the main part of slab 4 on the other side of the crack, which caused this significant increase in vertical movement.

4.2 Test Section 520FD

Test Section 520FD was conducted on slabs 7, 8 and 9 on the South Tangent, with the 8 × 1 m HVS test section located so that slab 8 (total length of 5.8 m) was fully tested along its edge. The temperature control box was used during this test. The test started with a 35-kN dual wheel load to 51,240 repetitions, and then the load was increased to 100 kN for just over another 20,000 repetitions. The test was stopped at 74,320 repetitions. An overhead photo of the entire section with cracks can be seen in Photograph 4.7; Figure 4.4 shows the crack development.

4.2.1 Visual Observations, Test Section 520FD

Prior to the start of the test, two cracks had already developed as shown in Photograph 4.8. While not attributable to the HVS loading, these initial cracks are likely to influence the subsequent crack development during the accelerated loading test. These are probably due to shrinkage and curling stresses, or less likely due to construction traffic.

After about 1,000 load repetitions at 35 kN, a longitudinal crack developed along nearly the entire length of the middle slab (slab 8) between both joints, about 1.1 m away from the edge (Photograph 4.9). After 2,000 repetitions, the longitudinal crack had extended to link up with the

Photograph 4.7. Composite photograph of final crack pattern, Test Section 520FD.

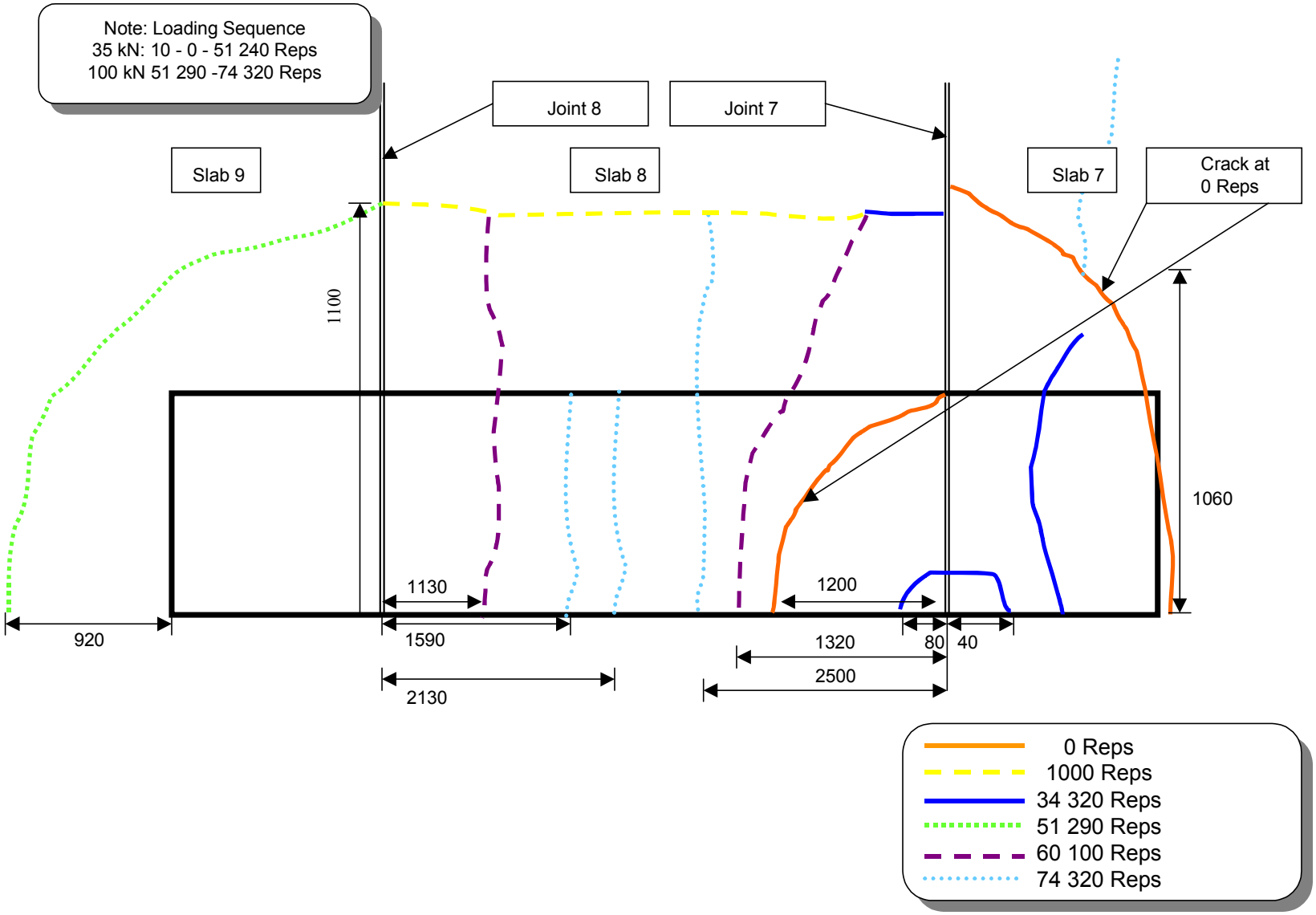

Figure 4.4. Schematic of crack development, Test Section 520FD (not to scale).

Photograph 4.8. Corner cracks at start of test, Test Section 520FD.

Photograph 4.9. Longitudinal crack after 1,000 repetitions, Test Section 520FD.

Photograph 4.10. Cracks at joint 7 (J2) after 2,000 repetitions, Test Section 520FD.

Photograph 4.11. Final crack pattern after 74,000 repetitions, Test Section 520FD.

existing corner crack (which existed prior to the start of the test), and a transverse crack starting about 500 mm right of joint 7 had developed in slab 7 (Photograph 4.10).

Various additional transverse cracks appeared in the mid-slab area during the test, which proceeded to 74,000 load repetitions. The final crack pattern can be seen in Photographs 4.7 and 4.11.

4.2.2 JDMD and EDMD Data, Test Section 520FD

Two Joint Displacement Monitoring Devices (JDMDs) were placed on either side of Joint 8 and one Edge Displacement Monitoring Device (EDMD) was placed on the edge at the longitudinal midpoint of slab 8. The results are summarized in Tables 4.4 and 4.5 for the 25-kN test load and the 35-kN test load, respectively.

Table 4.4 EDMD and JDMD Deflections, Test Load = 25 kN, Test Section 520FD

Repetitions	Deflections ($m \times 10^{-6}$)			Temperature Difference (Top-Bottom), °C
	Midpoint Edge, Slab 8	Corner, Joint 8		
		Slab 9 Side	Slab 8 Side	
10	1,107	2,836	1,632	-1.7
2,000	662	3,573	2,881	-1.7
25,190	615	4,140	3,240	-0.8
55,500	607	2,308	3,037	-1.5
60,100	749	1,929	690	-1.3

Table 4.5 EDMD and JDMD Deflections, Test load = 35 kN, Test Section 520FD

Repetitions	Deflections ($m \times 10^{-6}$)			Temperature Difference (Top-Bottom), °C
	Midpoint Edge, Slab 8	Corner, Joint 8		
		Slab 9 Side	Slab 8 Side	
10	1,309	3,052	4,007	-1.7
1,000	909	3,509	3,114	-1.7
2,000	802	3,810	3,043	-1.7
5,769	751	4,041	3,199	-0.8
40,000	671	4,186	3,304	-2.4
55,500	675	1,998	3,079	-1.5
60,100	920	2,134	825	-1.3

The results of the 35-kN test load are also shown in Figure 4.5. As noted for previous tests, the results should be viewed together with the crack pattern (Figure 4.4) for correct interpretation.

When the longitudinal crack appeared (at around 1,000 repetitions), the midpoint edge deflection and edge deflection of slab 8 close to joint 8 (right hand side of the joint) decreased significantly. This is similar to the behavior of the HVS test on Section 519FD. It is conjectured that an unsupported slab corner caused the initially high deflections measured at joint 8, and as seen on Section 519FD, could probably be due to warping in the slab causing it to curl permanently upwards.

As soon as the longitudinal crack developed, the midpoint edge deflections dropped. This indicated that the slab came into full contact with the base and thus the deflections decreased. These initially high deflections caused by slab curling have a significant impact on the backcalculated subgrade support values. Higher deflections suggest a lower subgrade support, but this is not necessarily the case.

After the longitudinal crack formed (at 1,000 repetitions), a loss in load transfer took place across joint 8 (see Table 4.6). This loss in distributed load across the joint caused higher corner deflections in slab 9. These high deflections stayed constant until a large corner crack developed at approximately 50,000 load applications (see Figure 4.4), after which the deflection decreased.

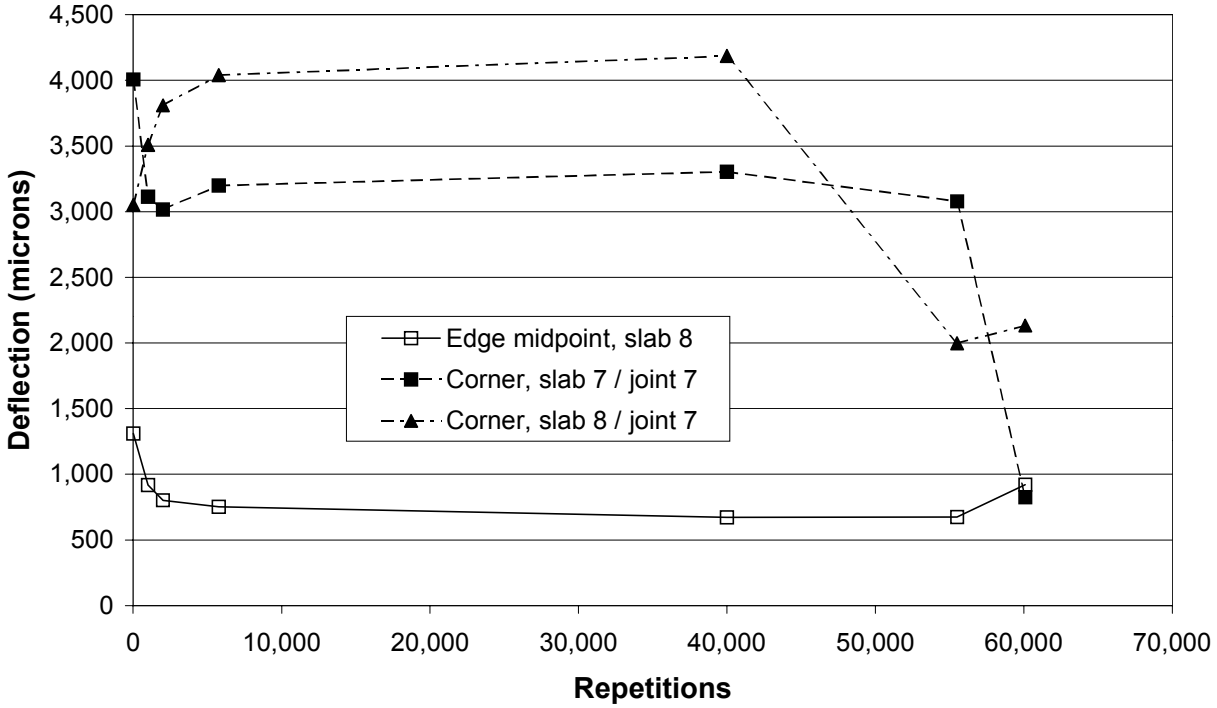

Figure 4.5. JDMD and EDMD deflections, test load = 35 kN, Test Section 520FD.

4.2.3 Load Transfer Efficiency, Test Section 520FD

The Load Transfer Efficiency (LTE) was calculated at joint 8 of the middle slab (slab 8). The results are summarized in Table 4.6. LTE was calculated for the HVS wheel running in both directions across the joint.

Table 4.6 Load Transfer Efficiency, Test Section 520FD

Repetitions	Load Transfer Efficiency (LTE), percent					
	From Slab 9 to Slab 8			From Slab 8 to Slab 9		
	$d_{unloaded}$, $m \times 10^{-6}$	d_{loaded}, $m \times 10^{-6}$	LTE	$d_{unloaded}$, $m \times 10^{-6}$	d_{loaded}, $m \times 10^{-6}$	LTE
10	1,437	1,564	*92*	1,907	2,493	*77*
1,000	1,804	3,468	*52*	2,174	3,138	*69*
2,000	1,409	2,987	*47*	1,913	3,031	*63*
40,000	1,492	4,214	*35*	1,396	3,298	*42*
60,100	839*	1,194*	*70**	1,121*	824*	*136**

* Results not reliable

The damaging effect of the repetitive load is clearly visible in the joint LTE data. After 40,000 repetitions, the joint load transfer had deteriorated to such an extent that only 35 percent of the deflection was transferred when the wheel was approaching from slab 9 (from the left) and 42 percent when the HVS wheel was approaching slab 8 (from the right).

Between 40,000 and 60,100 repetitions, additional transverse cracks developed (see Figure 4.4). As a result of the additional transverse cracking, the middle slab (slab 8) began to rock under the influence of the applied load, which affected the measurement of the load transfer efficiency as seen in Table 4.6.

4.2.4 Strain Gauge Data, Test Section 520FD

Test Section 520FD was the first section on the South Tangent equipped with strain gauges. The gauges were placed in the middle slab (slab 8), close to the edge of the slab. Two Dynatest and two PMR gauges were installed. The placement was as described in Section 3.2 (see Figure 3.1) and is not repeated here.

The output from these gauges is recorded in microstrain and represents the strain state of the gauges at the time of data collection. In order to calculate the change in the strain state, the strain gauge readings should be compared to baseline readings. In the case of the HVS test on Section 520FD, it was possible to collect strain readings during the construction of the section before the placement of the concrete. These strain readings (15 minutes prior to concrete placement) were used as the baseline readings and all subsequent readings during construction (up to 7 hours after the construction) were related to this data set. Construction took place on 10 June 1998.

Strain readings were collected during three stages:

1. at various intervals before, during, and after the construction of the concrete layer;
2. before, during, and after the HVS was moved onto Test Section 520FD, and
3. during the accelerated trafficking of the test section, after a prescribed number of applied load applications.

It was decided to collect data during stage 2 because there was a concern that the weight of the HVS on the thin 100-mm concrete section might influence the strain state of the various gauges. Another factor, likely to influence the strain state, was the drop in temperature due to the controlled temperature chamber placed on the section. It was therefore decided to collect strain data from just after the temperature control chamber was erected until the temperature inside the control chamber stabilized.

Between construction (10 June 1998) and the starting time of the HVS test on Section 520FD (23 July 1998), some change in the strain readings was observed, probably due to shrinkage. Because of this, another set of baseline readings were taken just before the HVS was positioned on Test Section 520FD. Static strain readings, without the influence of any load on the section, were also recorded during the test. The strain data of stages 1 to 3 are presented in Tables 4.7 and 4.8. The surface temperature during time of data collection is also given in the tables.

The strain gauges were wired so that tensile strains have positive values and compression strains have negative values.

Data collected from PMR-X (parallel to HVS traffic at mid-span) was not reliable and is therefore not presented. The behavior of the strain gauges immediately after placement of the

Table 4.7 Strain Gauge Data Before, During, and After Concrete Construction, Test Section 520FD

Stage	Time (min.)	Midspan Strain Gauges (microstrain)				Corner Strain Gauges (microstrain)				Surface Temp. (°C)
		Dynatest Bottom	PMR			Dynatest Bottom	PMR			
			X: Top Parallel	M: Top 45 Deg.	Y: Top Perpendicular		X: Top Parallel	M: Top 45 Deg.	Y: Top Perpendicular	
15 min. before	-15:00	0	0	0	0	0	0	0	0	19.0
1 min after	1	25	-119	-110	-107	17	-65	-66	-57	19.0
5 min after	5	39	-88	-78	-73	14	-58	-57	-53	22.0
30 min after	30	-17	194	155	137	-15	170	158	159	23.6
45 min after	45	-147	270	124	-12	-230	276	180	56	25.8
1 hour after	60	-132	268	116	-28	-301	277	168	15	25.8
2 hours after	120	-48	295	150	-17	-186	283	164	4	27.0
3 hours after	180	-43	285	160	-24	-173	192	91	-10	30.0
6 hours after	360	33	343	217	2	-127	185	105	9	22.0
7 hours after	420	21	360	213	-48	-152	158	76	-26	

Table 4.8 Strain Gauge Data Before, During, and After the HVS Was Positioned on Section, Test Section 520FD

Stage	Time (dd:hh:mm)	Midspan Strain Gauges (microstrain)				Corner Strain Gauges (microstrain)				Surface Temp. (°C)
		Dynatest Bottom	PMR			Dynatest Bottom	PMR			
			X: Top Parallel	M: Top 45 Deg.	Y: Top Perpendicular		X: Top Parallel	M: Top 45 Deg.	Y: Top Perpendicular	
Before HVS moved	00:10:40	0		0	0	0	0	0	0	32.0
while moving	00:11:10	-25		13	-11	-207		-24	96	35.0
while moving II	00:11:11	-26		9	-14	-207		-40	93	37.0
after HVS moved	01:11:14	-29		8	-17	-209		-21	84	39.0
Cooling down under temperature control	01:11:35	-56		-20	10	-21	14	-29	-121	24.0
	01:12:30	-56		-43	-10	20	20	-38	-172	21.7
	01:13:44	-62		-53	-16	44	21	-46	-178	21.5
	01:14:54	-52		-51	-14	74	23	-48	-183	21.4
	01:15:38	-37		-65	-18	70	27	-66	-185	21.6
HVS trafficking of Test Section 520FD	**Repetitions**									
	10	81		-12	119	15	128	89	-135	18.0
	1,000	-30		-54	59	42	-136	-124	-272	18.4
	2,000	26		-89	113	-46	-2	-8	-226	18.1
	5,769	29		-1	166	91	51	31	-161	17.6
	25,190	40		17	183	91	164	131	-208	19.7
	40,000	49		-6	180	257	196	154	-198	19.3
	55,500	48		-20	166	282	219	218	-307	21.1

Note: Missing data due to non-functioning instrument at time of data collection.

concrete is complicated by a number of factors. First, the gauges will not record any shrinkage or expansion until the concrete has set and hardened sufficiently to force the ends of the gauge to move with the concrete. Secondly, the concrete will expand as it heats (because if the exothermic reaction and from the heat of the day), and will contract when it cools (at night and after the reaction slows down). The final aspect is the permanent drying shrinkage in the slab. This shrinkage is more severe at the top of the slab than at the bottom because the top is exposed to wind, sunlight, and lower humidity.

Because of the complexity of the response during and immediately after construction, it is difficult to separate the various aspects of the concrete behavior. There appears to be a shift in the data at between 30 minutes and 2 hours after construction, which is probably caused by the concrete setting during this time range. However, it can be seen that the parallel strains at the top of the slab are higher than those at the bottom, indicating the development of a shrinkage gradient, and therefore tension at the top of the slab. It is not possible to distinguish the component of the average shrinkage through the slab that is caused by shrinkage from that caused by cooling, as both are occurring simultaneously.

The second set of data collection took place just before the HVS was moved on to the section on 23 July 1998. From the data presented in Table 4.8, it is clear that the weight of the HVS on the section did not influence the strain readings of the various gauges significantly (refer to the first block of data in Table 4.8). The surface temperature during this phase was around 39°C.

After the temperature control box was erected, the air temperature was cooled down to the desired level (20°C ± 7°C) and various strain readings were taken. The effect of the drop in temperature inside the box did not cause a consistent change in all the gauges. It seems as if the

surface of the concrete cooled down at a faster rate than the bottom of the concrete slab. This caused some upward curling, which caused some of the upper gauges to go further into compression and some of the bottom gauges to go into tension. However, this behavior was not consistently observed throughout all the gauges.

After the desired temperature was reached and before the start of HVS trafficking, some additional strain change was observed (as presented in Table 4.8). Although some variations occurred, the static strains stayed fairly constant throughout the test while the surface temperature was kept fairly constant (between 18 and 19°C). The variations in the strain reading might be due to the size of the cool box. The box itself does not cover the whole slab, rather only the section directly beneath the HVS. It is very likely that temperature variation outside the controlled area influenced the strain readings as observed in Table 4.8 (*2*).

The dynamic strain response of the gauges is presented in Table 4.9. The data given are the maximum tensile and compressive strains recorded while the 25-kN wheel moved over the test section. As expected, the dynamic load caused the gauges to go through phases of tensile and compressive strain (see Figure 3.3).

4.3 Test Section 521FD

HVS Test Section 521FD was completed on slabs 11, 12 and 13 on the South Tangent, with the 8 × 1 m HVS test section located so that slab 12 (total length of 5.8 m) was fully tested along its edge. This section was the final 100-mm FSHCC test pavement and was conducted with the temperature control chamber in operation.

Table 4.9 Elastic Strain Results, Test Load = 25 kN, Test Section 520FD

Instrument Type, Placement, and Orientation			Repetitions	Maximum Strain Recorded with a 25-kN Load (microstrain)				
				10	**2,000**	**25,190**	**55,000**	**60,100**
Midspan Strain Gauges	**Dynatest Bottom**		Tensile (+) Compression (-)	29 -2	18 -3	18 -4	17 -4	23 -3
	PMR Top	**X: parallel**	Tensile (+) Compression (-)	Data unreliable (readings from zero to more than 2,000 microstrain)				
		M: 45 degree	Tensile (+) Compression (-)	26 -25	17 -17	15 -18	13 -22	18 -20
		Y: perpendicular	Tensile (+) Compression (-)	11 -1	12 -2	12 -1	9 -3	13 -1
Corner Strain Gauges	**Dynatest bottom**		Tensile (+) Compression (-)	16 -14	32 -2	55 -2	45 -4	438 -4
	PMR Top	**X: parallel**	Tensile (+) Compression (-)	552 -364	414 -194	441 -185	507 -186	386 -4
		M: 45 degree	Tensile (+) Compression (-)	429 -143	358 -24	375 -55	428 -88	256 -14
		Y: perpendicular	Tensile (+) Compression (-)	42 -46	60 -12	46 -16	34 -24	185 -9
Temperature (°C)				*17.9*	*18.1*	*19.7*	*18.5*	*17.4*

Note: Shaded data sets have been included for completeness. The apparent high (unrealistic) tensile strains may be attributable to physical bridging of micro-cracks by the gauge.

The HVS dual wheel load was started at 20 kN instead of the higher 25 kN and 35 kN wheel loads used in Tests 519FD and 520FD. The frequency of data collection was also increased compared with these earlier tests (see Table 3.1). After 157,719 repetitions the load was increased to 80 kN to monitor the progression of deterioration at this higher wheel. The test was completed after 168,319 load applications.

4.3.1 Visual Observations, Test Section 521FD

An overhead photo of the entire section with cracks can be seen in Photograph 4.12; crack development is presented in Figure 4.6. Apart from a small corner crack at joint 12, the complete 8-m long test section was free of any cracks prior to the start of the test (see Photograph 4.13). The crack growth pattern for Test Section 521FD was somewhat different from those observed on Sections 519FD and 520FD (compare Figure 4.1 and 4.4 to Figure 4.6).

A short longitudinal crack appeared about 770 mm outside the test section after 500 repetitions (Photograph 4.14). This crack progressed towards the test pad and ended up as a corner crack after about 1,000 repetitions (see Photograph 4.15). A longitudinal crack similar to those seen on Sections 519FD and 520FD appeared after 142,072 load applications. A corner crack and some additional transverse cracks appeared after 157,719 repetitions (see Photographs 4.16). The final crack pattern can be seen in Photograph 4.17.

4.3.2 JDMD and EDMD Data, Test Section 521FD

Two Joint Displacement Monitoring Devices (JDMD) were placed on either side of Joint 11 and one Edge Displacement Monitoring Device (EDMD) was placed at the midpoint edge of the middle slab (slab 12). The results are summarized in Table 4.10, for the 20kN test load, and displayed in Figure 4.7.

During the first part of the test (0–140,000 repetitions), the deflections stayed relatively constant, the midpoint edge deflection being about 1.8 mm and the joint deflection around 5.3 mm and 4.2 mm on each side of joint 11. The initial cracking at joint 12 did not affect the deflections at the midpoint edge of slab 12 and joint 11. However, this would be considered structural failure in the analysis.

These corner and edge deflections are high for such a small load (20 kN). The most likely explanation is that the edge of the concrete slab, similar to the slabs in the two previous tests (519FD and 520FD), was permanently curled upwards from the initial construction. After 142,072 repetitions, a longitudinal crack about 1,200 mm from the edge appeared (see Figure 4.6) which caused the edge of the slab to come into full contact with the base. The final position of the tested slab with respect to the asphalt concrete shoulder is shown in Photograph 4.17.

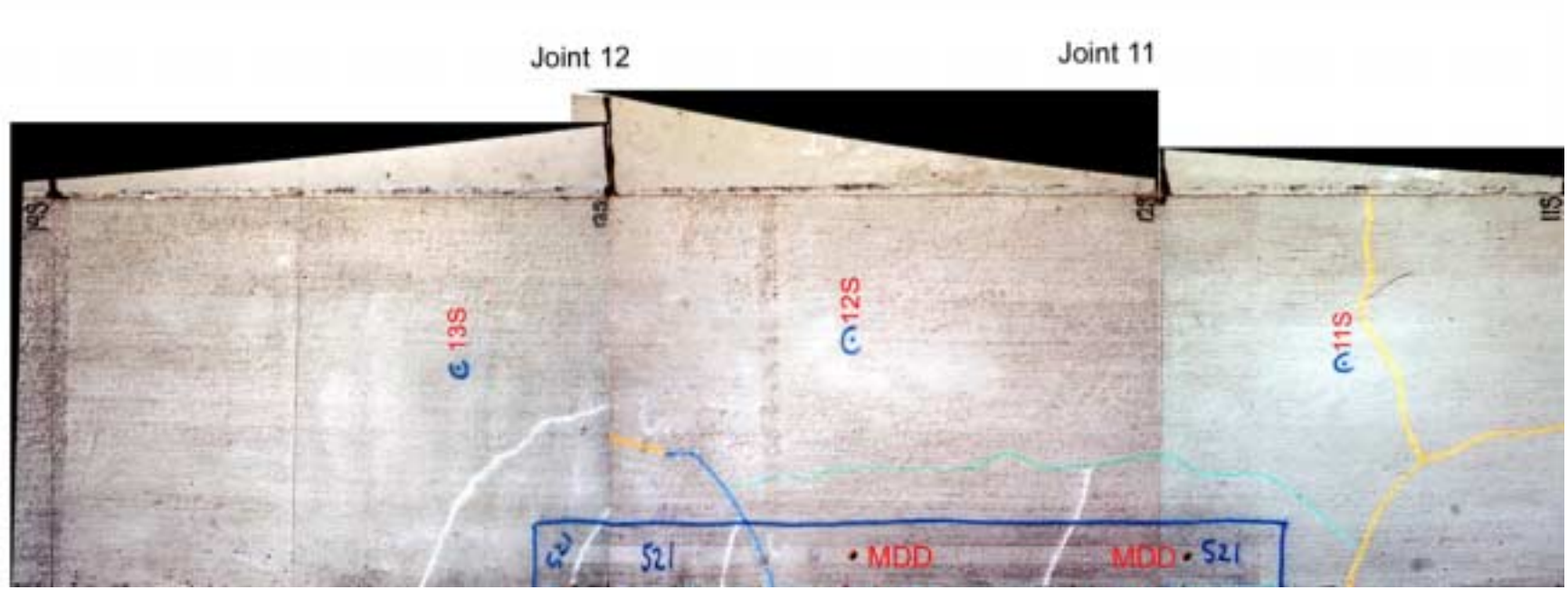

Photograph 4.12. Composite photograph of final crack pattern, Test Section 521.

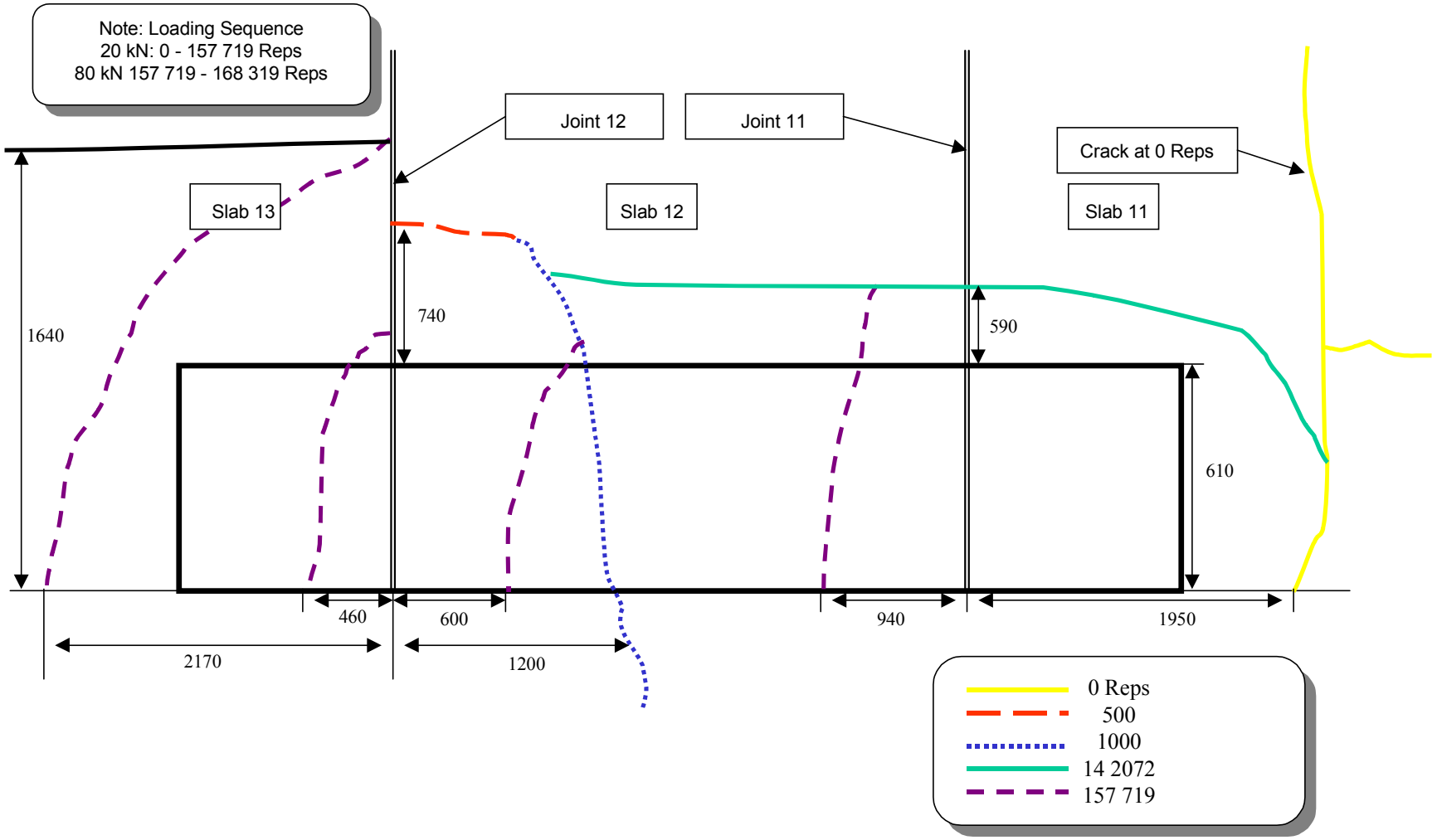

Figure 4.6. Schematic of crack development, Test Section 521 (not to scale).

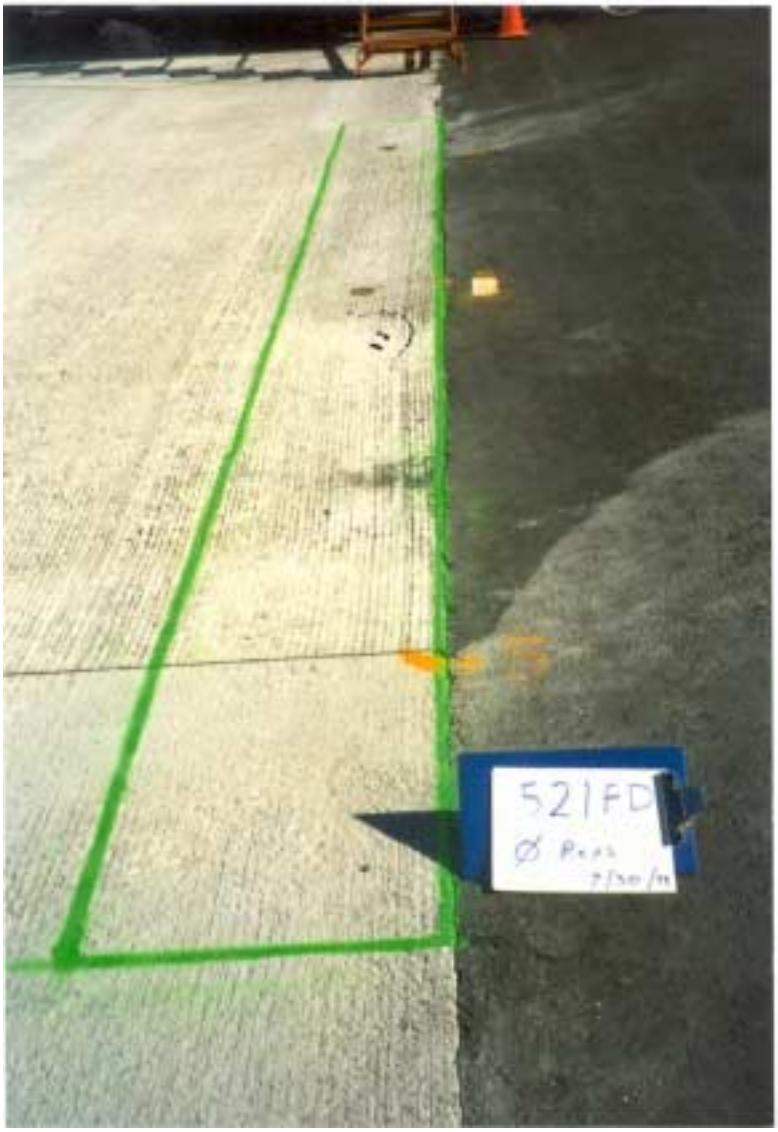

Photograph 4.13. Section at beginning of test, Test Section 521FD.

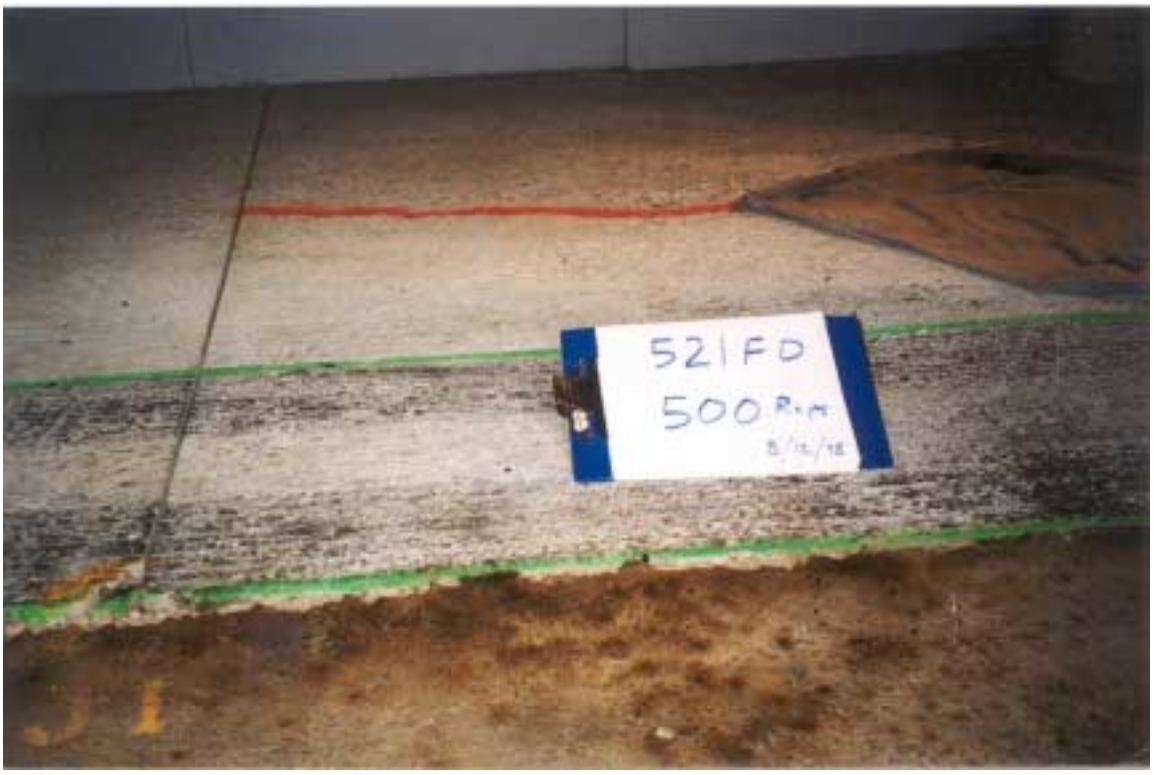

Photograph 4.14. Longitudinal crack on slab center after 500 repetitions, Test Section 521FD.

Photograph 4.15. Crack pattern after 168,000 repetitions, Test Section 521FD.

Photograph 4.16. Corner cracks at joint after 157,000 repetitions, Test Section 521FD.

Photograph 4.17. Final Crack pattern after 168,319 repetitions, Test Section 521FD.

Table 4.10 EDMD and JDMD Deflections, Test load = 20 kN, Test Section 521FD

Repetitions	Deflection (m × 10^{-6})			Temperature Difference (top-bottom), °C
	Midpoint Edge, Slab 12	Corner, Joint 11		
		Slab 12 Side	Slab 11 Side	
10	1,700	4,228	3,654	-1.3
500	1,767	4,205	3,514	NA
1,000	2,140	4,962	4,382	NA
5,000	1,728	4,409	3,420	-1.3
10,000	1,911	4,448	4,119	-0.8
20,000	1,809	4,445	3,555	NA
30,000	1,935	4,802	3,836	NA`
40,000	2,142	5,192	4,249	-0.4
50,000	1,926	5,122	3,962	-0.9
106,000	2,038	5,411	4,306	-0.5
125,000	**	5,390	4,162	-1.6
140,000	2,109	5,436	4,169	-0.8
157,719	718	674	2,263	-0.5
168,319	684	683	2,028	-0.2

** No data recorded

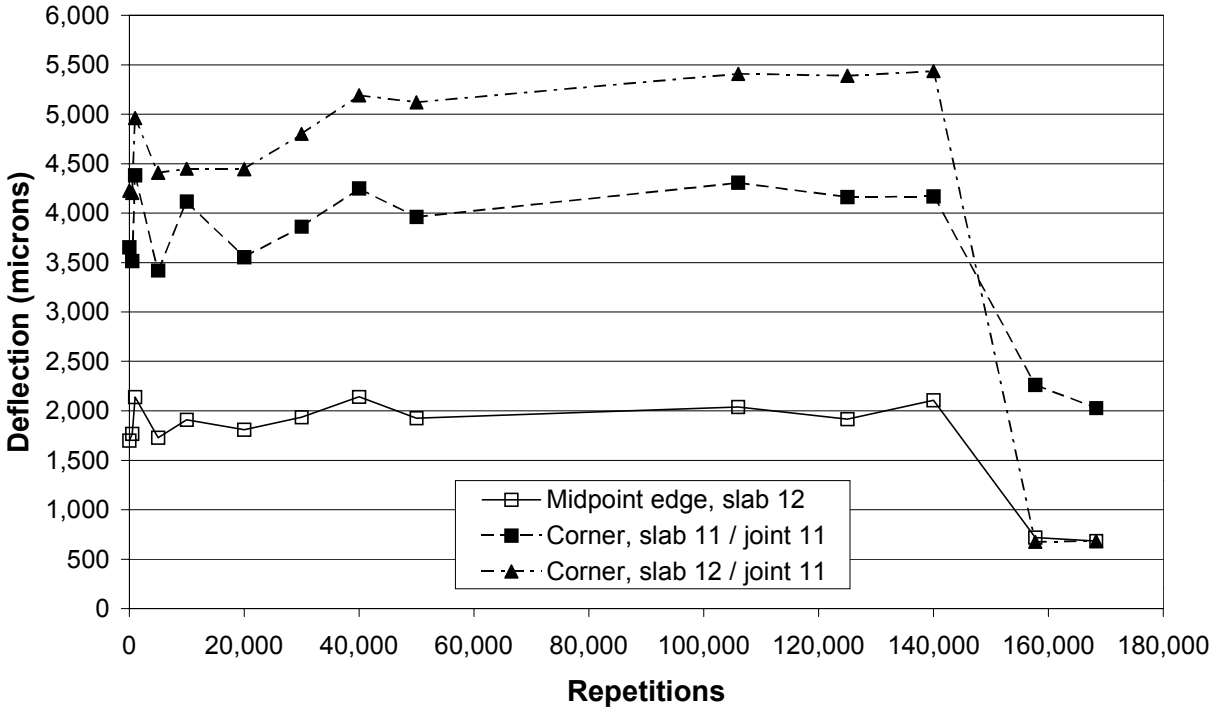

Figure 4.7. JDMD and EDMD deflections, test load = 20 kN, Test Section 521FD.

4.3.3 MDD Elastic Deflection Data, Test Section 521FD

Two MDDs were installed in the HVS wheelpath on Test Section 521FD, one at the midpoint of slab 12 (MDD4), and the other at the right hand side of joint 11 (MDD12, see Photographs 4.13 and 4.17). Both were installed between the contact areas for the HVS dual wheels, 300 mm from the edge of the slab. For both MDD installations, deflection-monitoring modules were installed at a depth of 50 mm (in the concrete slab), at a depth of 250 mm (bottom of the

base course) and at a depth of 425 mm (bottom of the aggregate subbase). The results of the peak MDD deflections can be seen in Table 4.11 and in Figure 4.8

The deflection trend is similar to that of the deflections measured by the JDMDs (see Table 4.10): a relatively constant phase (0-140,000 repetitions) followed by a significant decrease in the deflection occurring in the concrete slab once the load was increased and additional cracking occurred. The deflections measured by the MDD are lower than those recorded by the JDMDs and EDMD, but were located 305 mm from the edge of the pavement, in contrast to the JDMDs and EDMD, which were placed at the edge.

An important observation is that the deflections of the base course (MDDs at 250 and 425 mm depth) were close to zero during the first phase of testing (0–140,000 repetitions). This observation indicates that surface deflections originated from the 100-mm concrete slab and very little of the total surface deflection was transferred down to the deeper layers.

The very high elastic joint edge deflection (e.g., at MDD12, deflections of over 2,800 microns were recorded) gives more credence to the theory of a cavity between the concrete and the base course due to warping. It is conjectured that the slab was lifted off the ground so much that the effect of the deflection in the concrete was to make the slab plane with the ground

Table 4.11 MDD Deflections, Test Load = 20 kN, Test Section 521FD

Repetitions	In-depth Deflections at Depths as Indicated (m × 10^{-6})				
	Wheelpath, Longitudinal Midpoint Slab 12		Joint 11		
	50 mm	425 mm	50 mm	250 mm	425 mm
10	1,171	19	2,191	39	14
1,000	1,198	24	2,380	52	21
2,105	1,482	32	3,015	81	36
5,000	1,325	23	2,356	67	32
10,000	1,326	31	2,758	91	44
20,000	1,422	48	2,482	101	55
30,000	1,529	35	2,657	68	31
40,000	1,529	25	2,812	66	29
50,000	1,408	20	2,767	42	14
106,000	1,440	22	2,880	46	17
125,000	1,470	25	2,812	50	21
140,000	1,501	25	2,816	60	28
157,719	412	121	1,379	317	209
168,319	394	*	1,312	369	252

*Recorded data not reliable

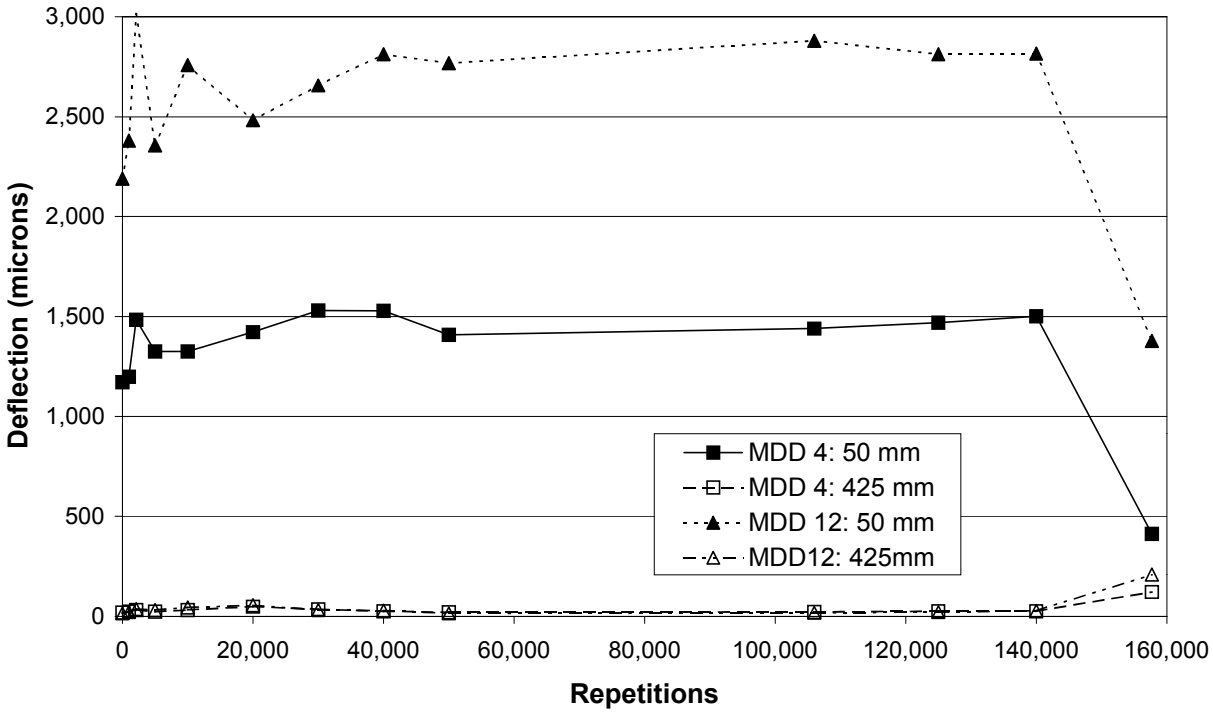

Figure 4.8. MDD deflections, test load = 20 kN, Test Section 521FD.

without mobilizing any significant deflection in the base layer. This would cause a very large stress in the slab corner.

After the longitudinal crack appeared at 142,072 repetitions (see Figure 4.6), the cavity closed and the concrete slab came in full contact with the base layer. This caused the surface deflections to decrease and mobilized deflections in the base layer as seen by the significant increase in deflections of the deeper layers from this point onwards.

Due to the unsupported nature of the slabs, a cantilever condition was present which supports the cracking observed at the corner. Heath et al. (*4*) found that the maximum stress in an edge-loaded slab is at the corner once the differential shrinkage strain exceeds 50 microstrain.(*4*)

4.3.4 MDD Permanent Deformation Data, Test Section 521FD

The permanent deformation of the upper part of the pavement was measured using the same MDDs. Permanent deformations at depths of 50, 250, and 425 mm were recorded and the results presented in Table 4.12 and Figure 4.9.

Table 4.12 MDD Permanent Deformation Data, Test Section 521FD

Repetitions	In-depth Deflections at Depths as Indicated (m × 10^{-6})				
	Wheelpath, Longitudinal Midpoint Slab 12		Joint 11		
	50 mm	425 mm	50 mm	250 mm	425 mm
10	0	0	0	0	0
1,000	284	22	240	-33	-38
2,105	374	16	53	-37	-44
30,000	527	-67	581	-62	-91
40,000	474	-70	427	-80	-108
50,000	418	-71	355	-61	-93
106,000	461	-90	197	-67	-98
125,000	509	-77	295	-69	-101
140,000	531	-79	364	-60	-96
157,719	3,407	113	4,173	560	235
168,319	3,677	331	4,724	813	405

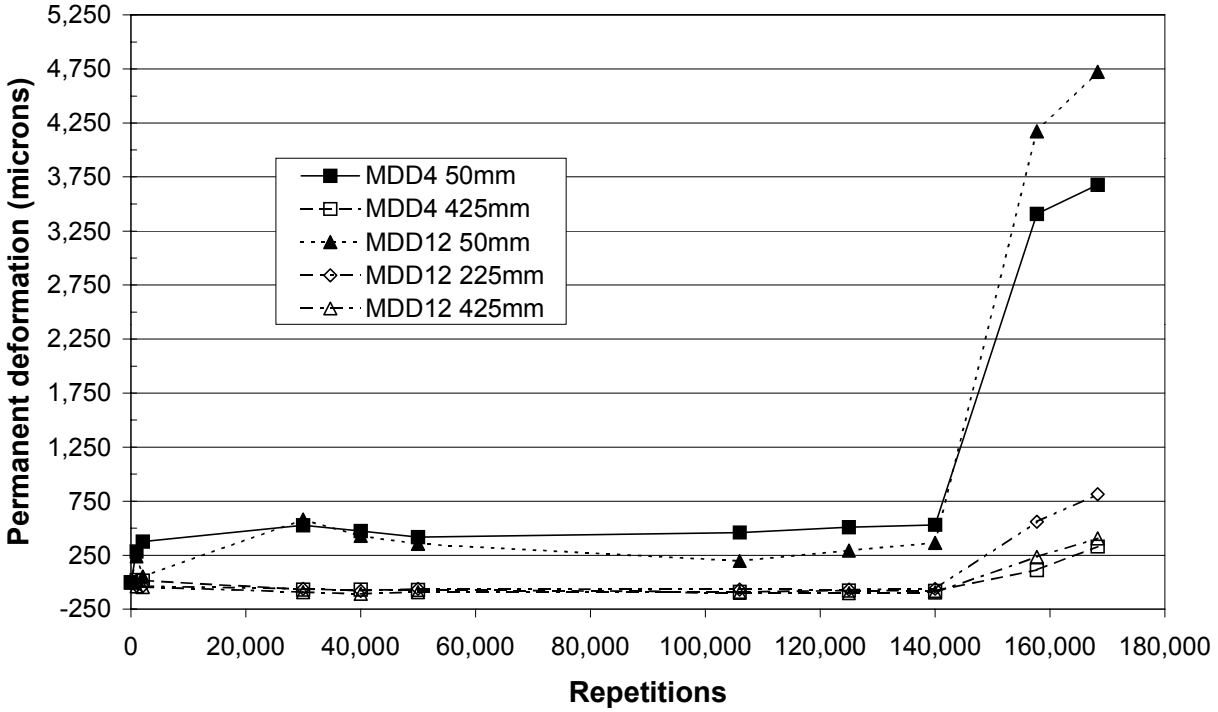

Figure 4.9. MDD permanent deformation, Test Section 521FD.

Figure 4.9 shows that the deeper MDDs have a slight negative deformation before going into positive values around 140,000 repetitions. This is probably due to small errors in the measurements (values are very small).

After the initial bedding-in of the slab on to the base course (due to the applied load from 0–30,000 repetitions), the deformation in the slab stayed relatively constant between 250 and 500 microns up to the point when the longitudinal crack appeared (around 140,000 repetitions, see Figure 4.6). At this point, the deformation of the concrete slab showed an abrupt increase to between 3,400 and 4,100 microns (3.4 and 4.1 mm).

This reaffirms the hypothesis that the concrete slabs initially had a warped up (concave) shape leaving the edges and corners unsupported. After this longitudinal crack, some deformation took place in the base layer, which is an indication that the concrete slab was in

better contact with the base layer and that some vertical load transfer took place from the concrete slab to the underlying granular base layers.

4.3.5 CAM Measurements, Test Section 521FD

Crack activity measurements were taken on the corner crack, which formed after 1,000 repetitions in the middle slab (Slab 12). The CAM was placed approximately 300 mm from the edge of the slab, between the contact areas of the HVS dual wheels (see Figure 4.6). The results can be seen in Table 4.13. The sign convention is similar to that discussed in Section 4.1.3 of this report.

Table 4.13 CAM Results, Test Section 521FD

Repetitions	Horizontal Movement (m × 10^{-6})		Vertical Movement (m × 10^{-6})	
	Closing (+)	Opening (–)	Positive	Negative
20,000	156	94	26	13
30,000	180	93	17	3
40,000	190	101	25	7
50,000	161	97	11	7
106,000	178	91	9	3
125,000	183	71	38	7
140,000	199	49	37	8
157,719	73	2	65	12
168,319	232	69	171	26

The crack activity at this location is relatively minor, indicating that there was effective aggregate interlock and base course support even after 168,000 20-kN load applications. The maximum horizontal movement was around 200 microns (after 140,000 repetitions) and maximum relative vertical movement was about 130 microns (after 168,000 repetitions).

Both these values are small indicating that although the crack was physically present, the load transfer across the crack and base support was still sufficient to carry the applied load.

4.4 Test Section 522FD

The HVS test on Section 522FD was a static test to determine the mid-slab edge flexural breaking strength of the 100-mm concrete slab. The HVS wheel was placed in the middle of slab 14 and surface edge deflections were measured with increases in the static hydraulic pressure exerted on the dual wheels of the HVS. This test was conducted without the use of the temperature control chamber. An overhead photograph of slab 14 is presented in Photograph 4.18; crack development is presented in Figure 4.10

Test Section 522FD was conducted on slab 14, which had two corner cracks prior to the start of the test (see Photograph 4.19). These cracks were caused by heavy construction equipment, which drove over the section after construction prior to the HVS being moved on to the South Tangent. The marked test section can be seen in Photograph 4.20

The test was conducted in two phases:

1. Stationary wheel load. The area in the middle of slab 14 was statically loaded by an increase in the hydraulic pressure exerted on the dual wheel of the HVS.
2. Moving wheel load. In this case, the HVS wheel was moved across the section at creep speed (less that 2km/h) and the deflection and crack development of the section was monitored with increases in wheel load.

The test was conducted in these two phases because during phase one, no additional cracks developed on the section even after the dual wheel load was increased to 100 kN. It was thought that the moving wheel load might assist in the establishment of the maximum flexural slab strength.

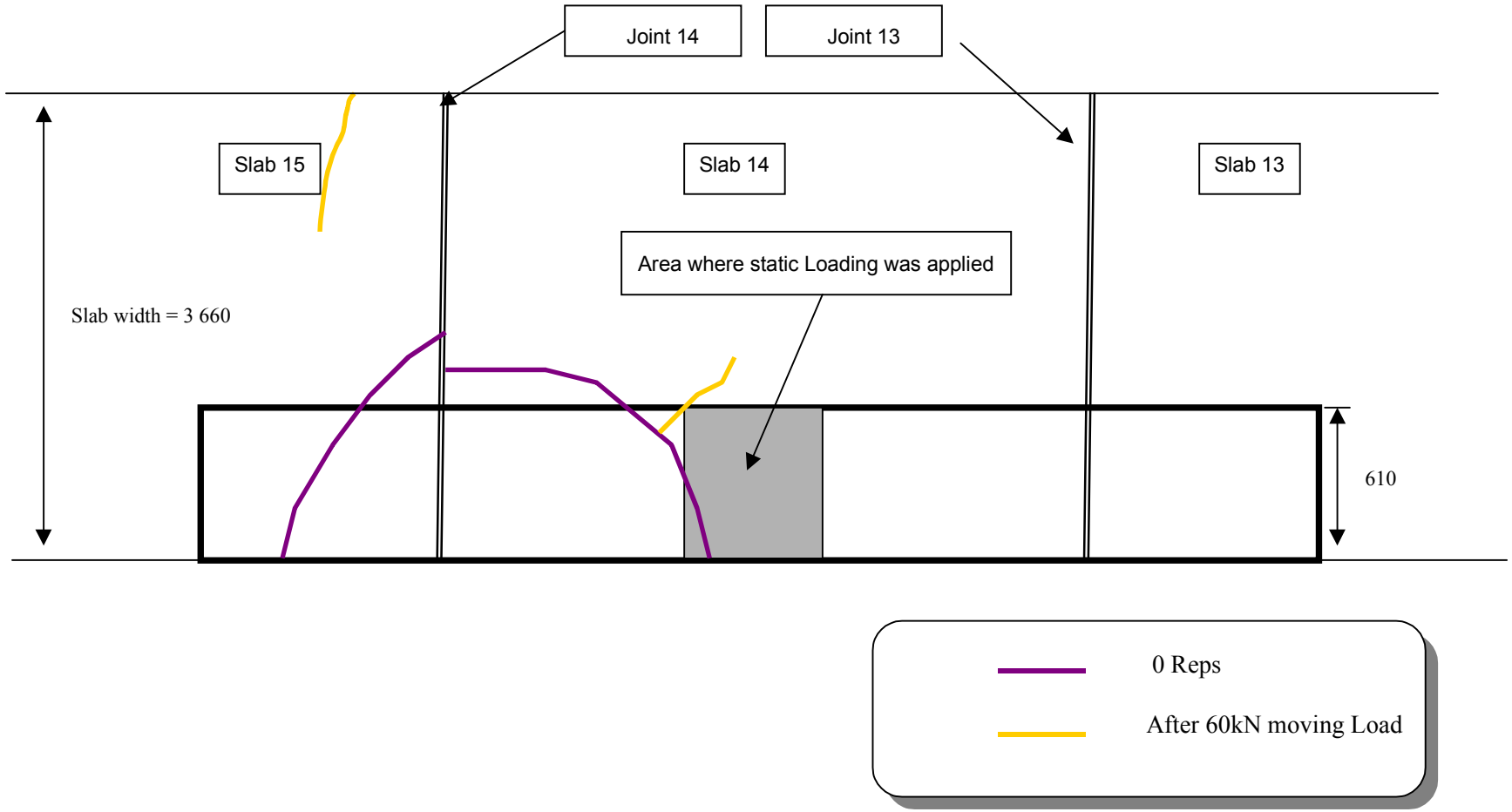

Figure 4.10. Schematic of crack development, Test Section 522FD (not to scale).

Photograph 4.18. Photograph of final crack pattern, Test Section 522FD.

Photograph 4.19. Crack pattern prior to HVS testing, Test Section 522FD.

Photograph 4.20. Position of static test, Test Section 522FD.

One EDMD was used to record the elastic deflections at the edge caused by the various load cases (Photograph 4.20) and the results are presented in Table 4.14 and Figure 4.11. The moving wheel test was only conducted to a maximum load of 60 kN.

Even with the application of a heavy load (100 kN) and high elastic edge deflections (3.3 mm), no additional cracks developed under the static load. The moving wheel caused higher deflections compared to the static case. After some applications of a 60-kN moving wheel two small cracks developed, one starting outside the trafficked area on slab 14 and one transverse crack on the untrafficked edge of the adjacent slab (slab 15). The final crack pattern can be seen in Photographs 4.18 and 4.20.

The flexural strength of the FSHCC at 90 days was approximately 5 MPa (*2*). A finite element analysis for a slab 100 mm thick indicated that the slab should crack under a load of approximately 25 kN.

Table 4.14 Elastic Edge Deflections at a Range of Loads, Test Section 522FD

Load (kN)	Edge Deflection (m × 10^{-6}) at Type of Load		Temperature Difference (top – bottom), °C
	Static	Moving Wheel	
20	1,552	1,808	5.5
25	1,556	1,926	7.5
30	1,614	2,115	7.7
35	1,683	2,322	8.1
40	1,694	2,469	8.1
45	1,819	2,538	8.3
50	1,942		8.4
55	2,095	2,585	8.5
60	2,232	2,673	8.7
65	2,426		8.9
70	2,584		9.3
75	2,725		9.2
80	2,855		9.5
85	2,972		9.6
90	3,075		9.9
95	3,197.7		9.7
100	3,339.7		9.3

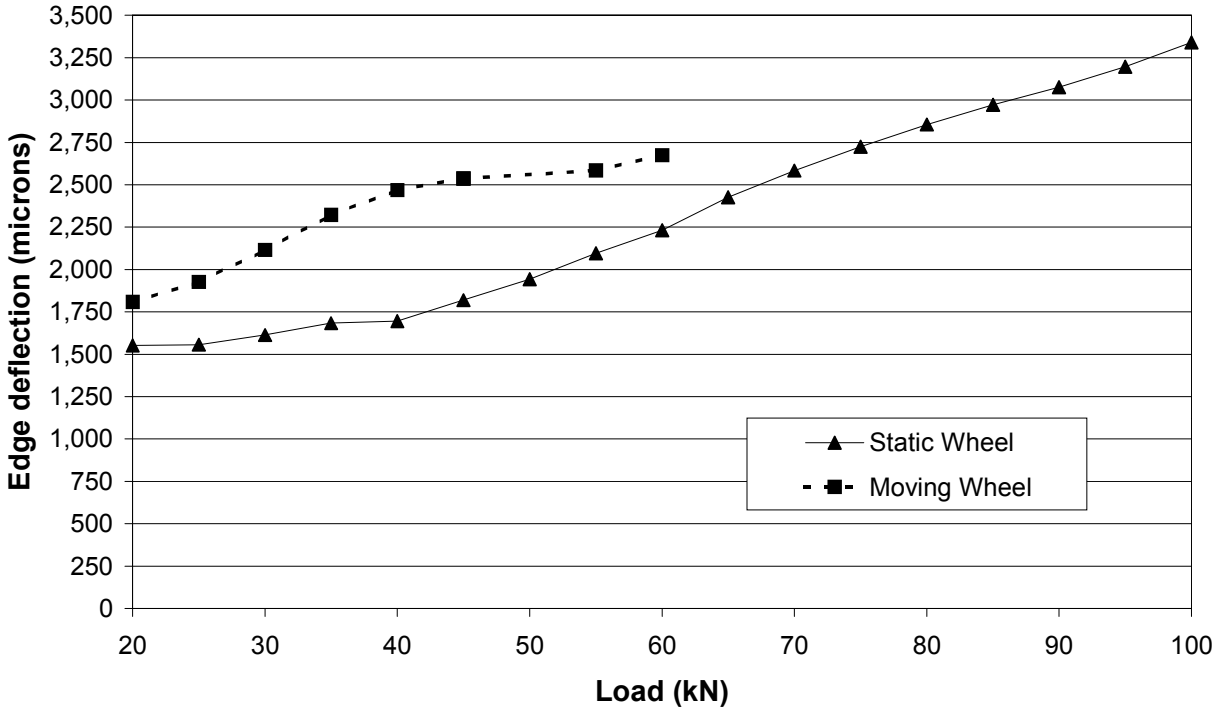

Figure 4.11. Elastic deflections at slab edge, Test Section 522FD.

This field test revealed a significantly higher load could be supported without the slab cracking, which indicates that the bending stress in the slab was substantially reduced due to the support from the underlying layers.

4.5 Test Section 523FD

The HVS test on Test Section 523FD was the first test on the 150-mm concrete slabs. The main objective of this series of tests was to evaluate the fatigue behavior of 150-mm thick Fast Setting Hydraulic Cement Concrete (FSHCC) on an aggregate base under the influence of bi-directional accelerated wheel loads with a temperature control box around the tested area and only dry conditions. This section has no dowel bars, tie bars or a widened lane. The results of these fatigue tests will be compared to the fatigue tests on 100- and 200-mm slabs on the same aggregate base.

The slab widths were 3.7 m with variable joint spacing from 3.7 m to 5.8 m. All the test sections on the South Tangent have 150-mm thick Class 2 aggregate base resting on a compacted granular subgrade. Sections have perpendicular transverse joints with the slab size matching the existing adjacent slabs.

4.5.1 Visual Observations, Test Section 523FD

Photograph 4.21 shows an overhead view of the test section and crack pattern. Figure 4.12 shows crack development for Section 523FD. Several cracks existed before trafficking began (see Photograph 4.22). The first crack under applied loading appeared at 89,963 repetitions on slab number 17 as a corner crack and as a longitudinal crack on slab number 16 (Photograph 4.23).

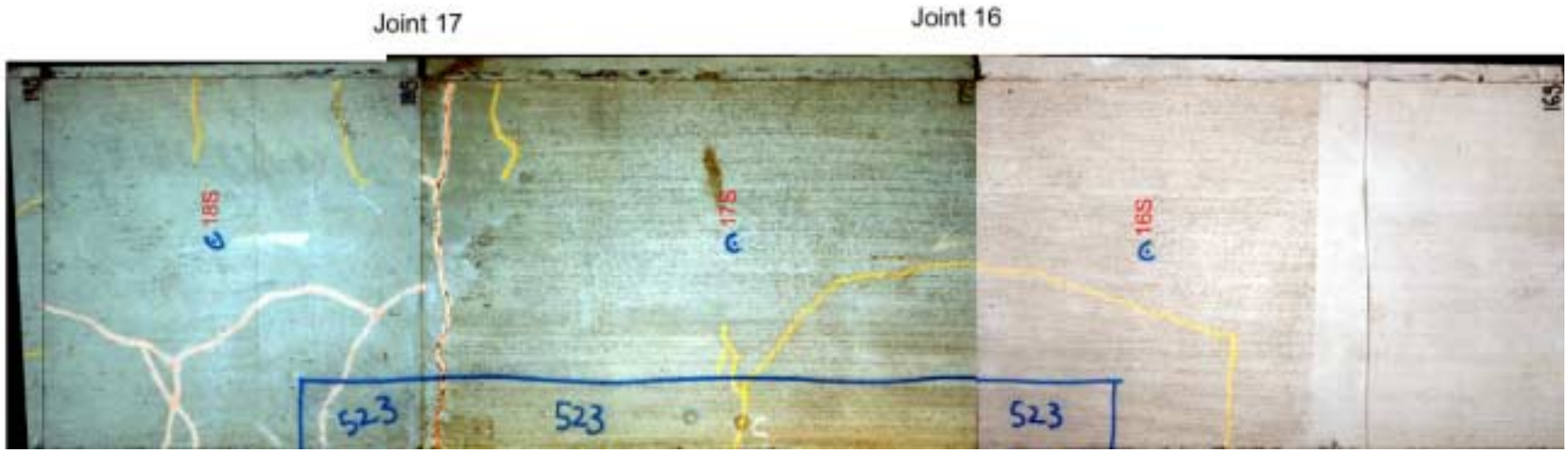

Photograph 4.21. Composite photograph of final crack pattern, Test Section 523FD.

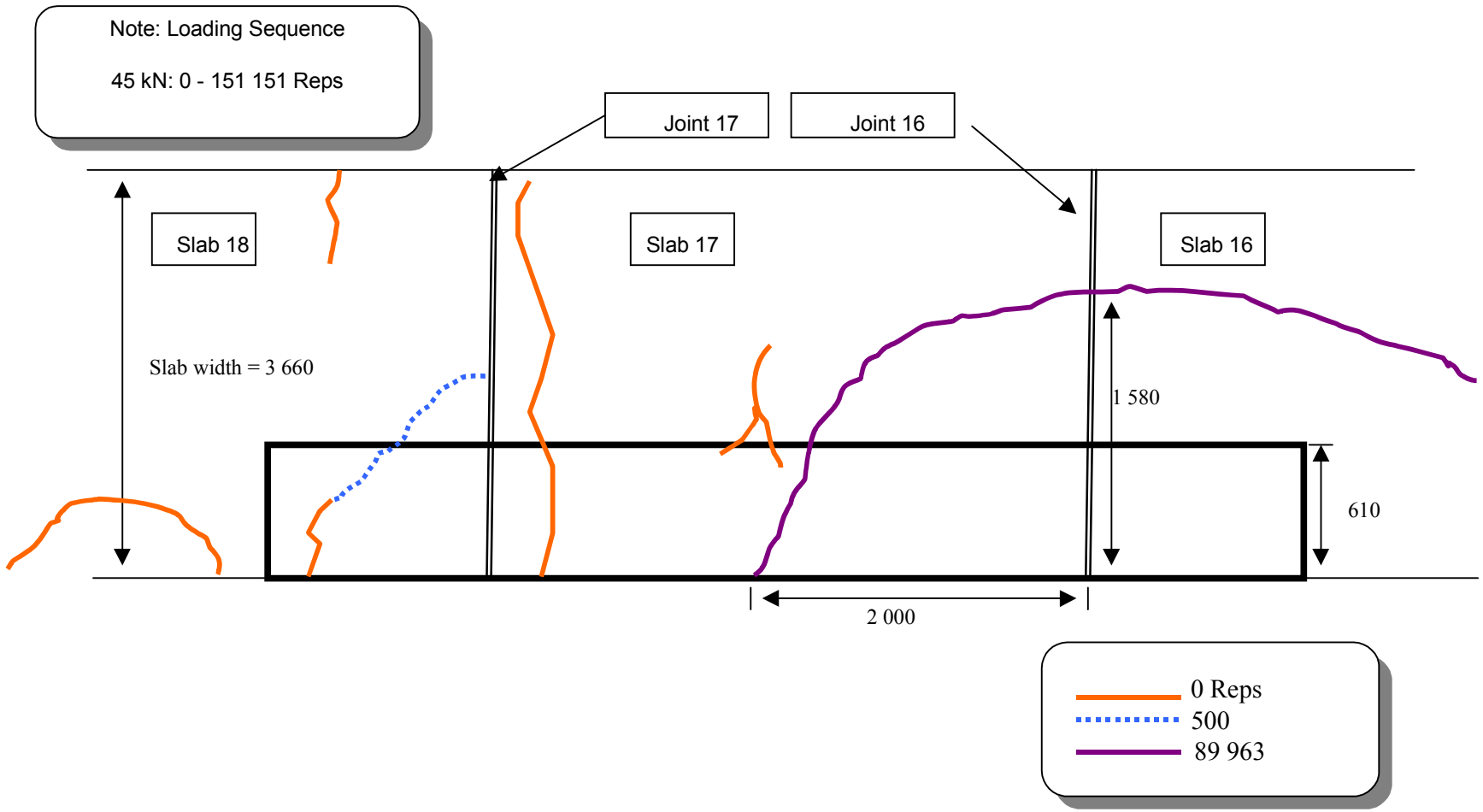

Figure 4.12. Schematic of crack development, Test Section 523FD (not to scale).

Photograph 4.22. Crack at transverse joint (joint 17) at start of test, Test Section 523FD.

Photograph 4.23. Crack pattern after 90,000 repetitions, Test Section 523FD.

4.5.2 JDMD and EDMD Data, Test Section 523FD

Tables 4.15 to 4.18 summarize the results of the maximum elastic deflection at the mid-slab edge of slab 17, as well as the maximum corner deflections on either side of joint 16. Table 4.19 summarizes the permanent deformations occurring at the edge and corner of the slab. Tables 4.15 to 4.17 show deflection data for when the HVS wheel is running in each direction across the joint. In terms of maximum mid-slab deflection, wheel direction does not seem to make a difference.

Table 4.18 and Figure 4.13 are the average displacements at the edge and slab corner over the loading history of Test Section 523FD. The corner displacements show a gradual increase with load repetitions until around 90,000 repetitions when the first crack appeared on slab numbers 16 and 17. Once this transverse crack appeared and propagated to the joint, the displacements at the slab corner decreased significantly. The edge deflections steadily increased throughout the test but were not affected by the corner crack.

The most likely reason that the corner displacements decreased once the crack developed was that the slab settled onto the base and was more fully supported. The edge of the slab was probably curled up throughout the test and was never in full contact with the base and therefore the deflection never decreased after first cracking. After first cracking the corner and edge displacements were not very sensitive to additional repetitions by the 45-kN wheel load.

When comparing the corner deflections at joint 16 from Table 4.18, there is a difference between the displacements even though the LVDTs are only 50 mm apart. This is evidenced by the relatively high coefficient of variation between the corner deflection measurements. The displacement on the slab 16 side of joint 16 was greater than that measured on the slab 17 side (left-hand side) until the first crack developed. After the corner crack formed on slab 17 and a

Table 4.15 Midpoint Edge Deflections under a 45-kN Wheel Load, Test Section 523FD

Repetitions	Midpoint Edge Deflections, Slab 17 (m × 10^{-6})					Temperature Difference (Top – Bottom), °C
	Load Direction		Avg.	Std. Dev.	C.O.V. (%)	
	From Slab 18	From Slab 16				
10	637	624	631	8.6	1.4	NA
100	665	685	675	14.4	2.1	-2.0
500	667	694	681	18.8	2.8	-2.0
1,000	664	655	660	6.6	1.0	-2.0
5,000	816	846	831	21.2	2.6	-1.0
10,000	702	780	741	55.1	7.4	-0.4
15,000	880	895	887	10.0	1.0	-1.0
20,000	694	680	687	9.8	1.4	-0.4
30,000	869	874	842	3.5	0.4	-1.3
40,000	883	911	897	20.0	2.2	-0.6
50,000	932	946	939	10.1	1.1	-0.3
60,000	936	951	943	11.0	1.2	-0.6
70,000	959	962	961	2.7	0.3	-1.0
89,963	970	974	972	3.0	0.3	-0.7
133,148	1,025	1,040	1,032	10.6	1.0	-0.7
151,151	1,015	1,041	1,028	19.0	1.9	-0.5

Table 4.16 Corner Deflections under a 45-kN Wheel Load, Slab 17, Test Section 523FD

Repetitions	Corner Deflections, Slab 17/Joint 16 (m × 10^{-6})					Temperature Difference (Top – Bottom), °C
	Load Direction		Avg.	Std. Dev.	C.O.V. (%)	
	From Slab 17	From Slab 16				
10	1,974	1,785	1,880	133.4	7.1	NA
100	2,145	2,116	2,131	21	1	-2.0
500	2,129	2,114	2,122	10.2	0.5	-2.0
1,000	2,213	2,176	2,194	26.2	1.2	-2.0
5,000	2,746	2,730	2,738	11.3	0.4	-1.0
10,000	2,600	2,586	2,593	9.8	0.4	-0.4
15,000	3,023	3,015	3,019	5.9	0.2	-1.0
20,000	2,618	2,619	2,618	0.5	0	-0.4
30,000	2,955	2,949	2,952	4.5	0.2	-1.36
40,000	3,079	3,076	3,078	2.4	0.1	-0.6
50,000	3,224	3,229	3,226	3.4	0.1	-0.3
60,000	3,304	3,317	3,310	8.8	0.3	-0.6
70,000	3,333	3,342	3,337	5.9	0.2	-1.0
89,963	2,080	2,104	2,092	16.7	0.8	-0.7
133,148	2,147	2,151	2,149	2.5	0.1	-0.7
151,151	2,237	2,249	2,243	8.8	0.4	-0.5

Table 4.17 Corner Deflections under a 45-kN Wheel Load, Slab 16, Test Section 523FD

Repetitions	Corner Deflections, Slab 16/Joint 16 ($m \times 10^{-6}$)					Temperature Difference (Top – Bottom), °C
	Load Direction		Avg.	Std. Dev.	C.O.V. (%)	
	From Slab 17	From Slab 16				
10	2,306	1,958	2,132	245.9	11.5	NA
100	2,623	2,594	2,609	20.5	0.8	-2.0
500	2,625	2,622	2,624	2	0.1	-2.0
1,000	2,691	2,958	2,674	23.2	0.9	-2.0
5,000	3,185	3,190	3,188	3.9	0.1	-1.0
10,000	3,092	3,067	3,080	17.5	0.6	-0.4
15,000	3,376	3,368	3,372	5.3	0.2	-1.0
20,000	2,958	2,933	2,946	176	0.6	-0.4
30,000	3,243	3,223	3,233	13.9	0.4	-1.3
40,000	3,343	3,350	3,347	4.8	0.1	-0.6
50,000	3,491	3,495	3,493	3.3	0.1	-0.3
60,000	3,595	3,591	3,593	3	0.1	-0.6
70,000	3,599	3,597	3,598	1.5	0	-1.0
89,963	1,607	1,610	1,660	2	0.1	-0.7
133,148	1,661	1,658	1,660	2	0.1	-0.7
151,151	1,582	1,584	1,583	0.9	0.1	-0.5

Table 4.18 Average of all Deflections under a 45-kN Wheel Load, Test Section 523FD

Repetitions	Deflections ($m \times 10^{-6}$)					Temperature Difference (Top – Bottom), °C
	Midpoint Edge, Slab 17	Corner Slab 17/ Joint 16	Corner Slab 16/ Joint 16	Std. Dev.	C.O.V. (%)	
10	631	1,880	2,132	218	10.8	NA
100	675	2,131	2,609	277	11.7	-2.0
500	681	2,122	2,624	290	12.2	-2.0
1,000	660	2,194	2,674	278	11.4	-2.0
5,000	831	2,738	3,188	260	8.8	-1.0
10,000	741	2,593	3,080	281	9.9	-0.4
15,000	887	3,019	3,372	204	6.4	-1.0
20,000	687	2,618	2,946	189	6.8	-0.4
30,000	872	2,952	3,233	163	5.3	-1.3
40,000	897	3,078	3,347	155	4.8	-0.6
50,000	939	3,226	3,493	154	4.6	-0.3
60,000	943	3,310	3,593	163	4.7	-0.6
70,000	961	3,337	3,598	150	4.3	-1.0
89,963	972	2,092	1,609	279	15.1	-0.7
133,148	1,032	2,149	1,660	283	14.8	-0.7
151,151	1,028	2,243	1,583	381	19.9	-0.5

Table 4.19 EDMD and JDMD Permanent Pavement Deformations, Test Section 523FD

Repetitions	Permanent Deformation (m × 10^{-6})		
	Midpoint Edge, Slab 17	Corner Slab 17/Joint 16	Corner Slab 16/Joint 16
20,000	0	0	0
30,000	-167	-271	-263
40,000	-93	-242	-313
50,000	-121	-303	-436
60,000	-199	-367	-530
70,000	-196	-378	-540
89,963	-185	2,178	1,157
133,148	-128	2,612	1,506
151,151	-100	2,816	1,535

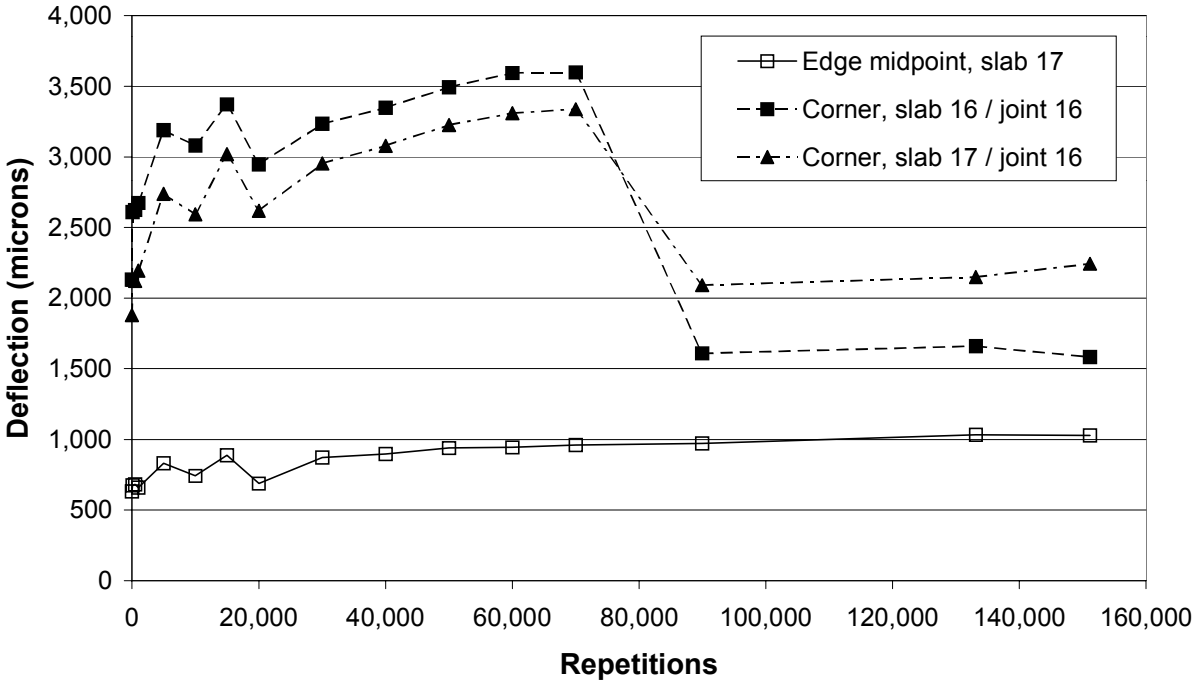

Figure 4.13. JDMD deflections, Test Section 523FD.

longitudinal crack formed on slab 16, the corner deflection on the slab 16 side was less than on the slab 17 side.

The reason for this change was probably due to the corner crack completely severing the corner from slab 17 while the longitudinal crack on slab 16 did not propagate all the away across. This also indicates, as expected, that the traveling wheel load drives crack propagation and since the wheel only loaded slab 16 for a 1-m length, the crack did not traverse the whole slab length of 4.0 m.

A chart showing permanent deformation at joint 16 and the slab midpoint edge versus HVS wheel repetitions is shown in Figure 4.14. There was minimal permanent deformation at the corner and slab edge midpoint until around 75,000 repetitions at which point corner permanent deformation in the pavement system started accumulating. This permanent deformation most likely began due to a loss in local stiffness of the slab, which in turn slightly increased the elastic deflection and the pressure on the base and subgrade.

After the first cracking at 90,000 repetitions, there was not a significant increase in permanent deformation at the corner or edge of the slab. This can be expected since the elastic deflections at the corner of the slab decreased between 40 and 50 percent after cracking. In Figure 4.14, there is a slight negative trend in the permanent deformation of the slab system in the beginning of the test. Because the base and subgrade cannot expand under wheel loading, the only explanation for this behavior is a different zero load position caused by either the rocking of the slab or the ambient temperature outside the box. The latter explanation (temperature effect) is probably the most likely answer.

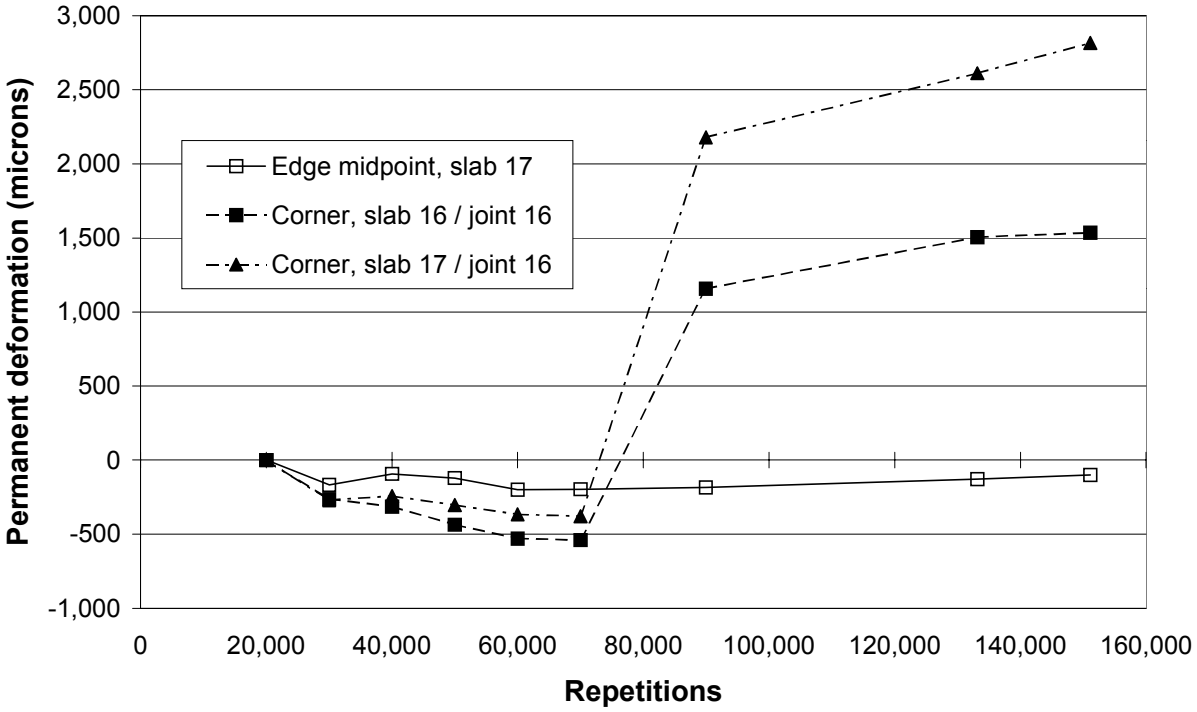

Figure 4.14. JDMD permanent deformation, Test Section 523FD.

Table 4.20 shows the load transfer efficiency (LTE) with the number of repetitions for both wheel directions and two wheel locations. LTE is calculated by dividing the unloaded slab corner deflection by the loaded slab corner deflection. The load transfer is calculated for the wheel load moving across the joint in each direction. For each wheel direction, LTE is calculated when the wheel is on each slab adjacent to the joint. Therefore, four LTEs are calculated for each joint at which deflection is measured.

Table 4.20 shows that the average LTE differs only little according to which direction the wheel load moved across the joint. The surface temperature of the slab was 26 degrees Celsius during the first reading, which probably affected the deflection measurements and the first LTE calculation. When deflection data was collected at 100 repetitions, the surface temperature was 19°C, which was near the target temperature of 20°C in the temperature control box. The LTE

Table 4.20 Load Transfer Efficiency at Joint 16, Test Section 523FD

Repetitions	Load Transfer Efficiency, LTE (%) at Joint 16						Temperature Difference (Top–Bottom), °C
	Slab17/Joint 16			Slab 16/Joint 16			
	From Slab 16 to 17	From Slab 17 to 16	Average	From Slab 16 to 17	From Slab 17 to 16	Average	
10	40.5	41.5	*41*	60.9	61.5	*61*	NA
100	43.9	44.7	*44*	45.0	46.8	*46*	-2.0
500	49.0	46.2	*48*	39.9	41.3	*41*	-2.0
1,000	47.9	46.2	*47*	38.4	39.0	*39*	-2.0
5,000	37.8	39.2	*38*	40.9	40.8	*41*	-1.0
10,000	32.6	31.3	*32*	33.9	35.0	*34*	-0.4
15,000	38.2	34.9	*37*	39.5	39.7	*40*	-1.0
20,000	23.0	23.3	*23*	30.3	31.9	*31*	-0.4
30,000	29.8	29.5	*30*	35.3	35.7	*35*	-1.3
40,000	32.3	29.5	*31*	37.6	36.8	*37*	-0.6
50,000	32.8	30.1	*31*	37.6	36.8	*37*	-0.3
60,000	33.5	32.5	*33*	37.0	36.6	*37*	-0.6
70,000	32.7	30.6	*32*	36.7	37.2	*37*	-1.0
89,963	8.9	10.2	*10*	30.5	39.9	*35*	-0.7
133,148	9.1	5.9	*7*	38.7	40.3	*39*	-0.7
151,151	3.6	6.0	*5*	44.7	67.2	*56*	-0.5

was also affected by the crack in the slab because the joint will behave differently depending on how close the crack is to the deflection sensors.

Table 4.20 shows that LTE is much more dependent on which side the slab is loaded than the direction of the wheel travel. This trend is consistent before and after cracking occurred on the test section. The difference in the measured LTE for the same wheel direction but different slabs is more extreme, especially after cracking began on slab 17.

Overall, the LTE shows a decrease with number of load repetitions. Furthermore the initial load transfer efficiency was quite low, approximately 45 percent. HWD testing measured the average LTE in section 3 (the 150-mm thick slabs) to be approximately 64 percent at 90 days after construction (*2*). The low LTE can be associated with shrinkage of the concrete, which opens the joints and decreases the aggregate interlock. The concrete used in Palmdale was found to have a higher free shrinkage as compared to normal Type I/II cement.(*4*)Table 4.20 shows that the deterioration of LTE occurs very quickly and levels off to a minimum value approaching 30

percent load transfer efficiency prior to cracking. Once cracking has occurred near the joint, the LTE can approach zero or even increase due to slab rocking or settling.

The most likely explanation for the directional behavior of the LTE at one joint is the shape of the joint crack. This trend was also seen in the 100-mm thick sections and in HVS Test Section 516CT (*3*). If the joint crack is not perpendicular to the surface, then LTE will be biased toward one slab. In this test, the top of the joint crack must have traveled down from the saw cut at the joint toward slab 17 in order to produce higher LTE on slab 16 compared with slab 17.

4.5.3 CAM Data, Test Section 523FD

Table 4.21 shows the results recorded with the Crack Activity Meter. These measurements were taken at two stages: at the beginning of the test, and after 10,000 load applications. The CAM was placed between the wheel paths of the dual wheels across joint 16.

Table 4.21 CAM Results, Test Section 523FD

Repetitions	**Horizontal Movement (m × 10^{-6})***		**Vertical Movement (m × 10^{-6})***	
	Closing (+)	**Opening (–)**	**Positive**	**Negative**
10	332	-20	962	-966
10,000	265	-96	352	-2,745**

* Symbols and explanations presented in Section 4.1.3 apply here as well.
** Data not reliable. LVDT probably went out of range.

The values presented in Table 4.21 are high, with the total vertical joint movement at the beginning of the test almost 2 mm (962 and 966 microns combined), which indicates a noticeable joint movement even at a test load of 45 kN. These results suggest that the aggregate interlock required to prevent vertical joint movement was low. At 10,000 repetitions, the vertical activity became so high that the LVDT recording the vertical movement went out of range and no useful conclusion from this data set can be drawn.

4.6 Test Section 524FD

The HVS test on Test Section 524FD was conducted on slab numbers 19, 20, and 21 on the South Tangent. Slab 20 (5.7-m total length) was fully tested, together with some area on either side of joints 19 and 20. The test section was trafficked with a 45-kN dual wheel load for the entire 119,784 repetitions. This test used the temperature control box and bi-directional trafficking. Photograph 4.24 shows an overhead view of the test section with cracks; Figure 4.15 shows the crack development.

4.6.1 Visual observations and JDMD and EDMD results, Test Section 524FD

A corner crack first appeared on slab 19 after 30,000 repetitions. The first crack appearing on the middle slab (20) was identified at 64,000 repetitions and started at joint 19, appearing initially to be a longitudinal crack, but ultimately turning into a large corner crack by 103,000 repetitions (Photograph 4.25).

4.6.2 JDMD and EDMD Data, Test Section 524FD

Tables 4.22 to 4.25 summarize the results of the maximum deflection at the mid-slab edge of slab 20, and the corner edge deflections on either side of joint 19. Table 4.22 shows that the repeatability of the midpoint edge deflections is less than 5 percent for the majority of the readings. Tables 4.23 and 4.24 show that there is little effect from wheel direction on the measured maximum corner deflections on either side of joint 19.

Table 4.25 summarizes the average maximum deflections of the mid-slab edge and corner deflections. The corner displacements measured on slab numbers 19 and 20 are very similar up to 30,000 repetitions. The coefficient of variation between corner measurements was less than 3

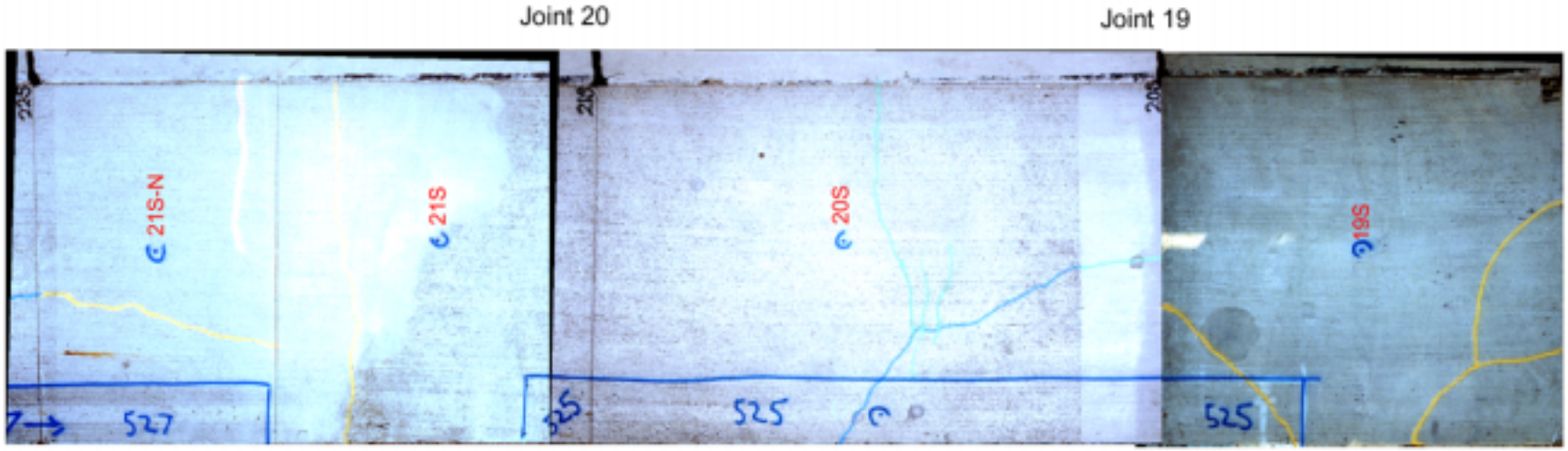

Photograph 4.24. Composite photograph of final crack pattern, Test Section 524FD.
Note: The paint indicating Section 525FD in this photograph is incorrect; test section is actually 524FD.

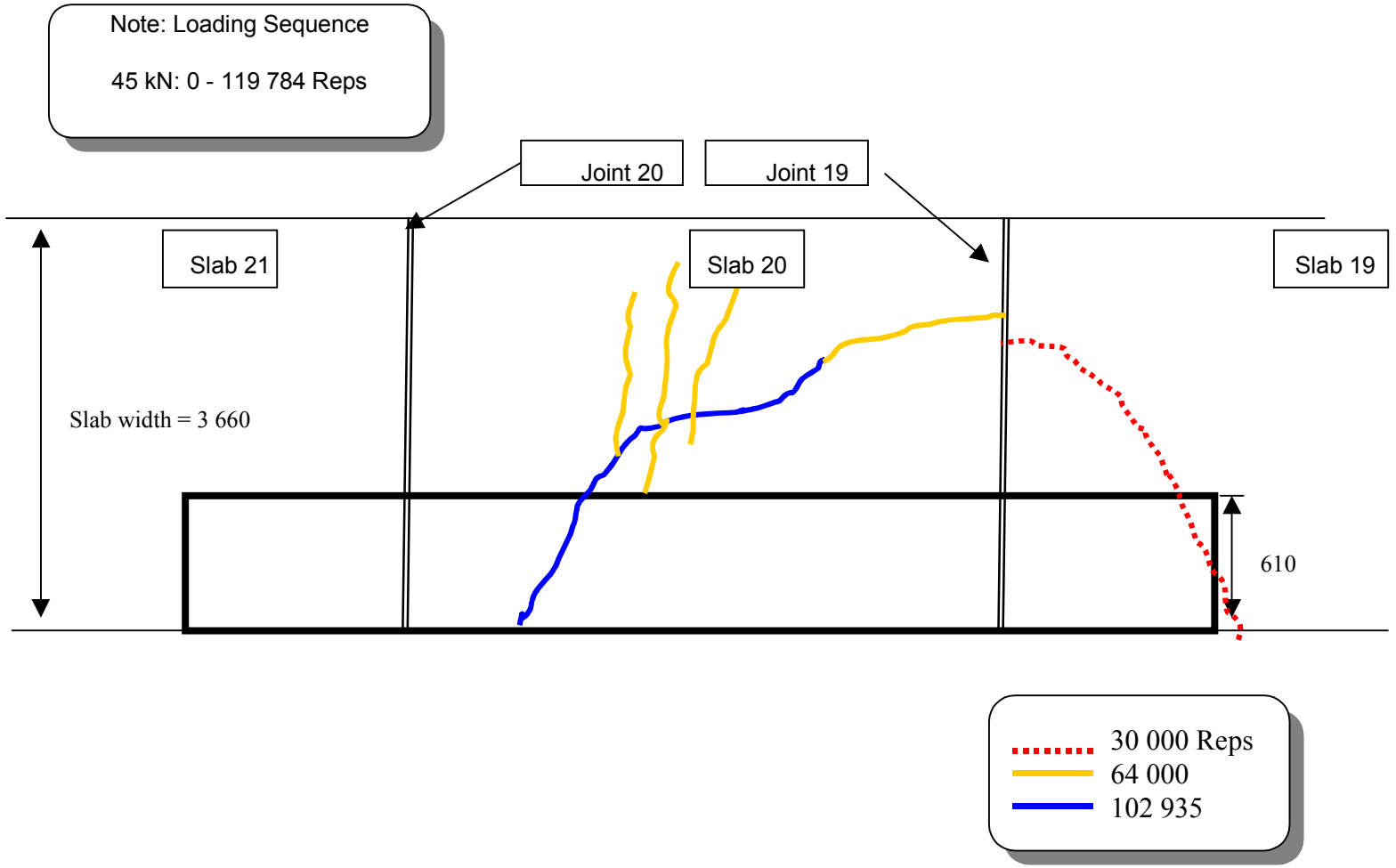

Figure 4.15. Schematic of crack development, Test Section 524FD (not to scale).

Photograph 4.25. Crack pattern at completion of HVS trafficking, Test Section 524FD.

Table 4.22 Midpoint Edge Deflections under a 45-kN Wheel Load, Slab 20, Test Section 524FD

Repetitions	Midpoint Edge Deflections (m × 10^{-6}) at Slab 20					Temperature difference (Top–Bottom), °C
	Load Direction		Average	Std. Dev.	C.O.V. (%)	
	From Slab 21	From Slab 19				
10	1,069	1,079	1,074	6.8	0.6	NA
100	1,115	1,089	1,102	18.9	1.7	NA
500	1,215	1,202	1,209	9.2	0.8	NA
1,000	1,248	1,170	1,209	55.1	4.6	-1.10
5,000	1,300	1,237	1,269	44.5	3.5	-0.30
19,353	1,415	1,291	1,353	87.7	6.5	-0.80
30,000	1,160	1,214	1,187	38.4	3.2	-0.40
40,000	937	913	925	17.0	1.8	NA
64,332*	914	853	883	43.0	4.9	-0.10
102,935	892	785	839	75.1	9.0	-0.10
119,784	898	794	846	73.2	8.7	0.10

*corner crack appeared

Table 4.23 Corner Deflections under a 45-kN Wheel Load, Slab 20, Test Section 524FD

Repetitions	Corner Deflections (m × 10^{-6}) at Slab 20/Joint 19					Temperature difference (Top–Bottom), °C
	Load Direction		Average	Std. Dev.	C.O.V. (%)	
	From Slab 20	From Slab 19				
10	2,624	2,645	2,635	15.1	0.6	NA
100	2,976	2,992	2,984	11.3	0.4	NA
500	3,188	3,194	3,191	3.7	0.1	NA
1,000	3,361	3,350	3,356	7.4	0.2	-1.10
5,000	3,532	3,549	3,540	11.8	0.3	-0.30
19,353	3,776	3,765	3,770	7.8	0.2	-0.80
30,000	3,294	3,323	3,308	19.9	0.6	-0.40
40,000	1,842	1,910	1,876	48.4	2.6	NA
64,332*	1,748	1,724	1,736	16.7	1.0	-0.10
102,935	1,361	1,341	1,351	13.7	1.0	-0.10
119,784	1,348	1,323	1,336	18.3	1.4	0.10

*corner crack appeared

Table 4.24 Corner Deflections under a 45-kN Wheel Load, Slab 19, Test Section 524FD

Repetitions	Corner Deflections (m × 10^{-6}) at Slab 19/Joint 19					Temperature difference (Top–Bottom), °C
	Load Direction		Average	Std. Dev.	C.O.V. (%)	
	From Slab 20	From Slab 19				
10	1,069	1,079	1,074	6.8	0.6	NA
100	1,115	1,089	1,102	18.9	1.7	NA
500	1,215	1,202	1,209	9.2	0.8	NA
1,000	1,248	1,170	1,209	55.1	4.6	-1.10
5,000	1,300	1,237	1,269	44.5	3.5	-0.30
19,353	1,415	1,291	1,353	87.7	6.5	-0.80
30,000	1,160	1,214	1,187	38.4	3.2	-0.40
40,000	937	913	925	17.0	1.8	NA
64,332*	914	853	883	43.0	4.9	-0.10
102,935	892	785	839	75.1	9.0	-0.10
119,784	898	794	846	73.2	8.7	0.10

*corner crack appeared

Table 4.25 Average of all Deflections under a 45-kN Wheel Load, Test Section 524FD

Repetitions	Average Deflections ($m \times 10^{-6}$)			Temperature difference (Top–Bottom), °C
	Midspan Edge, Slab 20	Corner Slab 20/Joint 19	Corner Slab 19/Joint 19	
10	1,074	2,635	2,556	NA
100	1,102	2,984	2,989	NA
500	1,209	3,191	3,234	NA
1,000	1,209	3,356	3,466	-1.1
5,000	1,269	3,540	3,522	-0.3
19,353	1,353	3,770	3,837	-0.8
30,000	1,187	3,308	3,259	-0.4
40,000	925	1,876	2,141	NA
64,332*	883	1,736	1,901	-0.1
102,935	839	1,351	1,310	-0.1
119,784	846	1,336	1,308	0.1

*corner crack appeared

percent until the appearance of the first crack. This differs from the measurements on Test Section 523FD where the coefficient of variation approached 13 percent. After 30,000 repetitions, a corner crack developed in slab 19 which affected the deflection measurement at the corner of slab 19 more than on the corner of slab 20.

Figure 4.16 is the plot of elastic deformation versus the number of HVS wheel repetitions (Tables 4.22 to 4.24). The plot of JDMD readings in Figure 4.16 shows a rapid increase in deflection values at the corners of the slab at the beginning of the test. After 30,000 repetitions a corner crack formed in slab 19 near joint 19, and resulted in a significant decrease of corner deflections on both sides of joint 19. The slab 20 side of the joint was a little higher than the other side (slab 19) because the crack initiated on slab 19. Similar decreases in deflection were seen previously on Test Section 523FD and on the 100-mm test sections.

The midpoint edge deflections increased until 20,000 repetitions then steadily decreased over the rest of the test, but did not decrease markedly when crack development began occurring

on the test section. However, the maximum deflections at the edge did show a similar shape to the corner deflections.

The permanent deformations at the corner and midpoint edge are given in Table 4.26 and Figure 4.17. The permanent deformation at joint 19 started accumulating significantly by 30,000 repetitions. At 40,000 repetitions, the permanent deformation at the joint was greater than 2 mm. The slab 19 side of the joint continued to accumulate permanent deformation at a higher rate than the other side due to the corner crack occurring on slab 19. The permanent deformation at the edge of the slab was similar in magnitude to the corners. By 30,000 repetitions, the permanent deformation was approximately 0.7 mm. The permanent deformation at the edge did not increase at the same rate as the corner deflections. This is most likely due to the lower displacements at the edge and thus less stress on the underlying layers. The permanent deformation at the edge did not accumulate significantly faster once cracking appeared on slab 20.

Table 4.26 EDMD and JDMD Permanent Deformation, Test Section 524FD

Repetitions	**Permanent Deformation ($m \times 10^{-6}$)**		
	Midpoint Edge, Slab 17	**Corner Slab 20/Joint 19**	**Corner Slab 19/Joint 19**
10	0	0	0
100	11	-205	-68
500	-11	-220	-157
1,000	132	-256	-192
5,000	395	205	299
19,353	538	400	264
30,000	666	1,967	1,055
40,000	1,307	3,318	2,926
64,332*	1,553	5,322	3,361
102,935	2,073	6,323	4,188
119,784	2,154	6,435	4,298

*corner crack appeared

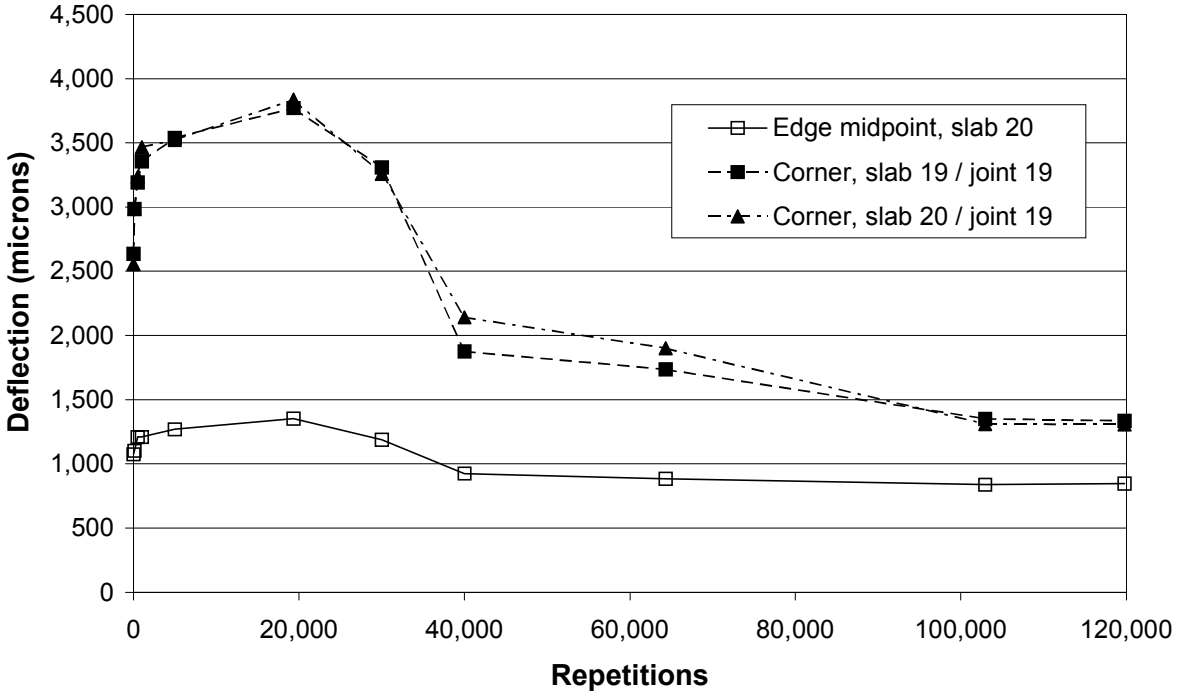

Figure 4.16. EDMD and JDMD elastic deflections, test load = 45 kN, Test Section 524FD.

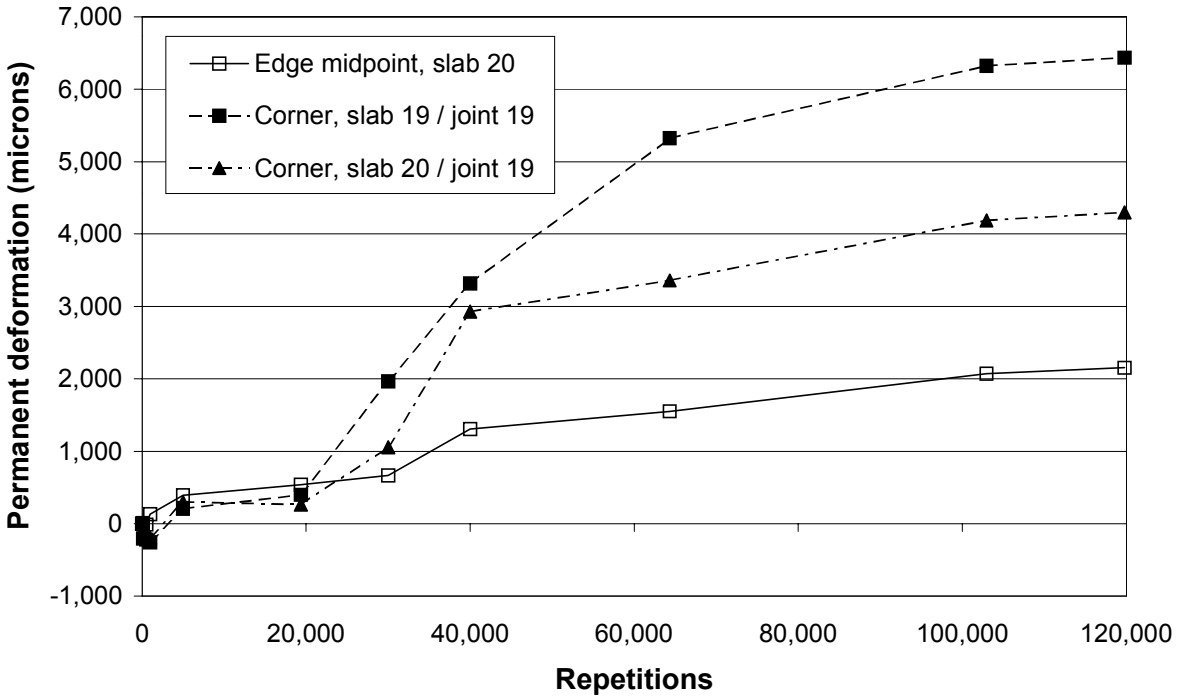

Figure 4.17. EDMD and JDMD permanent deformation, Test Section 524FD.

4.6.3 Load Transfer Efficiency, Test Section 524FD

Table 4.27 shows the change in load transfer efficiency (LTE) with the number of repetitions for Section 524FD. Overall, the LTE calculations show a decrease of the LTE with repetitions up until the first crack was observed on the section at 30,000 repetitions. The initial load transfer efficiency for joint 19 was low (approximately 60 percent), although this was 15 percent higher than observed on Section 523FD.

Table 4.27 Load Transfer Efficiency, Test Section 524FD

Repetitions	Load Transfer Efficiency, LTE (%) Joint 19						Temp Difference (top–bottom), °C
	Slab 20/Joint 19			Slab 19/Joint 19			
	From slab 19 to slab 20	From slab 20 to slab 19	Average	From slab 19 to slab 20	From slab 20 to slab 19	Average	
10	59.1	57.9	*59*	58.9	60.3	60	NA
100	53.3	49.9	*52*	54.4	57.1	56	NA
500	46.0	43.2	*45*	55.1	55.6	55	NA
1,000	46.2	45.4	*46*	51.7	51.8	52	-1.1
5,000	33.8	36.3	*35*	44.3	46.6	45	-0.3
19,353	41.3	40.7	*41*	36.1	36.3	36	-0.8
30,000	91.5	96.2	*94*	104.1*	94.7	99	-0.4
40,000	110.1*	110.1*	*110**	84.1	86.4	85	NA
64,332	104.2*	98.6	*101**	69.1	76.4	73	-0.1
102,935	89.8	92.4	*91*	79.5	76.3	78	-0.1
119,784	91.5	93.5	*92*	79.7	78.0	79	0.1

*LTE over 100% is due to rocking

After cracking occurred near the joint, the LTE actually increased to almost 100 percent. This would not normally be expected, but the slabs were now fully supported and this could be the likely reason. The average LTE stayed close to 80 to 90 percent until the test was completed, even after slab cracking occurred in slab 20.

The average LTE calculated was similar regardless of the direction of wheel travel. As seen on Test Section 523FD, the location of wheel load on the slab was more important in the LTE calculation than the direction of wheel travel. At 30,000 repetitions, the LTE on both slabs

approached 100 percent. There was no change in LTE after the middle slab (slab 20) had developed a larger corner crack.

4.6.4 Strain Gauge Data, Test Section 524FD

Strain gauge measurements were taken in order to monitor the change in dynamic strain within the concrete slab. The dynamic strain has two components: elastic and permanent. Figure 3.2 shows the instrument locations on Section 524FD. Strain gauges were installed at two locations in slab 20: at 2.87 m from joint 20 (near the middle of the slab) and the other one at 0.3 m from joint 19 (close to joint 19). The strain gauges consisted of Dynatest and Tokyo Sokki strain gauges, and their positions in the slab are described below.

- Dynatest in the middle of slab 20: Dynatest #0 (parallel to travel)
- Dynatest at joint 19: Dynatest #12 (perpendicular to travel)
- Tokyo Sokki in the middle slab 20:
  - Direction 1: PMR-X (parallel to travel)
  - Direction 2: PMR-M (45 degrees)
  - Direction 3: PMR-Y (perpendicular to travel)
- Tokyo Sokki at joint 19:
  - Direction 1: PMR-X (parallel to travel)
  - Direction 2: PMR-M (45 degrees)
  - Direction 3: PMR-Y (perpendicular to travel)

The Dynatest strain gauges were installed at 40 mm from the bottom of the slab and the Tokyo Sokki strain gauges were installed at 40 mm from the top of the slab. The distance from the slab edge and joint was 0.3 m.

4.6.4.1 Dynamic Response

Table 4.28 shows the strain gauge results when a moving 45-kN load was applied over the pavement surface. These results are elastic responses of the concrete slab, which was defined as the peak strain (positive or negative) minus the no-load (baseline) strain value. Figure 4.18 compares the maximum strain outputs at the same location. In the figure and table, positive numbers indicate tension and negative readings are compression.

Figure 4.18 shows that the maximum tensile stress occurred with the Dynatest strain at the bottom of the slab while the maximum compressive stress was measured with the PMR-X gauge. Both of these gauges are oriented parallel to the direction of wheel travel. Table 4.28 shows the PMR-X indicated slightly higher strains throughout the test but any deviation in strain gauge depth or slab thickness will cause these two gauges to provide different values. The PMR-M gauges should have the second highest compressive strain since they are oriented 45 degrees to the direction of travel. Finally, because the PMR-Y is oriented perpendicular to the slab edge, it should have a close to zero strain reading.

Figure 4.18 shows that the maximum strains parallel to the wheel are approximately constant until the large corner crack that began at joint 19 intersected the edge of the pavement (see Figure 4.15). At 30,000 repetitions, the corner crack on slab 19 was having no effect on the strain outputs at the slab midpoint edge. However, at 103,000 repetitions, all of the measured strain values at the slab midpoint edge dropped to almost zero strain. This can be attributed to

Table 4.28 Dynamic Strain Response under a 45-kN Test Load, Test Section 524FD

				Maximum Strain Recorded with a 45-kN Load (microstrain) at Given Repetitions										
	Instrument Type, Placement & Orientation			**10**	**100**	**500**	**1,000**	**5,000**	**19,353**	**30,000**	**45,386**	**64,332**	**102,935**	**119,784**
Midspan strain gauges	Dynatest bottom		Tensile (+)	57	60	58	65	62	69	63	62	62	3	63
			Compression (-)	-16	-13	-16	-12	-14	-14	-13	-8	-8	-3	-15
	PMR top	X: parallel	Tensile (+)	7	9	16	10	14	13	12	4	5	3	32
			Compression (-)	-66	-64	-58	-65	-64	-76	-74	-74	-76	-4	-60
		M: 45 degree	Tensile (+)	15	16	22	15	19	18	20	13	15	3	24
			Compression (-)	-33	-32	-29	-37	-34	-41	-37	-39	-38	-4	-26
		Y: perpendicular	Tensile (+)	5	6	8	6	7	8	7	6	7	2	9
			Compression (-)	-8	-3	-2	-3	-3	-3	-4	-3	-3	-4	-7
Corner strain gauges	Dynatest bottom		Tensile (+)	3	3	6	6	4	6	5	2	2	3	4
			Compression (-)	-15	-12	-10	-8	-8	-9	-9	-10	-10	-4	-7
	PMR top	X: parallel	Tensile (+)	15	15	19	15	17	19	20	18	18	3	20
			Compression (-)	-20	-23	-22	-22	-18	-17	-13	-11	-12	-4	-10
		M: 45 degree	Tensile (+)	6	9	0	0	0	9	10	7	7	3	7
			Compression (-)	-33	-31	0	0	0	-34	-29	-21	-20	-4	-16
		Y: perpendicular	Tensile (+)	9	9	0	0	0	10	10	7	7	4	8
			Compression (-)	-11	-12	0	0	0	-13	-13	-8	-7	-6	-6
Temperature (°C)				*17.4*	*17.4*	*18.2*	*17.0*	*18.5*	*18.8*	*19.3*	*20.0*	*20.0*	*20.0*	*20.0*

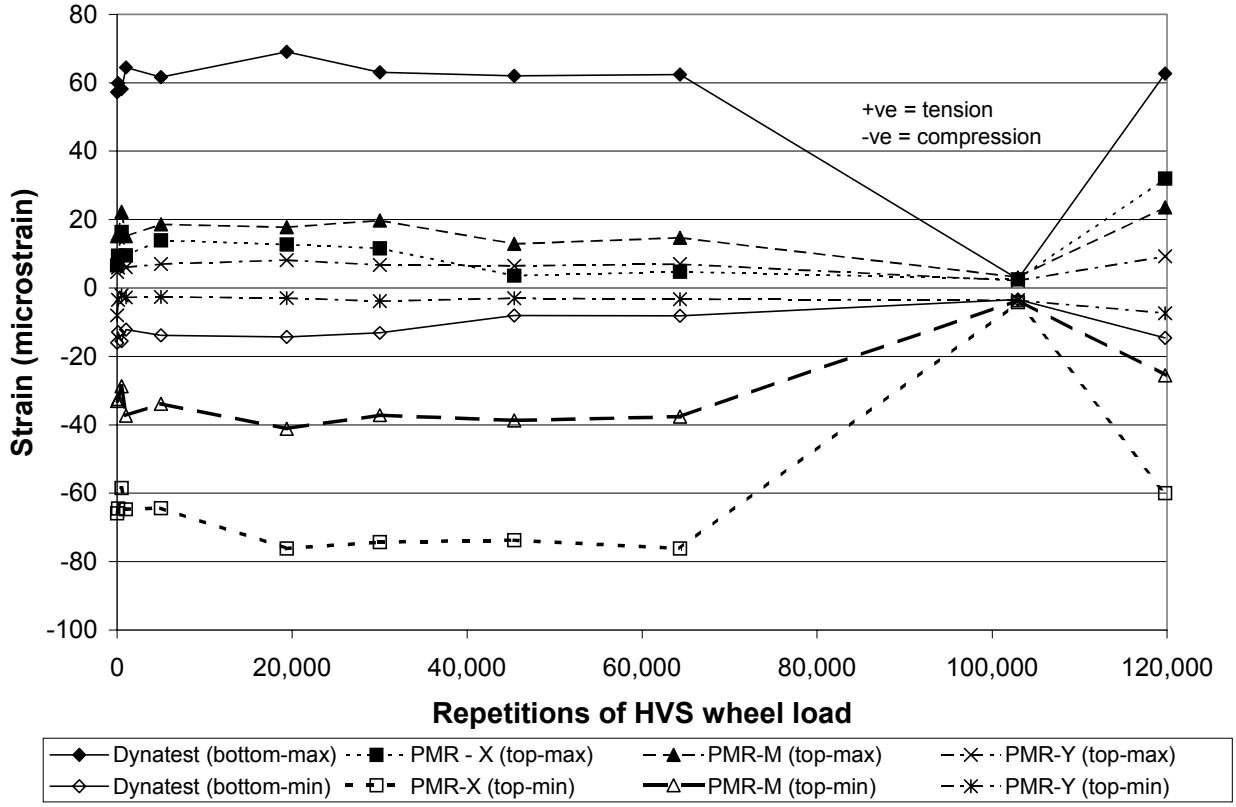

Figure 4.18. Dynamic strain response at edge midpoint, slab 20, Test Section 524FD.

the unloading of the slab due to the relative proximity of the gauges to the newly formed crack. After approximately 20,000 more repetitions (119,784), the elastic strain reading had increased again. This could be a result of more damage accumulating in the vicinity of the gauges.

The measurements at the corner of the slab give small strain values so it is difficult to make any meaningful comment about trends. There appears to be a drop in strain at 103,000 repetitions for PMR-X, which was the same time a corner crack fully developed on slab 20.

4.6.4.2 Permanent Strain Response

The permanent strain readings of the gauges located near the slab 20 midpoint edge and near joint 19 are shown in Table 4.29. Figure 4.19 shows the variations of the strain values for the strain gauges installed at the slab midpoint edge whereas Figure 4.20 shows the static

Table 4.29 Permanent Strain Gauge Response on Slab 20 and at Joint 19, Test Section 524FD

Repetitions	Mid-span Strains, Slab 20 (microstrain)				Corner Strain, Joint 19 (microstrain)				Temperature Difference (top–bottom), °C
	Dynatest Bottom	PMR			Dynatest Bottom	PMR			
		X: Top parallel	M: Top 45 degrees	Y: Top perpendicular		X: Top parallel	M: Top 45 degrees	Y: Top perpendicular	
10	0	0	0	0	0	0	0	0	NA
100	12	27	-9	25	-24	11	30	3	NA
500	-35	-32	-46	-15	-48	-19	30	3	NA
1,000	-13	34	-5	18	0	35	30	3	-1.10
5,000	-68	13	-22	17	-42	40	30	3	-0.30
19,353	-73	-5	-10	-17	-54	42	-9	30	-0.80
30,000	19	70	6	89	-31	79	94	30	-0.40
45,386	-6	68	53	52	44	140	63	72	NA
64,332	13	110	52	68	84	189	80	75	-0.10
102,935	-14	-46	0	-4	-24	203	31	88	-0.10
119,784	-18	-54	5	3	-9	217	41	101	0.10

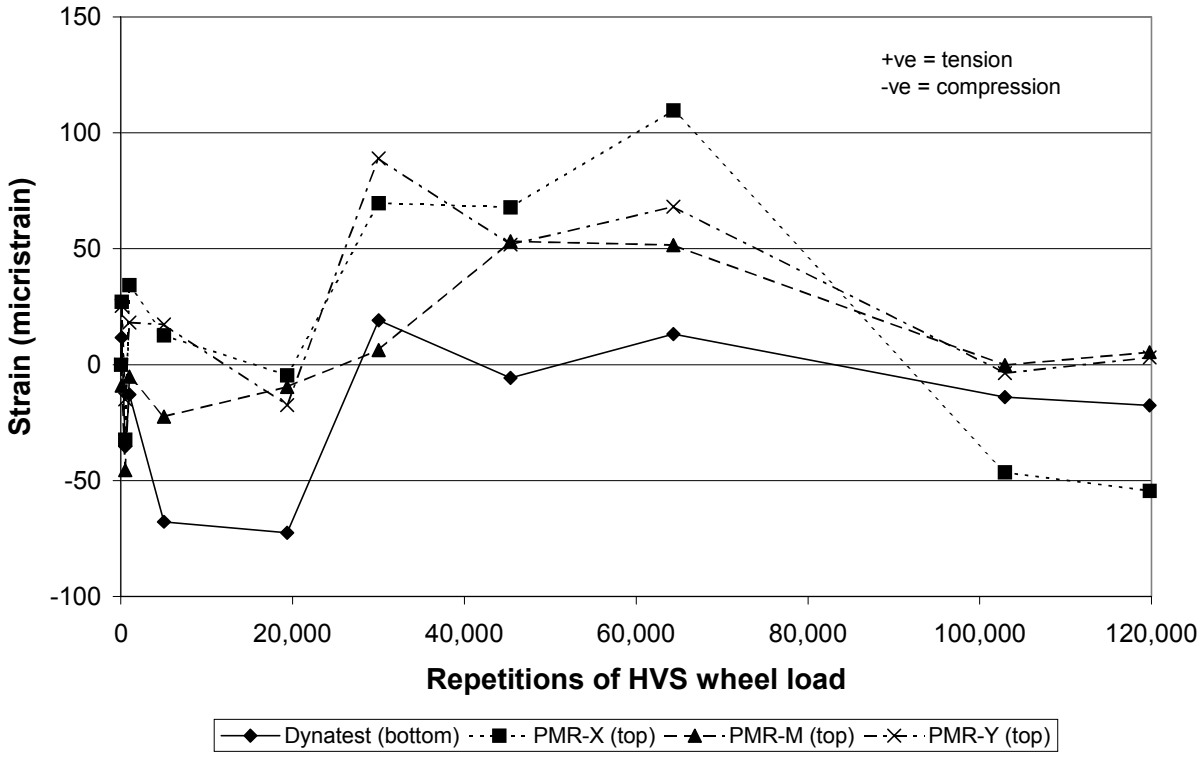

Figure 4.19. Static strain response, slab 20, Test Section 524FD.

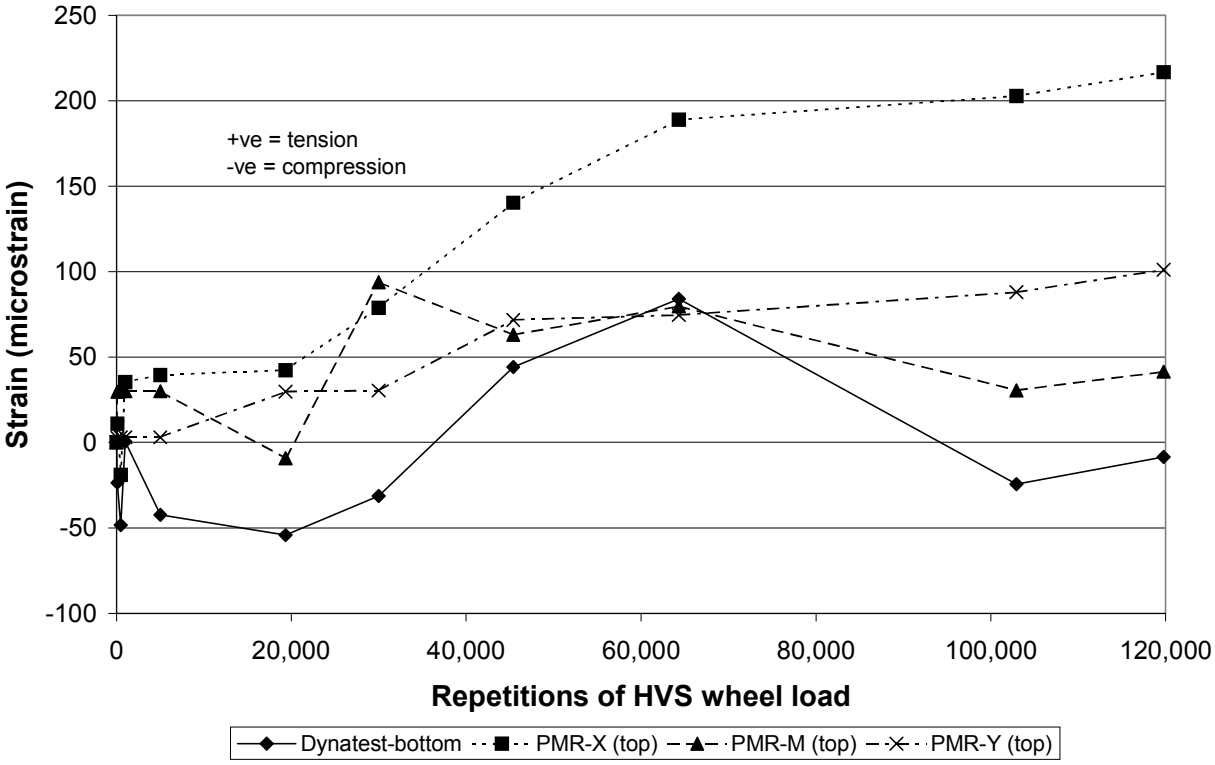

Figure 4.20. Static strain response near joint 19, Test Section 524FD.

responses recorded at joint 19. The permanent strain values from the edge midpoint showed no consistent trend, which indicates that there was no significant permanent strain or micro-cracking near the gauge.

At joint 19, the PMR-X gauge on the top of the slab showed significant permanent strain accumulation compared with the other gauges. The PMR-Y gauge also had a steady increase in permanent strain, but not as large as the PMR-X gauge. The Dynatest and PMR-M gauge did not show any consistent trend in permanent strain accumulation.

The varying results in permanent strain measurements make it very difficult to establish trends. Roesler (1998) found permanent strain results to be highly dependent on the location of the micro cracking area relative to the gauge (*5*).

4.7 Test Section 525FD

HVS Test Section 525FD was conducted on slab numbers 22, 23, and 24 on the South Tangent. Slab 23 (total length of 5.7 m) was fully tested, together with some area on either side of joints 22 and 23. A 45-kN dual wheel load was applied for the entire 5,000 repetitions with the HVS wheel run in the bi-directional trafficking mode. The temperature control box was not used in this test. Photograph 4.26 shows an overhead view of the test section with cracks at the end of HVS trafficking.

4.7.1 Visual Observations, Test Section 525FD

The first crack appeared on the middle slab (slab 23) by 1,000 repetitions. As seen in Photograph 4.26, the HVS produced a corner crack at joint 22 that was approximately symmetrical (1.7 by 1.66 m). This crack was similar to failure modes experienced on the other

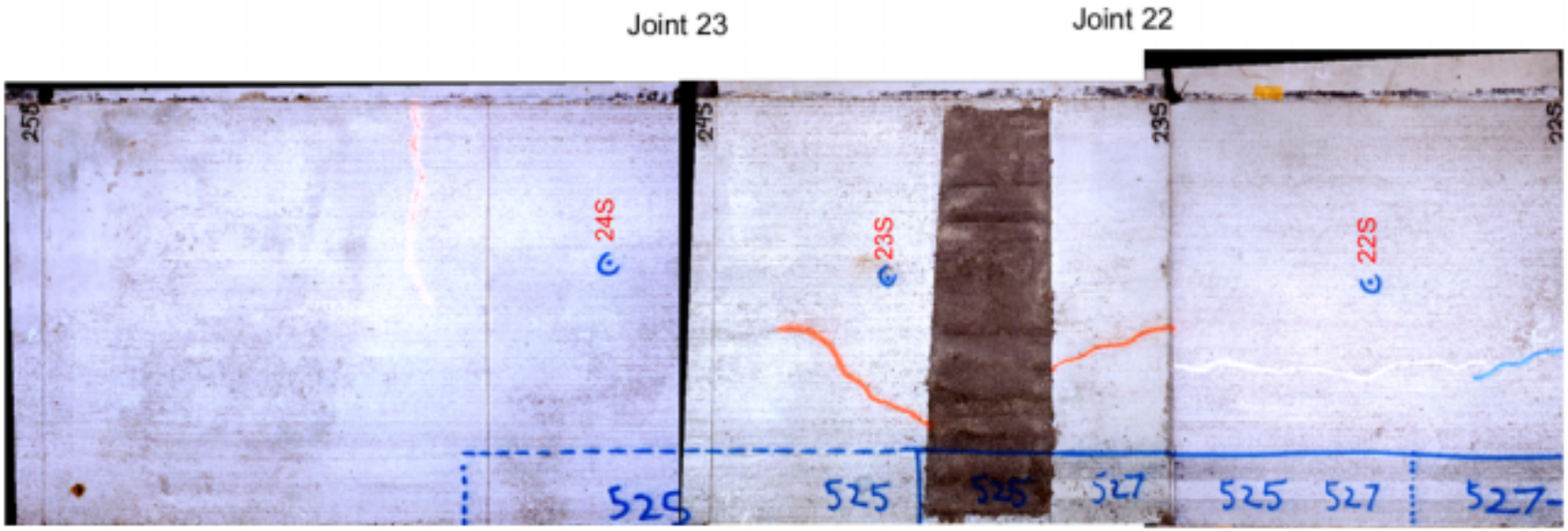

Photograph 4.26. Composite photograph of final crack pattern, Test Section 525FD.

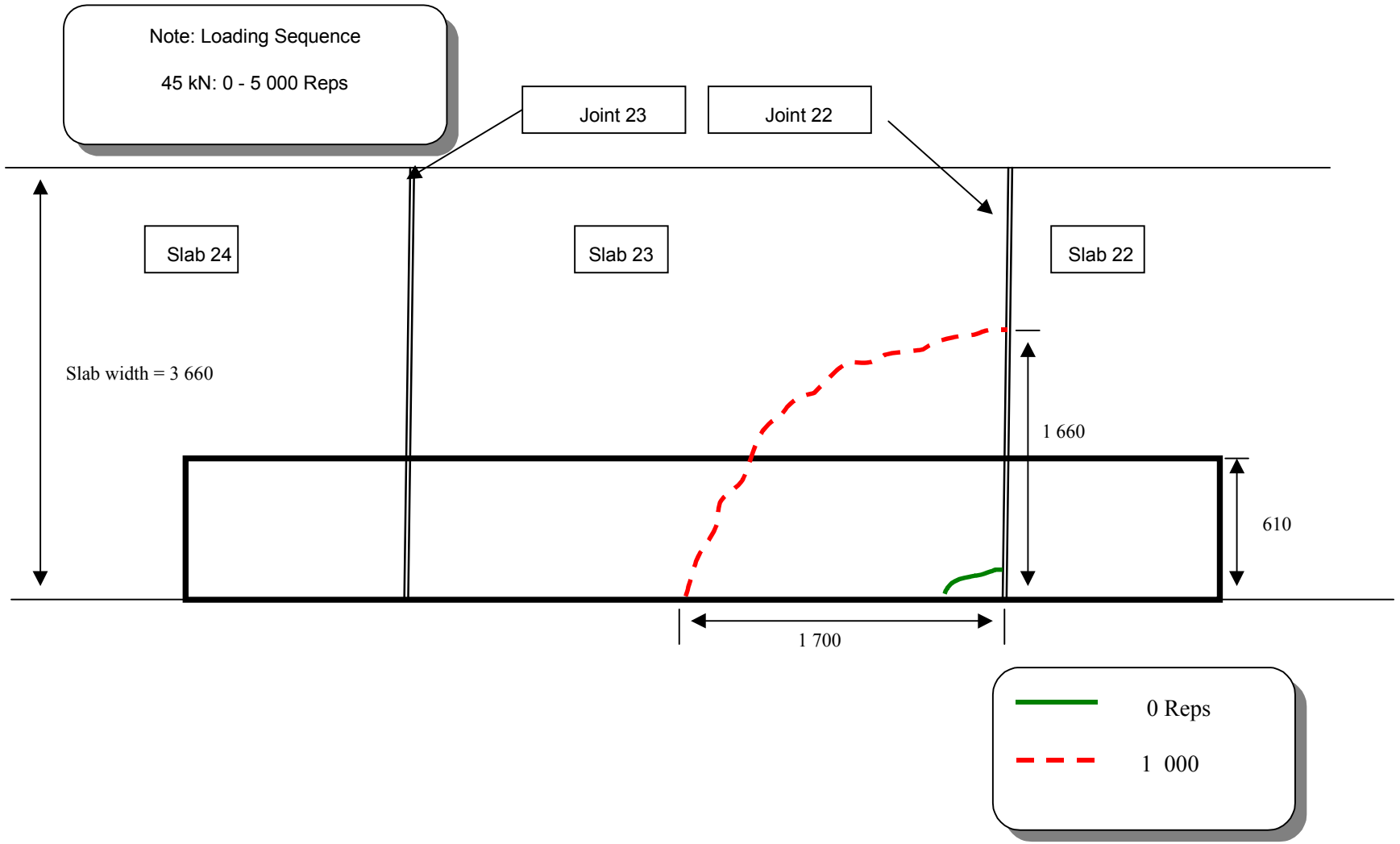

Figure 4.21. Schematic of crack development, Test Section 525FD (not to scale).

Photograph 4.27. Corner crack after 1,000 repetitions, Test Section 525FD.

150-mm thick test sections under accelerated trafficking mode (see Photograph 4.27).

4.7.2 JDMD and EDMD Data, Test Section 525FD

Tables 4.30 to 4.33 show the joint and edge deflection results on Section 525FD; Table 4.34 shows the permanent deformation values. The elastic deflections at the corners and edge were large from the beginning, which gave an indication that the slab would crack earlier than the other 150-mm sections. Tables 4.30 to 4.32 show that there is little difference in the measured slab deflections relative to the direction of wheel travel. The coefficient of variation is less than 5 percent for the majority of the measurements. The deflections at the corner were slightly higher when the wheel was traveling from slab 22 onto slab 23 (the main slab tested), while the edge midpoint deflection was higher when the wheel was traveling from slab 24 onto slab 23.

Table 4.30 Midpoint Edge Deflections under a 45-kN Wheel Load, Slab 23, Test Section 525FD

Repetitions	Midpoint Edge Deflections (m × 10^{-6})					Temperature Difference (top– bottom), °C
	Load Direction		Average	Std. Dev.	C.O.V. (%)	
	From Slab 24	From Slab 22				
10	1,565	1,503	1,534	43.7	2.9	4.0
100	1,559	1,498	1,529	43.3	2.8	4.0
500	1,322	1,258	1,290	45.1	3.5	5.3
1,000	1,435	1,388	1,412	33.5	2.4	5.3
5,000	1,082	1,053	1,067	20.3	1.9	0.3

Table 4.31 Corner Deflections under a 45-kN Wheel Load, Slab 23/Joint 22, Test Section 525FD

Repetitions	Corner Deflections (m × 10^{-6})					Temperature Difference (top–bottom), °C
	Load Direction		Average	Std. Dev.	C.O.V. (%)	
	From Slab 23	From Slab 22				
10	3,132	3,344	3,238	149.8	4.6	4.0
100	3,282	3,431	3,357	105	3.1	4.0
500	3,056	3,178	3,117	85.7	2.7	5.3
1,000	2,690	2,832	2,761	100.5	3.6	5.3
5,000	2,933	3,052	2,993	84.1	2.8	0.3

Table 4.32 Corner Deflections under a 45-kN Wheel Load, Slab 22/Joint 22, Test Section 525FD

Repetitions	Corner Deflections (m × 10^{-6})					Temperature Difference (top–bottom), °C
	Load Direction		Average	Std. Dev.	C.O.V. (%)	
	From Slab 23	From Slab 22				
10	2,962	3,323	3,142	255.7	8.1	4.0
100	3,147	3,401	3,274	179.2	5.5	4.0
500	3,078	3,185	3,132	75.8	2.4	5.3
1,000	1,382	1,441	1,411	41.2	2.9	5.3
5,000	1,333	1,342	1,338	6.2	0.5	0.3

Table 4.33 Average Midpoint Edge and Corner Deflections under a 45-kN Wheel Load, Test Section 525FD

Repetitions	Average Deflections (m × 10^{-6})			Temperature Difference (Top–Bottom),°C
	Edge Midpoint, Slab 23	Corner, Slab 23/Joint 22	Corner, Slab 22/Joint 22	
10	1,534	3,238	3,142	4.0
100	1,529	3,357	3,274	4.0
500	1,290	3,117	3,132	5.3
1,000	1,412	2,725	1,411	5.3
5,000	1,067	2,993	1,338	0.3

Table 4.34 Permanent Deformation Data, Test Section 525FD

Repetitions	Permanent Deformation (m × 10^{-6})			Temperature Difference (Top–Bottom),°C
	Edge Midpoint, Slab 23	Corner, Slab 23/ Joint 22	Corner, Slab 22/Joint 22	
10	0	0	0	4.0
100	228	245	413	4.0
500	876	861	1,486	5.3
1,000	958	1,405	4,722	5.3
5,000	1,781	1,265	5,431	0.3

Figure 4.22 shows the average measured deflections (from Table 4.33) and Figure 4.23 shows the permanent deformations (from Table 4.34). The plot of the elastic corner deflections shows the drop in response after slab 23 cracked at approximately 1,000 repetitions. The corner deflection measured on slab 23 dropped more markedly than the corner deflection measured on slab 22. This is due to the corner crack forming on slab 23, which caused the slab to come into full contact with the base again. The midpoint edge deflection did not decrease appreciably after the corner crack had formed, even though the final crack appeared only 100 mm from the gauge.

From Table 4.33 and Figure 4.22, it can be seen that there were high elastic deflections at the beginning of the test on both sides of joint 22.

After 1,000 repetitions, the development of the corner crack induced a steep increase in the permanent deformation (about 63 percent) and a sudden decrease of deflection (about 56 percent). These observations lead again to the assumption that the slab was curled upward prior to the start of the test and until the corner crack developed. The unsupported condition at the corner caused the formation of a corner crack and consequent slab failure.

The maximum permanent deformation (5 mm) occurred on the slab 23 side of joint 22 (refer to Figure 4.21 and Photograph 4.26 for the location). At the right side of the joint (slab 22), the permanent deformation was 1 mm. The 4-mm differential permanent vertical displacement between slabs at joint 22 shows that a significant faulting effect occurred. As can

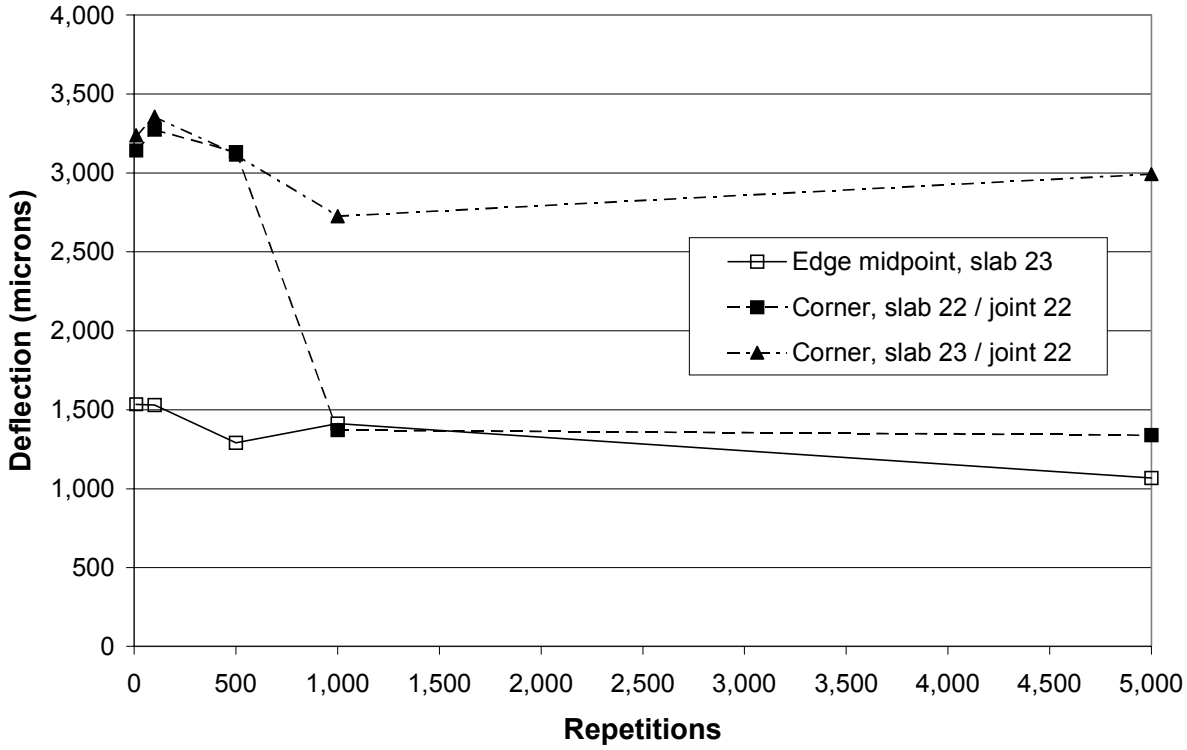

Figure 4.22. JDMD and EDMD deflections, Test Section 525FD.

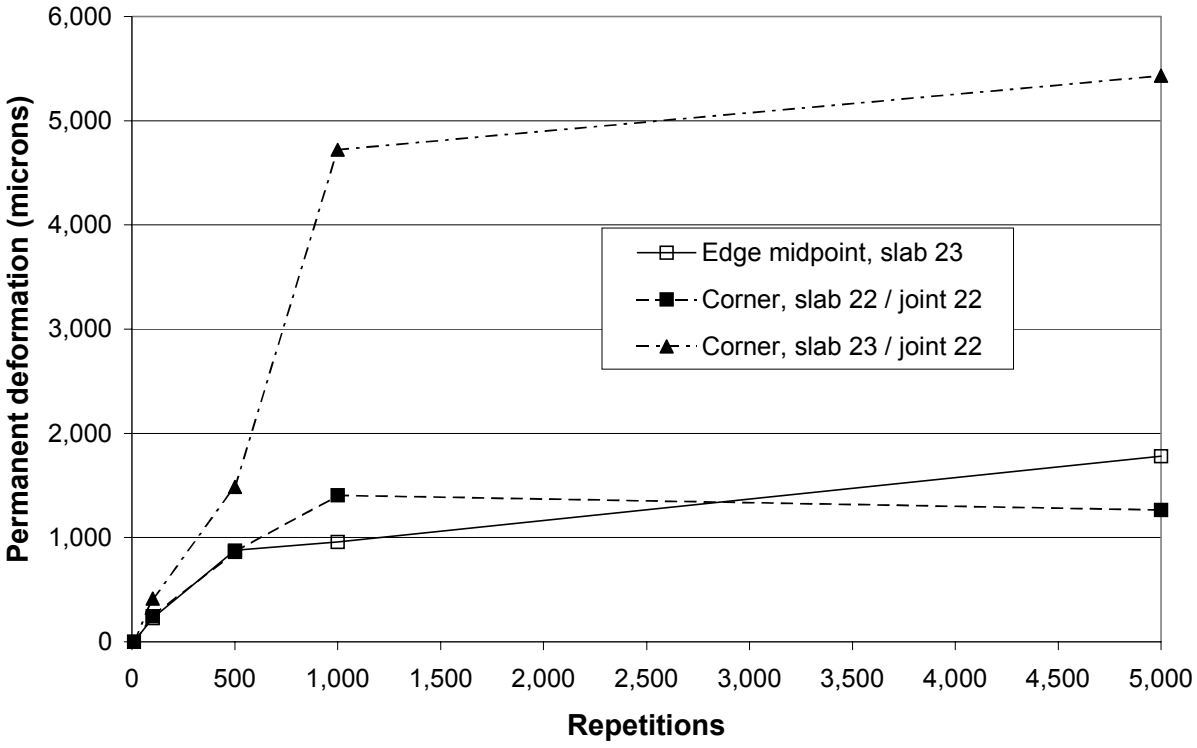

Figure 4.23. JDMD and EDMD permanent deformation, Test Section 525FD.

be seen in Table 4.35, the load transfer efficiency at the beginning of the test was quite poor (about 62 percent). The permanent deformation at the midpoint edge of the middle slab was approximately 2 mm.

Table 4.35 Load Transfer Efficiency (LTE), Test Section 525FD

Repetitions	Load Transfer Efficiency, LTE (%) at Joint 22		Temperature difference (top–bottom), °C
	From Slab 22 to Slab 23	From Slab 23 to Slab 22	
10	26.8	61.7	4.0
100	13.6	54.1	4.0
500	4.8	35.6	5.3
1,000	12.6	111.4	5.3
5,000	25.7	113.2	0.3

Other factors such as voids and concrete stiffness may have also contributed to the rapid failure of the slab since the initial deflections were not much higher than those recorded on the previously tested sections at the same 45-kN load.

4.7.3 Load Transfer Efficiency, Test Section 525FD

The Load Transfer Efficiency values (Table 4.35) calculated when the wheel moved from slab 23 to slab 22 show that the LTE decreased with load applications. After the crack occurred, the results became unreliable.

4.8 Test Section 526FD

HVS testing on Test Section 526FD was conducted on slabs 26, 27 and 28. An 85-kN load was used throughout the test. The test was completed after 23,625 load applications. The temperature control chamber was used.

4.8.1 Visual Observations, Test Section 526FD

The first mid-slab crack developed after only 100 repetitions (Photograph 4.28). This crack is attributable to the higher HVS wheel load of 85 kN compared with the previous tests (45-kN wheel load). After 500 repetitions, a longitudinal crack and a corner crack had developed (Photograph 4.29). The complete section is shown in Photograph 4.30; crack development is presented in Figure 4.24. Slab 28 had a transverse crack prior to the start of HVS testing of Test Section 526FD, caused by shrinkage and curling stresses without any traffic loading.

4.8.2 JDMD and EDMD Data, Test Section 526FD

The elastic deformation values recorded by the JDMD and EDMD are presented in Table 4.36 and the permanent deformation values in Table 4.37.

The midpoint edge and corner cracks that initially appeared on both sides of joint 26 are nearly symmetrical. They were followed by transverse cracks that occurred after 500 repetitions. In addition, they look almost symmetrical with respect to the two cracks that formed on each side of joint 26. Two other cracks formed after 500 repetitions on each side of joint 27.

Figures 4.25 and 4.26 show the deflection and permanent deformation during the test. The high test load (85 kN, see Table 3.4) applied from the beginning of the test caused high deflections compared to the responses measured during previous tests.

A significant decrease in deflection values was noticeable after 500 repetitions. After this point, all measured deflections stabilized at almost the same magnitude (between 1,100 microns and 1,900 microns), as shown in Figure 4.25.

Photograph 4.28. Corner cracks after 100 repetitions, Test Section 526FD.

Photograph 4.29. Crack pattern after 500 repetitions, Test Section 526FD.

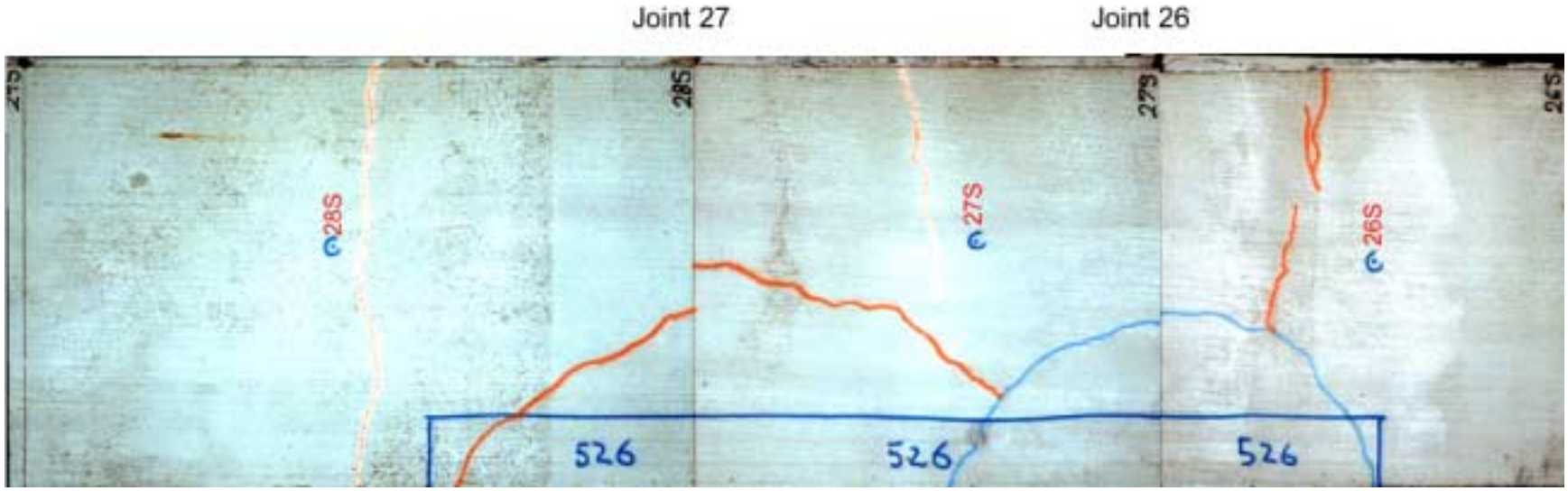

Photograph 4.30. Composite photograph of final crack pattern, Test Section 526FD.

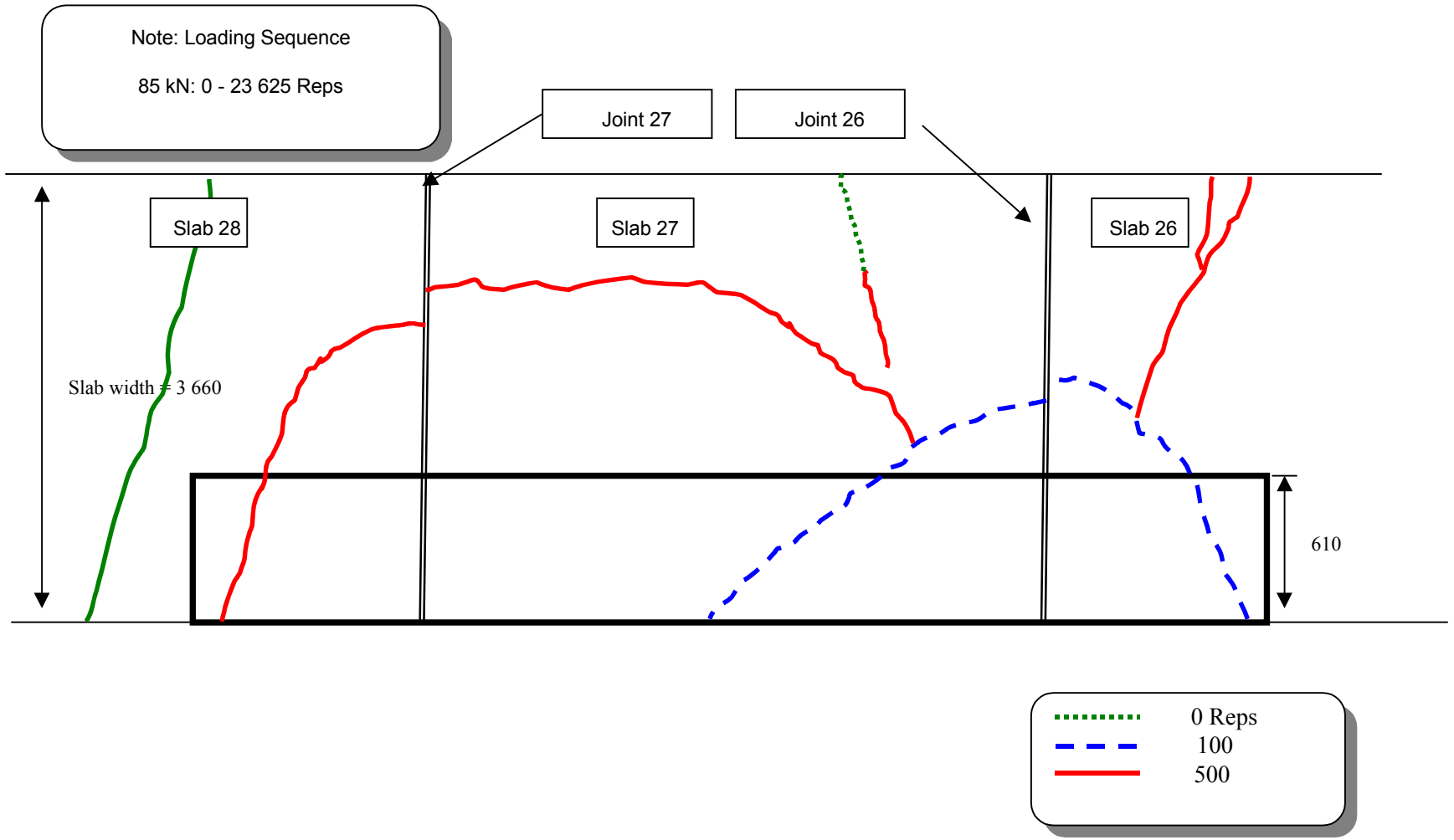

Figure 4.24. Schematic of crack development, Test Section 526FD (not to scale).

Table 4.36 EDMD and JDMD Deflections, 85-kN Test Load, Test Section 526FD

Repetitions	Deflections (m × 10^{-6})			Temperature Difference (top–bottom), °C
	Midpoint Edge, Slab 27	Corner, Joint 26		
		Slab 26 Side	Slab 27 Side	
10	2,131	4,604	4,510	NA
100	2,195	4,169	3,937	-0.6
500	1,095	1,914	1,415	0.2
1,000	1,137	1,838	1,355	0.2
5,000	1,173	1,592	1,361	0.4
10,000	1,148	1,455	1,351	0.9
23,625	1,172	1,496	1,268	NA

Table 4.37 EDMD and JDMD Permanent Deformation, Test Section 526FD

Repetitions	Permanent Deformation (m × 10^{-6})			Temperature Difference (top-bottom) (°C)
	Midpoint Edge, Slab 27	Corner, Joint 26		
		Slab 26 Side	Slab 27 Side	
10	0	0	0	NA
100	417	299	86	-0.6
500	3,066	6,666	7,680	0.2
1,000	3,258	7,116	8,133	0.2
5,000	3,768	7,905	8,906	0.4
10,000	4,166	8,323	9,248	0.9
23,625	4,644	8,691	9,826	NA

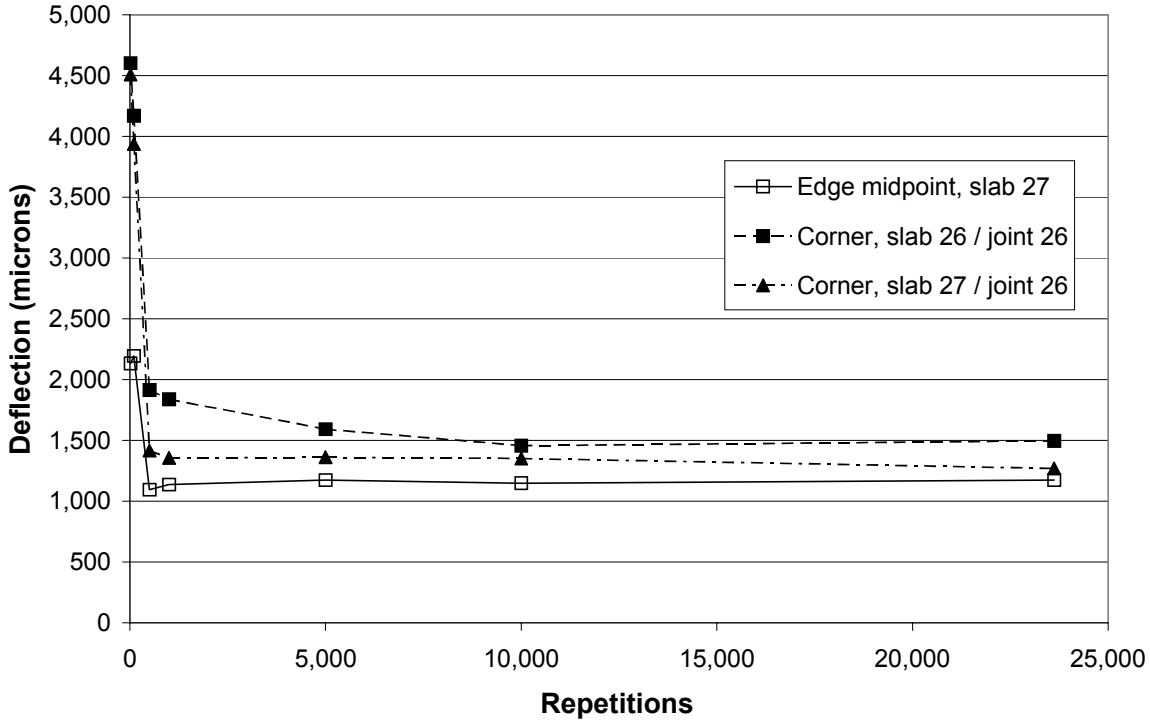

Figure 4.25. EDMD and JDMD deflections, Test Section 526FD.

This is probably an indication that the slab seated on the base course once the corner and transverse cracks developed, and because the seated slab received from more effective support from the base and underlying layers, the deflections decreased. No important variation in the deflection values was observed after 500 repetitions.

The permanent deformation values (Table 4.37) increased considerably at 500 repetitions on both sides of joint 26. The final recorded permanent deformation values at joint 26 were 10 mm on the slab 27 side (middle trafficked slab), and 9 mm on the slab 26 side. At the midpoint edge of the middle slab (slab 27), the permanent deformation was about 5 mm. The permanent deformation values are displayed in Figure 4.26.

The Load Transfer Efficiency values are shown in Table 4.38. The LTE is higher overall when the loaded wheel crosses joint 26 from slab 27 (the main test slab) compared to the opposite direction, and is on the order of 80 to 90 percent throughout. In contrast, the LTE for the other direction is significantly lower throughout, and typically 50 to 65 percent. In comparison with most of the previous tests, these values can still be regarded as relatively high.

As noted on the previous tests, there is usually a difference in LTE between the two sides of the joint, which can only be attributed to the asymmetrical conditions of the slabs on either side of the joint. Contributing factors include differences in crack development, slab support, and deterioration of the joint interlock due to this asymmetry.

4.9 Test Section 527FD

The HVS test on Test Section 527FD was the last in the series of 150-mm concrete tests, and over 1.2 million wheel load repetitions were applied to this section. The entire test was conducted without temperature control.

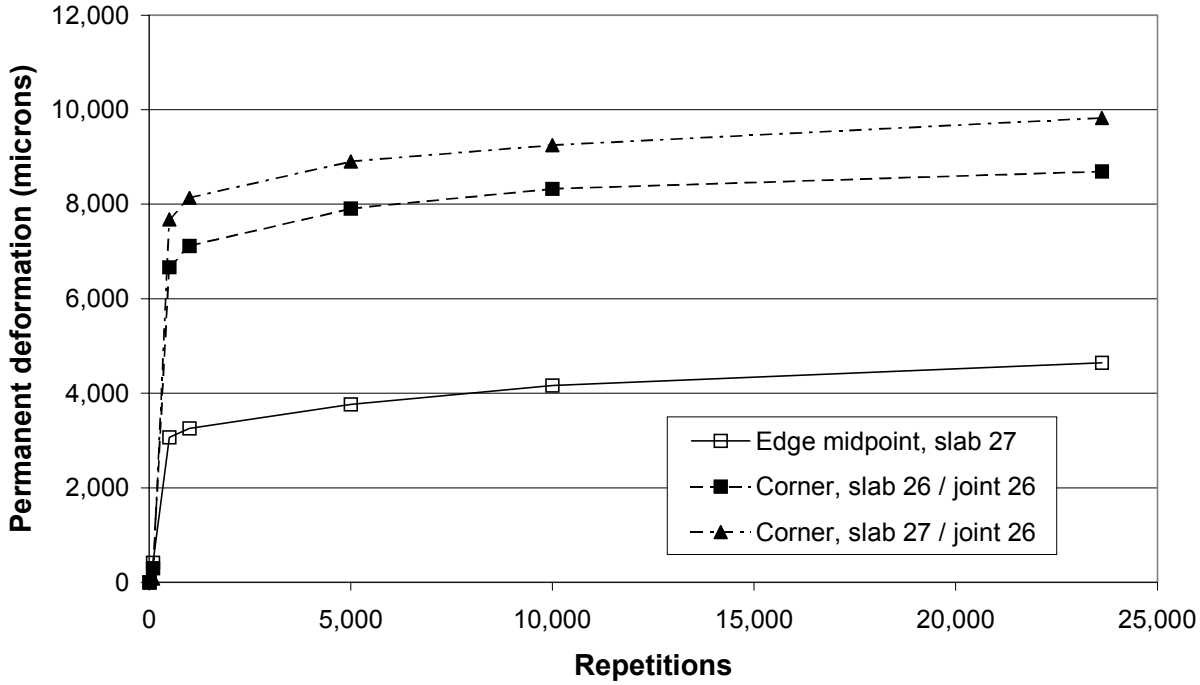

Figure 4.26. Permanent deformation, Test Section 526FD.

Table 4.38 Load Transfer Efficiency (LTE) at Joint 26, Test Section 526FD

Repetitions	Load Transfer Efficiency, LTE (%) Joint 26		Temperature Difference (top–bottom), °C
	From Slab 26 to Slab 27	From Slab 27 to Slab 26	
10	69	75	NA
100	64	91	-0.6
500	49	97	0.2
1,000	49	96	0.2
5,000	65	88	0.4
10,000	78	86	0.9
23,625	68	85	NA

This section was initially trafficked with a 35-kN dual wheel load (to 723,438 repetitions), and the load was then increased to 45 kN for the remainder of the test to a total of 1,233,969 repetitions. The test load levels when deflection measurements were taken were 35 kN for repetitions to 723,438 and 40 kN thereafter. This is normal HVS practice, especially for cemented slab or base pavements: not to use higher test loads when conducting measurements than those applied during the traffic history to ensure that inadvertent damage is not caused during deflection measurements. The 40-kN load represents a half Standard Axle load (variously defined as 80 kN, 8,160 or 8,200kg, or 18,000lb./18 kip) used as the primary standard for deflection measurements.

4.9.1 Visual Observations, Test Section 527FD

Test Section 527FD included slabs 21, 22, and 23. A photograph of the full test section with cracks at the end of HVS trafficking is presented in Photograph 4.31; crack development is presented in Figure 4.27.

4.9.2 JDMD and EDMD Data, Test Section 527FD

The JDMD and EDMD deflection data are presented in Table 4.39 and the permanent deformation data in Table 4.40; these data are presented graphically in Figures 4.28 and 4.29, respectively. A corner crack at slab 23 existed prior to the start of the test (see Photograph 4.32). The crack started at the edge of slab 23 and curled towards joint 22 (between slabs 23 and 22).

Table 4.39 indicates that the deflections were sensitive to temperature differentials within the slab. During the daytime, a positive temperature difference existed (surface temperature warmer than the bottom of the slab) which caused the slab to curl downwards, leading to

increased support at the edges of the slab. In this curled down state (daytime), the recorded deflections were lower than nighttime deflections. During the night, slab curling in the opposite direction occurred (slab curls up at the edges) so that less support was provided at the edges and thus, edge deflections were higher.

Deflections on both sides of joint 21 were broadly similar for the first part of the test (wheel load of 35 kN up to 723,438 repetitions) and in the order of 1,000 microns on the edge and 2,000 to 2,500 microns at the joint (Figure 4.28). This suggests that there was no significant deterioration under the trafficking load, with good slab support and aggregate interlock at the joint being maintained.

When the wheel load was increased to 40 kN, however, the joint deflections dropped noticeably (see Figure 4.28). In addition, deflections measured on each side of the joint differed until the end of the test: those on the slab 22 side (main trafficked slab) were generally higher than those on the slab 21 side.

At the end of the test, deflections on each side of the joint were approximately 1,500 microns. Deflection at the midpoint edge of slab 21 dropped to 350 microns. This may have been due to the cracks that formed on slab 21 at 890,000 repetitions and on slab 22 at 1,133,694 repetitions, which caused the slab to seat and come into full contact with the base layers similar to conditions observed in other tests.

The accumulation of permanent deformation at the joint is shown in Figure 4.29. The trend is similar to that of the elastic deflections. A steady increase in the permanent movement of the slab at all three recorded positions (midpoint slab edge and each side of joint 21) occurred

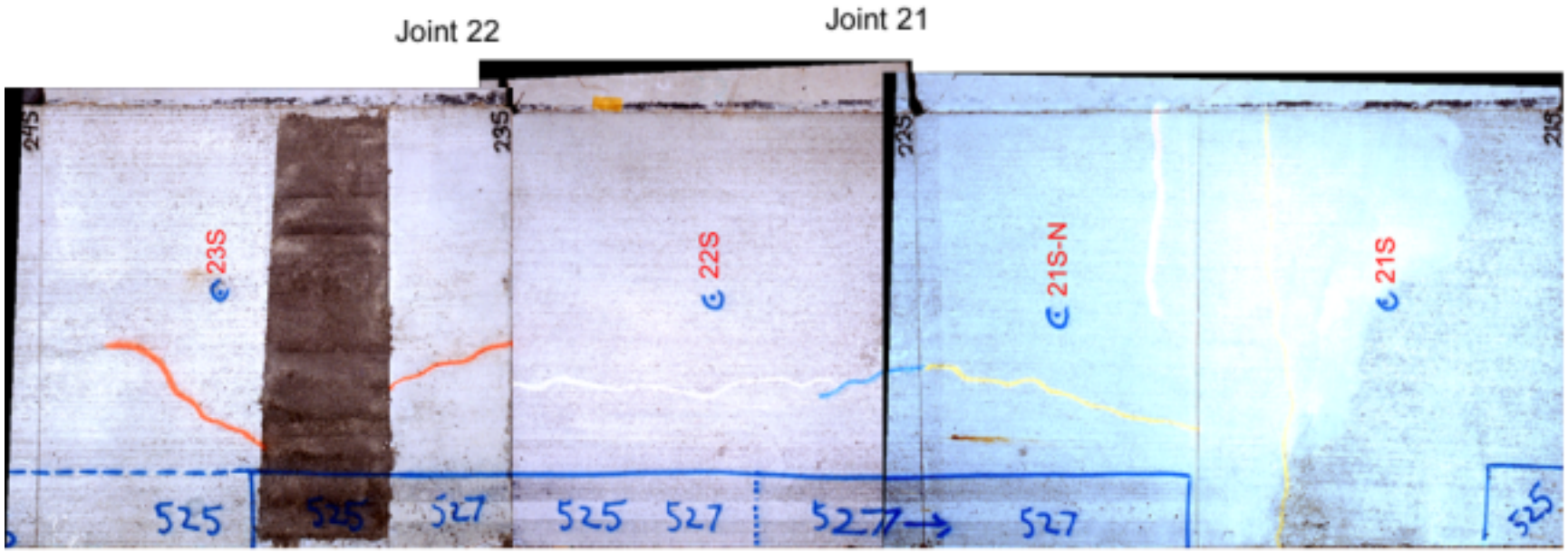

Photograph 4.31. Composite photograph of final crack pattern, Test Section 527FD.

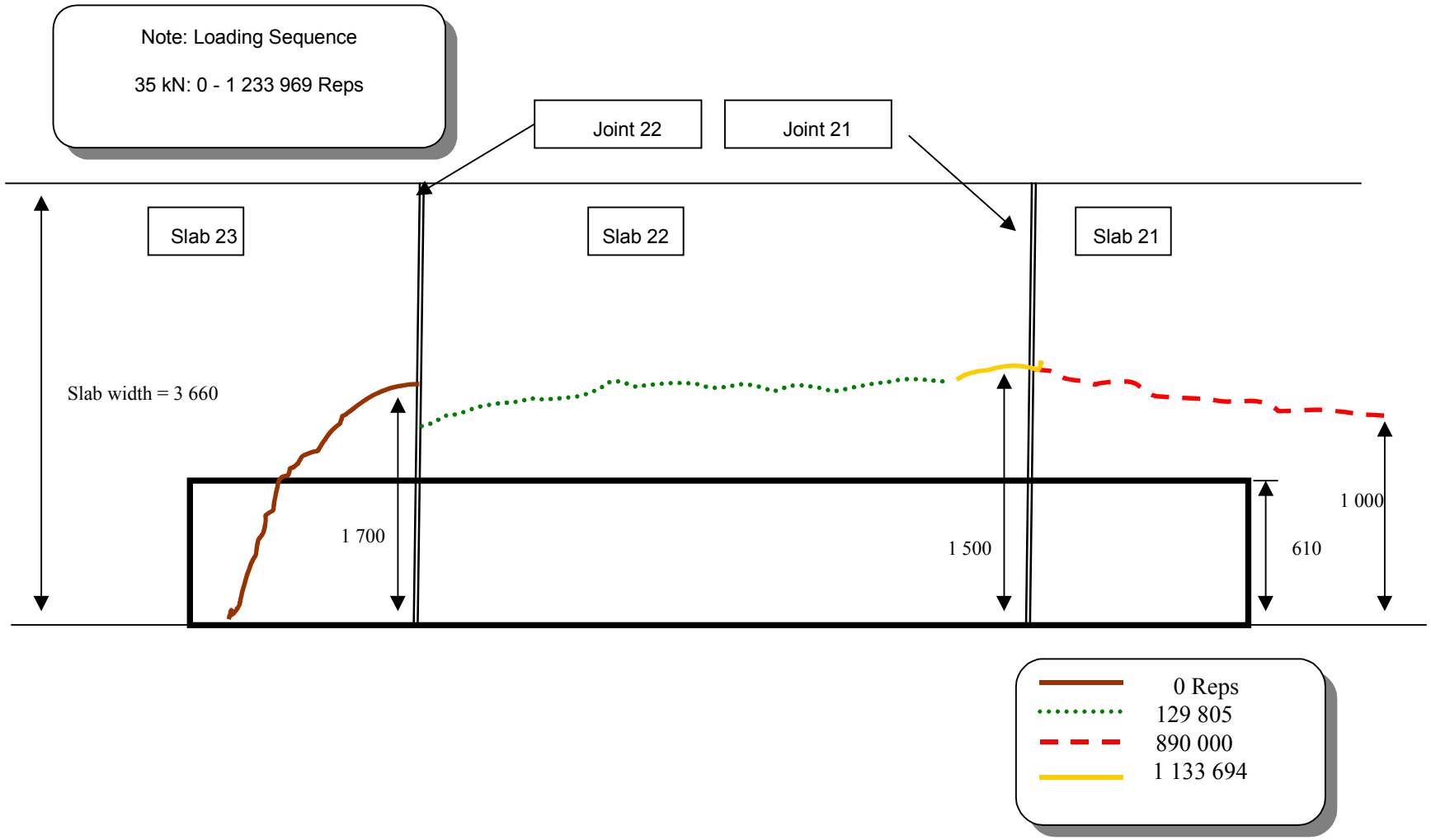

Figure 4.27. Schematic of crack development, Test Section 527FD (not to scale).

Photograph 4.32. Corner crack at start of test, Test Section 527FD.

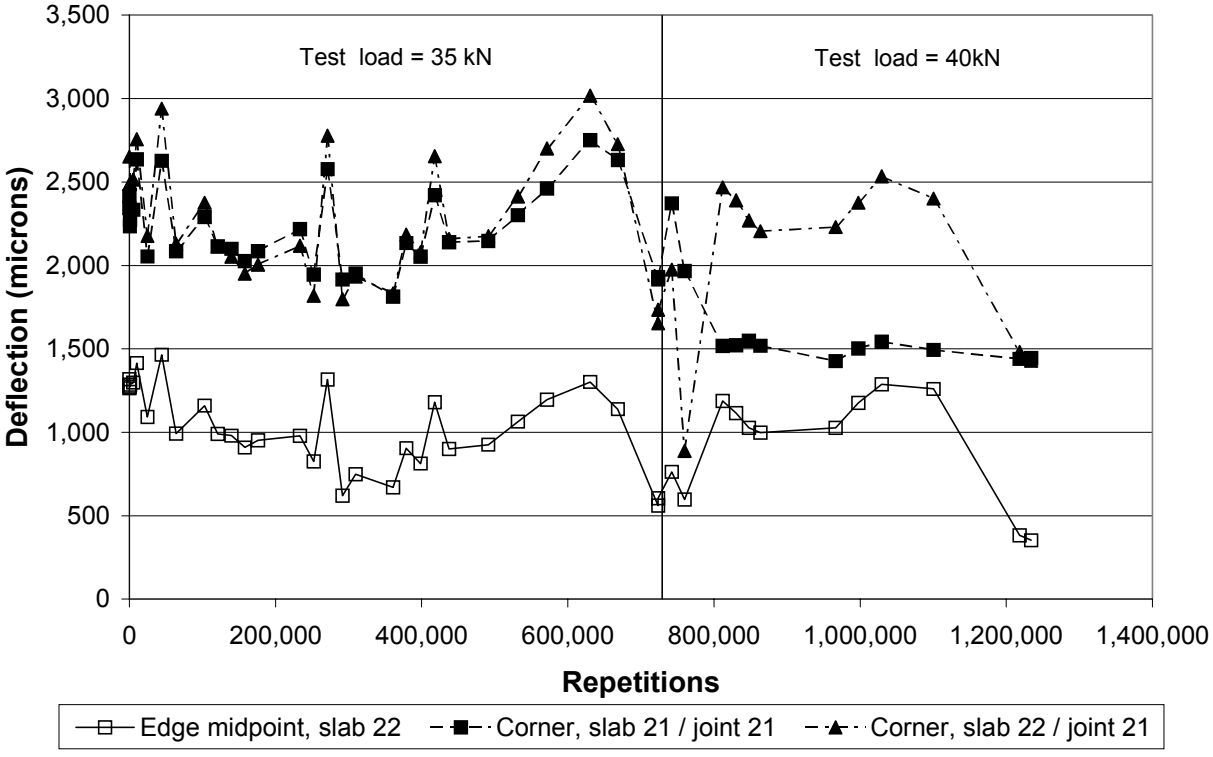

Figure 4.28. EDMD and JDMD deflections, test load = 35 and 40 kN, Test Section 527FD.

Table 4.39 EDMD and JDMD Deflections, Test Load = 35 and 40 kN, Test Section 527FD

Repetitions	Deflection (m × 10^{-6})			Temperature Difference (top-bottom), °C
	Midpoint Edge, Slab 22	Corner, Joint 21		
		Slab 21 Side	Slab 22 Side	
Test load = 35 kN				
10	1,264	2,343	2,485	-0.3
100	1,317	2,415	2,651	-0.3
500	1,274	2,234	2,485	0.0
1,000	1,285	2,273	2,493	0.4
5,000	1,298	2,334	2,515	-1.2
10,000	1,415	2,636	2,757	1.3
24,639	1,092	2,054	2,177	3.4
44,126	1,465	2,627	2,940	NA
63,823	991	2,085	2,130	-0.6
102,913	1,159	2,290	2,376	-3.0
120,837	990	2,114	2,113	0.2
139,543	980	2,100	2,053	3.5
157,820	909	2,025	1,952	3.4
175,869	951	2,085	2,005	2.7
233,374	978	2,218	2,119	-0.5
252,121	826	1,945	1,818	-1.5
271,306	1,316	2,576	2,778	-3.6
291,508	620	1,916	1,798	0.1
309,517	748	1,951	1,933	2.1
360,939	670	1,813	1,832	NA
378,914	905	2,134	2,185	NA
398,313	812	2,052	2,081	0.8
417,729	1,180	2,420	2,655	0.8
437,509	899	2,139	2,159	1.5
490,928	925	2,147	2,176	1.4
531,485	1,064	2,301	2,412	-0.3
571,386	1,195	2,461	2,701	-0.7
630,633	1,301	2,751	3,018	-3.8
668,205	1,139	2,633	2,727	NA
Test load increased to 40 kN				
723,438	560	1,916	1,653	5.8
723,600	604	1,930	1,735	5.7
742,218	763	2,372	1,975	NA
759,493	597	1,967	889	-0.5
811,727	1,187	1,517	2,468	-3.8
830,394	1,115	1,521	2,390	3.5
847,623	1,027	1,548	2,269	-1.3
863,483	998	1,519	2,205	0.3
966,586	1,026	1,427	2,231	1.0
997,540	1,175	1,503	2,375	2.8
1,029,411	1,287	1,542	2,534	5.6
1,100,314	1,259	1,494	2,401	NA
1,218,163	382	1,439	1,482	NA
1,233,969	352	1,445	1,429	NA

Table 4.40 Permanent Deformation, Test Section 527FD

Repetitions	Permanent Deformation (m × 10^{-6})		
	Midpoint Edge, Slab 22	Corner, Joint21	
		Slab 21 Side	Slab 22 Side
10	0	0	0
100	3,280	3,726	955
500	3,358	4,043	1,233
1,000	3,501	4,151	1,308
5,000	3,711	3,819	1,518
10,000	3,764	3,870	1,468
24,639	4,138	4,352	2,053
44,126	3,707	3,581	1,076
63,823	4,555	4,767	2,299
102,913	4,515	4,749	2,113
120,837	4,822	5,102	2,384
139,543	4,854	5,232	2,584
157,820	5,092	5,336	2,737
175,869	4,996	5,232	2,698
233,374	4,971	5,174	2,655
252,121	5,188	5,545	2,990
271,306	4,661	4,810	1,953
291,508	6,040	7,159	4,533
309,517	6,032	7,192	4,644
360,939	6,339	7,628	5,039
378,914	6,139	7,393	4,683
398,313	6,253	7,556	4,801
417,729	5,844	7,166	4,163
437,509	6,168	7,451	4,640
490,928	6,207	7,635	4,662
531,485	6,047	7,444	4,394
571,386	5,897	7,238	4,066
630,633	6,146	7,592	4,558
668,205	6,342	7,757	4,854
723,438	6,844	8,482	5,685
723,600	6,919	8,575	5,841
742,218	6,713	8,074	5,510
759,493	6,389	8,035	4,815
811,727	6,670	10,557	5,036
830,394	6,624	10,560	5,150
847,623	6,766	10,622	5,264
863,483	6,834	10,766	5,403
966,586	6,552	10,870	5,089
997,540	6,445	10,852	5,036
1,029,411	6,332	10,860	4,922
1,100,314	6,296	10,986	4,925
1,218,163	7,663	11,281	6,265
1,233,969	7,656	11,407	6,305

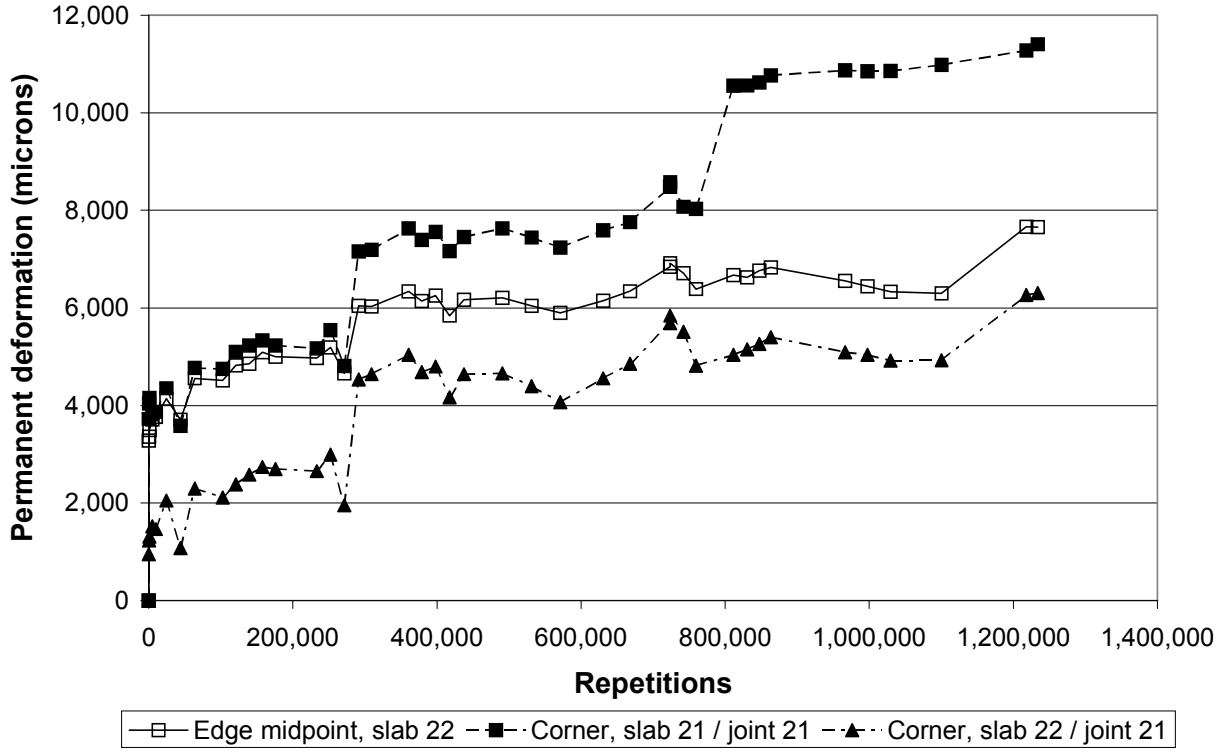

Figure 4.29. EDMD and JDMD permanent deformation, Test Section 527FD.

during the 35-kN loading phase. After the load was increased to 40 kN, an increased rate of permanent deformation was observed. The slab 21 side of joint 21 recorded the most movement, with over 11 mm at the end of the test, compared with the slab 22 side having 6.3 mm.

As seen in Photograph 4.31, slab 23 had a corner crack from the outset, about 1.7 m from the edge. After 129,805 repetitions, a new longitudinal crack at about 1.5 m from the edge of the tested slab (slab 22) formed. Shortly after the load was increased to 40 kN (after 890,000 repetitions), a longitudinal crack formed on slab 21. This new crack developed through the entire width of the slab, also about 1.5 m from the edge.

The Load Transfer Efficiency values for Section 527FD are shown in Table 4.41. For the first 271,306 repetitions, load transfer deteriorates progressively with the increased number of applied load cycles: from approximately 80 percent to 50 percent with the load wheel running

Table 4.41 Load Transfer Efficiency, Test Section 527FD

Repetitions	Load Transfer Efficiency, LTE (%) Joint 21		Temperature Difference (top–bottom), °C
	From Slab 22 to Slab 21	From Slab 21 to Slab 22	
Test load = 35 kN			
10	81.1	69.0	-0.3
100	83.3	64.9	-0.3
500	82.6	62.4	0.0
1,000	82.9	64.2	0.4
5,000	80.0	65.5	-1.2
10,000	81.2	72.7	1.3
24,639	77.4	66.2	3.4
44,126	83.2	65.3	NA
63,823	49.6	46.7	-0.6
102,913	53.9	59.0	-3.0
120,837	53.3	66.8	0.2
139,543	48.1	67.6	3.5
157,820	44.7	64.8	3.4
175,869	40.6	60.3	2.7
233,374	36.8	56.8	-0.5
252,121	29.7	51.5	-1.5
271,306	49.2	42.8	-3.6
291,508	3.2	8.7	0.1
309,517	5.4	4.9	2.1
360,939	10.1	3.8	NA
378,914	12.9	3.6	NA
398,313	12.3	11.1	0.8
417,729	20.3	7.3	0.8
437,509	15.7	25.3	1.5
490,928	23.0	12.6	1.4
531,485	23.0	7.2	-0.3
571,386	32.5	16.5	-0.7
630,633	25.7	15.8	-3.8
668,205	15.8	7.9	NA
723,438	8.9	12.7	5.8
Test load = 40 kN			
723,600	10.0	2.5	5.7
742,218	18.9	11.8	NA
759,493	5.8	1.4	-0.5
811,727	88.6	5.5	-3.8
830,394	73.8	3.7	3.5
847,623	67.0	1.6	-1.3
863,483	50.0	6.0	0.3
966,586	82.4	9.5	1.0
997,540	82.0	11.6	2.8
1,029,411	92.1	15.3	5.6
1,100,314	97.4	10.7	NA
1,218,163	41.0	14.3	NA
1,233,969	33.8	11.3	NA

from slab 21 to slab 22, and from roughly 70 percent to 40 percent when running in the opposite direction.

The readings taken from 291,508 repetitions onward show that a significant change had occurred (LTEs dropping to less than 10 percent initially) consistent with formation of new cracks. It will be noted, however, that this change was not detected in the visual crack observations (Figure 4.29), and that the appearance of visible cracks does not seem to necessarily coincide with any marked changes in LTE.

4.10 Test Section 528FD

The HVS test on Test Section 528FD was the first test conducted on the 200-mm thick concrete sections. It was performed on slabs 34, 35 and 36 on the South Tangent with temperature control. As shown in Figure 4.30, slab 35 (total length of 4.7 m) was fully tested, together with some area on either side of joints 34 and 35 (on slabs 34 and 36).

A 40-kN dual wheel load was used for the entire duration of the test to a total of 83,045 repetitions. An overhead photograph of the test section after HVS trafficking is presented in Photograph 4.33.

4.10.1 Visual Observations, Test Section 528FD

Prior to the start of the HVS test on Section 528FD, no cracks were visible on the test section. After approximately 56,912 load repetitions, a transverse crack developed in the middle slab (slab 35) between both joints (see Photograph 4.34). This crack pattern suggests that the slab failed due to fatigue and if time permitted, the crack may have developed into a corner

break. This crack extended with time and the final crack pattern can be seen in Figure 4.30 and Photograph 4.35.

4.10.2 JDMD and EDMD Data, Test Section 528FD

Two Joint Displacement Monitoring Devices (JDMDs) were placed on either side of joint 34 (between slabs 34 and 35) and one Edge Displacement Monitoring Device (EDMD) was placed on the edge of slab 35 at its midpoint. The results of the maximum deflection at the edge of the midpoint edge of the middle slab, as well as the corner edge deflections on either side of joint 34 are summarized in Table 4.42 and shown in Figure 4.31.

A significant increase in all deflections was recorded between the first and second set of readings (nominally 10 and 3,807 repetitions respectively). Broadly, all deflections tripled during this trafficking period. This is in marked contrast to previously observed behavior where deflections tended to decrease, attributable to better seating of the slab with trafficking and crack formation, and therefore suggests that the HVS trafficking disturbed the original slab seating and support without cracking the slab. It is possible that the short center slab was cracking.

After the transverse crack developed at approximately 57,000 repetitions, the midpoint edge deflections increased from 844 microns to 1,028 microns. This represents a 21 percent increase in the deflection at the midpoint edge. Similarly, the deflections on each side of joint 34 increased 15 to 18 percent.

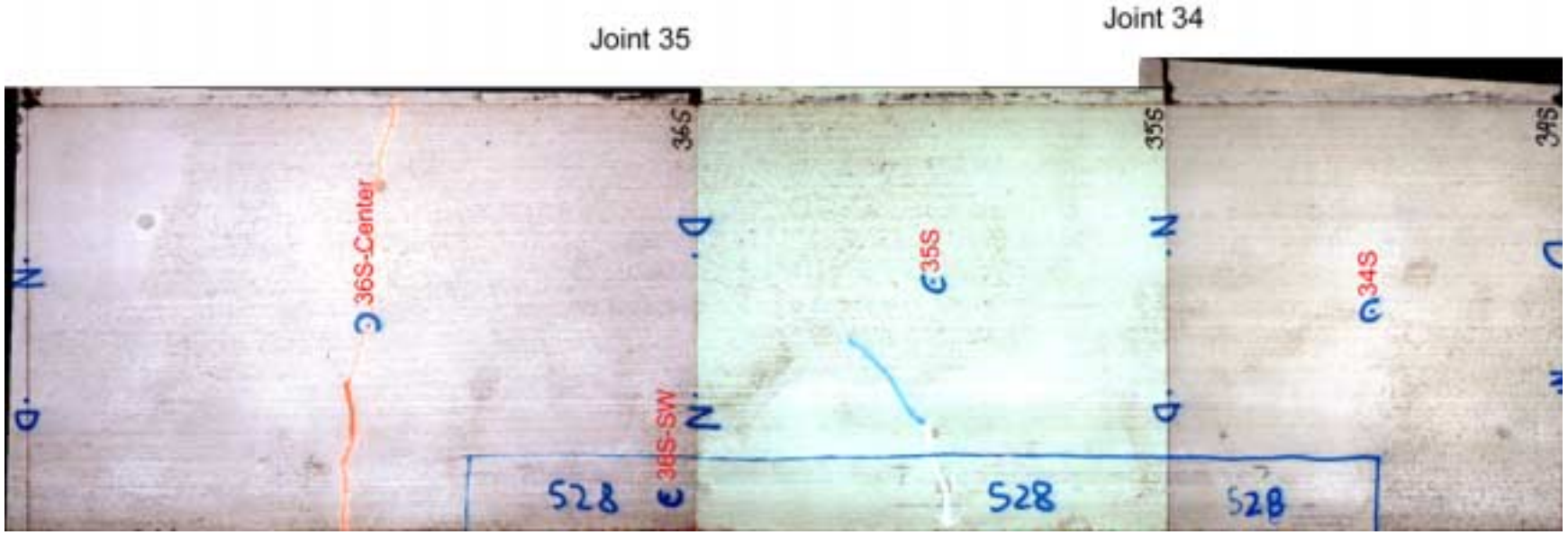

Photograph 4.33. Composite photograph of final crack pattern, Test Section 528FD.

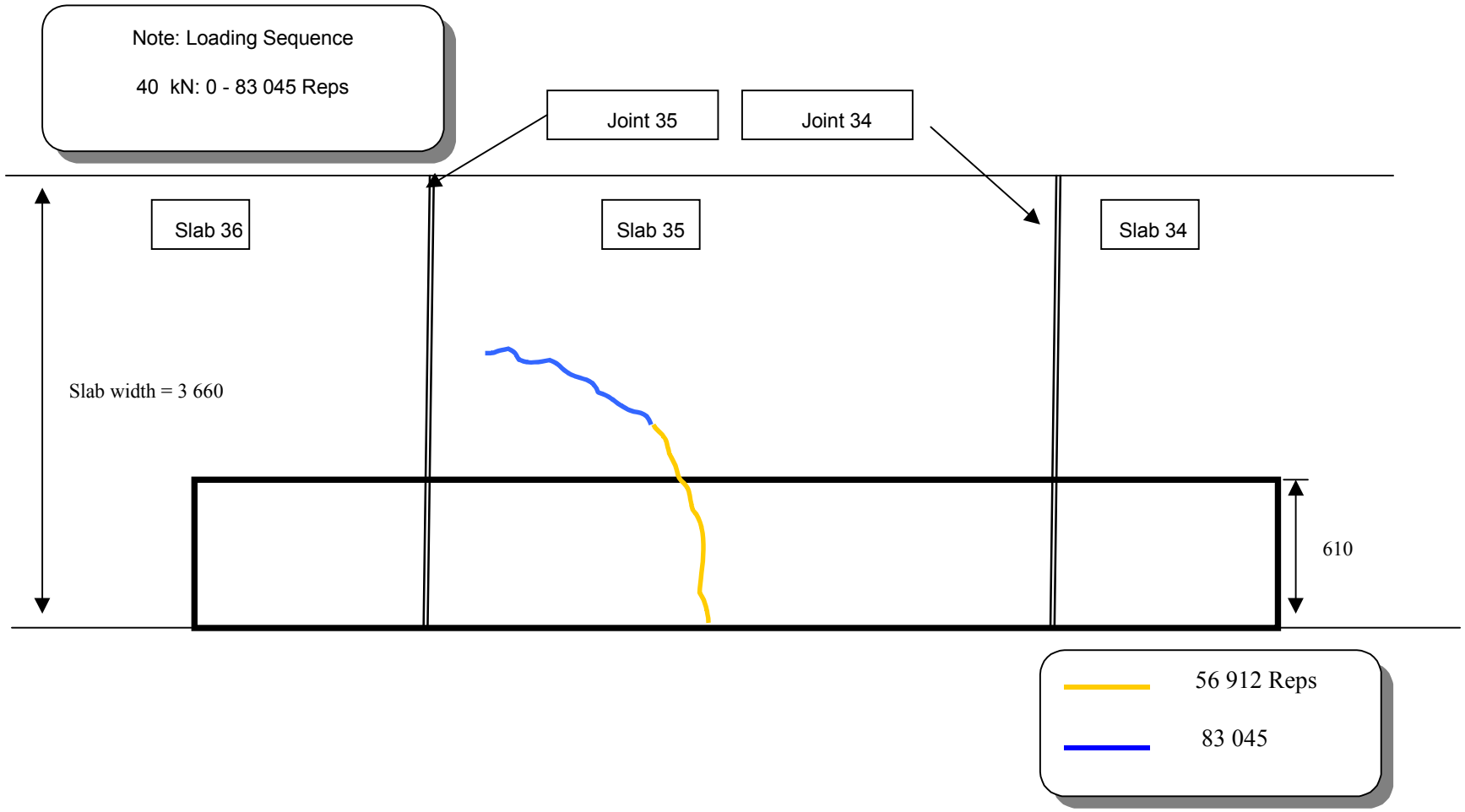

Figure 4.30. Schematic of crack development, Test Section 528FD (not to scale).

Photograph 4.34. Transverse crack after 52,000 repetitions, Test Section 528FD.

Photograph 4.35. Final crack pattern after 83,000 repetitions, Test Section 528FD.

Table 4.42 EDMD and JDMD Deflections, Test Load = 40 kN, Test Section 528FD

Repetitions	Deflection (m × 10^{-6})			Temperature Difference (top–bottom), °C
	Midpoint Edge, Slab 35	Corner, Joint34		
		Slab 35 Side	Slab 34 Side	
10	287	434	602	NA
3,807	819	1,287	1,751	-0.7
15,554	755	1,174	1,777	-0.2
27,347	958	1,324	1,954	-1.0
30,783	844	1,753	1,751	3.0
75,227	1,028	2,031	2,072	-1.1
83,045	992	1,951	2,066	-1.3

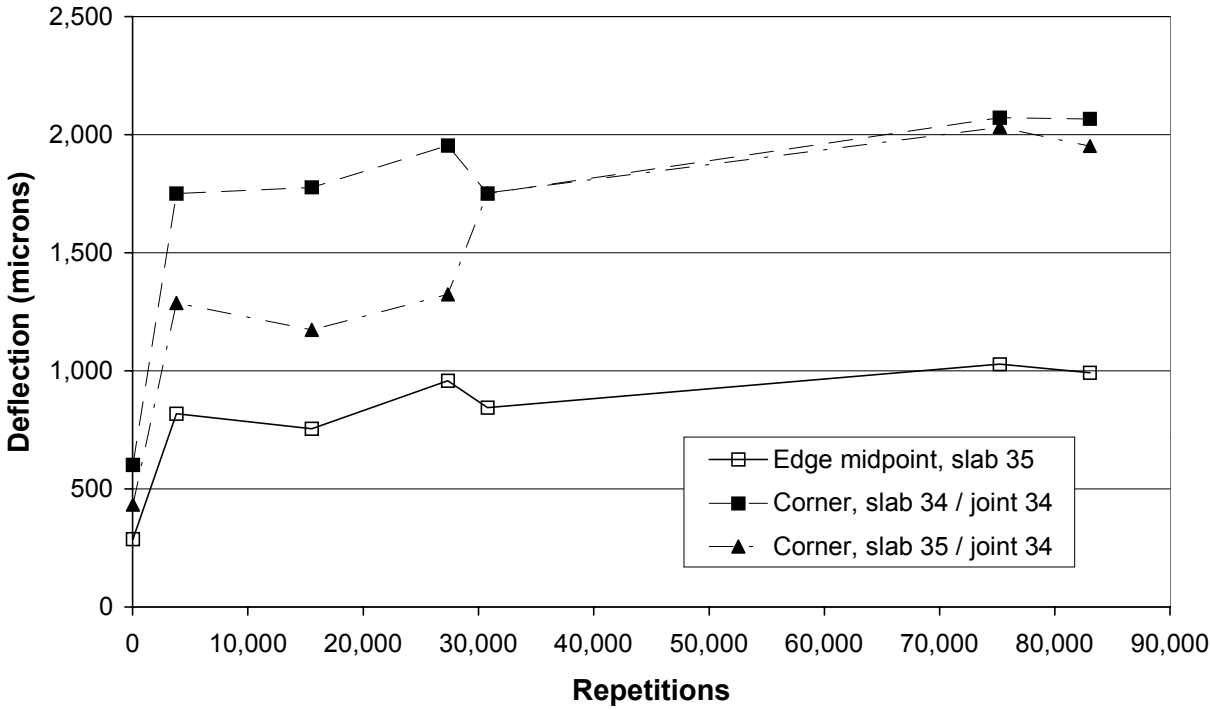

Figure 4.31. EDMD and JDMD deflections, test load = 40 kN, Test Section 528FD.

4.10.3 Load Transfer Efficiency, Test Section 528FD

The Load Transfer Efficiency (LTE) was calculated at joint 34 (the joint between slab 35 and slab 34), and the results are summarized in Table 4.43. It was calculated for the HVS wheel running in both directions. LTE is defined as the ratio of the deflection on the unloaded slab to the maximum deflection on the loaded slab at the joint.

Table 4.43 Load Transfer Efficiency at Joint 34, Test Section 528FD

Repetitions	Load Transfer Efficiency, LTE (%), Joint 34		Temperature Difference (top–bottom), °C
	From Slab 35 to Slab 34	From Slab 34 to Slab 35	
10	82.3	21.9	NA
3,807	86.3	31.9	-0.7
15,554	116.6	41.3	-0.2
27,347	100.7	31.9	-1.0
30,783	71.7	67.8	3.0
75,227	39.7	30.0	-1.1
83,045	42.2	22.9	-1.3

The LTE was always higher when the HVS loaded wheel approached the joint from slab 35 (the main trafficked slab) than when it approached from the opposite side. These results suggest that the crack which had formed at the bottom of the saw-cut joint is not perfectly vertical, propagated down toward the inner slab (35), thus providing more support (load transfer) when the load is approaching from slab 35.

It would be assumed that as the test progressed, the aggregate interlock between the two slabs would deteriorate causing a decrease in LTE. From Table 4.43 this tendency is not clearly apparent, possibly highlighting the fact that load transfer also depends on support conditions, cracking, and temperature/environmental conditions.

4.10.4 Strain Gauge Data, Test Section 528FD

Strain measurements were taken at two locations stated previously in Section 3.2. The gauges in the middle of the center slab (slab 35) did not produce any reliable results and the data were disregarded. The strain gauge adjacent to joint 35 was the only gauge that indicated significant differences in strain levels within the slab. However, the crack pattern suggests that

these strain levels had no direct correlation to the failure of the slab. The maximum tensile strains are summarized in Table 4.44.

Table 4.44 Dynamic Strain Data, Test Load = 40 kN, Test Section 528FD

Repetitions	Maximum Tensile Strain (microstrain)			
	Dynatest	PMR X	PMR M	PMR Y
10	0.0	231	0.0	0.0
3,807	359	92	166	805
15,554	198	103	150	890
27,347	388	69	122	795
30,783	300	57	358	513
75,227	284	95	130	884
83,045	267	64	408	514

4.11 Test Section 529FD

HVS Test Section 529FD was completed on slabs 30, 31 and 32 on the South Tangent, with the 8 ×1 m HVS test section located so that slab 31 was tested along its entire edge. The test started with a 40-kN dual wheel load, which was kept constant to 88,110 repetitions, after which it was increased to 60 kN for an additional 264,214 repetitions. The test was stopped at 352,324 load repetitions. The crack pattern, as it developed with time, can be seen in Figure 4.32. A composite photograph of Test Section 529FD can be seen in Photograph 4.36.

4.11.1 Visual Observations, Test Section 529FD

After 88,110 40-kN load repetitions and another 142,020 60-kN load repetitions (totaling 230,130 load applications), a corner crack developed on slab 30 which is directly adjacent to the middle slab (slab 31) (see Photograph 4.37). After an additional 92,403 60-kN load repetitions, a longitudinal corner crack developed at joint 30 and propagated toward the slab edge midpoint of slab 31. Finally, after 14,997 more repetitions at 60 kN, the crack initiating from joint 31 developed into a longitudinal and transverse break (Photograph 4.38).

4.11.2 JDMD and EDMD Data, Test Section 529FD

Two Joint Displacement Monitoring Devices (JDMDs) were placed on either side of joint 31 (between slabs 31 and 32) and one Edge Displacement Monitoring Device (EDMD) was placed on the edge at the midpoint of slab 31. The results are summarized in Table 4.45 for the 40-kN test load and Table 4.46 for the 60-kN test load.

The results are shown in Figure 4.33 (40-kN test load) and Figure 4.34 (60-kN test load). The joint where the deflections were monitored (joint 31) was not the joint where corner breaks occurred, and the only significant trend is that the deflections increase with increasing repetitions.

4.11.3 Load Transfer Efficiency, Test Section 529FD

The Load Transfer Efficiency (LTE) was calculated at joint 31, and the results are summarized in Table 4.47. LTE was calculated for the HVS wheel running in both directions.

From 29,000 load repetitions (when the LVDT was corrected) to the end of the loading cycle, there is little to suggest that any significant change in LTE occurred. There was, however, a marked difference in the values for the two directions. In the case of wheel travel from slab 32 to slab 31, the LTE remained in the order of 110 to 120 percent throughout. In contrast, crossing the joint in the opposite direction gave LTEs typically from 10 to 30 percent.

It is conjectured that the sawed joint did not propagate straight down to the base. It appears that the crack propagated down toward slab 32, which is directly to the left of the mid-slab (slab 31).

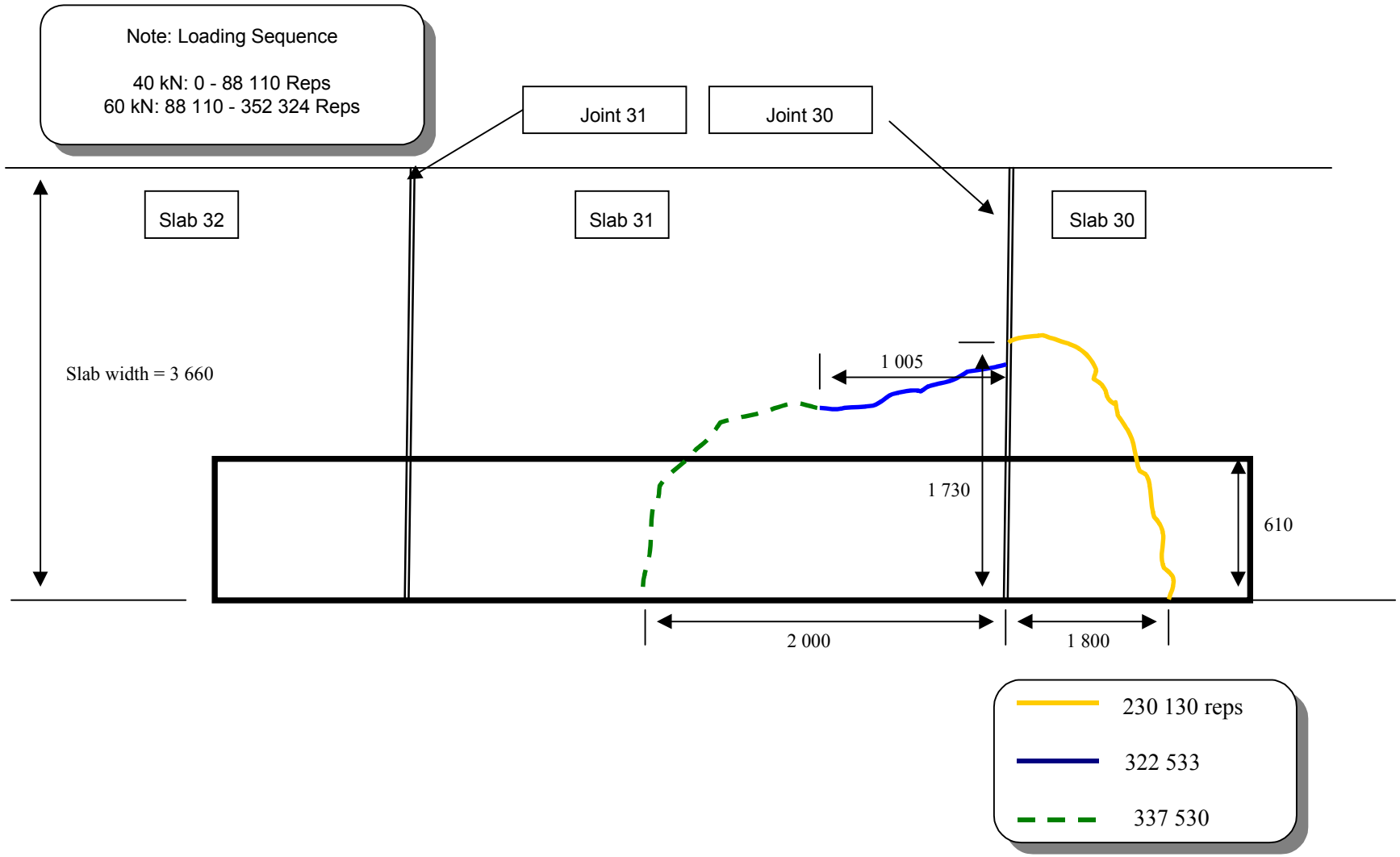

Figure 4.32. Schematic of crack development, Test Section 529FD (not to scale).

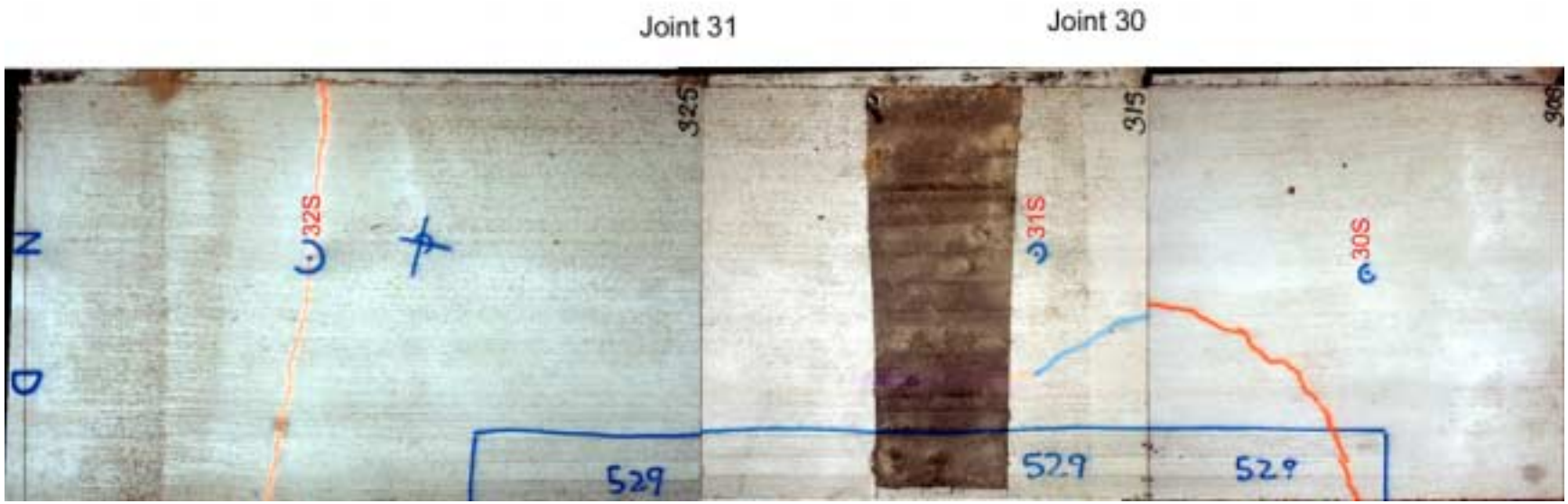

Photograph 4.36. Composite photograph of final crack pattern, Test Section 529FD.

Photograph 4.37. Corner crack after 230,000 repetitions, Test Section 529FD.

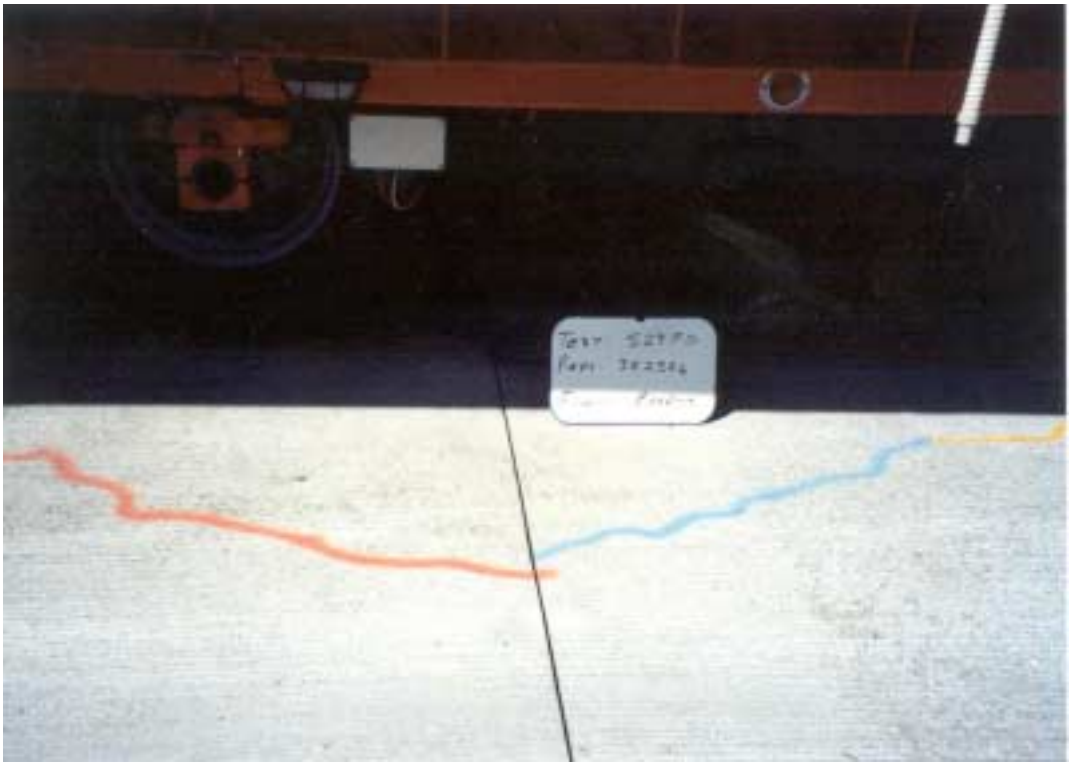

Photograph 4.38. Final crack pattern after 352,324 repetitions, Test Section 529FD.

Table 4.45 EDMD and JDMD Deflections, Test Load = 40 kN, Test Section 529FD

Repetitions	Deflection (m × 10^{-6})			Temperature Difference (top–bottom),°C
	Midpoint Edge, Slab 31	Corner, Joint 31		
		Slab 32 Side	Slab 31 Side	
10	188	748	11	7.5
3,641	667	1,249	11	5.5
16,641	779	1,388	9	2.4
29,015	840	1,646	784*	1.3
43,090	781	1,357	815	7.1
88,110	855	1,597	812	2.4

*Reset LVDT due to instrument failure

Table 4.46 EDMD and JDMD Deflections, Test Load = 60 kN, Test Section 529FD

Repetitions	Deflection (m × 10^{-6})			Temperature Difference (top–bottom), °C
	Midpoint Edge, Slab 31	Corner, Joint 31		
		Slab 32 Side	Slab 31 Side	
0	951	1,725	903	2.4
2,861	950	2,048	1,068	3.4
14,985	1,060	1,868	1,081	2.0
17,646	964	2,015	1,119	3.5
30,368	1,050	1,771	1,097	2.9
46,114	1,165	2,082	1,230	0.1
61,743	1,182	2,274	1,417	-1.4
109,788	1,127	1,910	1,117	0.6
126,306	906	1,646	1,050	1.6
142,020	824	1,621	1,176	2.8
157,811	885	1,572	1,122	2.2
174,249	1,023	2,100	1,178	
221,140	970	2,167	1,262	1.1
234,423	975	2,248	1,299	0.7
249,420	899	2,322	1,359	-1.1
264,214	907	2,339	1,325	-0.5

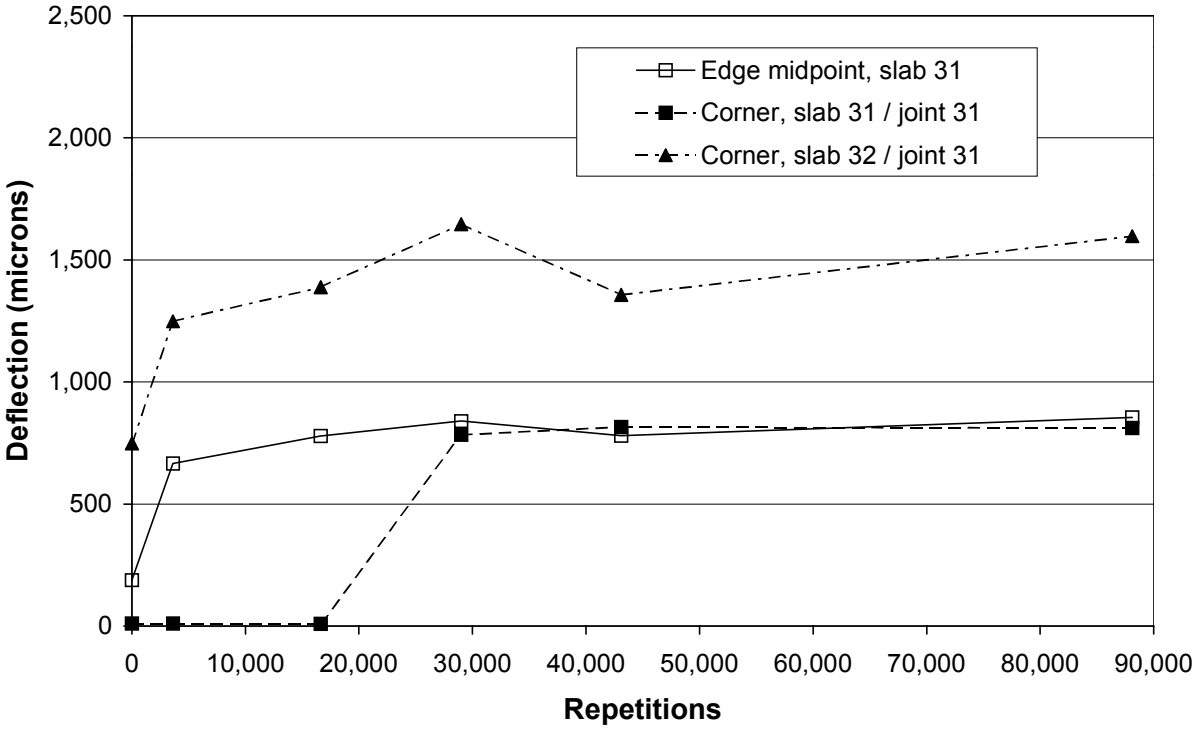

Figure 4.33. Elastic surface deflections, test load = 40 kN, Test Section 529FD.

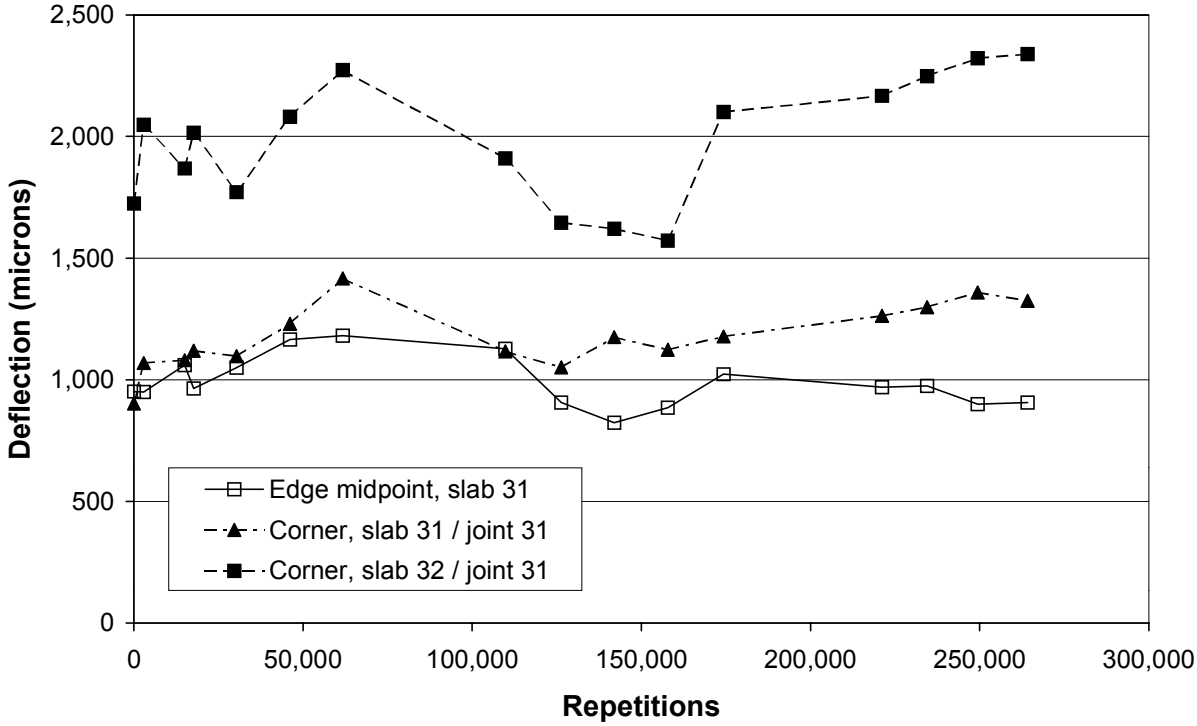

Figure 4.34. Elastic surface deflections, test load = 60 kN, Test Section 529FD.

Table 4.47 Load Transfer Efficiency, Joint 31, Test Section 529FD

Repetitions	Load Transfer Efficiency, LTE (%), Joint 31		Temperature Difference (top–bottom), °C
	From Slab 32 to Slab 31	From Slab 31 to Slab 32	
Test load = 40 kN			
10	-251.6*	0.1	7.5
3,641	-2,621.3*	0.3	5.5
16,641	-2,225.7*	0.0	2.4
29,015	123.0	-0.9	1.3
43,090	119.5	18.9	7.1
88,110	116.8	10.0	2.4
Test load = 60 kN			
88,110	114.0	11.6	2.4
90,971	113.6	9.4	3.4
103,095	113.5	21.3	2.0
105,756	115.9	13.2	3.5
118,478	117.6	26.6	2.9
134,224	116.7	16.1	0.1
149,853	108.9	25.9	-1.4
197,898	113.8	14.7	0.6
214,416	111.2	22.2	1.6
230,130	110.3	37.6	2.8
245,921	108.9	36.2	2.2
262,359	110.9	7.9	
309,250	110.2	12.1	1.1
322,533	110.5	13.7	0.7
337,530	111.7	15.2	-1.1
352,324	109.2	9.0	-0.5

* Not reliable due to LVDT failure

4.12 Test Section 530FD

The HVS test on Test Section 530FD was completed on slabs 38, 39 and 40 on the South Tangent, with the 8 × 1 m HVS test section located so that slab 39 was tested along its entire edge. The test started with a 40-kN dual wheel load, which was kept constant up to 64,227 repetitions, then increased to 60 kN for an additional 752,448 repetitions and finally up to 90 kN

for an additional 30,170 repetitions. The test was stopped at a cumulative total of 846,845 load repetitions. The test was conducted with temperature control.

The crack pattern, as it developed with time, can be seen in Figure 4.35. Photograph 4.39 presents an overhead view of the test section at the completion of HVS trafficking. Photograph 4.39 also clearly shows evidence of the Weigh-In-Motion piezometers that were installed on slab 40. Photograph 4.40 presents another view of the cracks on Test Section 530FD.

4.12.1 Visual Observations, Test Section 530FD

After 64,227 40-kN load repetitions and 227,457 60-kN load repetitions (totaling 291,684 load applications), a corner crack developed on slab 38. After an additional 524,991 60-kN load repetitions and 30,170 90-kN load repetitions (totaling 830,463 repetitions), a transverse crack developed at joint 38 and propagated toward the longitudinal edge of slab 39. This is the same failure mode as experienced on the previous section (529FD).

4.12.2 JDMD and EDMD Data, Test Section 530FD

Two Joint Displacement Monitoring Devices (JDMDs) were placed on either side of joint 38 (between slabs 38 and 39) and one Edge Displacement Monitoring Device (EDMD) was placed at the midpoint edge of the middle slab (slab 39). The results are summarized in Tables 4.48, 4.49 and 4.50 for the 40-, 60-, and 90-kN test loads, respectively. The surface deflections as detailed in these tables are shown in Figures 4.36 to 4.38.

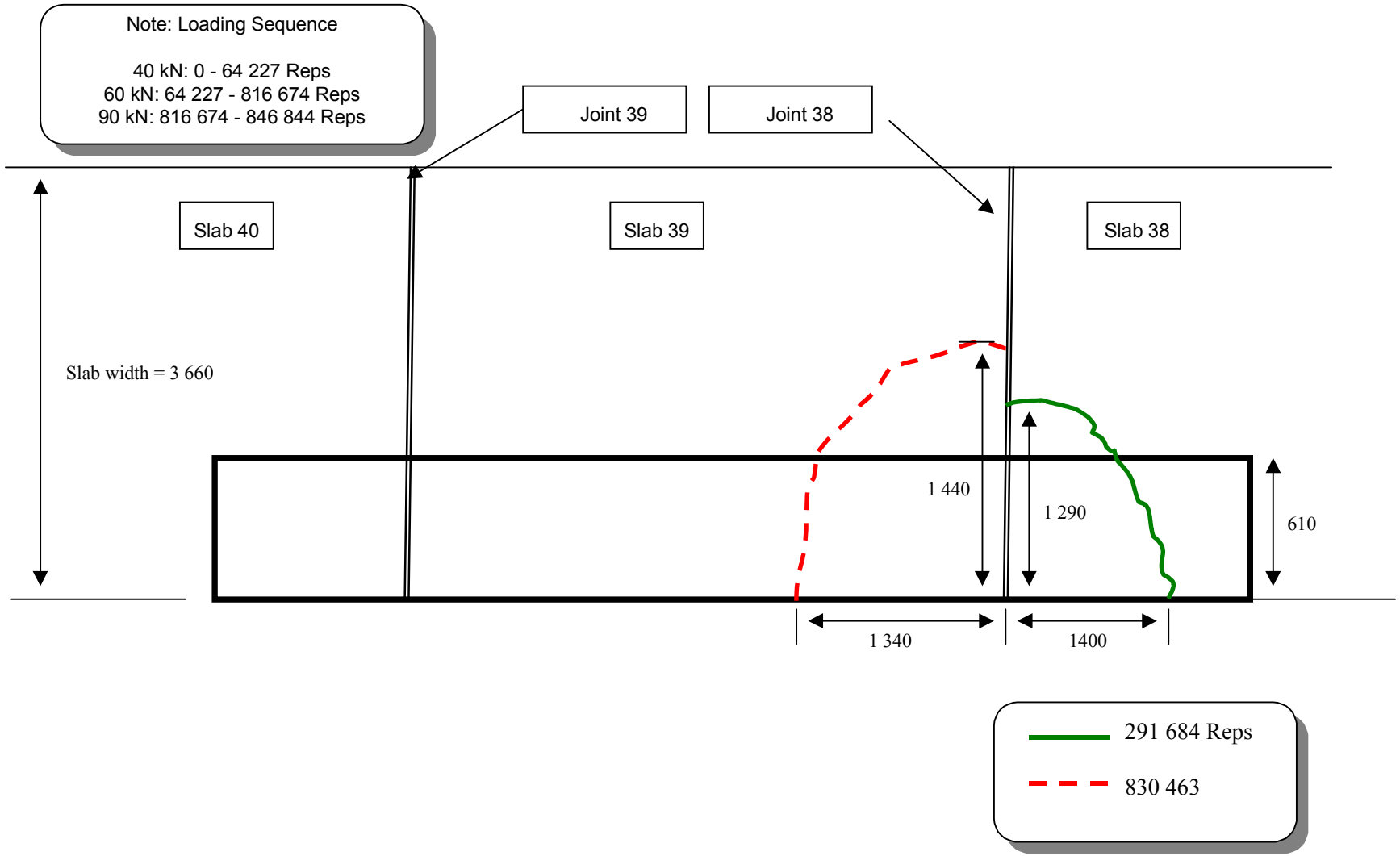

Figure 4.35. Schematic of crack development, Test Section 530FD (not to scale).

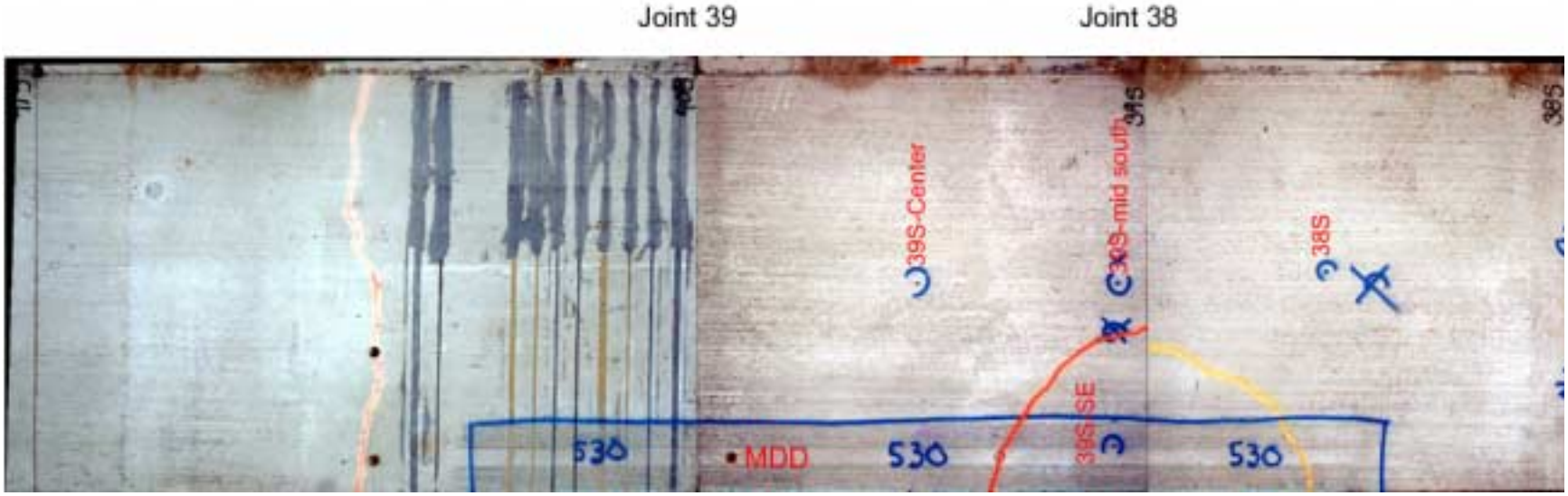

Photograph 4.39. Composite photograph of final crack pattern, Test Section 530FD.

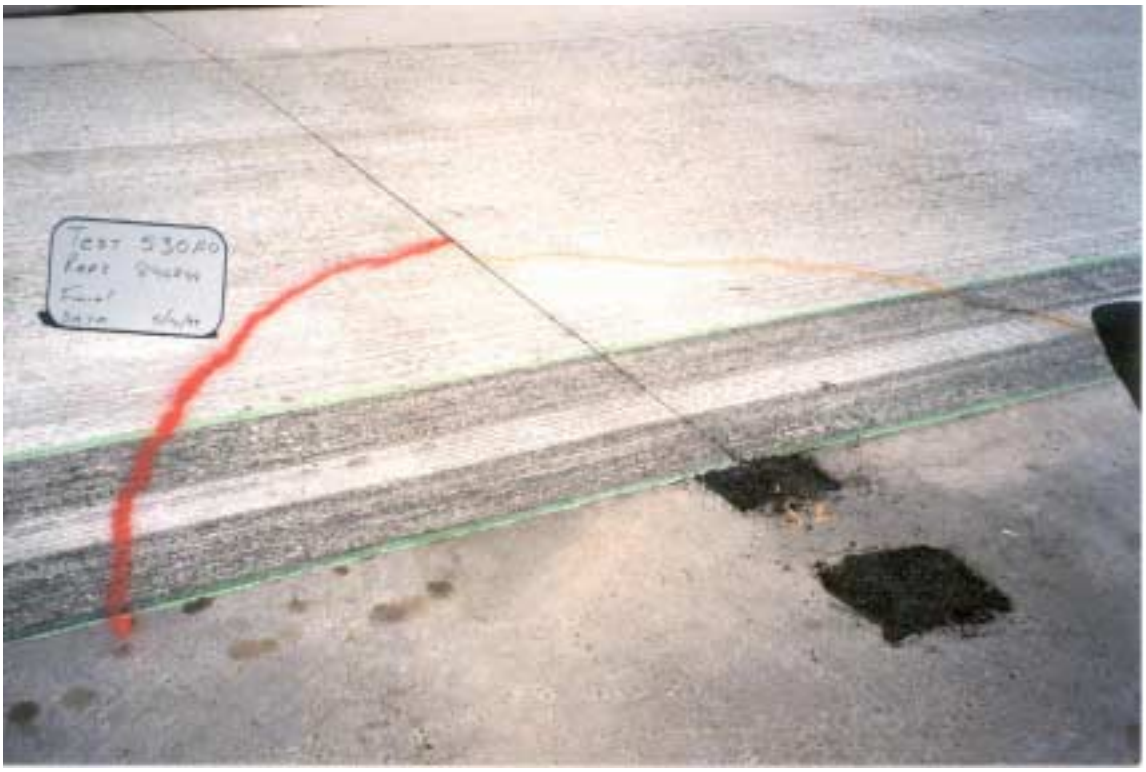

Photograph 4.40. Final crack pattern at the end of the test (846,844 repetitions), Test Section 530FD.

Table 4.48 EDMD and JDMD Deflections, Test Load = 40 kN, Test Section 530FD

Repetitions	Deflection (m × 10^{-6})			Temperature Difference (top–bottom), °C
	Edge Midpoint, Slab 39	Corner, Joint 38		
		Slab 39 Side	Slab 38 Side	
0	552	1,552	2,277	-1.1
2,500	642	1,674	2,053	-0.4
5,000	636	1,626	1,056	0.5
14,000	645	1,669	1,958	-0.2
63,157	700	1,811	2,201	1.0
64,227	557	1,362	2,002	3.2

Table 4.49 EDMD and JDMD Deflections, Test Load = 60 kN, Test Section 530FD

Repetitions	Deflection (m × 10^{-6})			Temperature Difference (top–bottom), °C
	Edge Midpoint, Slab 39	Corner, Joint 38		
		Slab 39 Side	Slab 38 Side	
40 kN Load				
0	711	1,699	2,408	3.2
973	909	2,267	2,746	-0.5
16,161	971	2,496	3,168	0.0
32,197	988	2,581	3,210	-0.2
47,558	995	2,511	3,153	2.4
97,539	988	2,512	3,102	1.5
111,092	1,062	2,743	3,343	-1.1
126,508	1,000	2,621	3,293	1.0
141,336	1,024	2,690	3,376	0.5
157,003	1,020	2,529	3,088	1.0
203,411	975	2,592	3,034	0.7
213,992	1,039	2,756	3,380	-1.1
227,457	989	2,676	2,425	-0.3
242,558	996	2,499	1,830	1.1
255,649	972	2,380	1,536	0.4
303,026	1,018	2,523	1,697	0.5
318,207	1,019	2,558	1,716	0.1
388,303	670	1,762	1,257	-0.9
404,454	715	2,097	1,680	3.1
447,175	906	2,421	1,782	-0.7
460,778	956	2,552	1,775	0.1
508,219	955	2,558	1,648	0.0
523,308	963	2,581	1,687	-0.2
538,949	967	2,698	1,775	-0.5
554,430	1,039	2,721	1,674	-0.5
570,085	1,026	2,794	1,742	-0.5
617,323	1,055	2,737	1,643	-0.4
633,148	887	2,685	1,526	-0.3
647,556	1,039	2,757	1,612	0.0
662,575	950	2,656	1,514	0.2
677,160	962	2,655	1,555	-0.1
724,820	794	2,583	1,406	-0.5
737,478	996	2,797	1,589	-0.3
752,448	1,007	2,815	1,649	0.1

Table 4.50 EDMD and JDMD Deflections, Test Load = 90 kN, Test Section 530FD

Repetitions	Deflection (m × 10^{-6})			Temperature Difference (top–bottom), °C
	Edge Midpoint, Slab 39	Corner, Joint 38		
		Slab 39 Side	Slab 38 Side	
0	1,160	3,065	1,744	NA
1,000	862	2,571	1,211	0.1
14,789	1,398	1,210	1,076	-1.2
30,170	1,446	1,239	1,297	-0.1

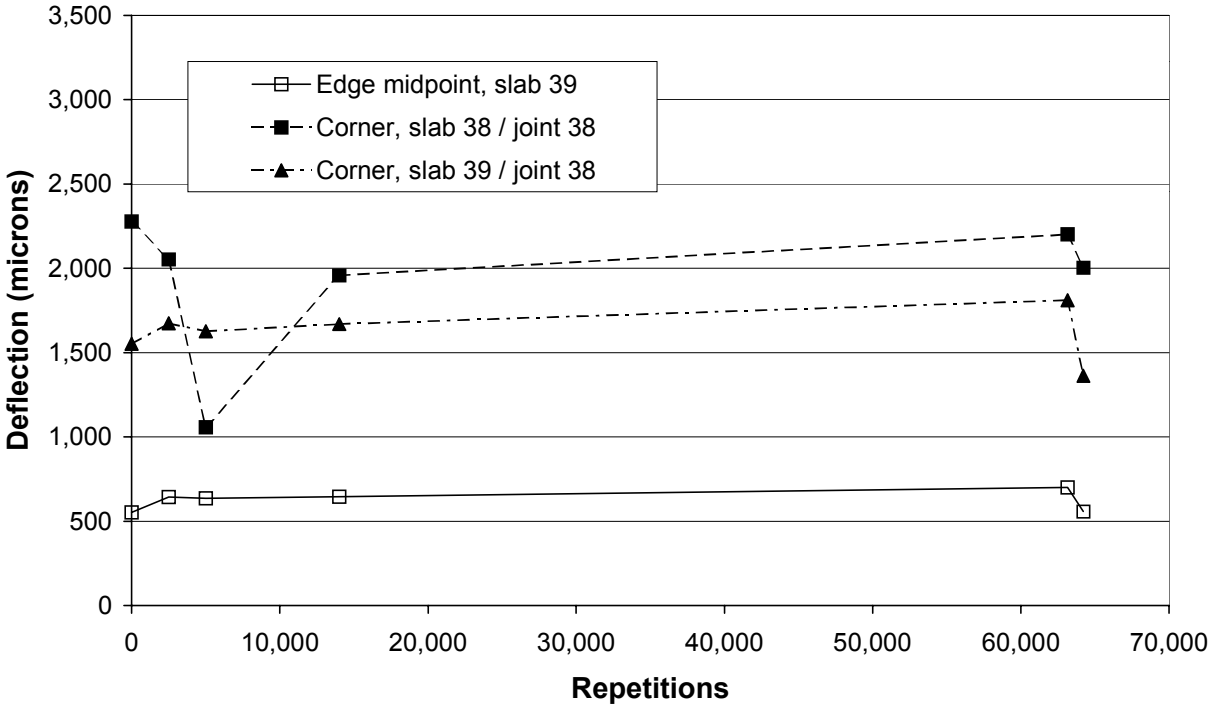

Figure 4.36. Elastic surface deflections, test load = 40 kN, Test Section 530FD.

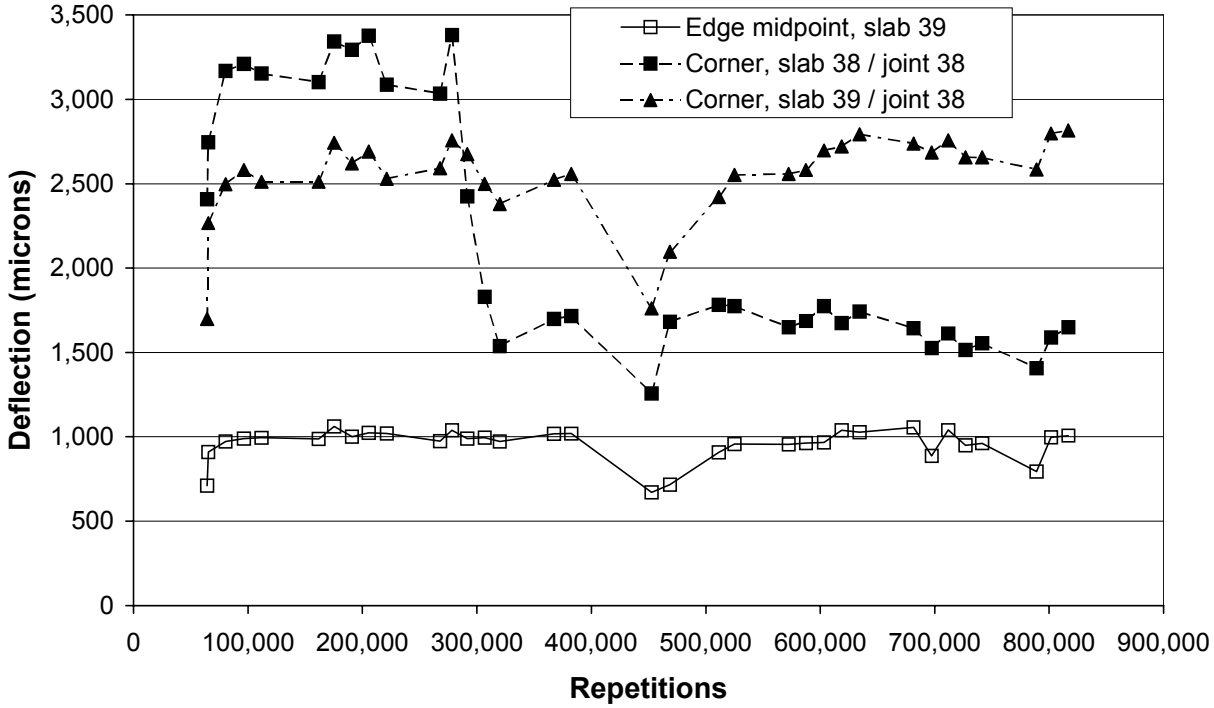

Figure 4.37. Elastic surface deflections, test load = 60 kN, Test Section 530FD.

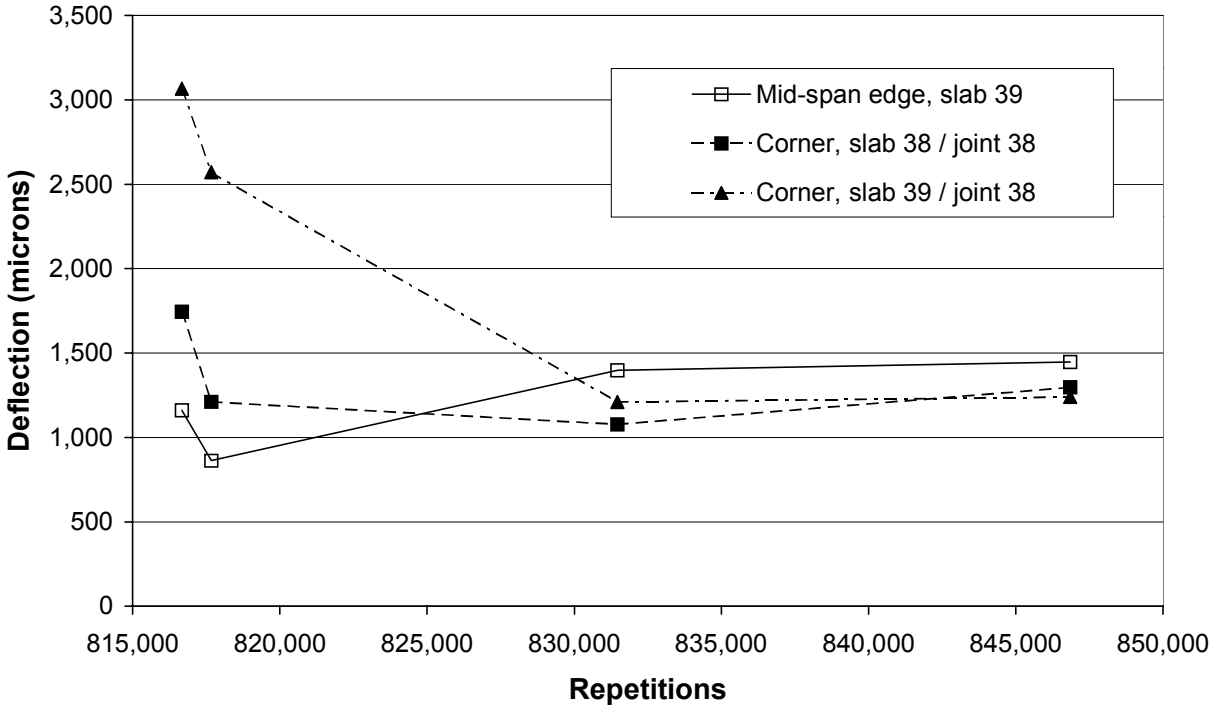

Figure 4.38. Elastic surface deflections, test load = 90 kN, Test Section 530FD.

While the test load was 40 kN (to 64,227 repetitions), the deflections stayed relatively constant, in the order of 0.6 mm at the edge midpoint and 1.6 to 2 mm on either side of joint 38. After 227,457 repetitions at 60 kN (291,684 total repetitions), a corner crack developed on slab 38. This is shown in Figure 4.37, where the deflection reading of the JDMD on the slab 38 side of the joint decreases significantly. When the load was raised to 90 kN, a corner crack developed on slab 39 at approximately 5,000 90kN load repetitions (830,463 total repetitions), which is shown by the drop in deflection for the slab 39 side of the joint in Figure 4.38.

4.12.3 Load Transfer Efficiency, Test Section 530FD

The Load Transfer Efficiency (LTE) was calculated at joint 38; the results are summarized in Table 4.51. LTE was calculated for the HVS wheel running in both directions across the joint.

Table 4.51 again highlights the difference in LTE between crossing the joint in different directions observed throughout this test series, and the underlying asymmetry between conditions of adjacent slabs. Until the appearance of the first visible crack at 290,000 repetitions, LTEs seemed to have settled around 25 and 35 percent for the both directions of wheel travel. A marked increase then occurred when running from slab 39 to slab 38 (which cracked), from approximately 25 percent to 70 percent and higher. The difference running across the joint in the other direction is far less, initially increasing from approximately 35 to approximately 45 percent, but then decreasing again to around 35 percent.

The formation of the visible crack in slab 39 near the end of the test at 830,000 repetitions seems to cause another change in LTEs as might be expected, but the limited data are inconclusive other than indicating a possible reduction in LTE.

4.12.4 MDD Elastic Deflection Data, Test Section 530FD

One MDD was installed on Section 530FD, near joint 39 on slab 39. This MDD was installed between the wheel paths of the dual wheels about 0.3 m from the edge of the slab. MDD modules were installed inside the 200-mm thick concrete slab at a depth of 50 mm as well as at the top of the base course (225 mm) and the top of the in-situ soil (425 mm). The results of the peak MDD deflections can be seen in Table 4.52 and Figure 4.39.

Figure 4.39 shows that the deflection of the concrete is significantly higher than the aggregate base or subgrade. This may result from curling of the slab in an upward direction. This same trend is noted for the 100- and 150-mm test sections.

Table 4.51 Load Transfer Efficiency, Joint 38, Test Section 530FD

Repetitions	Load Transfer Efficiency, LTE (%) Joint 38		Temperature Difference (top–bottom), °C
	From slab 38 to slab 39	From slab 39 to slab 38	
40-kN trafficking load			
0	16	83	-1.1
2,500	39	63	-0.4
5,000	93	14	0.5
14,000	55	70	-0.2
63,157	31	67	1.0
64,227	7	60	3.2
60-kN trafficking load			
64,227	10	65	3.2
65,200	15	50	-0.5
80,388	19	50	0.0
96,424	22	48	-0.2
111,785	29	51	2.4
161,766	30	43	1.5
175,319	26	41	-1.1
190,735	26	42	1.0
205,563	28	46	0.5
221,230	25.8	33	1.0
267,638	27	28	0.7
278,219	27	35	-1.1
291,684	70	46	-0.3
306,785	80	48	1.1
319,876	87	36	0.4
367,253	85.6	39	0.5
382,434	86	41	0.1
452,530	98	29	-0.9
468,681	89	39	3.1
511,402	102	50	-0.7
525,005	99	45	0.1
572,446	109	36	0.0
587,535	103	38	-0.2
603,176	99	42	-0.5
618,657	101	39	-0.5
634,312	108	40	-0.5
681,550	105	37	-0.4
697,375	110	31	-0.3
711,783	105	36	0.0
726,802	106	34	0.2
741,387	99	35	-0.1
789,047	109	30	-0.5
801,705	105	34	-0.3
816,675	101	37	0.1
90-kN trafficking load			
816,675	114	32	NA
817,675	138	19	0.1
830,464	67	48	-1.2
846,845	49	23	-0.1

4.12.5 MDD Permanent Deformation Data, Test Section 530FD

The permanent deformation for the pavement layers was measured using the same MDD; the results are presented in Table 4.53 and Figure 4.40.

From the preceding tables and Figure 4.40 at some 450,000 load repetitions, there is a significant increase in the concrete permanent deformation and a decrease in both the base and subgrade deformation values. This may be due to movement of the modules inside the MDD hole, or a crack in the concrete layer that was not discovered because it was either microscopic or initiated at the bottom of the layer.

4.13 Test Section 531FD

Test Section 531FD was conducted on slabs 41, 42 and 43 and was the last HVS test performed on the South Tangent. The test was conducted with temperature control. As shown in Figure 4.41, slab 42 (total length of 4.7 m) was fully tested, together with some area on either side of joints 41 and 42. The test started with a 40-kN dual wheel load, which was kept constant up to 31,318 repetitions, after which it was increased to 70 kN for an additional 33,997 repetitions. The test was stopped at 65,315 total load repetitions. The crack pattern, as it developed with time, can be seen in Figure 4.41. A photo composite of the test section with cracks after HVS trafficking is presented in Photograph 4.41.

It should be noted that Weigh-In-Motion piezometer instrumentation (WIM) was installed in slab 43.

Table 4.52 MDD Deflections, Joint 39, Test Section 530FD

Repetitions	MDD In-depth Deflections (m × 10^{-6}), Joint 39			Temperature Difference (Top–Bottom), °C
	Depth from Surface			
	50 mm	250 mm	425 mm	
40-kN trafficking load				
0	1,144	124	49	-1.1
2,500	1,161	121	49	-0.4
5,000	1,107	105	39	0.5
14,000	1,119	99	39	-0.2
63,157	1,236	105	40	1.0
64,227	1,074	273	129	3.2
60-kN trafficking load				
64,227	1,257	327	161	3.2
65,200	1,696	253	106	-0.5
80,388	1,881	188	92	0.0
96,424	1,925	172	85	-0.2
111,785	1,828	210	107	2.4
161,766	1,870	207	107	1.5
175,319	2,037	161	80	-1.1
190,735	1,932	188	96	1.0
205,563	1,970	183	95	0.5
221,230	1,865	203	110	1.0
267,638	1,932	175	92	0.7
278,219	2,033	164	85	-1.1
291,684	1,992	165	87	-0.3
306,785	2,002	174	96	1.1
319,876	1,959	169	93	0.4
367,253	2,080	163	89	0.5
382,434	2,115	140	76	0.1
452,530	1,447	278	137	-0.9
468,681	1,530	220	113	3.1
511,402	1,833	104	47	-0.7
525,005	2,045	135	68	0.1
572,446	2,019	114	62	0.0
587,535	2,036	124	67	-0.2
603,176	2,131	108	60	-0.5
618,657	2,166	90	50	-0.5
634,312	2,208	85	51	-0.5
681,550	2,175	90	56	-0.4
697,375	2,181	85	55	-0.3
711,783	2,170	85	55	0.0
726,802	2,061	92	58	0.2
741,387	2,063	96	60	-0.1
789,047	1,980	67	46	-0.5
801,705	2,128	72	50	-0.3
816,675	2,132	85	58	0.1
90-kN trafficking load				
816,675	2,240	154	104	NA
817,675	1,852	198	132	0.1
830,464	2,330	183	116	-1.2
846,845	2,319	201	124	-0.1

Table 4.53 MDD Permanent Deformation, Joint 39, Test Section 530FD

Repetitions	MDD In-depth Deflections (m × 10^{-6}), Joint 39			Temperature Difference (top – bottom) °C
	Depth from Surface			
	50 mm	250 mm	425 mm	
40-kN trafficking load				
0	0	0	0	-1.1
2,500	122	29	23	-0.4
5,000	144	15	13	0.5
14,000	165	34	23	-0.2
63,157	301	73	38	1.0
64,227	500	-90	-8	3.2
60-kN trafficking load				
64,227	587	-66	-9	3.2
65,200	584	-67	-9	-0.5
80,388	882	9	9	0.0
96,424	964	49	24	-0.2
111,785	1,2788	128	65	2.4
161,766	1,428	188	91	1.5
175,319	1,212	198	100	-1.1
190,735	1,388	222	113	1.0
205,563	1,369	226	115	0.5
221,230	1,531	234	120	1.0
267,638	1,477	255	135	0.7
278,219	1,359	261	143	-1.1
291,684	1,447	267	146	-0.3
306,785	1,434	271	146	1.1
319,876	1,481	281	155	0.4
367,253	1,376	284	158	0.5
382,434	1,310	288	164	0.1
452,530	1,915	149	94	-0.9
468,681	2,436	208	113	3.1
511,402	2,071	279	163	-0.7
525,005	1,920	284	163	0.1
572,446	1,974	300	171	0.0
587,535	1,975	300	171	-0.2
603,176	1,841	298	172	-0.5
618,657	1,762	303	176	-0.5
634,312	1,721	303	180	-0.5
681,550	1,771	309	182	-0.4
697,375	1,754	309	181	-0.3
711,783	1,787	317	189	0.0
726,802	1,912	320	193	0.2
741,387	1,893	320	193	-0.1
789,047	1,865	323	197	-0.5
801,705	1,788	328	274	-0.3
816,675	1,804	325	203	0.1
90-kN trafficking load				
816,675	1,810	321	203	NA
817,675	2,210	315	271	0.1
830,464	1,806	337	212	-1.2
846,845	1,880	354	220	-0.1

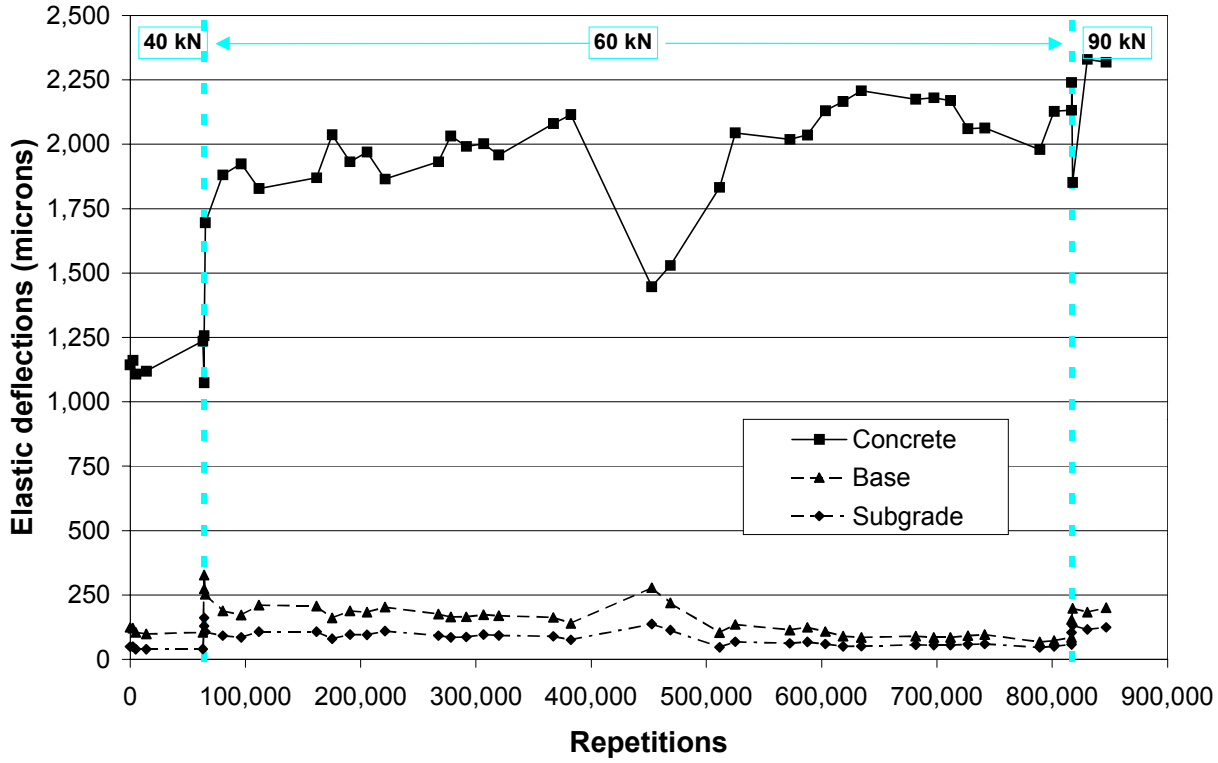

Figure 4.39. In-depth MDD deflections, Test Section 530FD.

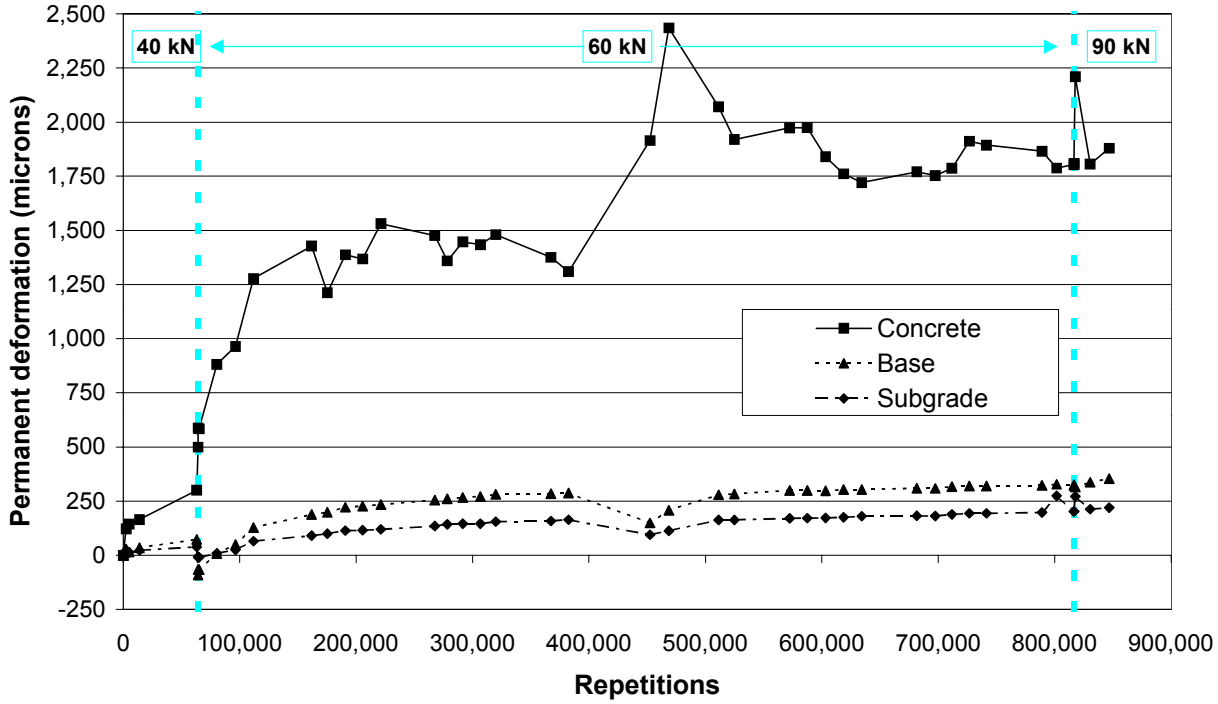

Figure 4.40. Permanent deformation, Test Section 530FD.

4.13.1 Visual Observations, Test Section 531FD

Prior to the start of HVS testing, no cracks were visible on the Section 531FD. After 31,318 40-kN load repetitions and 31,495 70-kN load repetitions (a total of 62,813 load repetitions), a transverse crack developed in the middle slab (slab 42) and a longitudinal crack developed across the WIM instrumentation in slab 43. This crack pattern suggests that the slab failed due to fatigue and if time permitted, the crack may have appeared to be a corner break (see Photograph 4.42).

4.13.2 JDMD and EDMD Data, Test Section 531FD

Two Joint Displacement Monitoring Devices (JDMDs) were placed on either side of joint 41 (between slabs 41 and 42) and one Edge Displacement Monitoring Device (EDMD) was placed on the edge of slab 42 at its edge midpoint (midway between the two joints). The maximum deflection at the midpoint edge of the middle slab, and the corner edge deflections on either side of joint 41, are summarized in Table 4.54 for the 40-kN loading and Table 4.55 for the 70-kN loading. The data are also shown in Figures 4.42 and 4.43 for the 40- and 70-kN load cases, respectively.

The deflections recorded at both load levels remained relatively constant. The failure that occurred (crack pattern) developed somewhat prematurely, which may be the result of a lack of aggregate interlock at joint 42 due to the installation of the WIM instrumentation.

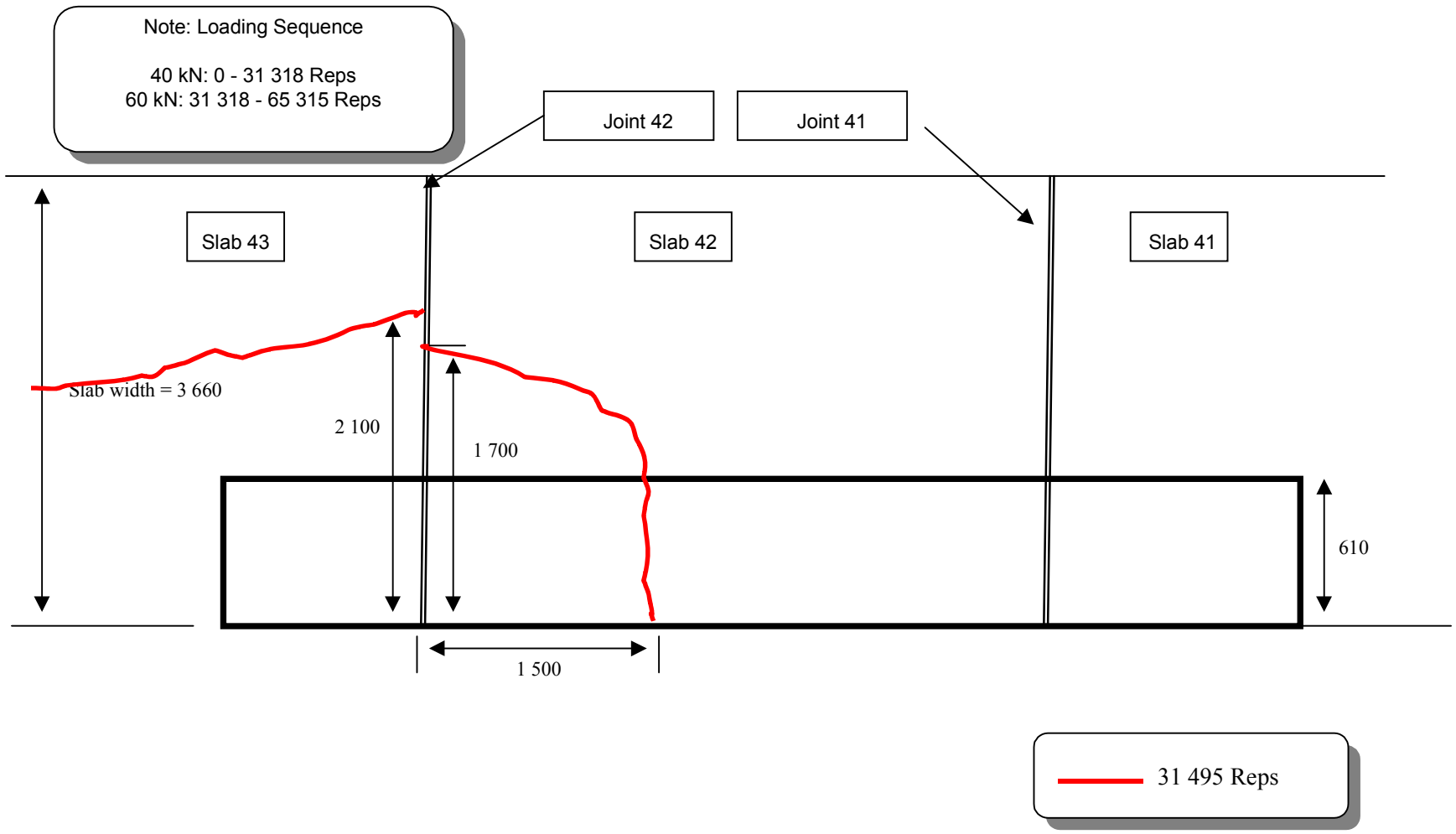

Figure 4.41. Schematic of crack development, Test Section 531FD (not to scale).

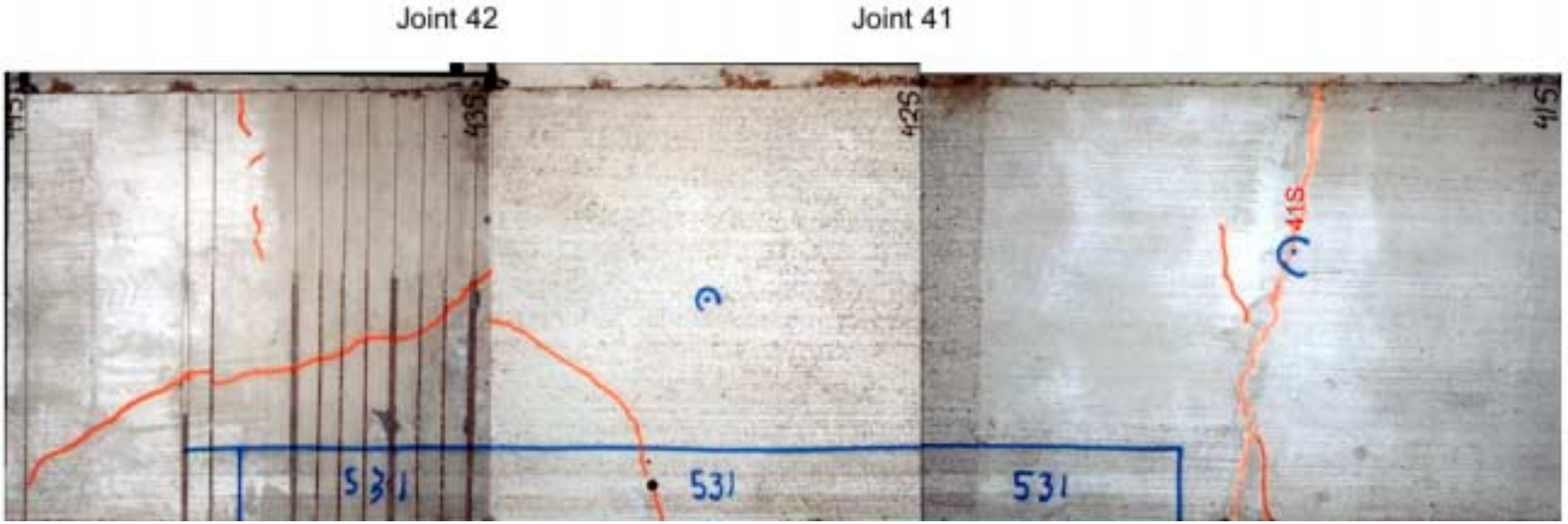

Photograph 4.41. Composite photograph of final crack pattern, Test Section 531FD.

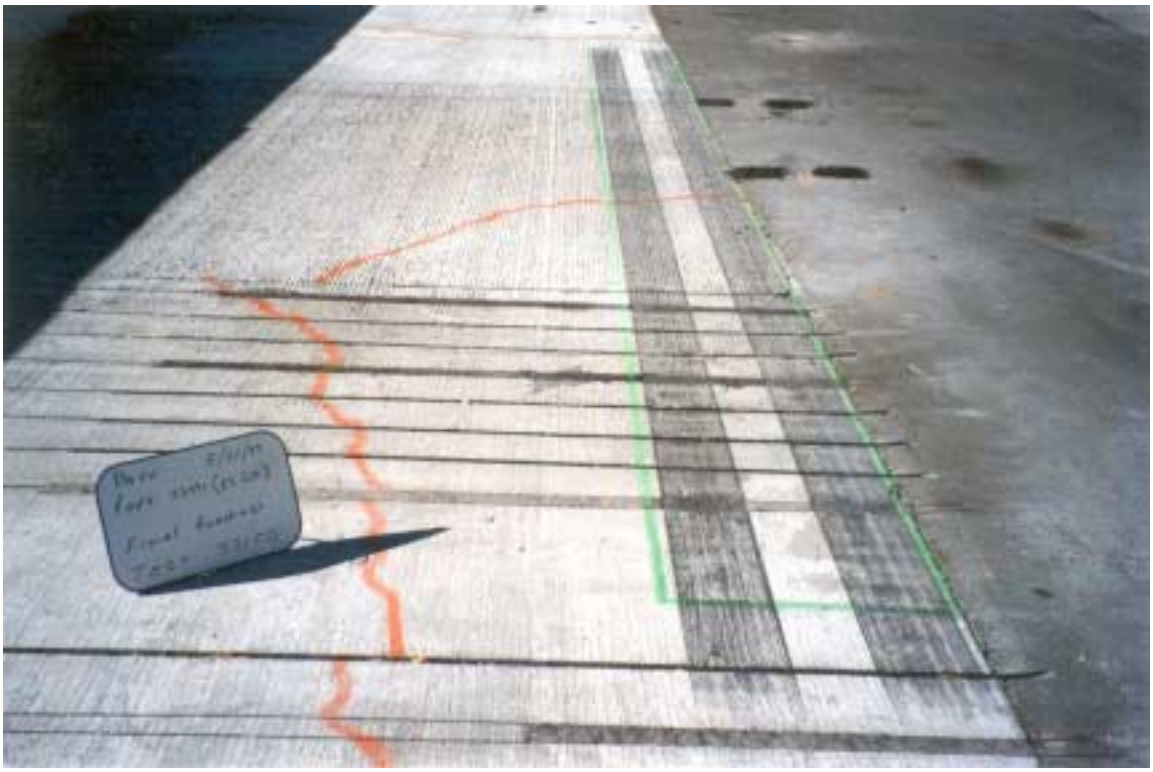

Photograph 4.42. Final crack pattern after 65,315 repetitions, Test Section 531FD.

Table 4.54 EDMD and JDMD Deflections, Test Load = 40 kN, Test Section 531FD

Repetitions	Deflection (m × 10^{-6})			Temperature Difference (top–bottom), °C
	Edge Midpoint, slab 42	Corner, Joint 41		
		Slab 42 Side	Slab 41 Side	
0	851	2,212	1,679	2.0
2,500	688	1,606	1,424	-0.5
5,000	754	1,652	1,600	0.9
15,259	752	1,792	1,651	0.4
31,318	682	1,618	1,559	-0.7

Table 4.55 EDMD and JDMD Deflections, Test Load = 70 kN, Test Section 531FD

Repetitions	Deflection (m × 10^{-6})			Temperature Difference (top–bottom), °C
	Edge Midpoint, slab 42	Corner, Joint 41		
		Slab 42 Side	Slab 41 Side	
0	932	2,241	1,784	0.6
2,500	891	2,063	2,159	2.0
14,191	957	2,422	2,520	-1.3
31,495	1,065	2,041	2,560	-1.5
33,997	1,012	2,254	2,083	-1.4

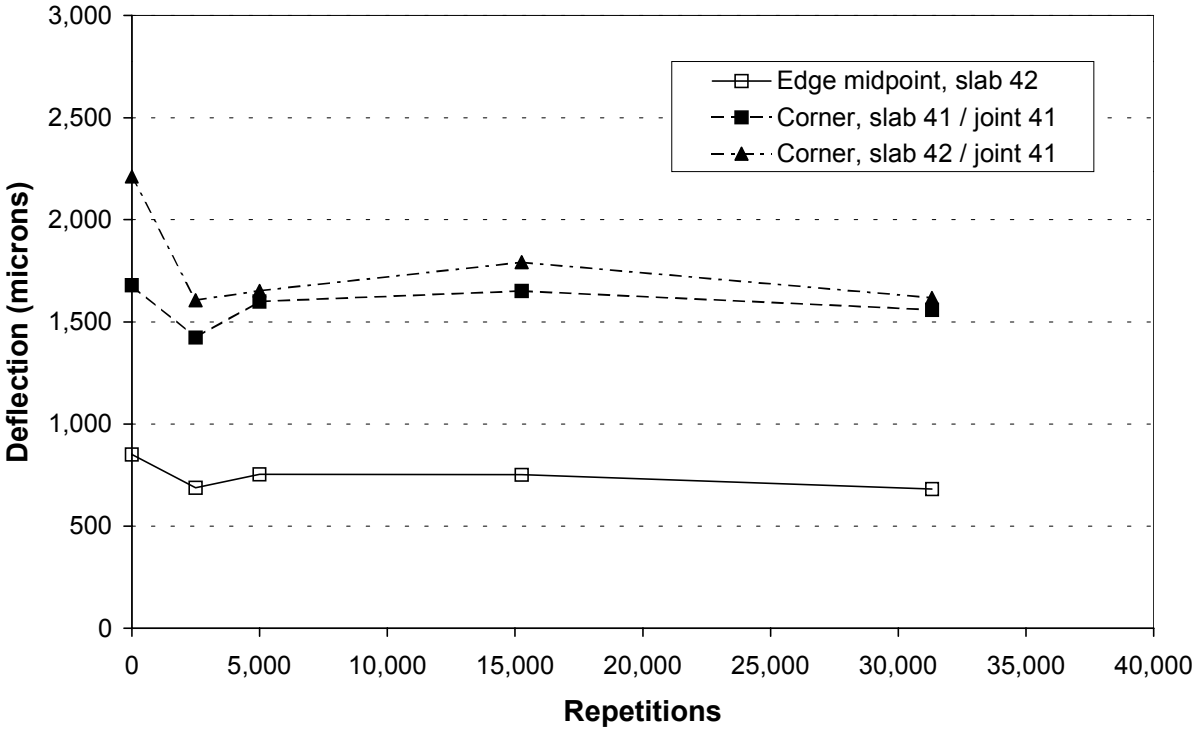

Figure 4.42. Elastic surface deflections, test load = 40 kN, Test Section 531FD.

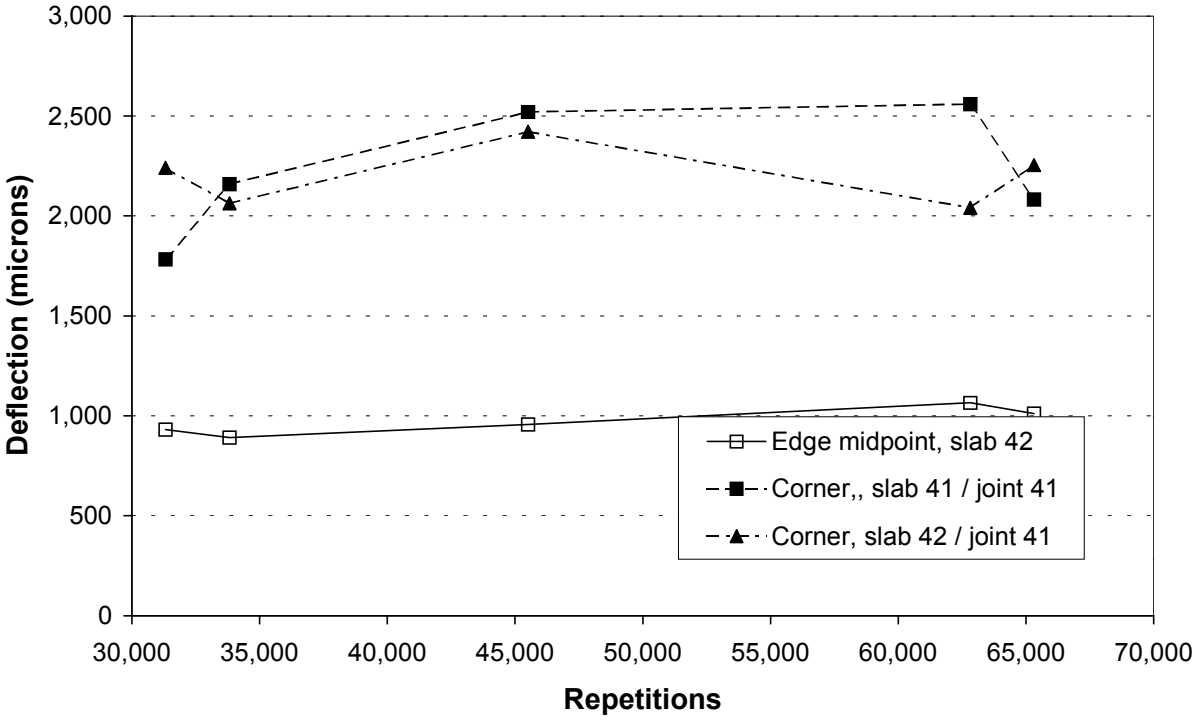

Figure 4.43. Elastic surface deflections, test load = 70 kN, Test Section 531FD.

4.13.3 Load Transfer Efficiency, Test Section 531FD

The Load Transfer Efficiency (LTE) was calculated at joint 41 (the joint between slabs 41 and slab 42) for the HVS wheel traveling in both directions. The results are summarized in Table 4.56.

The LTE was relatively constant throughout the entire test. These results suggest that the crack at the sawed joint propagated relatively straight down to the bottom of the concrete.

Table 4.56 Load Transfer Efficiency at Joint 41, Test Section 531FD

Repetitions	Load Transfer Efficiency, LTE (%), Joint 41		Temperature Difference (top–bottom), °C
	From Slab 41 to Slab 42	From Slab 42 to Slab 41	
Test load 40kN			
0	81.9	37.9	2.0
2,500	49.7	50.7	-0.5
5,000	59.0	70.4	0.9
15,259	68.1	64.8	0.4
31,318	73.3	72.1	-0.7
Test load 70 kN			
31,318	74.5	55.4	0.6
33,818	71.4	87.3	2.0
45,509	71.3	83.8	-1.3
62,813	51.2	101.6	-1.5
65,315	56.3	52.6	-1.4

5.0 TEST PITS

Three test pits were excavated during January 2000. The objectives of this effort were to:

- verify layer thicknesses of the concrete slabs and the subbase layers;
- visually inspect the crack growth patterns, and
- extract soil samples for further laboratory testing at UCB.

The three test pits were dug through previously tested HVS sections at the following locations:

- Test Section 519FD - Section 1A, Slab 4
- Test Section 525FD - Section 3C, Slab 23
- Test Section 529FD - Section 5A, Slab 31

Layer thicknesses were measured at three locations in each test pit and averaged, and any visible cracks were measured.

5.1 Test Pit Results

The layer thickness results are summarized in Table 5.1.

Table 5.1 Layer Thicknesses Measured by Direct Observation in Test Pit

HVS Test	Slab #	Concrete Thickness at location (mm)					Subbase Thickness (mm)				
		1	2	3	Average	Design	1	2	3	Average	Design
519FD	4	101.6	95.3	108.0	101.6	100.0	152	152	164	157	150
525FD	23	184.4	177.8	177.8	179.9	150.0	152	152	152	152	150
529FD	31	196.9	177.8	203.2	192.6	200.0	178	191	178	182	150

The concrete thicknesses matched the design thicknesses on the 100- and 200-mm sections. The 150-mm section, however, was measured to be 180 mm instead of the design 150 mm. This may only be a localized deviation.

The subbase thickness was consistent with the design thickness under the 100- and 150-mm concrete sections, but under the 200-mm concrete section, an average subbase thickness of 182 mm was measured for a design thickness of 150 mm.

The various layers seemed to be in good condition. The respective concrete slabs did not show any sign of a honeycomb structure and no air pockets were noted. The aggregate base layer, as well as the subgrade layer exhibited good compaction.

5.1.1 Crack Patterns

- **Section 1A, Slab 4, Test Section 519FD.** Two cracks were found in the first test pit (519FD). The first crack, on one face of the test pit, went completely through the concrete layer and the second crack (visible on the opposite face of the test pit) went 75 percent through the slab from its origin at the top. Photograph 5.1 shows the location of the test pit in relation to the HVS test pad. The crack, which was measured, had formed after 2,105 load applications (see figure 4.1) and can be seen in Photograph 5.2.
- **Section 3C, Slab 23, Test Section 525FD.** The crack observed on Test Section 525FD after 1,000 load applications (see Figure 4.20) is shown in Photograph 5.3. From the photograph it is clear that the crack went all the way through the 150-mm concrete slab.
- **Section 5A, Slab 31, Test Section 529FD.** On slab 31 on Section 529FD, a surface crack was reported after 337,530 load applications (see Figure 4.29) but after the test pit was dug it became evident that this was only a surface crack. This crack did not penetrate the concrete to any visible extent (see Photograph 5.4).

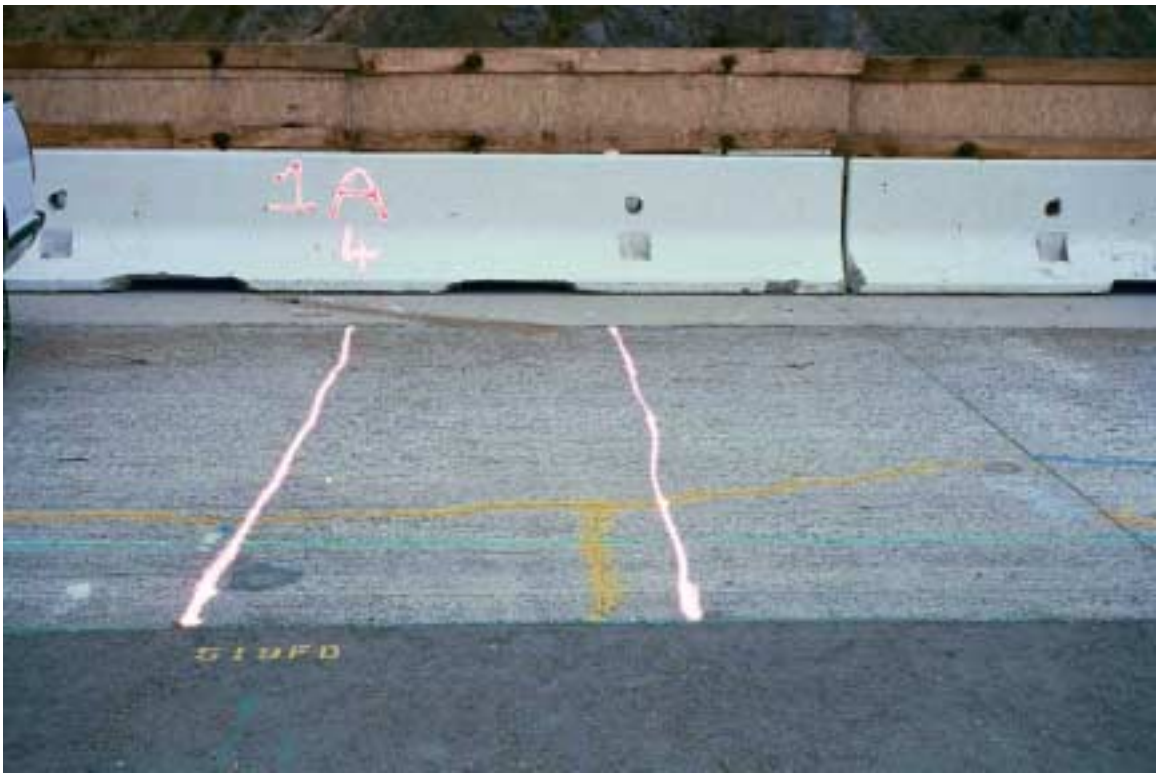

Photograph 5.1. Location of test pit prior to excavation on Test Section 519FD.

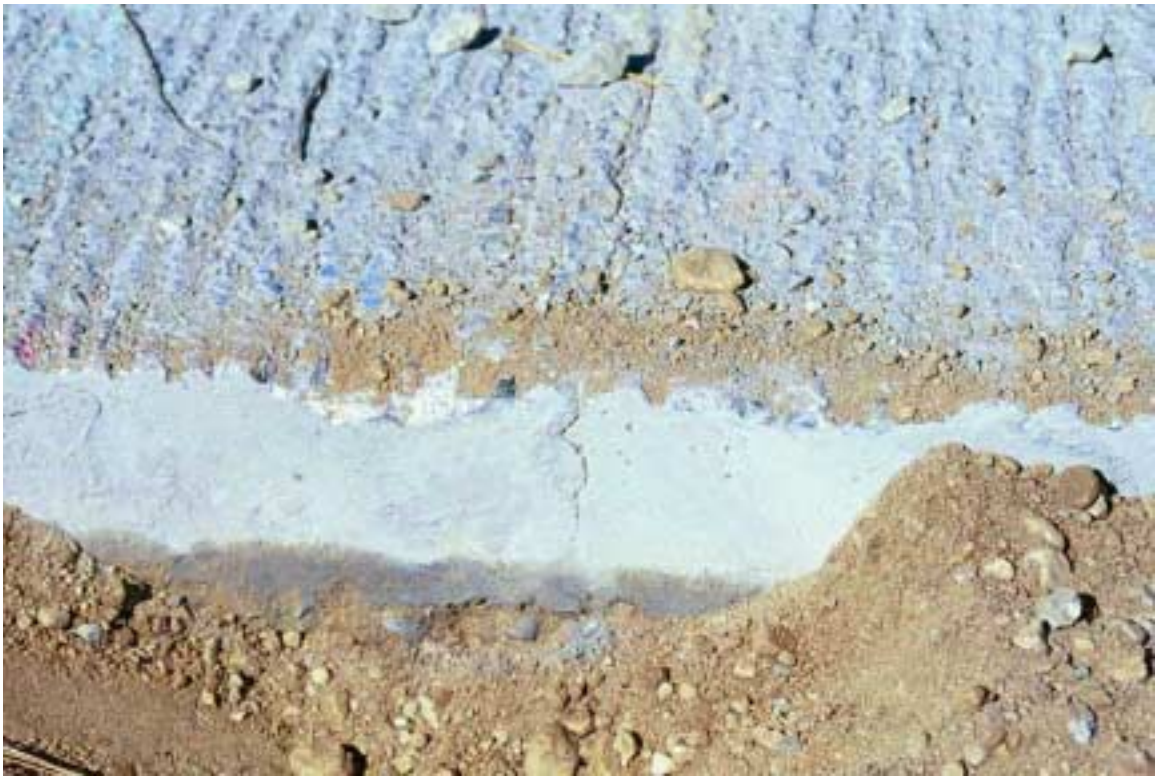

Photograph 5.2. Crack on Test Section 519FD.

Photograph 5.3. Crack on Test Section 525FD.

Photograph 5.4. Surface crack that did not propagate to bottom of concrete, Test Section 529FD.

6.0 FWD RESULTS

In this section, the Falling Weight Deflectometer (FWD) data recorded before and after HVS testing is presented. In view of the large data set, only processed data parameters are presented in this section. Raw deflection data is presented in Appendix A.

FWD measurements were taken at 1, 7, 50, 90, 200, and 270 days after construction of the concrete pavement. The sequence of these six test groups relative to the HVS testing is shown in Figure 6.1. It should be noted that the FWD testing was performed only on the concrete sections with a thickness of 200 mm or greater, thus only these HVS test sections are shown in Figure 6.1.

A spreadsheet macro was developed to transpose raw FWD data into an electronic format that is convenient for further processing and analysis. Instructions for using this macro are provided in Appendix A. This appendix also contains an explanation of the available data as well as of the directory structure for the data files. It should be noted that for second level data analysis purposes, all of the tables and figures contained in this section are mirrored by

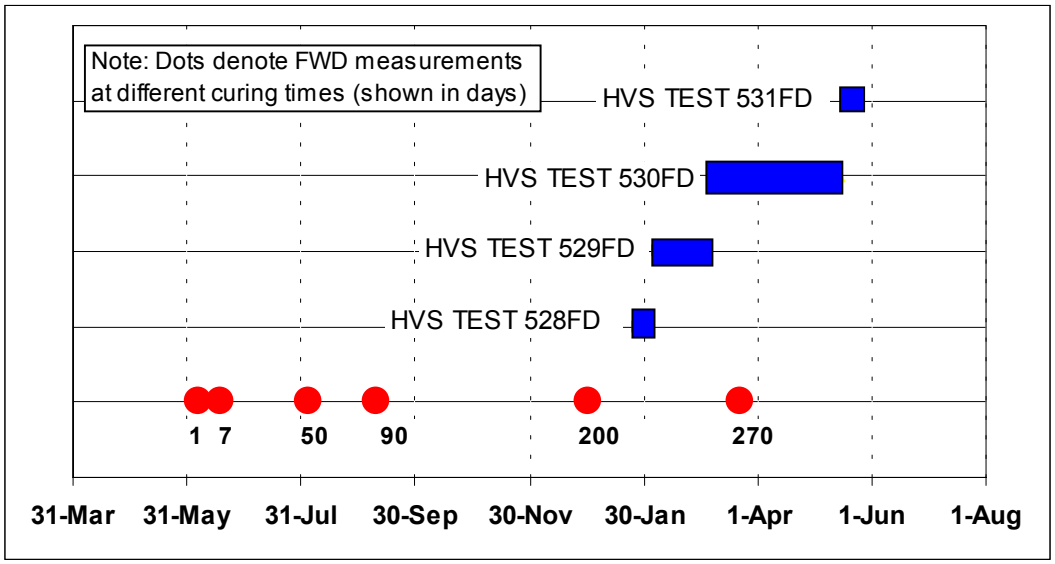

Figure 6.1. Timeline showing time of FWD testing and start and duration of HVS testing on 200-mm thick slabs.

spreadsheet files which are listed in Appendix A.

6.1 Effect of Curing on Backcalculated Stiffness

Concrete slab and subgrade stiffnesses were backcalculated using the ELMOD software. A two-layer model was assumed with the first layer being the concrete slab, and the second layer (referred to as the subgrade) consisting of the aggregate base and subgrade. Backcalculated stiffnesses for the concrete slabs and subgrade at different curing times are listed in Table 6.1. The change in concrete and subgrade stiffness with increasing curing time is shown in Figure 6.2. The trends observed from these figures are decreasing subgrade stiffness and a tendency for decreased stiffness versus curing age for the concrete. These trends are also reflected in the raw deflection data for the different HVS tests (see Appendix A).

The tendency for the deflections to increase with increased curing age may be attributable to curling effects, which cause less consistent seating of the concrete slab on the subgrade, rather than weakening of the concrete slabs. Care should therefore be taken in the interpretation of the backcalculated stiffnesses. For second level analysis, it is recommended that a more rigorous backcalculation study be undertaken for the slabs situated within the HVS sections, particularly with respect to temperature. It can particularly be seen that backcalculated concrete stiffness is lowest at 90 days during the hottest time of the year, and highest at 200 days in mid-winter.

6.2 Effect of Curing on Load Transfer Efficiency

The Load Transfer Efficiency (LTE) between different slabs at different curing ages is summarized in Table 6.2. No apparent relationship exists between the LTE and the curing age. It should be noted that temperature variations are not accounted for in these plots. The LTE percentages at different curing ages are shown in Figure 6.3.

Table 6.1 Concrete and Subgrade Stiffness for Different Curing Ages (Based on Deflections Measured at Slab Center)

Slab Number	Station (ft.)	Stiffness of		Curing Period (days)
		Concrete	Subgrade	
31 Middle slab for Test Section 529FD	230.1	27,428	386	1
	230.1	23,377	324	7
	230.1	23,460	173	50
	230.1	13,786	124	90
	230.1	24,378	152	200
32 Edge Slab for Test Section 529FD	211.1	36,694	276	1
	211.1	39,323	290	7
	211.1	40,406	317	50
	210.1	44,698	297	90
	210.1	48,169	221	200
33	197.1	25,765	262	1
	196.1	32,720	276	7
	197.1	23,281	324	50
	195.1	35,542	200	90
	195.1	23,771	262	200
34 Edge Slab for Test Section 528FD	183.1	22,908	262	1
	184.1	24,764	283	7
	183.1	29,718	235	50
	183.1	29,774	228	90
	183.1	43,870	145	200
35 Middle Slab for Test Section 528FD	167.1	34,942	290	1
	168.1	36,860	269	7
	167.1	43,235	290	50
	166.1	51,032	276	90
	167.1	85,636	179	200
36 Edge slab of Test Section 528FD	147.1	28,614	331	1
	150.1	26,462	290	7
	147.1	31,160	255	50
	147.1	39,765	262	90
	147.1	37,060	269	200
37	133.1	37,384	352	1
	133.1	53,641	228	7
	133.1	32,023	159	50
	133.1	32,264	186	90
	133.1	84,077	186	200

Slab Number	Station (ft.)	Stiffness of		Curing Period (days)
38 Edge Slab for Test Section 530FD	120.1	41,034	449	1
	120.1	56,235	290	7
	120.1	33,596	338	50
	120.1	36,453	338	90
	120.1	64,494	276	200
39 Middle slab for Test Section 530FD	105.1	38,233	435	1
	106.1	46,092	442	7
	105.1	66,123	421	50
	105.1	84,484	297	90
	105.1	62,652	248	200
40 Edge Slab for Test Section 530FD	85.1	40,234	421	1
	88.1	52,392	297	7
	84.1	26,489	269	50
	84.1	32,044	283	90
	83.1	66,585	242	200
41 Edge Slab for Test Section 531FD	72.1	25,026	352	1
	73.1	47,651	311	7
	72.1	59,726	242	50
	72.1	42,366	248	90
	72.1	63,066	242	200
42 Middle Slab for Test Section 531FD	60.1	33,341	338	1
	60.1	42,835	304	7
	60.1	42,918	255	50
	60.1	50,805	242	90
	60.1	51,819	193	200
43 Edge Slab for Test Section 531FD	44.1	31,436	317	1
	43.1	33,396	297	7
	44.1	20,528	69	50
	44.1	17,678	104	90
	44.1	16,325	90	200
44	27.1	24,350	352	1
	26.1	22,349	345	7
	26.1	30,395	262	50
	27.1	29,808	221	90
	27.1	23,067	193	200
45	8.1	49,390	380	1
	9.1	61,182	345	7
	8.1	57,229	317	50
	8.1	62,107	380	90
	8.1	52,406	248	200

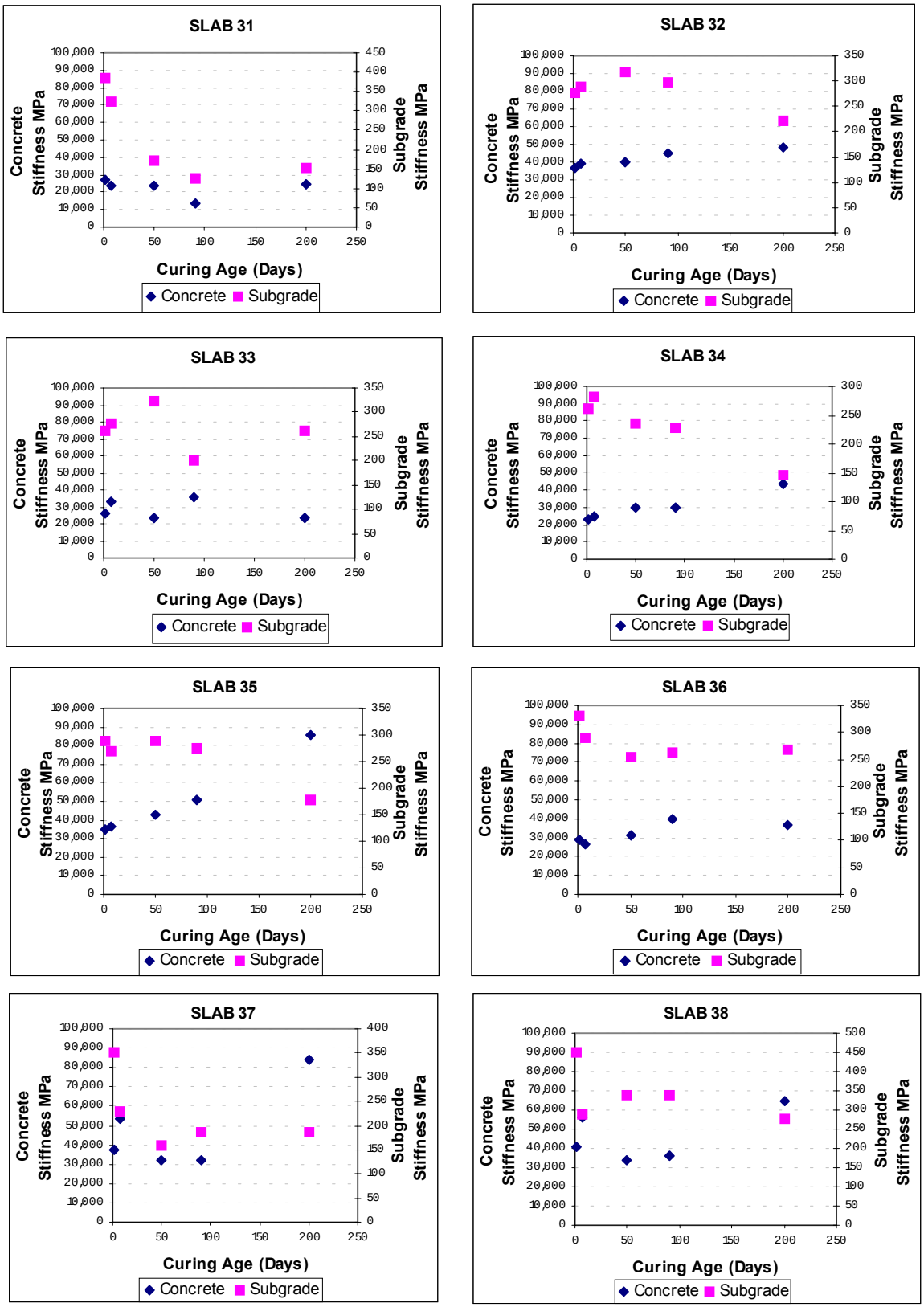

Figure 6.2. Curing age versus stiffness of the concrete and subgrade for different slabs (based on deflections measured at slab center).

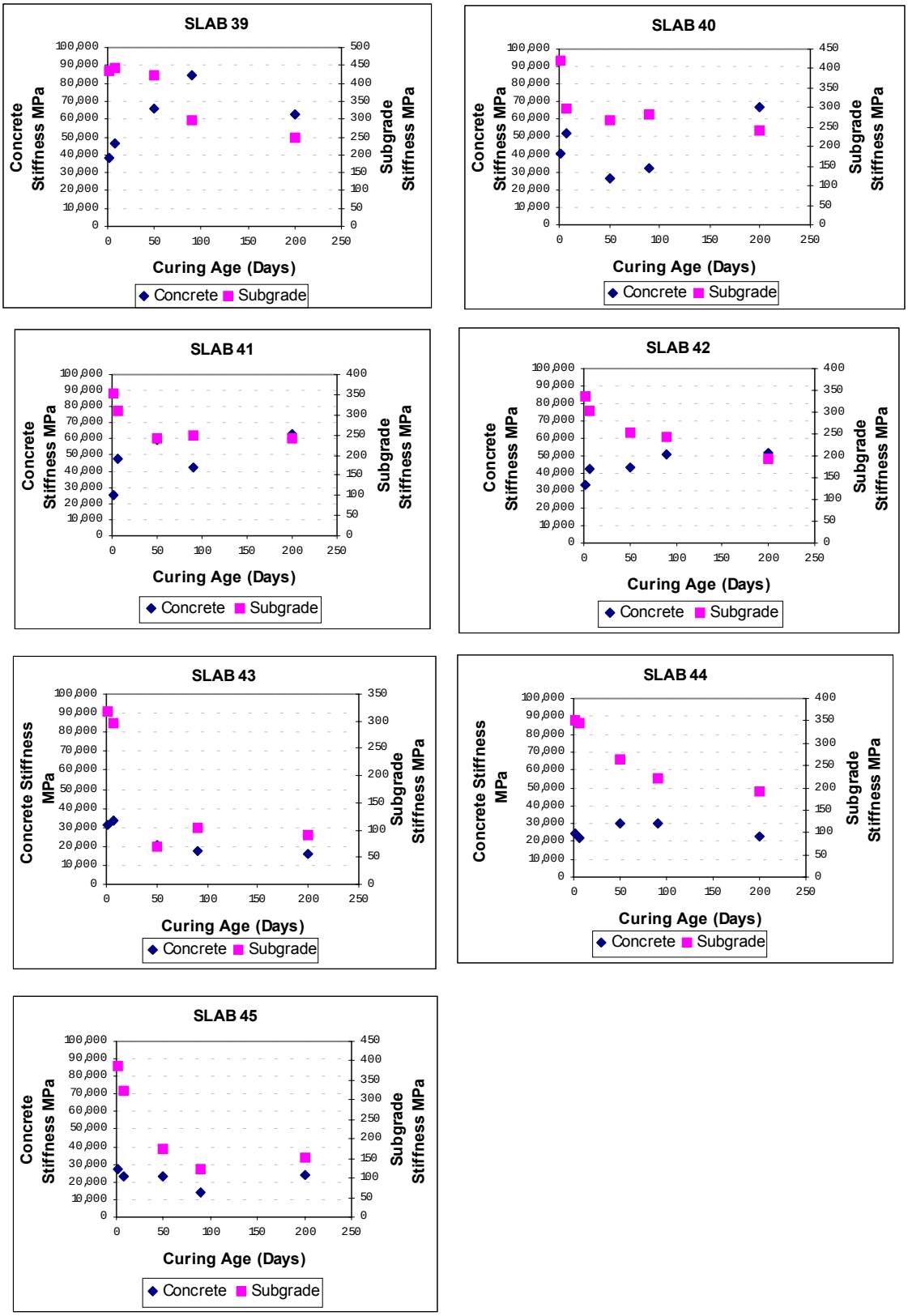

Figure 6.2 (Continued). Curing age versus stiffness of the concrete and subgrade for different slabs (based on deflections measured at slab center).

6.3 HVS Sections on 200-mm Thick Slabs: Effect of Curing on Centerline Deflections

The influence of curing time on the deflections taken within the HVS test sections is illustrated in Figures 6.4 through 6.6. The deflections shown in these figures have been normalized to 66.7 kN, and are centerline deflections taken at the transverse joints and at the center of the middle slab of each HVS test section. In all cases, the deflections at the transverse joints are significantly higher than those situated at the center of the given slab. A general increase in deflections with curing time is noted in all cases. This observation corresponds with the trend noted for some of the slabs in Figure 6.2.

6.4 Load Transfer Efficiency Recorded After HVS Testing

After all HVS tests were completed, FWD measurements were recorded across all joints as well as over visible cracks on the slabs. These measurements are summarized in Tables 6.3a through 6.3d. Measurements were taken approximately twelve hours apart during the coolest part of the night and hottest part of the day, at each of the following positions (See Figure 6.7):

- At the center of the transverse joint;
- At the corner of the slab on the shoulder side of the pavement;
- At the corner of the slab on the k-rail side of the pavement; and

At the longitudinal joint, on the k-rail side of the pavement.

6.5 Deflection Data Recorded after HVS testing

The deflection data measured during day and nighttime at the center of each slab are summarized in Table 6.4. Air and surface temperatures are also reported.

Table 6.2 Joint Load Transfer Efficiency at Various Curing Ages

Slab Number	Joint Number	Station (feet)	K-Joint	LTE (%)	Curing (days)
32: Edge Slab of Test Section 529FD	30	237.20	No Data	No Data	1
		237.20			7
		237.20			50
		237.20			90
32: Edge Slab of Test Section 529FD	31	221.20	627	70	1
		221.20	190	26	7
		221.20	78	47	50
		221.20	105	27	90
33	32	203.20	694	96	1
		203.20	351	75	7
		203.20	121	77	50
		203.20	172	65	90
34: Edge Slab of Test Section 528FD	33	191.20	698	81	1
		191.20	350	63	7
		191.20	79	84	50
		191.20	179	74	90
35: Middle Slab of Test Section 528FD	34	178.20	587	92	1
		178.20	313	66	7
		178.20	51	77	50
		178.20	71	69	90
36: Edge Slab of Test Section 528FD	35	159.20	774	77	1
		159.20	500	38	7
		159.20	65	52	50
		159.20	121	42	90
37	36	141.20	803	88	1
		141.20	417	58	7
		141.20	83	51	50
		141.20	130	44	90
38: Edge Slab of Test Section 530FD	37	129.20	689	67	1
		129.20	383	40	7
		129.20	86	66	50
		129.20	142	67	90
39: Middle Slab of Test Section 530FD	38	116.20	832	93	1
		116.20	578	44	7
		116.20	81	70	50
		116.20	161	45	90
40: Edge Slab of Test Section 530FD	39	97.20	827	52	1
		97.20	496	16	7
		97.20	229	69	50
		97.20	343	38	90

Slab Number	Joint Number	Station (feet)	K-Joint	LTE (%)	Curing (days)
41: Edge Slab of Test Section 531FD	40	79.20	700	74	1
		79.20	177	48	7
		79.20	44	66	50
		79.20	49	31	90
42: Middle Slab of Test Section 531FD	41	67.20	483	44	1
		67.20	228	22	7
		67.20	53	54	50
		67.20	82	45	90
43: Edge Slab of Test Section 531FD	42	54.20	599	41	1
		54.20	359	11	7
		54.20	95	64	50
		54.20	250	40	90
44	43	35.20	553	51	1
		35.20	185	47	7
		35.20	71	40	50
		35.20	168	23	90
45	44	17.20	351	48	1
		17.20	109	31	7
		17.20	29	63	50
		17.20	79	32	90

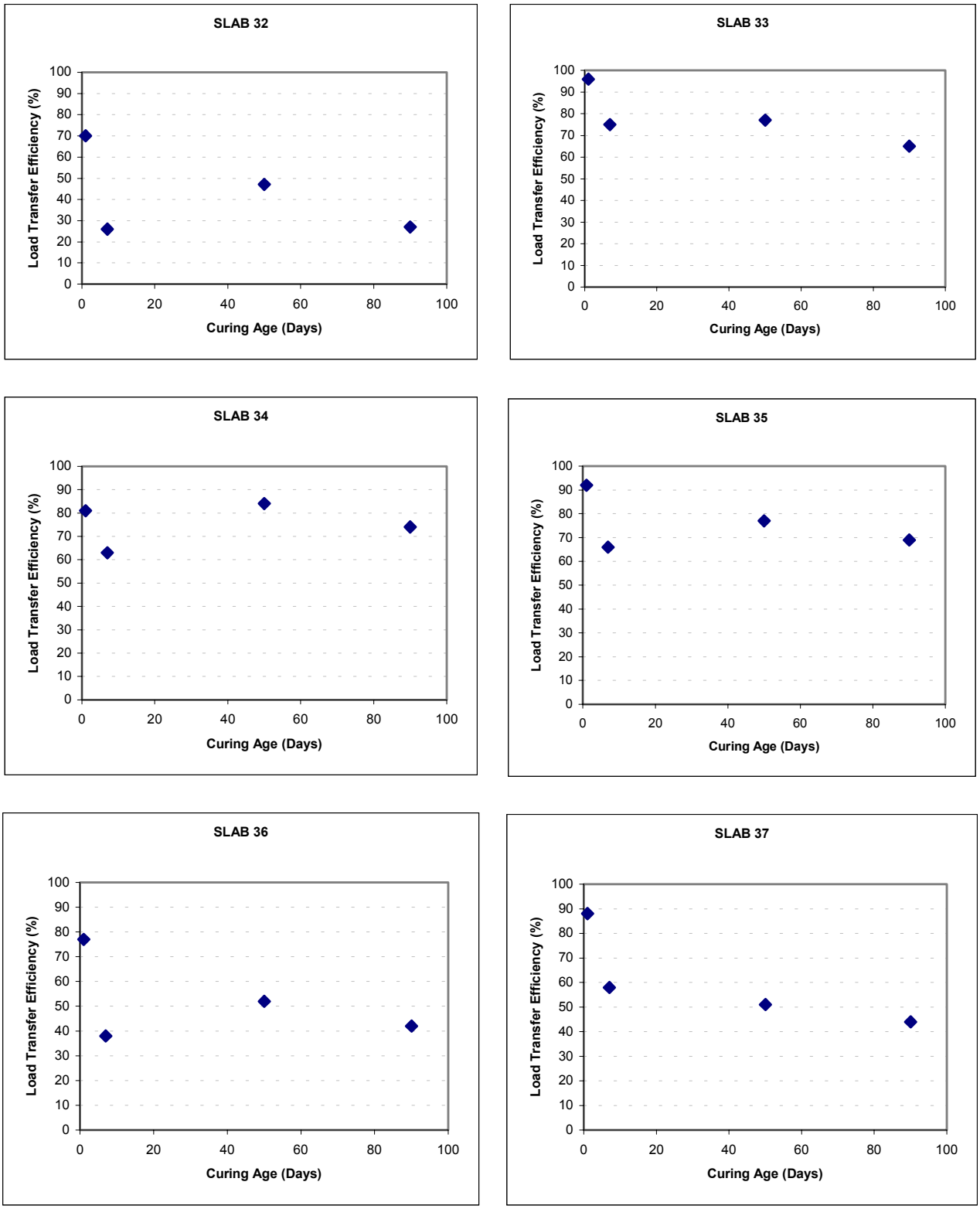

Figure 6.3. Load transfer efficiency versus curing age

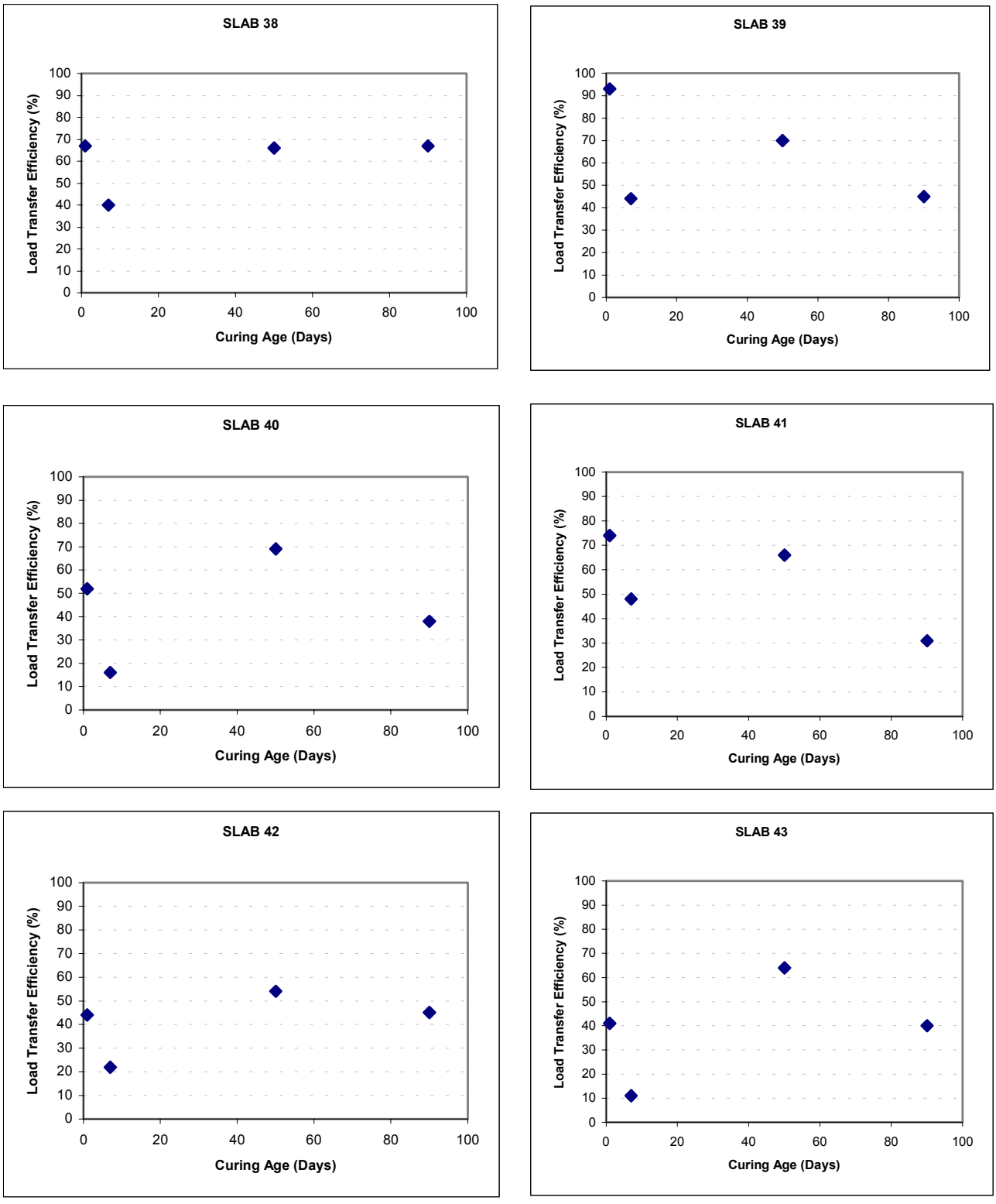

Figure 6.3. Load transfer efficiency versus curing age (continued).

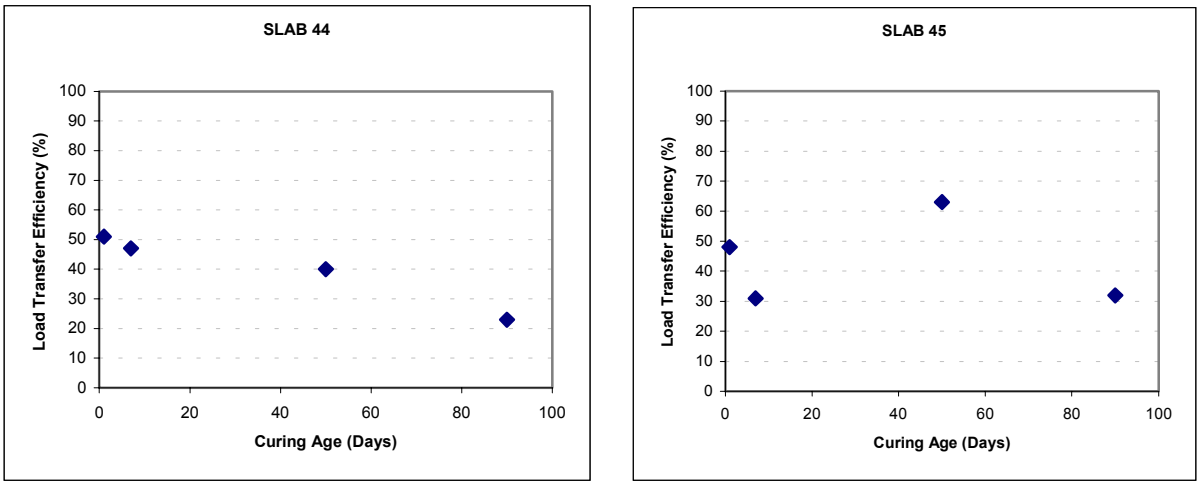

Figure 6.3. Load transfer efficiency versus curing age (continued).

HVS Test Section 528FD **Centreline Deflections Normalized to 66.7 kN**

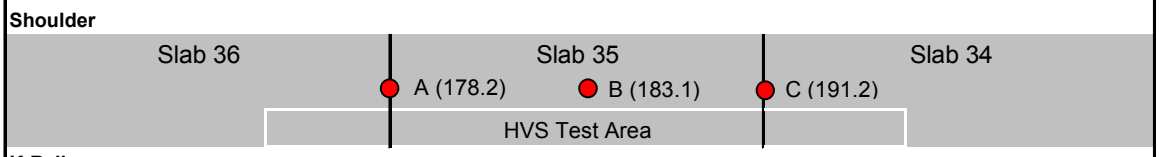

			Deflection (micron) for a Curing Time of (days)				
Position	**Station (ft)**	**Slab**	**1**	**7**	**54**	**90**	**200**
A	178.2	35	157	250	577	465	857
B	183.1	35	158	146	156	156	190
C	191.2	34	174	270	517	355	596

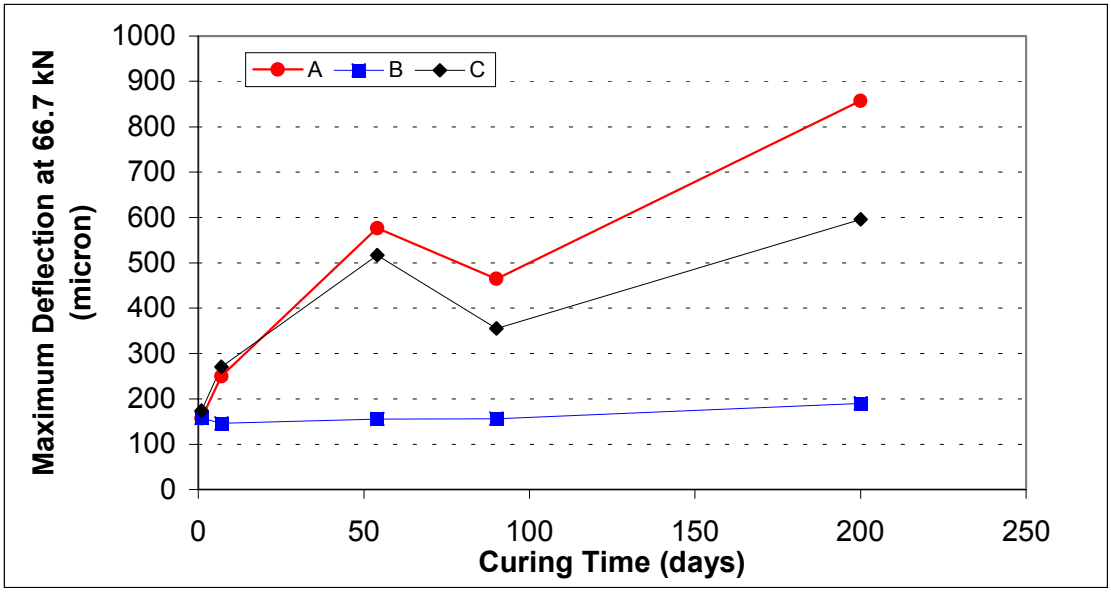

Figure 6.4. HWD deflections versus curing time, Test Section 528FD.

HVS Test Section 530FD **Centreline Deflections Normalized to 66.7 kN**

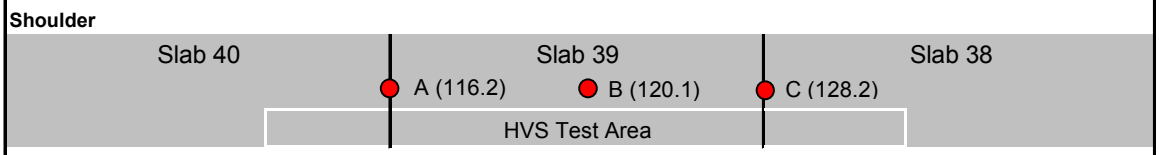

			Deflection (micron) for a Curing Time of (days)				
Position	**Station (ft)**	**Slab**	**1**	**7**	**54**	**90**	**200**
A	116.2	39	130	184	396	295	393
B	120.1	39	90	109	118	115	168
C	128.2	39	155	224	534	388	555

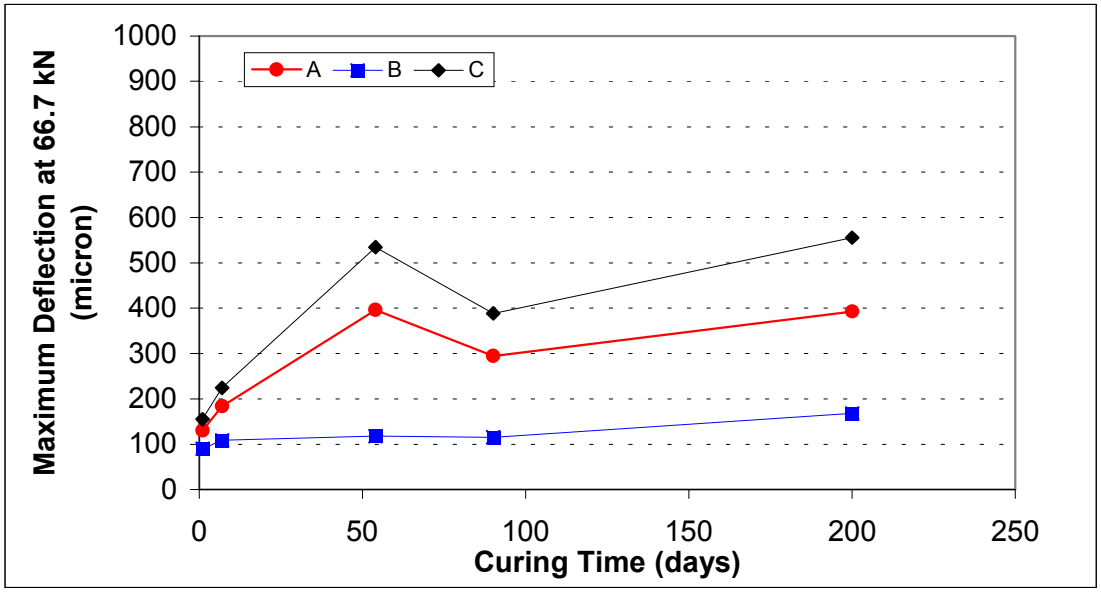

Figure 6.5. HWD deflections versus curing time, Test Section 530FD.

HVS Test Section 531FD **Centreline Deflections Normalized to 66.7 kN**

Shoulder

Slab 43 | Slab 42 | Slab 41

A (67.1) B (72.1) C (79.2)

HVS Test Area

K-Rail

			Deflection (micron) for a Curing Time of (days)				
Position	**Station (ft)**	**Slab**	**1**	**7**	**54**	**90**	**200**
A	67.2	42	242	375	694	506	570
B	72.1	42	127	110	120	131	147
C	79.2	41	176	348	571	561	779

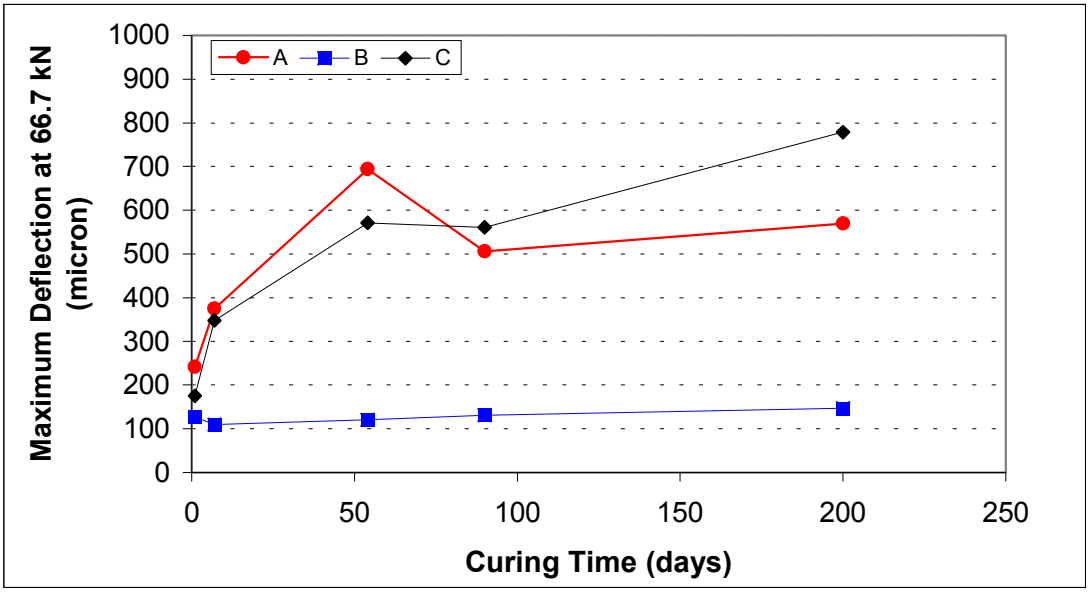

Figure 6.6. HWD deflections versus curing time, Test Section 531FD.

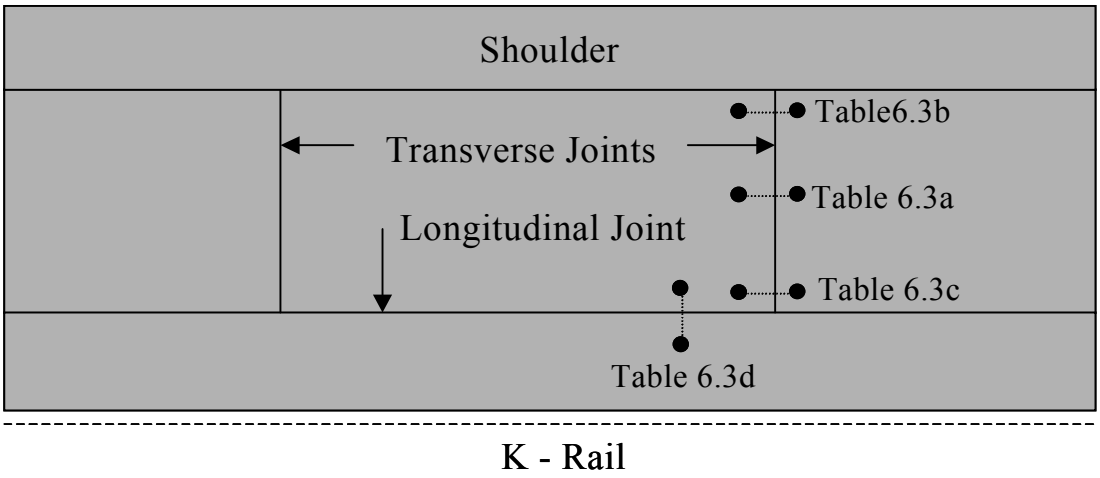

Figure 6.7. Positions at which load transfer efficiency was determined.

Table 6.3a Transverse Joint Load Transfer Efficiency, Center of Transverse Joint (Refer to Figure 6.4)

Location			Night Measurement						Day Measurement					
			Station (ft)	Load (kN)			Temperature (°C)		Station (ft)	Load (kN)			Temperature (°C)	
				44.5	66.7	89.0				44.5	66.7	89.0		
Slab	Section	Joint		Load Transfer Efficiency (%)			Surface	Air		Load Transfer Efficiency (%)			Surface	Air
45	N/A	45	17	24	22	23	0	2	17	9	22	33	8	7
44		44	35	25	24	31			35	19	31	41	9	7
44		Crack	44	46	60	68	-2	2	26	98	98	98	9	6
41	531	41	80	10	13	20	0	3	79	17	21	26	8	8
41		Crack	90	94	94	94	1	3	90	94	94	94	8	6
40	530	40	98	16	29	41	1	3	97	20	27	40	9	6
38		38	130	10	15	24	1	3	130	19	20	22	8	7
37	N/A	37	142	9	10	13	1	3	142	16	18	21	8	6
37		Crack	150	97	97	96	1	2	150	96	96	96	8	7
36	528	36	160	58	63	67	1	3	160	60	64	68	8	7
36		Crack	170	93	92	92	1	3	169	93	92	93	8	7
35		35	179	49	50	53	1	3	179	56	58	61	8	6
34		34	193	28	46	58	2	3	192	51	61	68	8	6
33	N/A	33	204	17	18	20	2	3	204	25	26	29	9	7
32	529	32	223	16	18	22	1	3	222	19	24	30	9	6
32		Crack	231	77	80	83	2	2						

Table 6.3b Corner Load Transfer Efficiency, Shoulder Side Corner (See Figure 6.4)

Location			Night Measurement						Day Measurement					
			Station (ft)	Load (kN)			Temperature (°C)		Station (ft)	Load (kN)			Temperature (°C)	
				44.5	66.7	89.0				44.5	66.7	89.0		
Slab	Section	Joint		Load Transfer Efficiency (%)			Surface	Air		Load Transfer Efficiency (%)			Surface	Air
45	N/A	45	18	24	38	46	-1	2	17	22	37	49	8	6
44	N/A	44	35	19	27	35	0	2	35	7	20	31	8	6
		Crack	44	84	86	87	0	3						
43	531	43	55	56	64	68	0	3	54	50	57	63	8	6
41	531	41	80	40	48	56	0	3	79	35	39	45	8	6
		Crack	89	96	96	96	1	3	88	94	95	95	8	7
40	530	40	98	38	47	55	2	3	97	24	36	47	8	7
		Crack	107	77	78	79	1	3						
38	530	38	130	29	33	37	2	2	129	33	39	42	7	7
		Crack	134	62	67	71			134	52	59	64	8	5
37	N/A	37	142	17	26	35	2	3	141	13	24	36	8	6
		Crack	151	99	99	99	1	2	151	97	97	97	8	6
36	N/A	36	160	96	95	95	2	2	160	95	95	95	7	6
		Crack	169	95	95	94	1	2	169	90	91	92	7	5
35	N/A	35	179	30	32	34			179	36	38	39	8	6
34	N/A	34	192	22	33	41	1	2	192	23	27	33	7	7
33	N/A	33	204	11	15	26	1	2	204	10	12	22	6	7
32	529	32	222	16	24	34	1	2	222	18	28	38	6	6
		Crack	229	97	97	96		3						
31	529	31	242	7	15	19								
		Crack	255	49	53	56								
		Crack	261	93	94	94								
		Crack	267	24	39	49	1	3						

Table 6.3c Corner Load Transfer Efficiency, K-rail Side Corner (See Figure 6.4)

Location			Night Measurement						Day Measurement					
			Station (ft)	Load (kN)			Temperature (°C)		Station (ft)	Load (kN)			Temperature (°C)	
				44.5	66.7	89.0				44.5	66.7	89.0		
Slab	Section	Joint		Load Transfer Efficiency (%)			Surface	Air		Load Transfer Efficiency (%)			Surface	Air
45	N/A	45	17	8	10	10	0	3	18	9	11	13	9	8
		Crack	26	12	11	11	0	3	27	13	15	15	9	7
44	N/A	44	36	13	14	15	0	3	36	13	14	16	9	8
		Crack	45	7	9	10	0	3						
43*	531	43	55	6	7	8	0	4	55	7	9	10	9	8
41	531	41	80	18	19	20	0	4	79	22	23	25	9	8
		Crack	91	5	6	6	1	3	91	14	16	17	10	8
40	530	40	98	4	5	5	1	4	98	12	14	15	10	8
38	530	38	130	5	6	6	1	4	129	9	10	11	10	8
37	N/A	37	142	4	4	4	1	4	142	8	9	6	10	8
		Crack	149	5	5	6	2	3	149	22	23	25	10	7
36	528	36	160	6	7	8	2	3	160	10	11	12	10	8
		Crack	170	10	10	10	2	4	170	28	27	25	9	8
35	528	35	180.3	11	11	12	2	4	179	13	15	16	9	8
34	528	34	192	12	13	13	2	3	192	16	18	19	9	9
33	N/A	33	204	12	13	13	2	3	204	12	13	15	8	8
32	529	32	223	9	10	11	3	3	223	18	18	19	9	8
		Crack	231	9	9	9	2	3						

Table 6.3d Longitudinal Joint Load Transfer Efficiency, K-rail Side Longitudinal Joint (See Figure 6.4)

Location			Night Measurement						Day Measurement					
			Station (ft)	Load (kN)			Temperature (°C)		Station (ft)	Load (kN)			Temperature (°C)	
				44.5	66.7	89.0				44.5	66.7	89.0		
Slab	Section	Joint		Load Transfer Efficiency (%)			Surface	Air		Load Transfer Efficiency (%)			Surface	Air
46	N/A	46	10	17	19	20	0	3	10	17.9	20.4	22.8	8	8
45	N/A	45	21	12	12	13	0	2	20	19.0	21.6	23.2	8	8
		Crack	30	7	8	10	0	3	30	13.3	16.5	18.1	9	8
44	N/A	44	38	13	15	13	0	3	37	10.3	12.4	13.3	8	8
		Crack	48	8	11	13	0	4	48					
42	531	42	74	7	9	10	-1	4	73	18	21	19	8	9
41	531	41	84	10	12	13	0	4	84	25	25	25	10	7
40	530	40	101	3	5	5	1	3	100	13	15	16	10	7
39	530	39	123	10	11	11	0	4	123	15	17	18	10	8
38	530	38	136	9	10	10	1	4	135	17	19	19	10	8
37	N/A	37	144	5	6	7	1	4	143	19	19	18	10	8
		Crack	154	7	7	8	2	3	154	17	19	19	10	7
36	528	36	165	13	12	11	2	4	164	36	35	33	9	8
		Crack	173	10	11	11	1	3	173	16	17	18	9	7
35	528	35	185	12	13	14	2	3	185	15	17	17	9	8
34	528	34	200	13	14	14	2	3	197	16	18	19	8	9
33	N/A	33	212	12	14	14	3	3	213	21	22	22	9	8
32	529	32	225	34	32	29	2	3	225					
		Crack	235	3	4	8	2	4	235	8	10	11	9	8

Table 6.4 Maximum Deflection at Center of Slabs, Day and Night

Slab Number	Station (ft.)	Time	Surface Temperature (°C)	Air Temperature (°C)	Deflection (m × 10^{-6}) @ Given Load		
					44.5 kN	66.7 kN	89 kN
46	10	Day	8	6	277	369	470
	11	Night	-1	2	336	482	631
45	26	Day	8	6	311	429	552
	27	Night	0	2	381	523	683
44	37	Day	8	6	586	773	962
	38	Night	0	3	569	751	948
	48	Day	8	6	362	498	641
	49	Night	0	3	343	468	606
42 (Section 531FD Center Slab)	72	Day	8	6	297	425	571
	74	Night	0	3	346	473	626
41 (Section 531FD Edge Slab)	82	Day	8	7	557	770	989
	83	Night	1	3	615	809	1,019
	91	Day	8	7	469	629	793
	92	Night	2	3	441	604	777
40 (Section 530FD)	101	Day	7	6	252	348	450
		Night	1	3	307	418	535
39 (Section 530FD Center Slab)	119	Day	7	7	308	411	520
	123	Night	2	2	334	447	571
38 (Section 530FD Edge Slab)	136	Day	8	5	528	713	911
37	144	Day	8	6	797	1,056	1,288
	145	Night	2	3	820	1,079	1,347
	154	Day	8	6	517	709	908
		Night	1	2	581	789	1,024
36 (Section 528FD Edge Slab)	162	Day	7	6	666	902	1,139
	164	Night	2	2	614	835	1.080
	172	Day	7	5	370	516	675
		Night	1	2	395	548	724
35 (Section 528FD Center Slab)	185	Day	8	6	233	332	452
	186	Night	1	2	213	303	413
34 (Section 528FD Edge Slab)	197	Day	7	7	229	321	431
	198	Night	1	2	221	312	417
33	212	Day	6	7	289	419	567
		Night	1	2	253	365	495
32 (Section 529FD Edge Slab)	223	Day	6	6	573	808	1,066
	233	Day	7	7	399	529	666
	234	Night	1	3	407	557	716
31 (Section 529FD Center Slab)	272	Night	1	3	524	709	922

7.0 CONCRETE CORE MEASUREMENTS

Two sets of cores are described in this section. The first set was taken from the South tangent approximately 40 days after construction. The second set was taken after all HVS testing had been completed on the South Tangent early in 2001.

7.1 40-Day Core Properties

All the measured core properties with some useful statistics are shown in Tables 7.1–7.3 for Sections 1, 3, and 5, respectively. The following sections further describe the data.

7.1.1 Slab Thicknesses

The true uncut lengths of the cores were measured to determine the as-built slab thicknesses. In the case of Section 1 where the specified slab thickness is 100 mm, the average slab thickness was 107.3 mm with a high of 124.5 mm and a low of 81.3 mm. In the case of Section 3 (specified thickness 150 mm) the average value was 163 mm with a maximum value of 200 mm and a minimum of 135.5 mm. For Section 5 (specified thickness 200 mm), the average thickness was 211.4 mm with a maximum of 227.5 mm and a minimum of 196 mm.

In general, it can be said that the slab thicknesses as measured from the four cores that were extracted from each section tend to be slightly thicker than the design thicknesses. The variability in core lengths is of concern, especially for an experimental concrete slab. With the limited samples taken the distribution of the slab thickness also seem to be skewed toward the thick side.

Table 7.1 Palmdale South Tangent Section 1 Cores Properties, 44 Days After Construction

Core Number	Location	Uncut Length (cm)	Density (kg/m^3)	Compressive Strength (MPa)
1A-4	Section 1-A	8.1	2,321	37.8
1B-8	Section 1-B	11.0	2,397	26.4
1C-12	Section 1-C	12.5	2,375	31.8
1D-14	Section 1-D	11.4	2,389	23.4
	Average	*10.7*	*2,370*	*31.1*
	Low	*8.1*	*2,321*	*26.4*
	High	*12.5*	*2,397*	*37.7*
	Std. Dev.	*1.8*	*34*	*5.0*
	50th Percentile	*11.2*	*2,382*	*30.1*
	90th Percentile	*12.1*	*2,395*	*36.0*
	10th Percentile	*9.0*	*2,337*	*27.0*

Table 7.2 Palmdale South Tangent Section 3 Cores Properties, 44 Days After Construction

Core Number	Location	Uncut Length (cm)	Density (kg/m3)	Compressive Strength (MPa)
3A-17	Section 3-A	15.1	2,117	12.2
3B-20	Section 3-B	16.6	2,382	22.0
3C-25	Section 3-C	13.6	2,348	45.6
3D-28	Section 3-D	20.0	2,383	34.0
	Average	16.3	2,307	28.4
	Low	13.6	2,117	12.2
	High	20.0	2,383	45.6
	Std. Dev.	2.8	129	14.5
	50th Percentile	15.8	2,365	28.0
	90th Percentile	19.0	2,383	42.1
	10th Percentile	14.0	2,186	15.1

Table 7.3 Palmdale South Tangent Section 5 Cores Properties, 44 Days After Construction

Core Number	Location	Uncut Length (cm)	Density (kg/m3)	Compressive Strength (MPa)
5A-32	Section 5-A	19.6	2,337	36.5
5B-36	Section 5-B	21.7	2,445	27.9
5C-40	Section 5-C	22.8	2,434	34.7
5D-44	Section 5-D	20.5	2,312	21.7
Average		21.1	2,445	30.2
Low		19.6	2,312	21.7
High		22.8	2,397	36.5
Std. Dev.		1.4	67	6.8
50th Percentile		21.1	2,385	31.3
90th Percentile		22.4	2,442	35.9
10th Percentile		19.9	2,320	23.5

7.1.2 Core Densities

Some useful statistics of the core densities taken from Sections 1, 3 and 5 (South Tangent) are also shown in Tables 7.1–7.3. Only the bulk densities calculated using Parafilm™ procedure are shown in the table. The corresponding volumetric densities as calculated from measured sample dimensions and weights are (as can be expected) somewhat higher than the densities obtained using Parafilm with an average conversion factor of 0.9768. The conversion factor is fairly consistent. The average Parafilm densities of all the samples taken on the South Tangent is 2,353 kg/m^3, with a maximum value of 2,444 kg/m^3 and a minimum value of 2,116 kg/m^3.

7.1.3 Compressive Strength

The well-known fact that concrete strength development is very dependent on concrete density is well demonstrated by the compressive strength data obtained from the Palmdale cores. It can be seen that when Parafilm density values approach 2,300 kg/m^3, the compressive strength

drops significantly. The average compressive strength of all the samples taken from Sections 1, 3, and 5 is 29.9 MPa. The lowest strength recorded is 12.2 MPa and corresponds to the lowest Parafilm density measured of 2,116.97 kg/m^3. Slab strengths, where the early setting of concrete occurred during construction vibration, may be affected due to voids. Samples taken during construction and tested at 8 hours, 7 days and 90 days are included in Reference (*2*).

7.2 Observations from Cores Taken after HVS Testing

After all HVS testing was completed, 37 100-mm diameter cores (9 from Section 1 and 14 each from Sections 3 and 5, respectively) were extracted from the South Tangent for more detailed investigation. The time of coring was approximately 960 days after construction. Most of these cores were taken from concrete judged intact and uncracked while the positions of others correspond to cracks and instrument positions. Some useful statistics from these cores are shown in Tables 7.4–7.7.

7.2.1 Core Lengths

In general, the measured uncut core lengths confirms the observations from the cores taken earlier, i.e., that the slabs are somewhat thicker than called for in the design specifications. The average slab thicknesses (from uncut core dimensions) are 111.9, 178.3, and 200.4 mm for Sections 1, 3, and 5, respectively.

Core lengths from Section 3, however, show a 50th percentile thickness of 177.5 mm and a high of 200 mm as compared to the design specification of 150 mm. The variability in slab thickness, especially for Section 3, must be noted for further analysis.

7.2.2 Core Densities

Only volumetric densities were calculated from core dimensions and weights. Parafilm densities were however estimated using the average conversion factor of 0.9768. The densities from this set of cores are very similar to those of the 40-day cores (2,360 kg/m^2 estimated average Parafilm for the post-HVS testing cores and an average of 2,353 kg/m^3 from the 40-day cores, with a maximum of 2,425 kg/m^3 and a minimum of 2,240 kg/m^3).

7.2.3 Compression Strength of Cores

The relationship between compressive strength and core density is more clear in the set of cores taken after HVS testing. Seven cores were tested and show a definite trend (refer to Figure 7.1). The straight line fit to the trend is:

$$\textit{Compressive strength (MPa)} = 0.1998 \times \textit{Parafilm density (kg/m}^3\textit{)} - 410.16$$

The highest measured compressive strength was 74.6 MPa, corresponding to an estimated Parafilm density of 2,425 kg/m^3; the lowest value was 42.8 MPa, corresponding to an estimated Parafilm density of 2,272 kg/m^3. Cylindrical specimens taken during construction, cured under standard laboratory conditions, and tested after 90 days had a maximum compressive strength of approximately 55 MPa and an average strength of approximately 44 MPa. When these strengths are compared to the average of 61.7 MPa and high of 74 MPa of the cores taken after HVS testing, it is evident that significant strength development took place after 90 days.

Table 7.4 Properties of Palmdale cores, South Tangent, Section 1, Sample Size = 9

	Uncut Length (cm)	Volumetric Density (kg/m^3)	Estimated Parafilm Density* (kg/m^3)
Average	11.2	2,449	2,392
Low	9.4	2,437	2,381
High	12.9	2,476	2,419
Std. Dev.	1.2	12	11
50th Percentile	10.9	2,446	2,389
90th Percentile	12.3	2,458	2,401
10th Percentile	10.0	2,439	2,382
5th Percentile	9.7	2,438	2,381

Table 7.5 Properties of Palmdale cores, South Tangent, Section 3, Sample Size = 14

	Uncut Length (cm)	Volumetric Density (kg/m^3)	Estimated Parafilm Density* (kg/m^3)
Average	17.8	2,402	2,346
Low	16.5	2,294	2,241
High	20.2	2,441	2,384
Std. Dev.	1.0	37	36
50th Percentile	17.8	2,403	2,347
90th Percentile	18.8	2,429	2,373
10th Percentile	16.9	2,366	2,311
5th Percentile	16.7	2,338	2,284

Table 7.6 Properties of Palmdale cores, South Tangent, Section 5, Sample Size = 14

	Uncut Length (cm)	Volumetric Density (kg/m^3)	Estimated Parafilm Density* (kg/m^3)
Average	20.0	2,417	2,361
Low	18.2	2,326	2,272
High	21.7	2,483	2,425
Std. Dev.	1.2	46	45
50th Percentile	20.2	2,420	2,364
90th Percentile	21.6	2,467	2,409
10th Percentile	18.6	2,375	2,312
5th Percentile	18.4	2,351	2,296

Table 7.7 Properties of Palmdale cores, South Tangent, all Sections Average, Sample Size = 37

	Uncut Length (cm)	Volumetric Density (kg/m^3)	Estimated Parafilm Density* (kg/m^3)
Average	N/A	2,417	2,360
Low	N/A	2,294	2,241
High	N/A	2,483	2,425
Std. Dev.	N/A	41	40
50th Percentile	N/A	2,422	2,366
90th Percentile	N/A	2,453	2,396
10th Percentile	N/A	2,374	2,319
5th Percentile	N/A	2,342	2,288

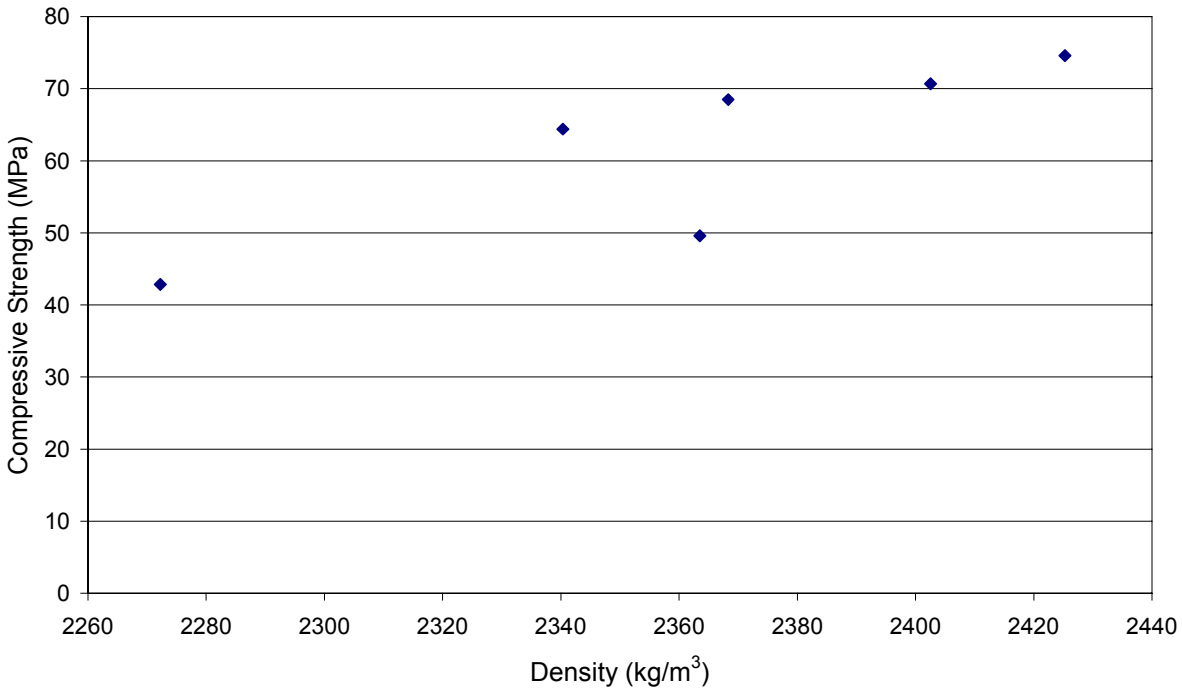

Figure 7.1. Density versus compressive strength, cores taken after HVS testing.

7.2.4 Instrument Position

Instrument positions were measurable on two cores. Both of these cores were extracted from Section 5, slab 39. The position of the one core was center and the other mid-south. In both cases, the instrument was the Carlson A-8 strain meter. The distance of the instruments from the pavement surface was 68 mm and 75 mm, respectively; (the design location depth was 40 mm).

7.3 Observations and Comment on Day/Night Cores

Six pairs of cores were extracted from Section 5 (South Tangent). These cores were taken on joints, one of each pair during daytime and one during nighttime on the same joint. The joints were fixed in place using an injected methacrylate epoxy adhesive to "capture" the joint width at the specified day and night times (3–5 a.m. for night, 1–3 p.m. for day). The goal of this procedure was to observe joint shrinkage and contraction due to thermal effects. Measurements taken of these cores include saw cut depth, saw cut width (both at the top and bottom of the cut) as well as the crack opening at the bottom of the core.

7.3.1 Saw cut depth and width

The saw cut depths from all the cores were very consistent with an average depth of 63.08 mm, a low of 62 mm and a high of 65 mm. There was also no significant difference observed between the top and bottom of the saw cuts on the cores. The average saw cut opening was about 5.9 mm. More statistics are shown in Table 7.8.

Table 7.8 Saw Cut Statistics: Day and Night Cores

	Saw cut depth (mm)	Day Time Readings				Night Time Readings			
		Opening at Saw Cut Top (mm)		Opening at Saw Cut Bottom (mm)		Opening at Saw Cut Top (mm)		Opening at Saw Cut Bottom (mm)	
		Side 1	Side 2	Side 1	Side 2	Side 1	Side2	Side1	Side2
Average	63.1	5.8	5.9	5.6	5.8	6.3	6.2	6.0	5.6
Low	62.0	5.5	5.6	5.4	5.4	5.7	5.7	5.6	5.3
High	65.0	6.4	6.1	6.2	6.1	6.5	6.7	6.4	6.6
Std. Dev.	0.8	0.3	0.3	0.3	0.3	0.3	0.4	0.4	0.5
50th Percentile	63.0	5.7	5.9	5.5	5.8	6.3	6.1	6.1	5.7
90th Percentile	63.9	6.1	6.1	6.0	6.1	6.5	6.6	6.4	6.4
10th Percentile	62.1	5.5	5.6	5.4	5.5	6.0	5.9	5.6	5.4

7.3.2 Day/night measurements of saw cut openings and cracks at the bottom of the cores

From the statistics shown in Table 7.8, no significant difference can be detected between day/night measurements of the saw cut openings.

Six pairs of day/night measurements of crack openings at the bottom of the cores are shown in Table 7.9. At first glance, there seem to be a more or less 50 percent decrease in crack opening at night on three pairs of the cores. The day/night crack openings for the remaining three pairs are generally lower in magnitude and the differences between day and night openings for these pairs are less significant to insignificant.

It should be noted that this experiment was performed during the winter with snow present on one of the days when coring took place. Therefore, the temperature difference and resulting thermal expansion and contraction of the slabs between day and night would not be as great as would be expected during the summer months. Further investigation and a repetition of the experiment during a period of greater daily temperature fluctuation is required before any meaningful conclusions can be drawn.

Table 7.9 Day/Night Measurements of Crack Openings at Bottom of Cores

Position	Joint	Opening at Crack Bottom (mm)		Comments
		Bottom Side 1	Bottom Side 2	
A	32S/33S DAY	1.1	1.1	Joint clogged
B	32S/33S NIGHT	0.55	0.55	Joint clogged
B	33S/34S DAY	0.94	0.94	Joint clogged
A	33S/34S NIGHT	1.1	0.94	Joint clogged
A	34S/35S DAY	1.4	1.4	Joint clogged
B	34S/35S NIGHT	0.7	0.7	Joint clogged
B	35S/36S DAY	0.7	0.7	Joint clogged
A	35S/36S NIGHT	0.7	0.7	Joint clogged
A	36S/37S DAY	1.6	1.6	Joint clogged
B	36S/37S NIGHT	0.82	0.82	Joint clogged
B	37S/38S DAY	0.9	0.9	Joint clogged
A	37S/38S NIGHT	0.7	0.7	Joint clogged

Note: Position A: Core position close to center of slab
Position B: Core position closer to barrier

8.0 TEMPERATURE DATA

Temperatures were collected from thermocouples every 2 hours for the duration of each HVS test. This section summarizes all temperature data in graphical format. The complete raw temperature data can be found in Appendix B.

The following temperature data were recorded:

- Air temperature outside the temperature control chamber
- Air temperature inside the temperature control chamber
- Surface temperature inside the temperature control chamber
- In-depth concrete pavement temperatures at 50, 100, 150, and 200-mm depths

Only the temperature of the concrete slab has been recorded and in cases where the concrete thickness was less than 200 mm, the temperature at the bottom of the concrete layer is reported (i.e. for the 100-mm sections, in-depth temperatures were recorded at 0, 50, and 100 mm). In some cases, more than one thermocouple was installed. Appendix B details all collected thermocouple data.

9.0 REFERENCES

1. CAL/APT Contract Team. "Test Plan for CAL/APT Goal LLPRS—Rigid Phase III," Institute of Transportation Studies, Pavement Research Center, University of California, Berkeley, April 1998.

2. Roesler, J., Scheffy, C., Ali, A., and Bush, D. "Construction, Instrumentation, and Material Testing of Fast-Setting Hydraulic Cement Concrete Pavement in Palmdale, California," Institute of Transportation Studies, Pavement Research Center, University of California, Berkeley, *Draft Report to Caltrans*, March 1999.

3. Roesler, J., du Plessis, L., Hung, D., Bush, D., Harvey, J. "CAL/APT Goal LLPRS – Rigid Phase III: Concrete Test Section 516CT Report," Institute of Transportation Studies, Pavement Research Center, University of California, Berkeley, *Draft Report to Caltrans*, September, 1998.

4. Heath, A. C., J. R. Roesler, J. T. Harvey. "Quantifying Longitudinal, Corner and Transverse Cracking in Jointed Concrete Pavements." *Transportation Research Board Annual Meeting CD-ROM*. 2000.

5. Roesler, J. *Fatigue of Concrete Beams and Slabs.* Ph.D. Thesis, University of Illinois, Urbana-Champaign, IL, 1998.

APPENDIX A: FWD DEFLECTIONS

This appendix includes the following information:

- Documentation of raw and processed data files
- Deflections versus age and curing (Graphical Representation)
- FWD Deflections (Raw data)

Documentation of Raw and Processed Data Files

All FWD related files are contained in the directory named CAL-APT FWD Data. The figure below shows the directory structure with an explanation of the contents.

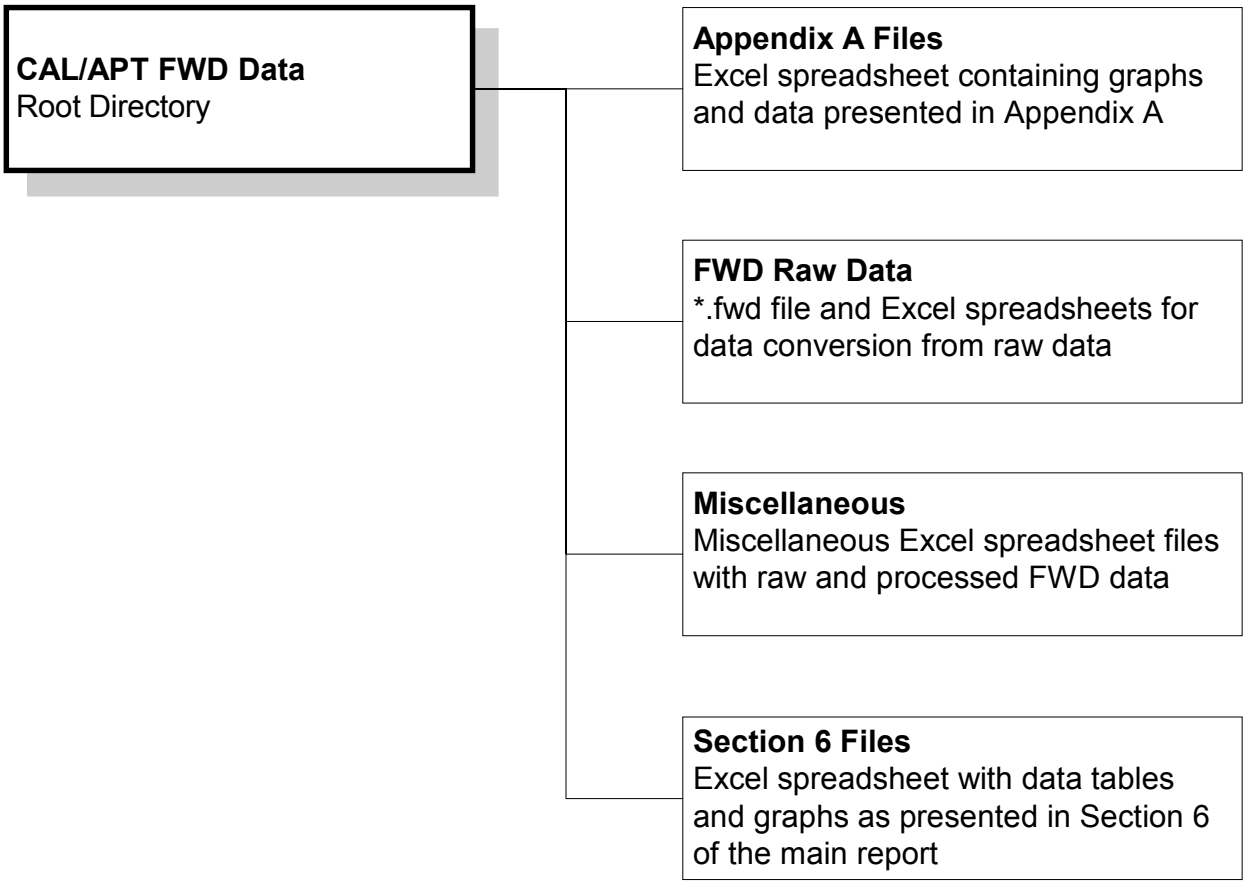

The raw data files containing the Falling Weight Deflectometer (FWD) data (*.fwd files) are contained in the directory named "FWD Raw Data". A hardcopy of most of these files is provided in translated format in the following sections. For second level analysis, the data can be electronically accessed by means of the spreadsheet titled "FWD conversion 1.xls". This spreadsheet contains a macro that processes the raw FWD data into a format from which data can be readily processed for graphical representation and further analysis.

The macro is run from the command button called "Import FWD," which is embedded in the first page of the spreadsheet. When this button is clicked, a file-open dialog box appears. Users can use this dialog to browse and select any file with the "FWD" extension. When the file is selected, the data is extracted from the raw data file to the first sheet of the spreadsheet. The data shows all relevant information from the raw data file, including:

- File name;
- Data of file creation (as entered by the operator at the time of measurement);
- Comments;
- Plate and sensor configuration;
- Station position for all deflections (all drops);
- Surface and air temperature for all deflections (all drops);
- Time of measurement for all deflections (all drops);
- Plate pressure for all deflections (all drops);
- Deflections for all stations (all drops);

The Autofilter property (Data→Filter→Autofilter) can be used to filter the data for a specific criterion (e.g., range of stations, drop number). The filtered data can be copied and pasted to another sheet for further analysis.

Deflections versus Curing Age for HVS Sections

The graphs show the variation in the normalized maximum deflection at different curing ages. The HVS test position is also indicated in the figures. The deflections were recorded along the slab centerline and were normalized for an applied load of 66.7 kN (943.6 kPa).

Deflections versus Curing Age for all 200 mm thick slabs

The attached graphs show the FWD maximum deflections at different times after construction. Slab numbers are also indicated in the graphs. The deflections (in micron) were normalized for an applied load of 66.7 kN (943.6 kPa).

FWD Deflections (Raw Data)

Charts plotting the converted raw FWD data are shown below. The data can be accessed in the Pavement Research Center Database.

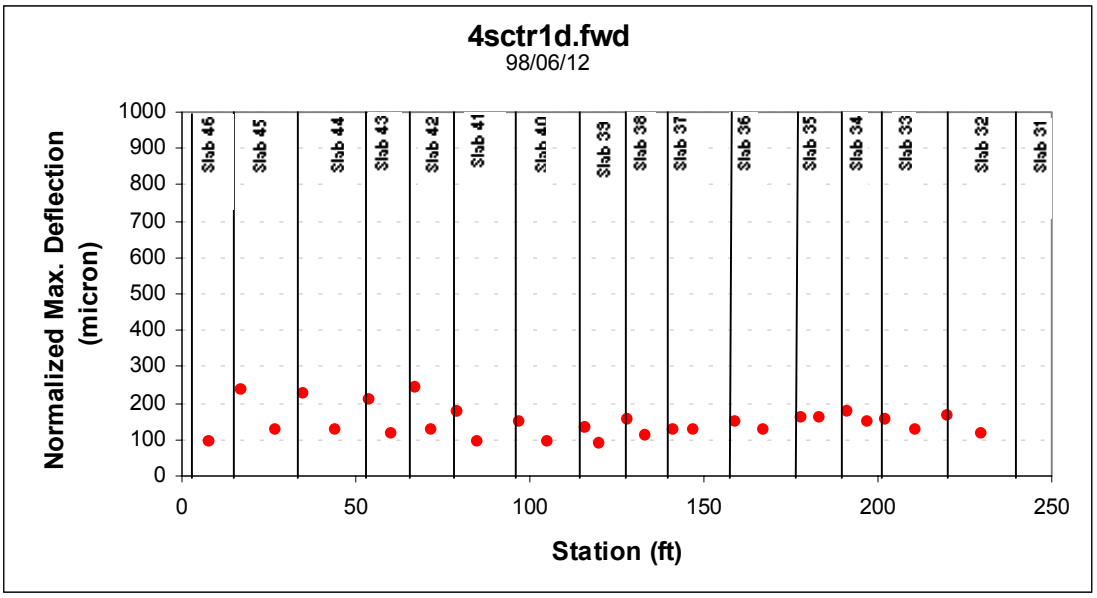
4sctr1d.fwd
98/06/12
Normalized Max. Deflection (micron)
1000
900
800
700
600
500
400
300
200
100
0
Slab 46
Slab 45
Slab 44
Slab 43
Slab 42
Slab 41
Slab 40
Slab 39
Slab 38
Slab 37
Slab 36
Slab 35
Slab 34
Slab 33
Slab 32
Slab 31
0
50
100
150
200
250
Station (ft)

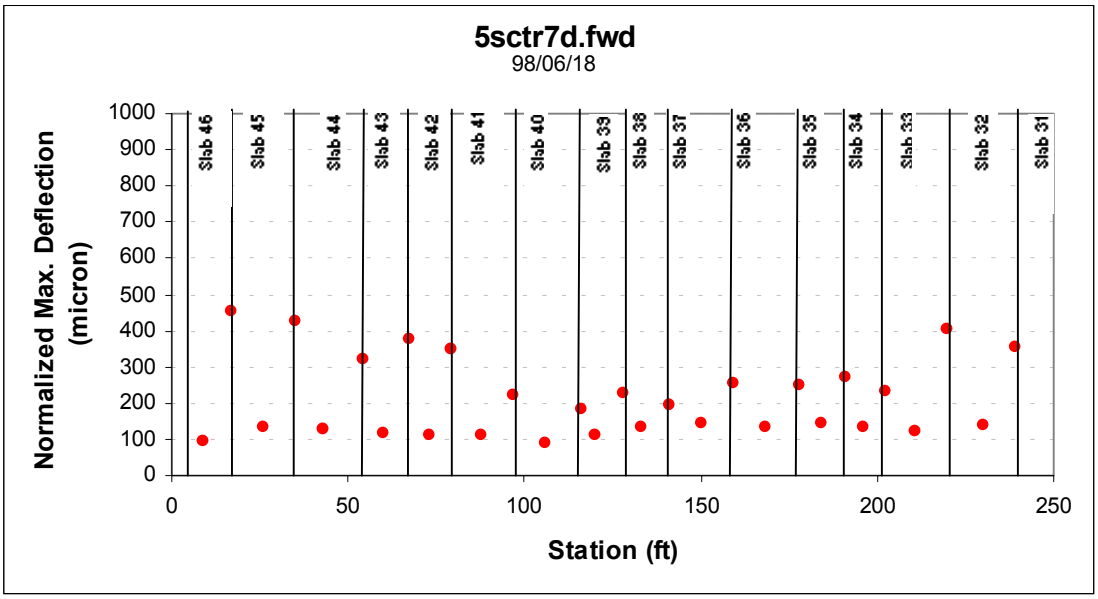
5sctr7d.fwd
98/06/18
Normalized Max. Deflection (micron)
1000
900
800
700
600
500
400
300
200
100
0
Slab 46
Slab 45
Slab 44
Slab 43
Slab 42
Slab 41
Slab 40
Slab 39
Slab 38
Slab 37
Slab 36
Slab 35
Slab 34
Slab 33
Slab 32
Slab 31
0
50
100
150
200
250
Station (ft)

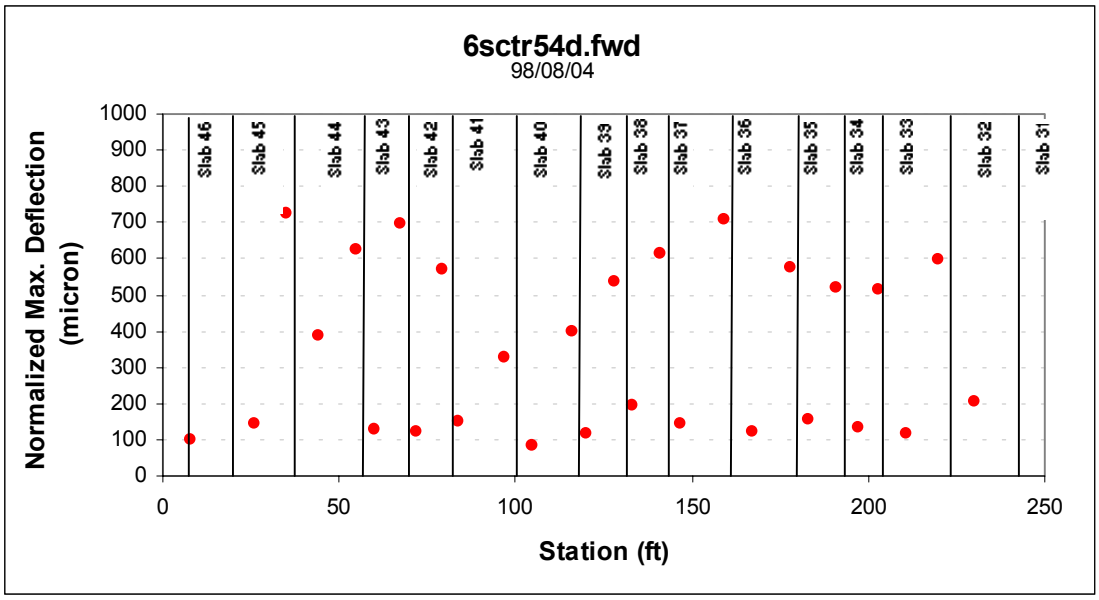
6sctr54d.fwd
98/08/04
Normalized Max. Deflection (micron)
Station (ft)
Slab 46
Slab 45
Slab 44
Slab 43
Slab 42
Slab 41
Slab 40
Slab 39
Slab 38
Slab 37
Slab 36
Slab 35
Slab 34
Slab 33
Slab 32
Slab 31

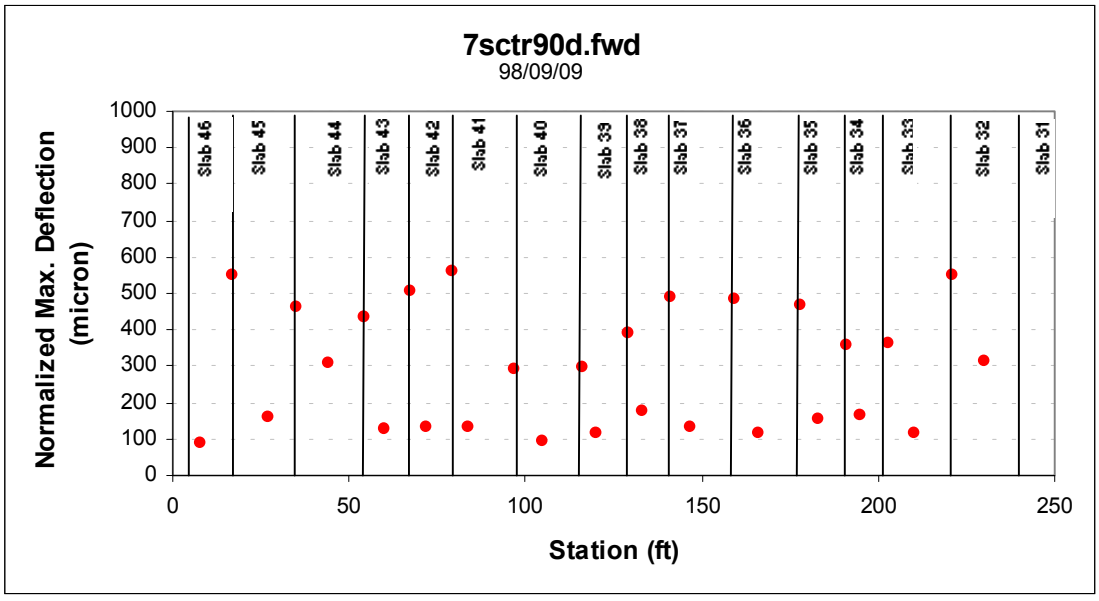
7sctr90d.fwd
98/09/09
Normalized Max. Deflection (micron)
Station (ft)
Slab 46
Slab 45
Slab 44
Slab 43
Slab 42
Slab 41
Slab 40
Slab 39
Slab 38
Slab 37
Slab 36
Slab 35
Slab 34
Slab 33
Slab 32
Slab 31

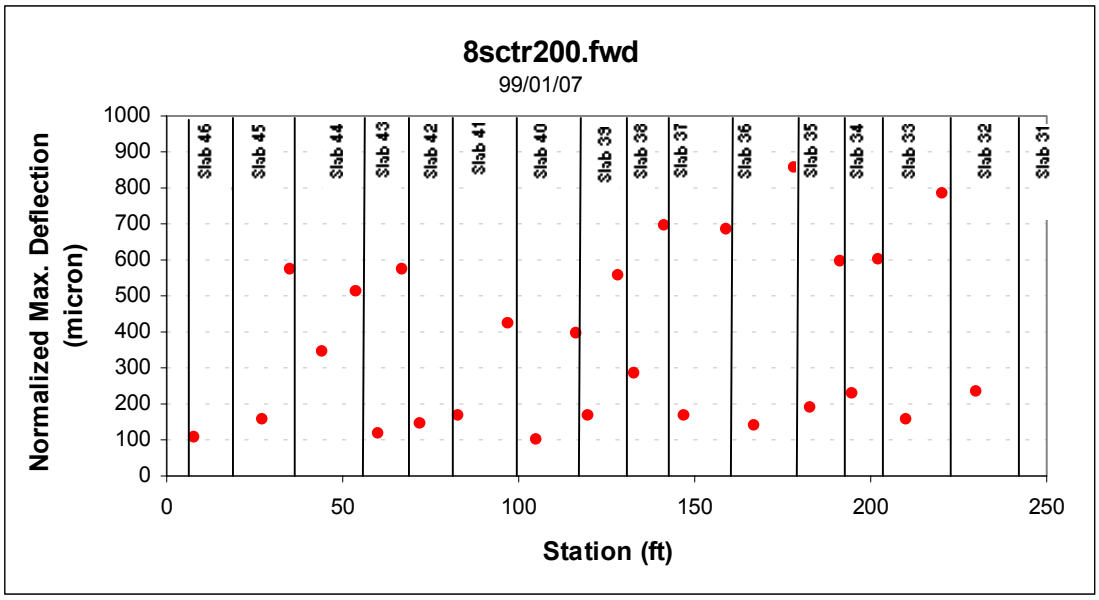
8sctr200.fwd
99/01/07
Normalized Max. Deflection (micron)
Station (ft)
Slab 46
Slab 45
Slab 44
Slab 43
Slab 42
Slab 41
Slab 40
Slab 39
Slab 38
Slab 37
Slab 36
Slab 35
Slab 34
Slab 33
Slab 32
Slab 31

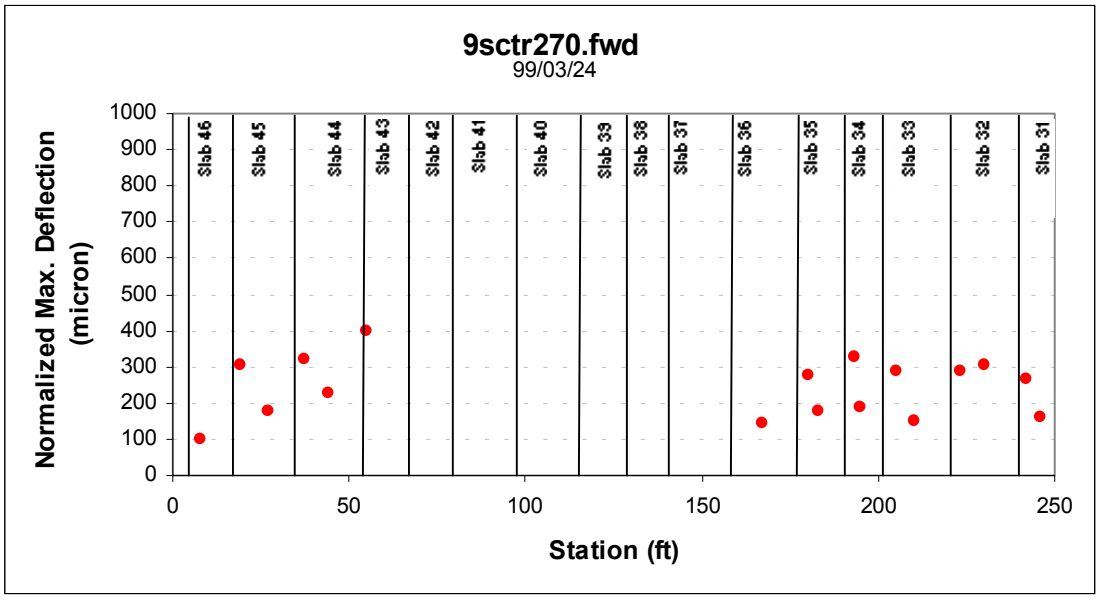
9sctr270.fwd
99/03/24
Normalized Max. Deflection (micron)
Station (ft)
Slab 46
Slab 45
Slab 44
Slab 43
Slab 42
Slab 41
Slab 40
Slab 39
Slab 38
Slab 37
Slab 36
Slab 35
Slab 34
Slab 33
Slab 32
Slab 31

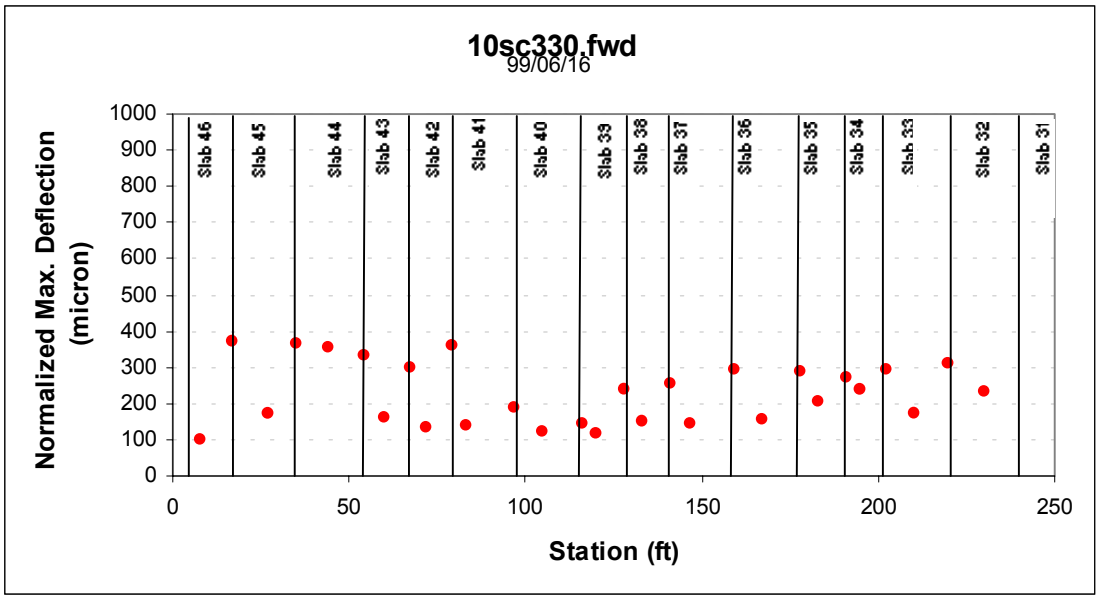
10sc330.fwd
99/06/16
Normalized Max. Deflection (micron)
Station (ft)
Slab 46
Slab 45
Slab 44
Slab 43
Slab 42
Slab 41
Slab 40
Slab 39
Slab 38
Slab 37
Slab 36
Slab 35
Slab 34
Slab 33
Slab 32
Slab 31

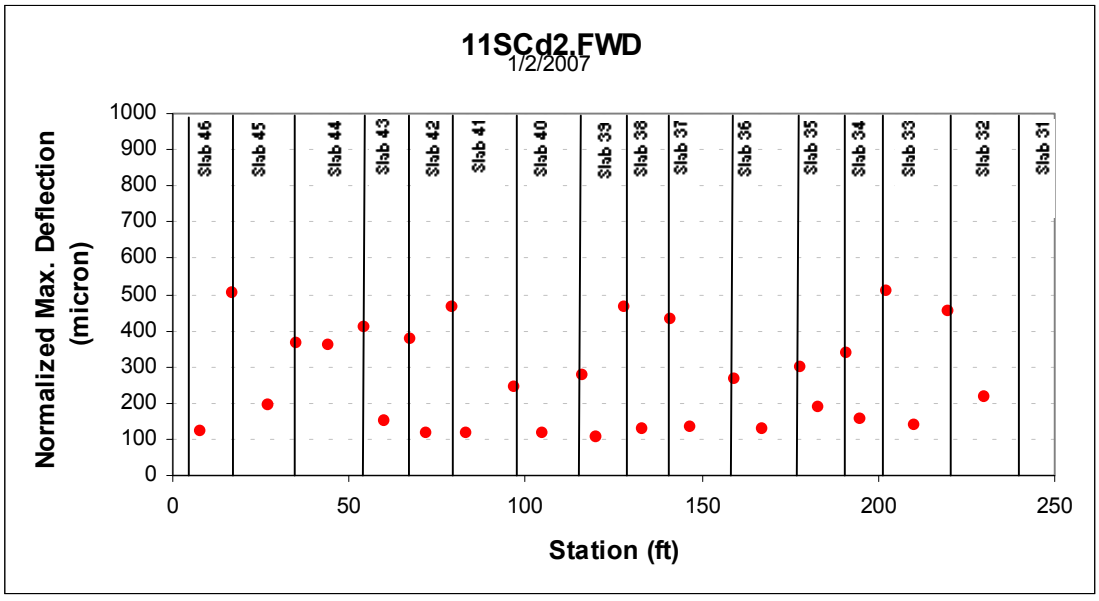
11SCd2.FWD
1/2/2007
Normalized Max. Deflection (micron)
Station (ft)
Slab 46
Slab 45
Slab 44
Slab 43
Slab 42
Slab 41
Slab 40
Slab 39
Slab 38
Slab 37
Slab 36
Slab 35
Slab 34
Slab 33
Slab 32
Slab 31

APPENDIX B: THERMOCOUPLE DATA

This appendix presents an example of the thermocouple data generated during the testing of the South Tangent pavement test sections. The complete data can be accessed using the Pavement Research Center Database.

Test Section 520FD

520FD													
Hourly Temperature Data (degrees C)					Thermocouple # 40			Thermocouple # 37			Thermocouple # 38		
Section	Date	Time	Air Outside	Air Inside	100 mm	50 mm	0 mm	100 mm	50 mm	0 mm	100 mm	50 mm	0 mm
520FD	22/7/98	11h30	30	24.2	26.1	25.7	24.8	25.5	25.4	24.7	25.2	24.9	24
520FD		12h00	31	20.7	26	24.9	22.5	25.5	24.9	23.6	25.1	24.3	22.6
520FD		13h30	31	19.9	25.1	23.6	21.3	25.1	24.3	22.8	24.5	23.4	21.7
520FD		14h30	29	19.2	24.7	22.1	20.8	25	24.2	22.8	24.2	23.2	21.5
520FD		15h30	28	19.9	24.2	22.6	20.4	24.9	24	22.8	24	23	21.4
520FD		17h00	26	18.5	24.1	22.6	20.5	24.9	24.3	23	24.1	23.2	21.6
520FD		18h00	25	18.2	23.9	22.9	21.4	24.1	24.1	22.7	23.8	22.2	20.3
520FD		20h00	23	16.3	23.1	22.1	20.6	24.2	23.9	21.3	22.7	21.2	19.2
520FD		22h00	21	16.3	23.1	22.2	20.9	23.7	22.7	20.9	22.3	22.7	18.8
520FD		24h00	19	18.1	23	22.3	21.2	23.4	22.4	2.09	22	20.6	18.5
520FD	23/7/98	2h00	17	16.4	22.9	22.2	21.1	23	22.1	20.4	21.5	20.2	18.6
520FD		4h00	16	15.4	22.8	22.1	21	22.7	21.7	20.2	21.2	20	18.3
520FD		6h00	16	16.3	22.6	21.8	20.9	22.3	21.4	19.9	20.9	19.8	18.2
520FD		8h00	20	15.6	22.3	21.7	20.6	22	21.1	20.2	20.7	19.4	17.7
520FD	N10	9h30	24	16.6	22.2	21.5	20.5	21.8	21.1	19.9	20.3	19.2	17.9
520FD		11h00	26	17.5	22	21.1	19.7	21.7	20.1	19.9	20.4	19.2	18
520FD		13h00	28	18.9	21.7	20.8	19.5	21	21.2	20.6	20.3	19.2	17.8
520FD		15h00	29	21.5	20.7	20.9	20	22.1	21.6	21	20.2	19.2	17.9
520FD		16h00	28	22.6	22.3	21.8	20.9	22.6	22.2	21.7	20.5	19.6	18.4
520FD		18h00	23	17.3	22.3	21.5	20.1	22.7	22.2	21.5	20.2	19	17.3
520FD		20h00	21	17.6	22.1	21.1	19.6	22.7	22.1	21	19.8	18.5	16.9
520FD		22h00	18	16.2	21.8	20.9	19.4	22.6	21.9	20.8	19.6	18.4	17
520FD		24h00	17	15.3	21.5	20.7	19.3	22.4	21.7	20.5	19.6	18.3	16.9
520FD	24/798	02h00	16	14.8	21.2	20.3	19	22.1	21.3	20.2	19.4	18.3	16.8
520FD		04h00	16	15.7	20.9	20.1	18.9	21.8	21	19.9	19.3	18.2	17

520FD													
Hourly Temperature Data (degrees C)					**Thermocouple # 40**			**Thermocouple # 37**			**Thermocouple # 38**		
Section	**Date**	**Time**	**Air Outside**	**Air Inside**	**100 mm**	**50 mm**	**0 mm**	**100 mm**	**50 mm**	**0 mm**	**100 mm**	**50 mm**	**0 mm**
520FD		06h00	16	15.2	20.8	19.9	18.7	21.6	20.8	19.6	19.1	18.1	17.2
520FD		08h00	19	18.6	20.7	20	19.2	21.4	20.7	20.2	19.3	18.5	17.8
520FD		9h30	23	19.6	20.8	20.2	19.8	21.4	20.9	20.5	19.4	18.7	18.1
520FD		11h00	27	21	20.7	20.1	21.6	21.2	19.8	19.4	18.9	18.9	18.2
520FD		12h00	29	22	22.2	20.8	20.5	21.8	21.6	21.8	19.6	19.1	18.5
520FD		16h00	31	24.5	22.1	21.8	21.5	22.8	22.8	23	19.9	19.3	18.5
520FD		18h00	26	22.1	22.4	22	21.6	23.2	23.1	22.8	20.9	19.4	19.2
520FD		20h00	23	20.9	22.5	22.1	21.7	23.3	23	22.7	20.1	19.5	18.9
520FD		22h00	20	20.2	22.7	22.3	21.8	23.4	23.2	22.8	20.1	19.5	18.9
520FD		24h00	19	20.1	22.7	22.4	22.1	23.3	22.9	22.2	20.3	19.8	19
520FD	25/7/98	02h00	19	20.3	22.6	22.4	22.4	23.2	22.6	22.1	20.4	19.6	19.2
520FD		04h00	20	19.9	23	22.7	22.3	22.9	22.4	21.8	20.4	19.8	19.1
520FD		06h00	20	20.3	23	22.8	22.5	22.8	22.3	21.7	20.4	19.8	19.2
520FD		08h00	25	20.7	23	22.8	22.5	22.7	22.3	22.1	20.2	19.7	19.1
520FD		10h00	30	19.4	22.7	22.4	21.7	22.6	22.1	21.6	20.2	19.5	18.3
520FD		12h00	37	21.8	22.8	22.5	22.2	22.6	22.3	22.2	19.9	19.4	18.7
520FD		14h00	36	23.9	22.9	22.6	22.3	22.9	22.8	22.9	20	19.5	18.9
520FD		16h00	35	24.7	23.1	22.8	22.5	23.4	23.3	23.7	20.2	19.8	19.3
520FD		18h00	32	23.7	23.3	22.9	22.5	23.8	23.8	24	20.3	19.9	19.4
520FD		22h00	24	21.2	23.2	22.9	22.3	23.8	23.4	22.9	20.4	19.8	19
520FD		24h00	24	20.2	23.3	22.9	22.5	23.6	23.1	22.5	20.2	19.7	18.8
520FD	26/7/98	02h00	26	20	23.2	22.9	22.4	23.3	22.8	22.1	20	19.3	18.2
520FD		04h00	23	20.7	23.2	22.9	22.4	23	22.5	21.8	19.9	19.3	18.7
520FD		06h00	26	20.8	23.4	22.8	22.4	22.8	22.3	21.6	19.8	19.2	18.4
520FD		08h00	29	21.5	23.1	22.7	22.2	22.8	22.3	22	19.8	19.2	18.5
520FD		10h00	32	20.1	22.7	22.1	21.1	22.8	22.5	22.1	19.5	18.7	17.6
520FD		12h00	35	21.7	22.4	21.9	21.3	22.8	22.5	22.4	19.4	18.9	18.5

520FD													
Hourly Temperature Data (degrees C)					Thermocouple # 40			Thermocouple # 37			Thermocouple # 38		
Section	Date	Time	Air Outside	Air Inside	100 mm	50 mm	0 mm	100 mm	50 mm	0 mm	100 mm	50 mm	0 mm
520FD		14h00	39	22.7	22.8	21.4	23.1	22.9	23	22.9	19.4	19.4	19.2
520FD		16h00	37	25.5	22.4	22	21.2	23.4	23.4	23.8	19.9	19.6	19.2
520FD		18h00	34	23.2	22.5	21.2	20.1	23.8	23.5	22.8	20.1	19.8	19.7
520FD		20h00	30	21.8	22.5	21.9	20.6	23.7	23.4	23	20.2	19.7	18.9
520FD		22h00	28	21.2	22.6	22.1	21.5	23.7	23.3	22.7	20.1	19.4	18.5
520FD		24h00	28	20.5	22.6	22	21.4	23.5	23	22.3	19.7	19.1	18.2
520FD	27/7/98	02h00	28	20.1	22.6	22.1	21.3	23.2	22.8	21.9	19.6	18.9	17.9
520FD		04h00	27	19.1	22.5	21.9	21.2	23	22.6	21.5	19.4	18.9	18.2
520FD		06h00	27	20.2	22.3	21.8	21	22.8	22.3	21.5	19.5	18.8	17.9
520FD		08h00	30	20.3	22.1	21.5	20.9	22.5	21.9	21.1	19.2	18.6	17.8
520FD		10h00	32	20.5	22	21.1	20.6	22.6	22.3	21.3	19.1	18.4	17.6
520FD		12h00	34	21.7	22.1	21.7	21.2	22.9	22.7	22.8	19.2	18.8	18.5
520FD		14h00	38	22.8	22.2	22.1	21.6	23.4	23.1	22.9	19.1	19.5	19.3
520FD		16h00	37	25.3	22.3	21.4	20.8	23.7	23.5	23.1	20	19.6	19.5
520FD		18h00	36	24.7	22.5	22.9	20.4	23.8	23.6	23.5	20.1	19.8	19.6
520FD		20h00	32	22.9	22.5	21.9	21	24	23.9	23.7	20.2	19.8	19.3
520FD		22h00	28	22.8	22.5	21.9	21.2	24.2	23.9	23.6	20.1	19.7	19.1
520FD		24h00	28	17.9	22.5	21.8	20.8	24.2	23.7	23.1	20	19.2	17.8
520FD		02h00	27	17.1	22.1	21.5	20.4	23.7	23.2	22.2	19.2	18.3	16.8
520FD		04h00	27	17.1	22	21.3	20.3	23.4	22.8	21.8	18.8	17.9	16.8
520FD	28/7/98	06h00	25	17.8	21.8	21.1	20.2	23	22.4	21.4	18.6	17.9	16.9
520FD		08h00	29	18.9	21.6	20	20.2	22.8	22.3	21.7	18.6	17.9	17.3
520FD		12h00	37	21.3	21.9	20.2	20.7	23.2	22.9	22.8	19	18.8	18.5
520FD		14h00	37	24.9	21.8	21.4	21	23.3	23.4	23.7	19.2	18.9	18.9
520FD		16h00	37	31.4	22.3	22	22.1	24.1	24.3	25.6	19.7	19.8	20.3
520FD		18h00	34	27.8	22.8	22.7	22.6	24.8	25.1	25.7	20.3	20.5	20.7
520FD		20h00	29	23.6	23	22.6	22.1	25	24.9	24.8	20.5	20.4	20.2

520FD													
Hourly Temperature Data (degrees C)					**Thermocouple # 40**			**Thermocouple # 37**			**Thermocouple # 38**		
Section	**Date**	**Time**	**Air Outside**	**Air Inside**	**100 mm**	**50 mm**	**0 mm**	**100 mm**	**50 mm**	**0 mm**	**100 mm**	**50 mm**	**0 mm**
520FD		22h00	26	23.3	22.9	22.5	21.8	25.1	25.1	25	20.5	20.1	19.5
520FD		24h00	24	21.3	22.7	22.2	21.3	25	24.8	24.3	20.3	19.8	19
520FD	29/7/98	02h00	23	21.6	22.6	22	21.2	24.8	24.6	24.2	20.1	19.5	18.7
520FD		04h00	23	21	22.4	21.8	20.9	24.6	24.4	24	19.8	19.2	18.4
520FD		06h00	21	22.2	22.2	21.6	20.9	24.7	24.5	24	19.6	19.1	18.3
520FD		18h00	28	16.6	21.3	20.5	19.4	23.3	22.8	21.7	18.6	18	17.1
520FD		20h00	23	18.2	21.2	20.3	18.8	23.1	22.4	21.4	18.6	17.9	17.2
520FD		22h00	20	18.3	20.9	19.9	18.6	22.9	22.3	21.4	18.6	18.1	17.6
520FD		24h00	17	16.7	20.6	19.8	18.7	22.9	22.1	21.1	18.6	18.2	17.8
520FD		02h00	17	16.6	20.5	19.7	18.8	22.9	22.3	21.6	18.7	18.3	17.8
520FD		04h00	17	16.9	20.6	19.6	18.7	22.8	22.2	21.7	18.8	18.4	17.9
520FD	30/7/98	06h00	15	16.8	20.5	19.8	19	22.7	22.3	21.4	19	18.4	18
520FD		14h00	29	22.7	20.1	19.9	19.6	22.4	21.9	21.8	18.7	18.6	18.4
520FD		16h00	28	19.3	20.6	20.3	20.1	22.2	21.8	21.4	18.9	18.4	17.9
520FD		18h00	25	18.6	20.7	20.1	21.8	22.1	21.4	21.3	18.6	18.2	17.6
520FD		20h00	19	17.2	20.8	19.4	22.2	22.3	21	21.1	18.8	18.4	17.7